

**Palladium-Catalyzed Cyclopropanation Reactions and Site
Selectivity in Palladium-Catalyzed Oxidative Cross-Coupling
Reactions**

by

Thomas W. Lyons

A dissertation submitted in partial fulfillment
of the requirements for the degree of
Doctor of Philosophy
(Chemistry)
in The University of Michigan
2011

Doctoral Committee:

Professor Melanie S. Sanford, Chair
Professor Adam J. Matzger
Professor Philip E. Savage
Associate Professor John P. Wolfe

© Thomas W. Lyons

2011

To my Mother and Father

Acknowledgments

I would like to thank Melanie for taking a chance on a lost P-chemist who wanted to learn about physical organic chemistry. It has been a pleasure working with you and learning from you over the last several years. Not many graduate students are as fortunate as we have been to have such a supportive and hard working advisor.

I would also like to thank my committee members for their service and support during my time at Michigan. Professors Matzger and Wolfe in particular, have been invaluable in solving problems with various projects throughout my graduate school career.

I have had the good fortune of working with a number of talented and supportive colleagues while at Michigan. Aside from Melanie I'd like to particularly thank Lopa, Dipa, and Kami who were instrumental in assisting me during my formative years as a chemistry graduate student. Additionally I'd like to thank Kara, Yingde, Asako, Kevin, Andrew, and Matt, for being great benchmates. I have worked closely with them over the last several years and they have served as a great sounding board for ideas and solving problems. Many other people have been great at discussing the litany of challenges that were overcome while pursuing the projects discussed in this thesis. Particularly I'd like to thank the other members of my incoming class in the lab; Nick, Matt, and Andrew who have been with me from the beginning. Sharon, Brannon, Amanda, and Joy have also been great for discussing organic, computational, and inorganic questions. I'd like to thank Sharon especially for her generous work editing this entire thesis. Finally, I'd like to thank all those people who baked so many goodies over the years. They may have added to my waste line, but also added to my wellbeing.

Finally, I'd like to thank my family. Without their support, none of this would have happened.

Table of Contents

Dedication	ii
Acknowledgements	iii
List of Tables.....	vi
List of Figures.....	viii
Abstract	x
Chapter 1	
Introduction	1
1.1 References	10
Chapter 2	
Palladium-Catalyzed Cyclopropanation Reactions.....	12
2.1 Background and Significance	12
2.2 Methodology Development and Scope	15
2.3 Mechanistic Investigations	24
2.4 Conclusion	36
2.5 Subsequent Work.....	37
2.6 Experimental Procedures	39
2.7 References.....	66
Chapter 3	
Controlling Site Selectivity in Palladium-Catalyzed Aryl-Aryl' Oxidative Cross-Coupling Reactions	69

3.1 Background and Significance	69
3.2 Methodology and Stoichiometric Selectivity Studies	78
3.3 Application to Diverse Substrates	96
3.4 Studies to Understand Selectivity in Carbonate Systems	101
3.5 Conclusions	114
3.6 Experimental Procedures	114
3.7 References	138

Chapter 4

Progress Toward Catalytic Regioselective Oxidative Cross-Coupling Reactions and Application to Direct Arylation	142
4.1 Background and Significance	142
4.2 Methodology Development and Oxidant Screening	147
4.3 Applications to Direct Arylation	157
4.4 Conclusion	160
4.5 Experimental Procedures	160
4.6 References.....	162

List of Tables

Chapter 2

Pd-Catalyzed Cyclopropanation Reactions

Table 2.1: Optimization of Enyne Cyclopropanation.....	16
Table 2.2: Pd-Catalyst Screening for Cyclopropanation	17
Table 2.3: Cyclopropane Formation Dependence as a Function of Bipy	18
Table 2.4: Substrate Scope of Pd-Catalyzed Enyne Cyclizations	20
Table 2.5: Effect of Oxidant on Yield of Cyclopropane 2	26
Table 2.6: CP/RE-1 as a Function of Aryl Substituent X	36

Chapter 3

Controlling Site Selectivity in Palladium-Catalyzed Aryl-Aryl' Oxidative Cross-Coupling Reactions

Table 3.1: Site Selectivity as a Function of Quinone Substitution.....	81
Table 3.2: Site Selectivity as a Function of Quinone Substitution (Electronic Effects)	82
Table 3.3: Site Selectivity as a Function of Carboxylate Substitution	83
Table 3.4: Effect of Exogenous AcOH on Selectivity in Regime 1	84
Table 3.5: Site Selectivity as a Function of Carboxylate Substitution	85
Table 3.6: Effect of Exogenous AcOH on Selectivity in Regime 2.....	85
Table 3.7: Effect of AcOH on Selectivity with Sterically Differentiated Quinones ...	86
Table 3.8: Site Selectivity as a Function of Benzoate Substitution (Electronic Effects)	87
Table 3.9: [(bzq)Pd(OPiv)] ₂ Studies with Substituted Quinones	88
Table 3.10: Site Selectivity as a Function of Ag Salt.....	93

Table 3.11: Influence of Ag ₂ CO ₃ Stoichiometry on Selectivity	94
Table 3.12: Selectivity and Yield as a Function of M ₂ CO ₃	95
Table 3.13: Application Oxidative Coupling to 1,3-Diisopropoxybenzene	97
Table 3.14: Substituted Quinones with 1,3-Diisopropoxybenzene	98
Table 3.15: Oxidative Coupling Arene Substrate Scope	99
Table 3.16: Scope of Oxidative Coupling Cyclometallating Ligands with DMB	101
Table 3.17: Calculated p-orbital Coefficients	102
Table 3.18: Energy Calculations for A' and B'.....	103
Table 3.19: Calculated pK _a values.....	106
Table 3.20: Calculated C–H Bond Lengths and Selectivities	108
Table 3.21: Arene Electronics Competition Study.....	110
Table 3.22: H/D Exchange Experiments.....	113

Chapter 4

Progress Toward Catalytic Regioselective Oxidative Coupling Reactions and Application to Direct Arylation

Table 4.1: Catalyst Screening for Pd/CO ₃ -Catalyzed Oxidative Coupling	148
Table 4.2: Stoichiometric Studies with Pd Salts	150
Table 4.3: Oxidant Screening with Bzq and DMB.....	151
Table 4.4: Oxidant Screenings with O ₂ and Cu ^{II} Co-oxidants	152
Table 4.5: O ₂ as the Terminal Oxidant with HPA Co-oxidants	153
Table 4.6: Additive Screening.....	154
Table 4.7: Oxidant Screening with Ag ^I and Cu ^{II} Salts	155

List of Figures

Chapter 2

Pd-Catalyzed Cyclopropanation Reactions

Figure 2.1: Chiral Ligands Screened in Pd-Catalyzed Cyclopropanation.....	23
Figure 2.2: X-ray Crystal Structure of Product 54	31
Figure 2.3: Crystal Structure of Oxime	44
Figure 2.4: Crystal Structure of Oxime of 44	53

Chapter 3

Controlling Site Selectivity in Palladium-Catalyzed Aryl-Aryl' Oxidative Cross-Coupling Reactions

Figure 3.1: Initial Rate vs. Equiv of BQ in the Coupling of 1 with 1,2-Dimethoxybenzene.....	78
Figure 3.2: A : B versus Equiv of BQ for the Reaction of 1 with DMB	80
Figure 3.3: Selectivity Hammett Plot	82
Figure 3.4: Steric Congestion in BQ Complexation.....	90
Figure 3.5: Site Selectivity (B : A) as a Function of Equiv of BQ for the Coupling of 5 / Cs_2CO_3 with DMB	96
Figure 3.6: Plot of B : A Ratio (Experimental from Reactions of 5 / Cs_2CO_3) versus $E_{\text{A}'} - E_{\text{B}'}$	104
Figure 3.7: Plot of Selectivity (B : A , experimental) versus ΔpK_{a}	107
Figure 3.8: H_6 -benzene Reaction Kinetics with $[(\text{bzq})\text{PdCl}]_2/\text{CO}_3$	133
Figure 3.9: D_6 -benzene Reaction Kinetics with $[(\text{bzq})\text{PdCl}]_2/\text{CO}_3$	134
Figure 3.10: Transition State Theory Equation.....	135

Figure 3.11: Example pK_a from Computational ΔG_{rxn} Calculations 137

Chapter 4

Progress Toward Catalytic Regioselective Oxidative Coupling Reactions and Application to Direct Arylation

Figure 4.1: Potential Arene and Aryl Halide Coupling Partners 159

Abstract

Palladium-Catalyzed Cyclopropanation Reactions and Site Selectivity in Palladium-Catalyzed Oxidative Cross-Coupling Reactions

by

Thomas W. Lyons

Chair: Melanie S. Sanford

This thesis describes our efforts at the discovery, optimization, and mechanistic study of two new and fundamentally different Pd-mediated reactions for the construction of bicyclic cyclopropanes as well as biaryl products. Palladium-catalyzed intramolecular carbocyclizations of alkenes and alkynes allow the assembly of complex carbo- and heterocycles from readily available starting materials. We have demonstrated the development of a tandem Pd-catalyzed bis-cyclization/oxidative cleavage sequence with enyne substrates resulting in the formation of cyclopropyl-containing fused heterocycles. Using a Pd^{II} catalyst such as Pd(OAc)₂, a stoichiometric oxidant such as iodobenzene diacetate, as well as a bidentate ligand such as bipyridine, the assembly of complex bicycles can be achieved with inversion of the starting alkene geometry. Stereochemical and electronic studies indicate the reaction proceeds via a Pd^{III/IV} catalytic cycle and has important implications for Pd^{IV} reductive elimination processes. This reaction has shown to be tolerant of substituted aryl groups, esters, and tosyl protected amines. Both the synthetic scope and recent mechanistic investigations of this reaction will be discussed in detail.

The second major topic discussed in this thesis is a detailed investigation of the factors controlling site selectivity in the Pd-mediated oxidative coupling of 1,3-disubstituted and 1,2,3-trisubstituted arenes (Aryl-H) with cyclometalating substrates (L~C-H). The influence of both the concentration and the steric/electronic properties of

the quinone promoter are studied in detail. In addition, the effect of steric/electronic modulation of the carboxylate ligand is discussed. Finally, we demonstrate that substitution of the carboxylate for a carbonate X-type ligand leads to a complete reversal in site selectivity for many arene substrates. The origins of these trends in site selectivity are discussed in the context of the mechanism of Pd-catalyzed oxidative cross-coupling.

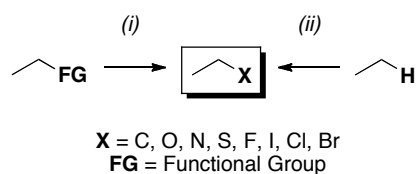
The final topic of this thesis addresses our efforts at developing a catalytic system for oxidative cross-coupling with new control of site selectivity. A variety of oxidation protocols are described which thus far have failed to produce catalytic turnover.

Chapter 1

Introduction

The site-selective and chemoselective functionalization of C–H bonds to form more modifiable C–X bonds (X = O, C, N, F, S, Cl, Br, I) remains an important challenge in modern chemistry.¹⁻⁶ The ability to functionalize a C–H bond found in aryl, alkenyl, or alkyl substrates would preclude the need for pre-functionalized starting materials that have traditionally been required to access new complex molecules (Scheme 1.1).

Scheme 1.1 Strategies for C–H Bond Functionalization



One successful strategy to meet this challenge that our group as well as others have developed, is a C–H activation/oxidative functionalization sequence.⁷⁻⁹ In such an approach, a metal catalyst is employed to *activate* a specific C–H bond by transforming it into a C–[M] bond. The resulting intermediate is much more reactive than a C–H bond, and can undergo functionalizations in the presence of electrophilic oxidants (Scheme 1.2).

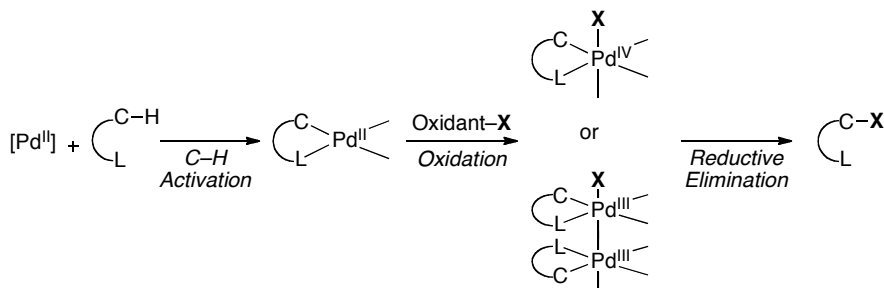
Scheme 1.2 Pathway for Metal-Catalyzed C–H Activation



The metal catalyst of choice for many of these transformations has been a Pd^{II} complex for three key reasons: (i) Pd^{II} salts are less susceptible to oxidation prior to generating the C–Pd^{II} complex, (ii) C–Pd^{II} bonds can be converted to a variety of C–FG bonds using commercially available oxidants, and (iii) the newly formed C–FG moieties are generally unreactive towards Pd^{II} catalysts.

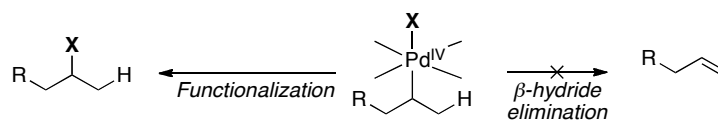
Over the past several years our group has demonstrated that substrates bearing a ligand can direct Pd^{II} catalysts to a proximal C–H bond for activation/functionalization.^{6, 10, 11} Using this method, our group has been able to demonstrate the regio- and chemoselective conversion of C–H bonds into diverse C–X bonds (X = OAc, Cl, Br, I, F, C, CF₃).⁶ The overall sequence is represented below in Scheme 1.3 and has been used with a variety of directing groups including pyridines, pyrimidines, amides, and oxime ethers for both aryl sp² C–H bonds and alkyl sp³ C–H bonds. Importantly, the key C–X bond forming step in these reactions is proposed to involve reductive elimination from a monomeric Pd^{IV} or dimeric Pd^{III}–Pd^{III} species.¹²⁻¹⁶ Accessing this high-oxidation state species is key to obtaining these new C–X bond constructions under mild conditions.

Scheme 1.3 Proposed Mechanism for Pd-Catalyzed Oxidative Functionalization



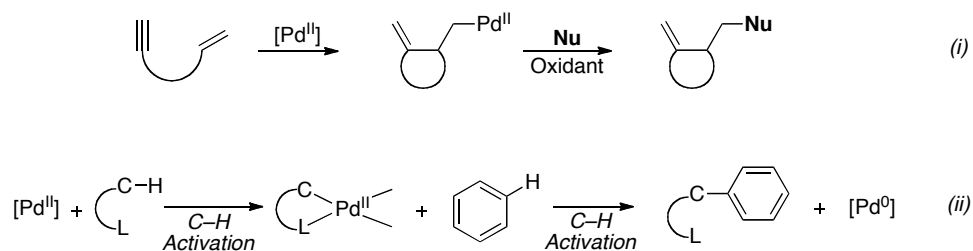
Another key advantage of employing methods using a Pd^{IV} intermediate is the ability to circumvent side reactions common with analogous Pd^{II} intermediates.¹⁷ Alkyl Pd^{IV} species, for example, are uniquely resistant to β-hydride elimination because the Pd center is coordinatively saturated (Scheme 1.4). This property makes Pd^{IV} intermediates very attractive for accessing new modes of functionalization in alkyl sp³ systems.

Scheme 1.4 Pd^{IV} Intermediates Resistant to β-Hydride Elimination



We set out to use the principal steps of ligand-directed C–H activation/oxidative functionalization for two new modes of reactivity. In the first, we sought to expand the scope of oxidative functionalization to Pd^{II} intermediates accessed via methods other than C–H activation (Scheme 1.5, *i*). In the second, we aimed to divert intermediates of ligand-directed C–H activation toward a new pathway involving cross coupling with simple arenes (Scheme 1.5, *ii*).

Scheme 1.5 Two New Modes of Reactivity with Pd Catalysis

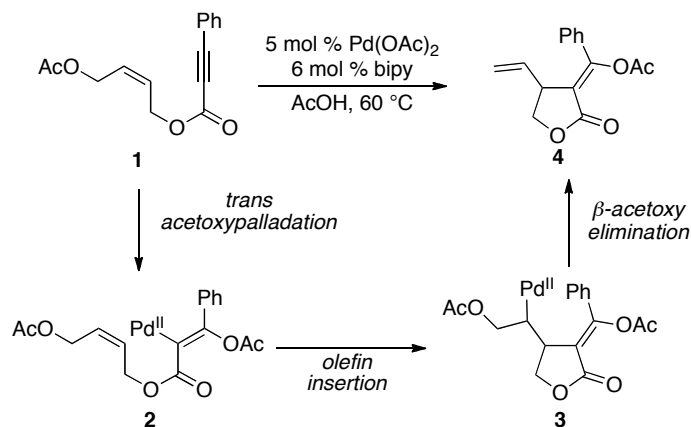


Our approach to the first new mode of reactivity was to expand the scope of oxidative functionalization beyond substrates bearing a directing group by taking advantage of another strategy to generate C–Pd^{II} bonds. Among the many approaches to generate alkyl–Pd^{II} intermediates is the Pd-catalyzed cyclization of enynes. These cyclizations have proven to be one of the most significant methods of generating functionalized cyclic products. The importance of these methods stems from the rapid increase in structural complexity they afford starting from relatively simple acyclic fragments.¹⁸⁻²¹

One important example comes from Lu and coworkers, who have shown that enynes of the type **1** could be readily cyclized in the presence of a Pd(OAc)₂ catalyst and 2,2'-bipyridine ligand (bipy) to yield highly functionalized lactones (Scheme 1.6).²² The proposed mechanism involves *trans*-acetoxypalladation to give the vinyl Pd^{II}

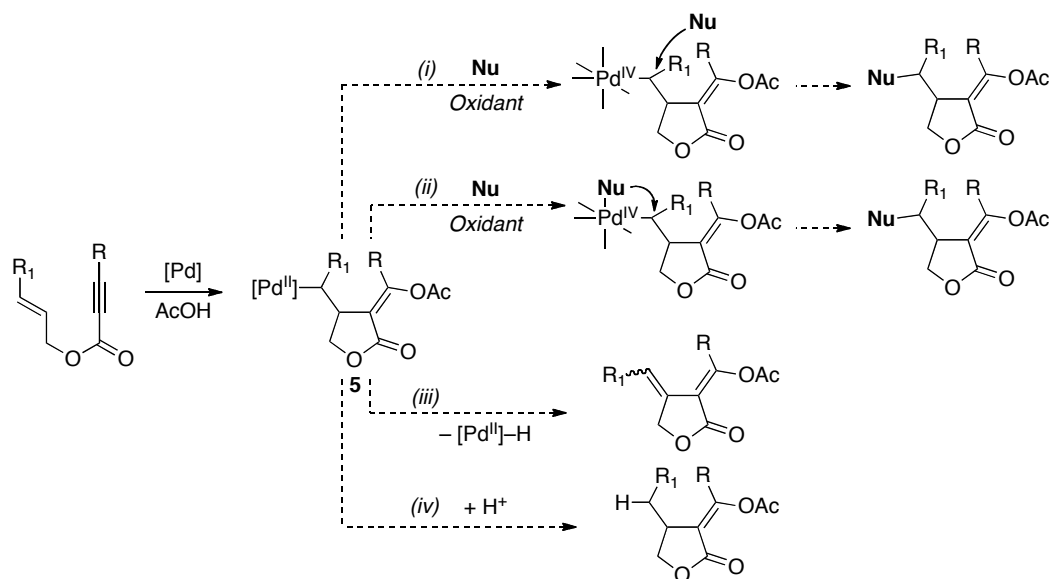
intermediate **2**, olefin insertion to give **3**, and finally, β -acetoxy elimination to yield the olefin product **4** and regenerate the Pd^{II} catalyst.²²⁻²⁴

Scheme 1.6 Lu's Pd-Catalyzed Functionalization of Enynes



We envisioned generating Pd^{II} σ -alkyl intermediates similar to **3** and functionalizing them using the oxidative functionalization strategy employed in the ligand directed C–H activation system described above (Scheme 1.7). In traditional Pd^{II} catalysis, such intermediates would be expected to undergo β -hydride elimination (Scheme 1.7, *iii*) or C–Pd bond protonation (*iv*). However, we reasoned that if **5** were intercepted with a strong oxidant, a Pd^{IV} intermediate would result, allowing access to a variety of highly functionalized products through either direct reductive elimination (*i*) or S_N2-type attack of the C–Pd^{IV} intermediate (*ii*).

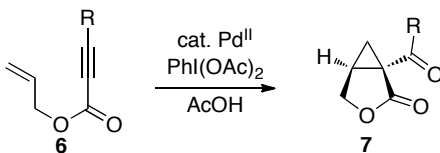
Scheme 1.7 Mechanistic Pathways for Pd-Catalyzed Enyne Cyclization



The overall strategy would form a C–O bond, C–Nu bond and one C–C bond, including two new stereocenters. Additionally, this method would provide the flexibility to introduce varying functionality from the nucleophile or oxidant, making this an attractive route to the preparation of highly functionalized heterocycles from acyclic starting materials.

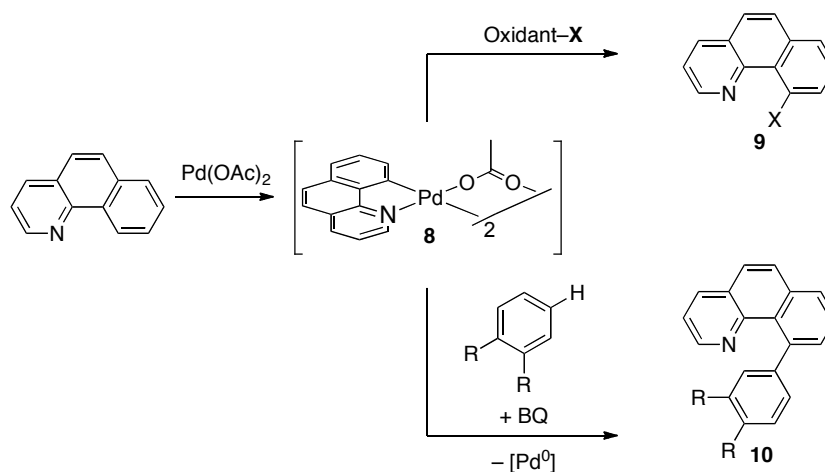
Chapter 2 details our investigations into this approach for enyne oxidative functionalization. Our initial efforts at this approach were quickly diverted when my former colleague Dr. Leilani Welbes observed the surprising formation of the bicyclo[3.1.0]hexane product **7** when enynes of the type **6** were exposed to our initial reaction conditions (Scheme 1.8). As such we pursued a detailed exploration of the scope of this reaction as well as mechanistic investigations into the cyclopropane ring-forming step.^{25, 26}

Scheme 1.8 Observed Bicyclo[3.1.0]hexane Product



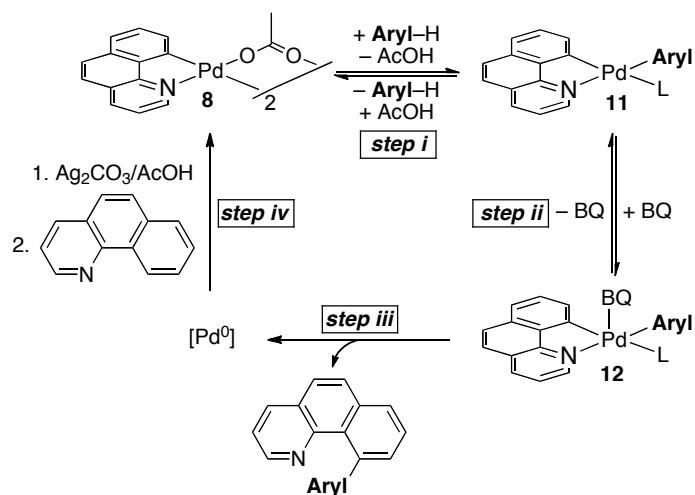
The second new mode of reactivity discussed in this thesis involves expanding the reactivity of cyclopalladated intermediates such as **8** beyond oxidative functionalization. As discussed above, ligand-directed oxidative functionalization enables the incorporation of a wide variety of functional groups through the use of electrophilic oxidants to give products such as **9**. In a related transformation, our group has shown these cyclopalladated intermediates can undergo a second C–H activation with simple arenes in the presence of a benzoquinone (BQ) promoter to afford oxidative cross-coupling products (Scheme 1.9).²⁷

Scheme 1.9 Pd-Catalyzed Oxidative Coupling Pathway



These reactions proceed through a ligand-directed C–H activation giving **8**, followed by a second non-directed C–H activation to afford the diaryl intermediate **11**, and finally benzoquinone (BQ) promoted reductive elimination from **12** to give the aryl–aryl coupled product (Scheme 1.10).²⁸

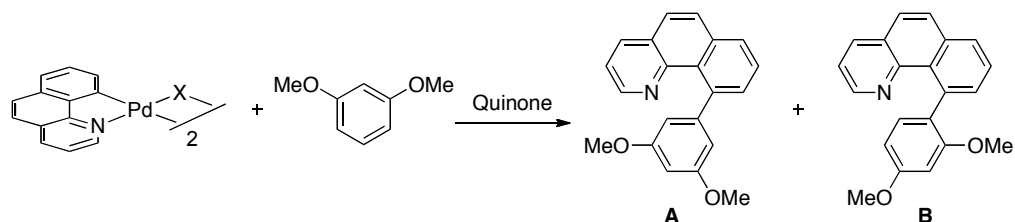
Scheme 1.10 Mechanism of Pd-Catalyzed Oxidative Cross Coupling



This exciting methodology illuminated a new selective approach to the cross coupling of arenes without the need for the prefunctionalized starting materials typically required to obtain selectivity and reactivity. The selectivity in this system was subject to the factors controlling each of the C–H activation steps in the reaction. The site selectivity of first C–H activation was governed by the ligand (quinoline in Scheme 1.10 above) directing the Pd catalyst to the proximal C–H bond, while the second C–H activation proceeded under steric control (with the least sterically hindered isomer as the predominant product).

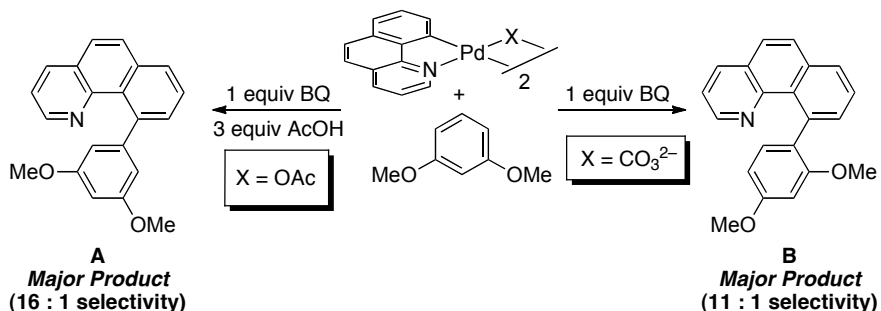
The factors controlling selectivity in ligand directed C–H activation have previously been fully investigated.^{29, 30} In contrast, the factors controlling the second undirected C–H activation in our system had not been explored. To that end, we chose to study in detail the factors controlling site selectivity in Pd-catalyzed oxidative coupling reactions with benzo[*h*]quinoline and simple arenes. In Chapter 3 we evaluate the effect of systematic changes to the ancillary ligands on selectivity using dimethoxybenzene (DMB) as the model arene substrate (Scheme 1.11).

Scheme 1.11 Model System for Site Selectivity Investigations



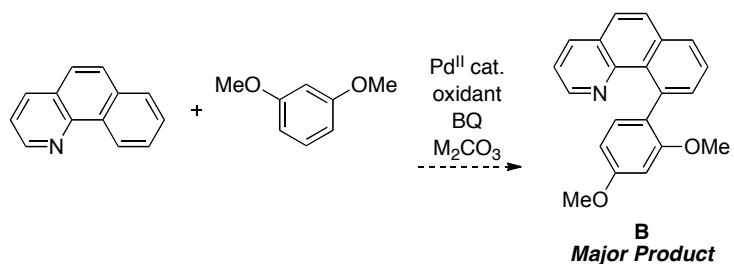
As part of these investigations we found that changing ligand X from OAc^- to CO_3^{2-} was effective in reversing the site selectivity of our model system (Scheme 1.12 below). This result was unprecedented in the literature and demonstrates a new level of control over site selectivity through the use of appropriate ligands. We further pursued the origin of this reversal in selectivity via a number of mechanistic investigations discussed in the later half of Chapter 3.³¹

Scheme 1.12 Ligand-Controlled Site Selectivity in Oxidative Coupling

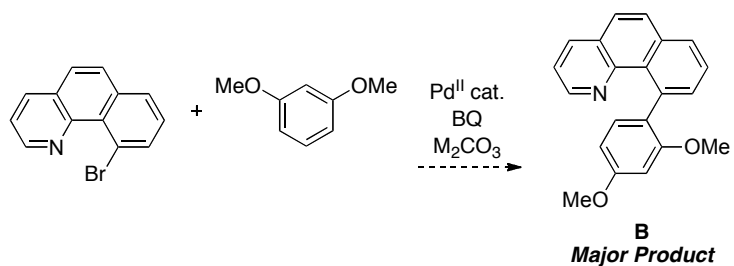


Following this discovery, we pursued extensive screening to develop a catalytic variant of the results found with carbonate salts (Scheme 1.13). These studies are described in Chapter 4. Additionally, we applied these newfound ligand effects to a direct arylation reaction using bromobenzo[*h*]quinoline as the starting aryl halide (Scheme 1.14). As with oxidative coupling, the factors controlling site selectivity in direct arylation with simple arenes have not been studied and remain a crucial challenge in the field.

Scheme 1.13 Potential Catalytic Reaction to afford Isomer **B**



Scheme 1.14 Potential Pd-Catalyzed Direct Arylation Reaction for Isomer **B**



In conclusion, a long-term goal of research in the Sanford laboratory is to develop and understand new modes of reactivity with transition metal catalysts. This thesis describes my efforts at the discovery, optimization, and mechanistic study of two new and fundamentally different Pd-mediated reactions for the construction of bicyclic cyclopropanes as well as biaryl products.

1.1 References

1. Kalyani, D.;Sanford, M. S., Chelate-Directed Oxidative Functionalization of Farbon-Hydrogen Bonds: Synthetic Applications and Mechanistic Insights. In *Topics in Organometallic Chemistry*, Chatani, N., Ed. Springer: New York, 2007; Vol. 24, pp 85-121.
3. Labinger, J. A.;Bercaw, J. E. *Nature* **2002**, *417*, 507-514.
4. Shilov, A. E.;Shul'pin, G. B. *Chem. Rev.* **1997**, *97*, 2879-2932.
5. Godula, K.;Sames, D. *Science* **2006**, *312*, 67-72.
6. Lyons, T. W.;Sanford, M. S. *Chem. Rev.* **2010**, *110*, 1147-1169.
7. Dick, A. R.; Hull, K. L.;Sanford, M. S. *J. Am. Chem. Soc.* **2004**, *126*, 2300-2301.
8. Maleczka, R. E.; Shi, F.; Holmes, D.;Smith, M. R. *J. Am. Chem. Soc.* **2003**, *125*, 7792-7793.
9. Ishiyama, T.; Takagi, J.; Ishida, K.; Miyaura, N.; Anastasi, N. R.;Hartwig, J. F. *J. Am. Chem. Soc.* **2001**, *124*, 390-391.
10. Ritleng, V.; Sirlin, C.;Pfeffer, M. *Chem. Rev.* **2002**, *102*, 1731-1770.
11. Kakiuchi, F.;Murai, S. *Acc. Chem. Res.* **2002**, *35*, 826-834.
12. Dick, A. R.; Kampf, J. W.;Sanford, M. S. *J. Am. Chem. Soc.* **2005**, *127*, 12790-12791.
13. Racowski, J. M.; Dick, A. R.;Sanford, M. S. *J. Am. Chem. Soc.* **2009**, *131*, 10974-10983.
14. Deprez, N. R.;Sanford, M. S. *J. Am. Chem. Soc.* **2009**, *131*, 11234-11241.
15. Powers, D. C.; Geibel, M. A.; Klein, J.;Ritter, T. *Nat. Chem.* **2009**, *1*, 302-309.
16. Powers, D. C.; Geibel, M. A. L.; Klein, J. E. M. N.;Ritter, T. *J. Am. Chem. Soc.* **2009**, *131*, 17050-17051.
17. Beller, M.; Zapf, A.;Riermeier, T. H., In *Transition Metals for Organic Synthesis*, Beller, M.; Bolm, C., Eds. Wiley: Weinheim, Germany, 2004; pp 271-305.
18. Ojima, I.; Tzamarioudaki, M.; Li, Z.;Donovan, R. J. *Chem. Rev.* **1996**, *96*, 635-662.
19. Michelet, V. C., L.; Gladiali, S, Genet, J. P. *Pure Appl. Chem.* **2006**, *78*, 397-407.

20. Trost, Barry M.; Hashmi, A. Stephen K.; Ball, Richard G. *Adv. Synth. Catal.* **2001**, *343*, 490-494.
21. Aubert, C.; Buisine, O.; Malacria, M. *Chem. Rev.* **2002**, *102*, 813-834.
22. Zhang, Q. H.; Lu, X. Y. *J. Am. Chem. Soc.* **2000**, *122*, 7604-7605.
23. Zhang, Q.; Lu, X. *J. Am. Chem. Soc.* **2000**, *122*, 7604-7605.
24. Xu, W.; Kong, A.; Lu, X. *J. Org. Chem.* **2006**, *71*, 3854-3858.
25. Welbes, L. L.; Lyons, T. W.; Cychosz, K. A.; Sanford, M. S. *J. Am. Chem. Soc.* **2007**, *129*, 5836-5837.
26. Lyons, T. W.; Sanford, M. S. *Tetrahedron* **2009**, *65*, 3211-3221.
27. Hull, K. L.; Sanford, M. S. *J. Am. Chem. Soc.* **2007**, *129*, 11904-11905.
28. Hull, K. L.; Sanford, M. S. *J. Am. Chem. Soc.* **2009**, *131*, 9651-9653.
29. Desai, L. V.; Stowers, K. J.; Sanford, M. S. *J. Am. Chem. Soc.* **2008**, *130*, 13285-13293.
30. Stowers, K. J.; Sanford, M. S. *Org. Lett.* **2009**, *11*, 4584-4587.
31. Lyons, T. W.; Hull, K. L.; Sanford, M. S. *J. Am. Chem. Soc.* **2010**, *In Press*.

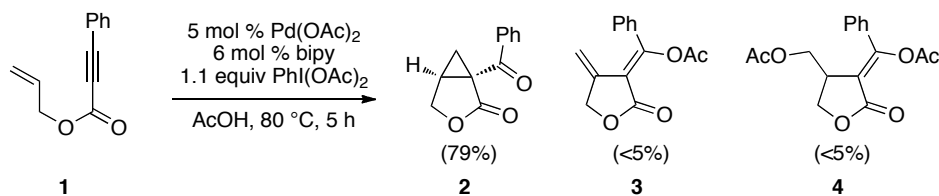
Chapter 2

Pd-Catalyzed Cyclopropanation Reactions

2.1 Background and Significance

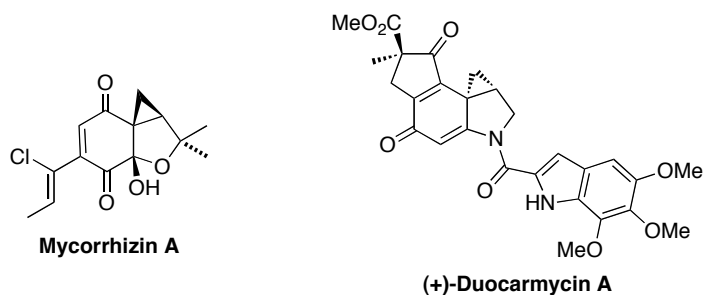
Our first efforts to develop a new functionalization of enynes were carried out by my former colleague Dr. Leilani Welbes and involved exposing enyne **1** to $\text{PhI}(\text{OAc})_2$ under conditions analogous to Lu's.¹ We anticipated such conditions would afford acetoxyated product **4**, because previous work by our lab had shown that $\text{PhI}(\text{OAc})_2$ could oxidize related aryl- and alkyl-Pd intermediates to generate acetoxyated organic compounds. However, we were surprised to discover the major product of this reaction was not the anticipated reductive elimination product **4**, or the β -hydride elimination product **3**, but instead was the bicyclo[3.1.0] ketolactone **2** (Scheme 2.1).

Scheme 2.1 Initial Enyne Functionalization Reaction



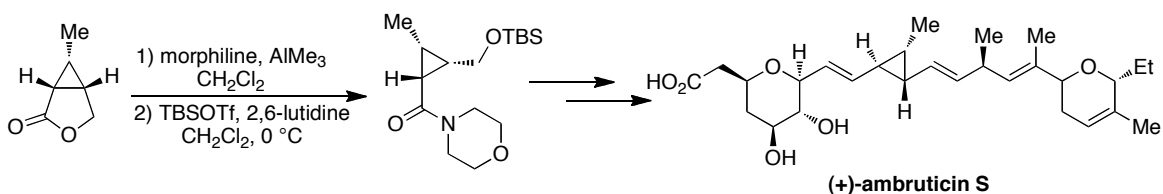
In light of these findings we decided to further investigate the construction of these bicyclo[3.1.0]hexanes starting with relatively simple acyclic enyne starting materials. Bicyclo[3.1.0] and [4.1.0] ring systems are important components of biologically active molecules and also serve as key intermediates in the construction of many functionalized organic products. For example, the natural products mycorrhizin A and duocarmycin A both contain a bicyclo[3.1.0]hexane as a key component of their structures (Scheme 2.2). Importantly, these natural products are known to possess potent antibiotic and antitumor properties.²⁻⁶

Scheme 2.2 Biologically Active Cyclopropane-Containing Natural Products



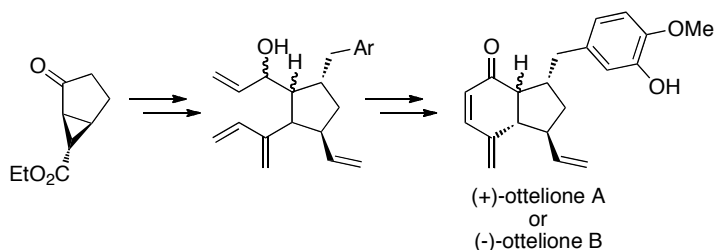
The bicyclo[3.1.0] ring system has been used in recent years as an advanced intermediate in the total synthesis of ambruticin S by Martin and coworkers (Scheme 2.3).⁷ Nucleophilic ring opening of the bicyclo[3.1.0]lactone with morpholine allowed for the stereoselective construction of the natural product. This intermediate also served as the source for the highly functionalized cyclopropane unit maintained through the remaining steps of the synthesis to the final product.

Scheme 2.3 Martin's Route to (+)-Ambruticin S



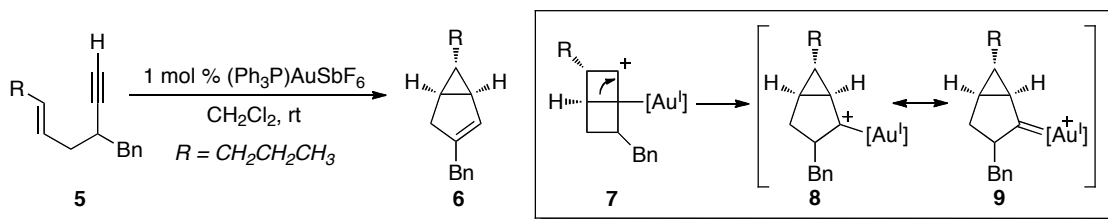
Another example of the utility of bicyclo[3.1.0] and [4.1.0]hexanes is their use as substrates in stereoselective nucleophilic ring opening to generate alkoxy- and alkyl-substituted lactones and furans.⁸⁻¹¹ For example, Clive and coworkers synthesized the antitumor agents (+)-ottelione A and (-)-ottelione B from an optically pure bicyclo[3.1.0] intermediate (Scheme 2.4).¹⁰ One key feature of their synthetic route is that the cyclopropyl group controls the stereochemistry in the attachment of the C-aryl and C-vinyl bonds in the final product.

Scheme 2.4 Clive's Route to Ottelione A and B



An attractive synthetic route to bicyclo[3.1.0] and [4.1.0] ring systems involves transition metal-catalyzed transformations of readily accessible enyne starting materials. As summarized in Schemes 2.5 and 2.6, two mechanistically distinct pathways have been reported for the metal-catalyzed construction of bicyclo[3.1.0]hexanes from enynes. In the first, electrophilic Pt and Au catalysts promote the rearrangement of 1,5- or 1,6-enynes (**5**) to afford bicyclo[3.1.0] and [4.1.0] ring systems, respectively (Scheme 2.5).¹²⁻¹⁸ These transformations are believed to proceed via nucleophilic attack of the alkene on the metal-coordinated alkyne to produce a bicyclic carbocation such as **7**. This intermediate rearranges to form a metalcarbene **8**, which can then undergo a 1,2-hydride shift/elimination sequence to afford cyclopropane **6**. These transformations typically proceed with high levels of stereoselectivity, affording products where the geometry of the cyclopropane substituents (*cis* vs *trans*) is the same as that in the alkene starting material.

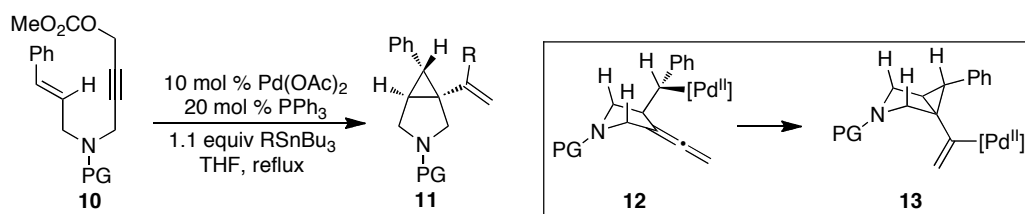
Scheme 2.5 Representative Example of Au^I-Catalyzed Cyclization of Enynes



The cyclization of enynes can also be catalyzed by Pd^{II} and proceeds through a different mechanism than that shown in Scheme 2.5. For example, Grigg and coworkers demonstrated the formation of bicyclo[3.1.0]hexanes from enynes using 10 mol % of Pd(OAc)₂ as a catalyst, 20 mol % of PPh₃, and 1.1 equiv of RSnBu₃.¹⁹ As shown in

Scheme 2.6, the key cyclopropane-forming step of these transformations proceeds via intramolecular *syn* olefin insertion, which transforms the σ -alkyl Pd^{II} intermediate **12** into cyclopropane **13**. Complex **13** is then captured with RSnBu₃ to generate product **11**. Importantly, these reactions proceed with high levels of stereoselectivity, affording retention of the olefin geometry (*cis* vs *trans*) in the cyclopropane product.²⁰⁻²⁴

Scheme 2.6 Representative Example of Pd^{II/0}-Catalyzed Cyclization of Enynes



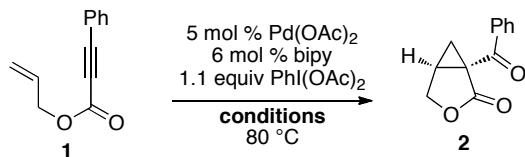
Our initial findings in this area suggested that our reaction was proceeding through a new mechanistic manifold involving a Pd^{II/IV} catalytic cycle (*vide infra*). This chapter describes the development of Pd-catalyzed reactions of enyne substrates with strong oxidants like PhI(OAc)₂ to afford cyclopropane products. The optimization, substrate scope, and limitations of these transformations are described in detail.²⁵ Additionally, several experiments designed to elucidate the mechanism of the cyclopropane-forming step are discussed, implicating an S_N2-type attack of the C_α-Pd bond.²⁶

2.2 Methodology Development and Scope

Reaction Development. We were surprised to see our initial reaction conditions provided clean conversion to the cyclopropane product, and we next sought to investigate the effect of the reaction conditions on the yield of this product. We first examined the influence of ambient water and air on the reaction (Table 2.1). A comparison of reactions run using rigorously dried AcOH (entry 3) versus those with commercial solvent taken directly from the bottle showed that the yield is slightly higher in the latter case (entry 1). Similarly, the presence or absence of air had a negligible effect (entry 2). These results demonstrate that rigorous purification of reaction solvent and exclusion of air are

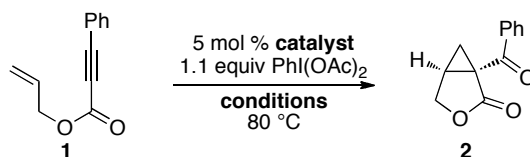
unnecessary, which enhances the ease of reaction set up and practicality of these transformations.

Table 2.1 Optimization of Enyne Cyclopropanation



Entry	Conditions	Yield
1	Ambient	88%
2	N ₂	71%
3	Dry AcOH	83%

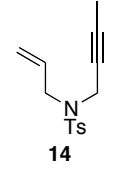
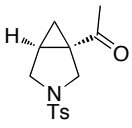
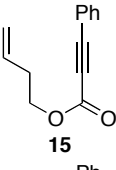
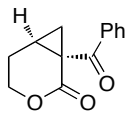
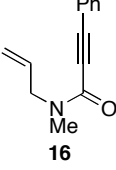
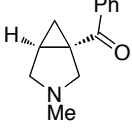
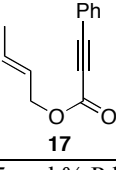
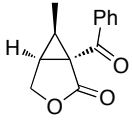
We next examined the role of bipyridine ligand, since it was initially hypothesized to be critical for achieving the desired reaction. As shown in Table 2.2, entry 1, the use of 5 mol % of the pre-formed catalyst (bipy)Pd(OAc)₂ afforded similar yield to the *in situ* combination of 5 mol % of Pd(OAc)₂ and 6 mol % of bipy. Further studies revealed that bipy is not essential for this transformation, and 93% yield was obtained with just Pd(OAc)₂ as the catalyst (entry 2). In addition, other Pd^{II} complexes also served as effective catalysts for this transformation in the absence of bipy, although the yields were lower than that with Pd(OAc)₂ (entries 3-8). Based on these studies, 5 mol % of Pd(OAc)₂ was identified as the optimal catalyst for cyclization of **1**, and these reaction conditions provided the cyclopropane product in 88% isolated yield.

Table 2.2 Pd-Catalyst Screening for Cyclopropanation

Entry	Catalyst	Conditions	Yield
1	(bipy)Pd(OAc) ₂	Ambient	80%
2	Pd(OAc) ₂	Ambient	93%
3	Pd(TFA) ₂	Ambient	81%
4	PdCl ₂	Ambient	72%
5	PdCl ₂ (CH ₃ CN) ₂	Ambient	65%
6	PdCl ₂ (PPh ₃) ₂	Ambient	62%
7	PdCl ₂ (PhCN) ₂	Ambient	60%
8	Na ₂ PdCl ₄	Ambient	51%

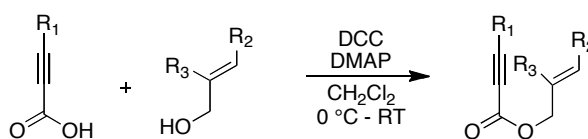
In contrast to the results with substrate **1**, the presence/absence of bipy did have a substantial effect on the Pd-catalyzed cyclization of other enynes. As shown in Table 2.3, entry 3, a significant enhancement in yield was observed when 6 mol % bipy was used in this system with **16** (9% versus 54% yield). However, with substrates, **14**, **15**, and **17** (Table 2.3, entries 1, 2, and 4), the addition of bipy with Pd(OAc)₂ led to a decrease in yield relative to Pd(OAc)₂ alone. The origin of these ligand effects is unclear, however it appears to be very substrate dependent. Since the Pd catalyst is involved in several steps of the catalytic cycle (*vide infra*), the influence of the ligand on each of these steps may change as a function of substrate.

Table 2.3 Cyclopropane Formation Dependence as a Function of Bipy

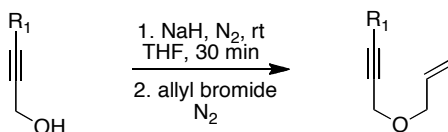
Entry	Substrate	Product ^a	Yield ^b with 6 mol% bipy	Yield ^b without bipy
1			61 %	71%
2			9%	59%
3			54%	9%
4			29%	59%

^aReaction conditions: 5 mol % Pd(OAc)₂, 0 or 6 mol % bipy, 1.1-4 equiv PhI(OAc)₂, 80 °C, 1-16 h. ^b Yields determined by GC relative to an internal standard.

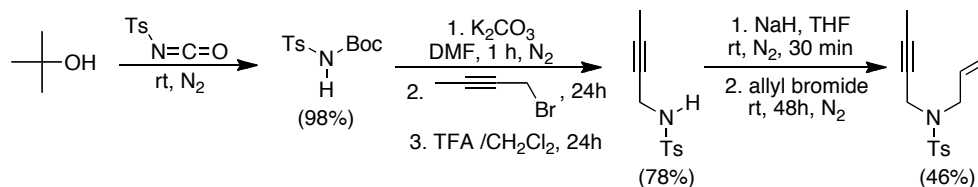
Substrate Scope. The scope of this reaction was next explored with a number of different enyne substrates. The substrates used in this reaction were generally synthesized in one of three ways. The lactone-bearing substrates were prepared by standard DCC coupling procedures in good yields (Scheme 2.7).²⁷ The ether-linked enynes were synthesized using an S_N2'-type reaction pathway involving deprotonation of the propargyl alcohol with NaH, followed by addition of the allyl bromide electrophile (Scheme 2.8).²⁸ Synthesis of the tosyl protected amine-containing enyne involved preparation of the Boc- and Ts-amine from *t*-butyl alcohol and N-tosyl-isocyanate (Scheme 2.9).²⁸ Cleavage of the Boc group and addition of propargyl bromide gave the corresponding propargyl amine. Finally, S_N2' addition of allyl bromide afforded the desired enyne.

Scheme 2.7 Synthesis of Lactone Containing Enynes

Scheme 2.8 Synthesis of Ether Containing Enynes



Scheme 2.9 Synthesis of N-Ts Enyne



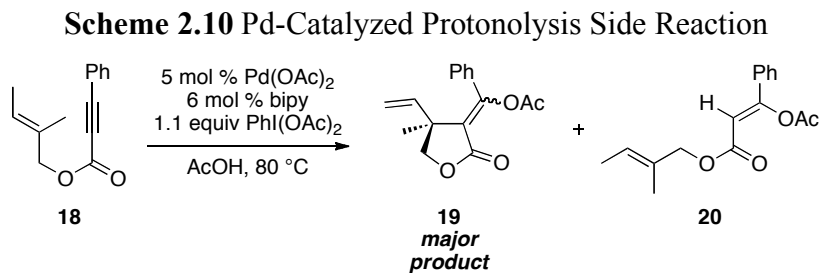
In general, we found that some optimization of the reaction for each substrate improved the yields substantially. As a result, each was optimized for: (i) the presence/absence of bipy, (ii) the amount of oxidant (ranging from 1.1 to 4 equiv), (iii) the reaction temperature (between 60 and 80 °C), and (iv) the reaction time (between 1 and 16 h). Upon optimization, moderate to good yields of 41–79% were obtained with all of the substrates in Table 2.4. These transformations produced bicyclo[3.1.0] and [4.1.0] ring systems containing lactones, tetrahydrofurans, pyrrolidines, and lactams. Both alkyl and aryl substituents were tolerated on the alkyne, and both electron donating (*p*-OMe) and electron withdrawing (*p*-CF₃) groups on the aryl ring were also compatible with the reaction conditions. Furthermore, both 1,1- and 1,2-disubstituted enynes were effective substrates. In the latter case, with an ester substituent on the alkene, the product was formed with > 20:1 dr.

Table 2.4 Substrate Scope of Pd-Catalyzed Enyne Cyclizations^a

Entry	Substrate	Product	Yield ^b
1			79%
2			55%
3			78%
4			66%
5			70%
6			55%
7			48%
8			41%
9			44%
10			71%
11			47%

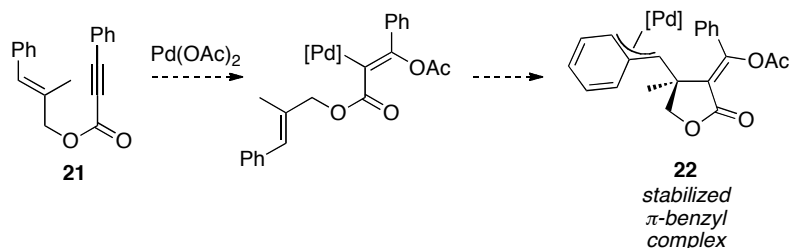
^a Reaction conditions: 5 mol % Pd(OAc)₂, 0–6 mol % bipy, 1.1–4 equiv PhI(OAc)₂, 60–80 °C, 1–16h. ^b Isolated yields (average of two runs).

One major limitation of these transformations is that trisubstituted enynes did not react to form cyclopropane products under the standard reaction conditions. Our first efforts to construct a cyclopropane with trisubstituted enynes involved using a 1,2-dimethyl substituted alkene moiety **18**. This substrate was synthesized from readily available starting materials via DCC coupling. Despite efforts to optimize this reaction, no cyclopropane product was observed. Instead the β -hydride elimination product **19** predominated along with isolable amounts of **20** (Scheme 2.10). Product **20** most likely arises from acetoxypalladation across the alkyne and subsequent protonolysis of the vinyl–Pd bond. Literature precedent suggests that this undesired side reaction takes place because olefin insertion to form the lactone ring is slow with highly substituted derivatives.^{29, 30} Presumably, the alkene product arises because β -hydride elimination is faster than the desired cyclopropanation.



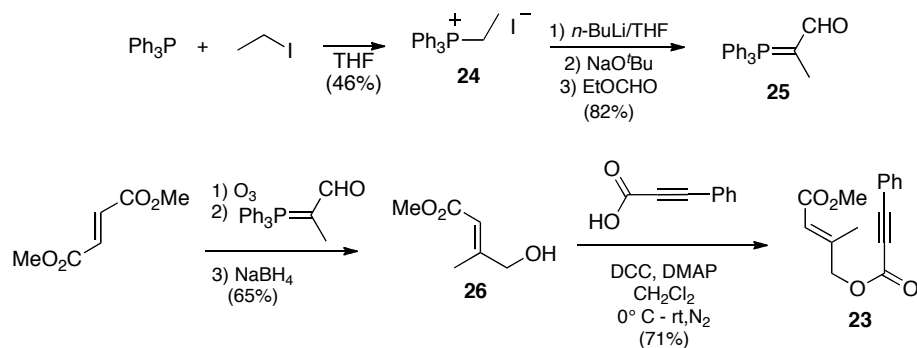
After struggling to find suitable conditions for the cyclization of enyne **18** to form cyclopropane products, we hypothesized that the stability of the vinyl insertion intermediate could be influenced by an appended phenyl or ester group on the alkene moiety. To that end, enyne **21** was synthesized according to literature methods from the alcohol. We anticipated a phenyl group would facilitate the formation of a stabilized π -benzyl complex **22**, allowing cyclopropanation to occur (Scheme 2.11). However, no cyclopropane product was observed and only starting material, the protonated product, and several unidentified side products were detected.

Scheme 2.11 Potential π -Benzyl Complex Formation



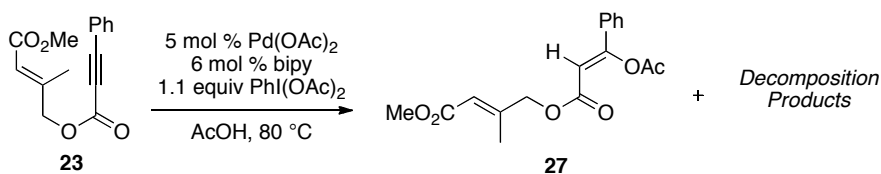
Alternatively, we hoped to obtain cyclopropanation with trisubstituted enynes by installing an electron-withdrawing group (ester) on the alkene. Electron-withdrawing groups have been shown to increase the rate of related Pd-catalyzed Heck-type olefin insertions.^{31, 32} As shown in Scheme 2.12 substrate **23** was synthesized by making the phosphorous ylide from PPh_3 and ethyl iodide. Deprotonation of ylide **24** with *n*-BuLi and reaction with ethylformate in the presence of a strong base gives the Wittig reagent **25**. Ozonolysis of dimethyl fumarate, followed by an *in situ* Wittig reaction with **25** and reduction with NaBH_4 gave the desired alcohol **26** in 65% yield. Finally, DCC coupling of the alcohol with phenylpropionic acid afforded the desired enyne.

Scheme 2.12 Synthesis of Enyne **23**



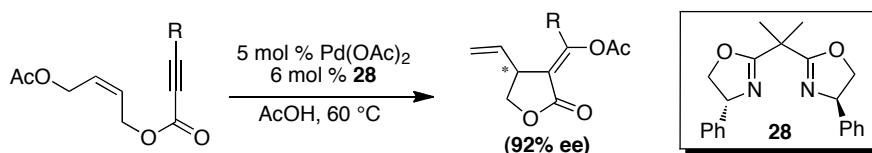
Unfortunately, this substrate also failed to afford the cyclopropane product under a variety of conditions. Instead only the protonation product and unidentified side products were generated. (Scheme 2.13) From these experiments it seems likely that the relative rate of olefin insertion/cyclopropanation is slow relative to protonolysis or undesired decomposition pathways with tri-substituted enynes.

Scheme 2.13 Undesired Product Formation From **23**



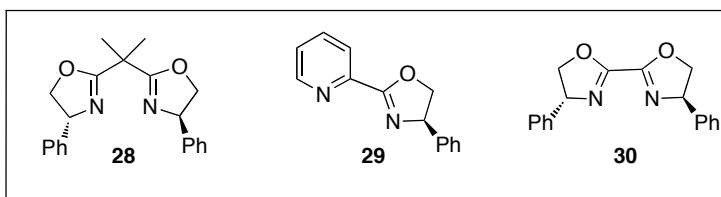
Asymmetric Studies. Previous work by Lu had shown that the Pd-catalyzed cyclization of similar enyne substrates could proceed with high levels of asymmetric induction upon the addition of a chiral ligand (Scheme 2.14). We hypothesized that a similar enantioselectivity-determining step could be at work in our Pd-catalyzed cyclopropanation reaction and sought to use similar ligands in our transformation.

Scheme 2.14 Lu's Asymmetric Enyne Cyclization

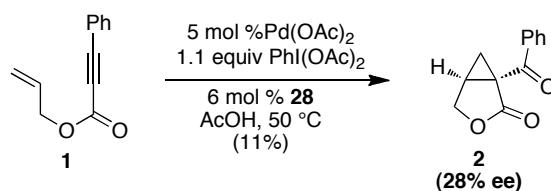


After screening several ligands for the reaction of **1** with 5 mol % Pd(OAc)₂, 1.1 equiv PhI(OAc)₂, and 6 mol % chiral ligand to form **2**, we found that only **28** was able to induce enantioselectivity to an appreciable degree. Lowering the temperature to 50 °C, in the presence of 5 mol % of Pd(OAc)₂, and 1.1 equiv of PhI(OAc)₂ gave the cyclopropane product in 28% *ee*. While this was an exciting first step, further optimization failed to improve the yield beyond 11% or resulted in lower asymmetric induction. In light of these complications and a greater interest in pursuing the mechanism of this reaction, we halted these investigations in pursuit of mechanistic studies.

Figure 2.1 Chiral Ligands Screened in Pd-Catalyzed Cyclopropanation



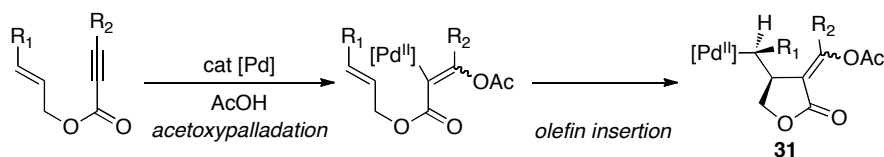
Scheme 2.15 Enantioselective Pd-Catalyzed Cyclopropanation



2.3 Mechanistic Investigations

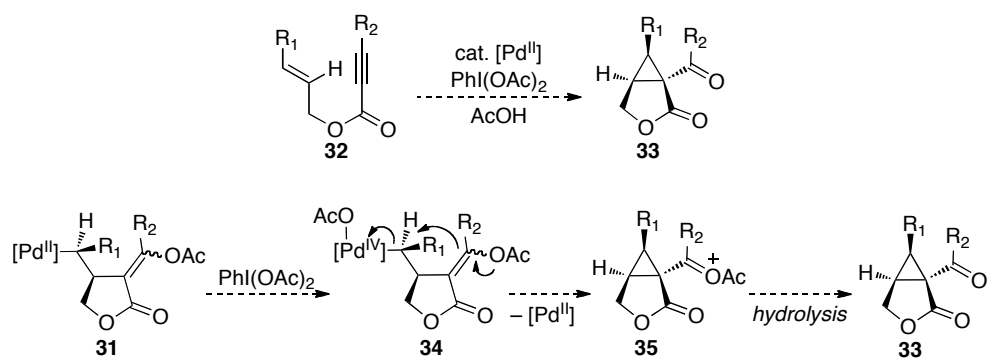
Mechanistic Studies and Reaction Mechanism. We envisioned two potential mechanisms for the Pd-catalyzed cyclization of enynes that would both involve a high oxidation state Pd^{IV} intermediate. Both proceed via the key intermediate **31**, which is accessed through the well-precedented sequence of alkyne acetoxypalladation followed by *syn* olefin insertion (Scheme 2.16).^{27, 28, 33-35}

Scheme 2.16 Mechanism for Access to Intermediate **31**



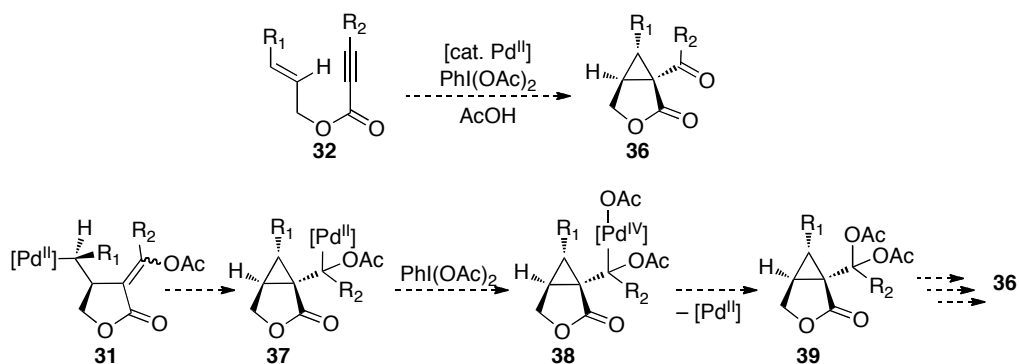
In our first proposed mechanism (Mechanism A) we hypothesized that **31** could be intercepted with the strong oxidant PhI(OAc)₂ to generate the Pd^{IV} complex **34** (Scheme 2.17). Such Pd^{IV} intermediates are highly susceptible to S_N2-type nucleophilic attack at the α-carbon,³⁶⁻³⁸ and we reasoned that the adjacent vinyl acetate moiety of **34** could serve as an effective nucleophile for cyclopropane formation. Notably, related S_N2-type cyclopropane-forming reactions with nucleophilic olefins are well preceded in the organic literature.^{39, 40}

Scheme 2.17 Pd^{II/IV}-Catalyzed Cyclopropanation via Mechanism A



An alternate Pd^{II/IV} mechanism (Mechanism B) involving Heck-type olefin insertion from **31** could also be possible (Scheme 2.18). Importantly, such reactivity has significant precedent in Pd^{II/0}-catalyzed cyclopropane forming reactions. Mechanism B would involve Heck-type olefin insertion to form **37**, followed by oxidation, then C–OAc bond-forming reductive elimination to give the di-acetoxyated intermediate **39**. Hydrolysis would then afford the final ketone product **36**.

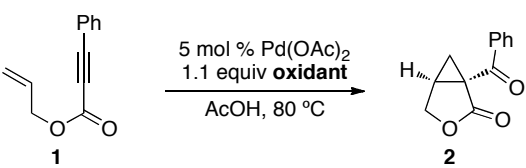
Scheme 2.18 Pd^{II/IV}-Catalyzed Cyclopropanation via Mechanism B



We first sought to gain evidence to support a Pd^{II/IV} mechanism for these transformations by focusing on the oxidant required. As such, our initial mechanistic investigations focused on replacing PhI(OAc)₂ with a variety of alternative stoichiometric oxidants in the Pd-catalyzed cyclization of **1**. As shown in Table 2.5, these studies revealed that the use of both Oxone[®] and K₂S₂O₈ as terminal oxidants resulted in significant quantities of cyclopropane product **2**. Importantly, both of these are strong oxidants that have been previously implicated in Pd^{II/IV} catalytic cycles.^{41, 42} In contrast,

neither Cu^{II}-based oxidants, nor benzoquinone nor air provided any of the desired product **2** (entries 4-7). With CuCl₂, Cu(OAc)₂, and benzoquinone, starting material **1** was completely consumed and a complex mixture of products was formed. With air as the oxidant, a significant quantity of **1** (40%) remained at the end of the reaction, along with a mixture of unidentified products. The requirement for strong two-electron oxidants in this transformation provided initial evidence to support the possibility of Pd^{IV} intermediates.

Table 2.5 Effect of Oxidant on Yield of Cyclopropane **2**

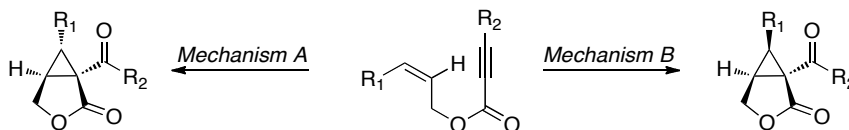


Entry	Oxidant	Yield of 2
1	PhI(OAc) ₂	94%
2	Oxone	50%
3	K ₂ S ₂ O ₈	27%
4	CuCl ₂	0%
5	Cu(OAc) ₂	0%
6	Benzoquinone	0%
7	Air	0%

Stereochemical Studies. The next set of experiments focused on the stereochemical outcome of this transformation. As discussed earlier, Pd-catalyzed cyclopropanation of enynes is generally known in the literature to proceed with retention of stereochemistry, relative to the starting olefin geometry. These literature examples proceed through Pd^{II/0} catalytic cycles, and we hypothesized that a Pd^{II/IV} process might result in a complementary stereochemical outcome. If a Pd^{IV} intermediate were involved in our transformation, we envisioned it could participate in one of two mechanisms: A or B (Schemes 2.17 and 2.18). These two mechanisms should be readily distinguishable through the use of enynes containing 1,2-disubstituted olefins. In Mechanism A, S_N2-type reductive elimination would result in net inversion of olefin geometry in the

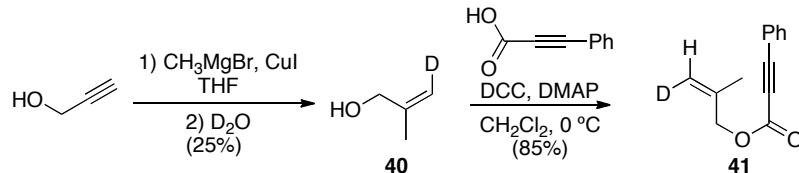
cyclopropane product. In contrast, *syn* olefin insertion in Mechanism B would lead to retention of the alkene geometry in the final cyclopropane (Scheme 2.19).

Scheme 2.19 Potential Mechanisms for Cyclopropane Formation



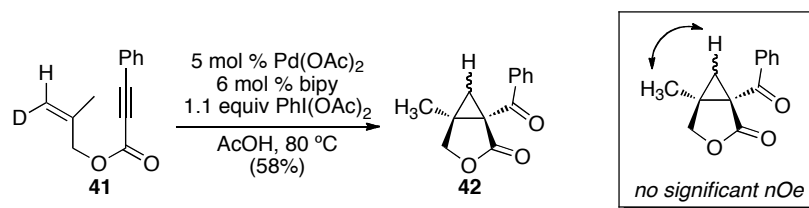
To explore which of these mechanisms was operative in this system we designed substrates with substitution at R₁. Our first efforts at distinguishing the stereochemistry involved synthesis of deuterium-labeled enyne **41** by the following sequence. Methyl cuprate was added to propargyl alcohol and quenched with D₂O, to afford alkene **40**. Subsequent DCC coupling with phenylpropionic acid gave the desired enyne (Scheme 2.20).

Scheme 2.20 Synthesis of Deuterium Labeled Enyne



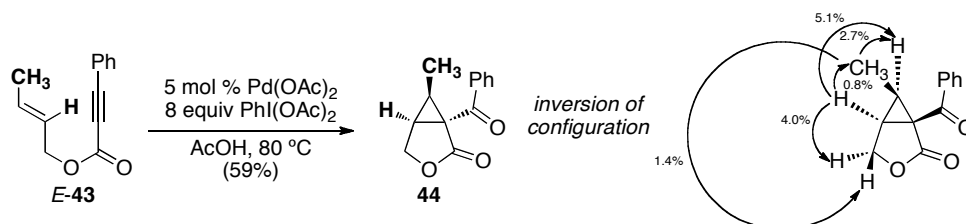
Subjection of enyne **41** to our optimized reaction conditions gave the desired cyclopropane product in 58% isolated yield (Scheme 2.21). Several attempts were made to characterize the stereochemistry of the cyclopropane product through NOE ¹H NMR experiments; however, no significant correlation was observed when the methyl protons were irradiated. This result suggests one of two conclusions: (i) the geometry of the cyclopropane does not allow for a through-space NOE interaction to be observed, or (ii) the reaction has proceeded with inversion of configuration putting the deuterium rather than the proton in proximity to the adjacent methyl.

Scheme 2.21 NOE Experiment with D-Labeled Cyclopropane

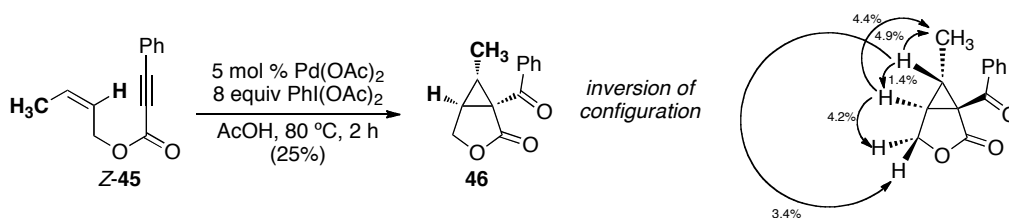


To overcome this uncertainty, we pursued substrates more amenable to ¹H NMR characterization. Two stereochemically pure enynes *E*-**43** and *Z*-**45** were synthesized by DCC coupling with the corresponding *cis*-crotyl alcohol, derived from H₂/Pd reduction of the corresponding propargyl alcohol and the commercially available *trans*-crotyl alcohol, respectively. After some optimization we found the *E*-**43** and *Z*-**45** enynes reacted with 5 mol % of Pd(OAc)₂ and 8 equiv of PhI(OAc)₂ in AcOH at 80 °C for 2 h to form the desired cyclopropane as the major product in 59% and 25% yield, respectively. Interestingly, each of the enynes reacted with clean inversion of olefin geometry. The stereochemistry was confirmed by several NOE ¹H NMR experiments highlighted below in Schemes 2.22 and 2.23. Additionally, an X-ray crystal structure of the hydroxyl oxime of **46** was obtained, confirming the inversion of stereochemistry (Figure 2.4, experimental section). These data gave us definitive evidence that an inversion of configuration was taking place and suggested Mechanism A was at work in our system.

Scheme 2.22 *E*-43 Enyne Cyclization

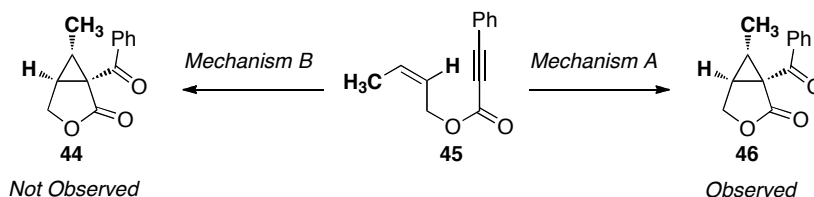


Scheme 2.23 *Z*-45 Enyne Cyclization



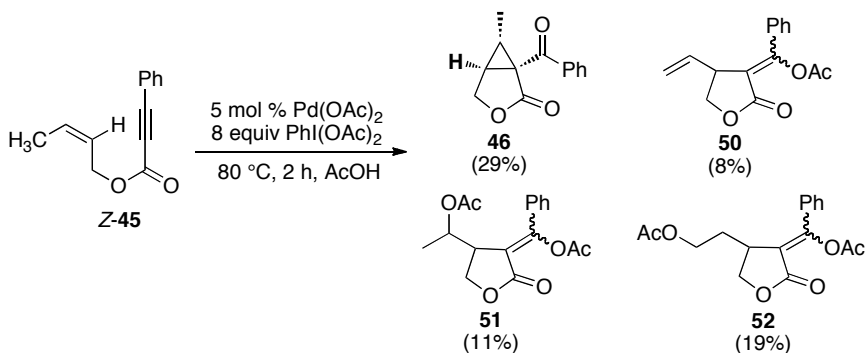
The stereochemical course of cyclopropane formation from substrate *E*-**43** as well as from isomeric *Z*-**45** provided key insights into the mechanism of these transformations. As outlined previously in Scheme 2.24 for substrate *Z*-**45**, cyclopropane ring formation via *syn* olefin insertion into the C–Pd bond (Mechanism B) would afford cyclopropane **44**, which is clearly not observed in the above experiment. In contrast, cyclopropane formation via nucleophilic substitution (Mechanism A) would afford the *cis*-cyclopropane **46** with net inversion of the alkene geometry, which is consistent with our experimental results.

Scheme 2.24 Potential Mechanism for Cyclopropane Formation with **43**



Over the course of these studies we observed and isolated a number of interesting side products that provided additional mechanistic insight. As shown in Scheme 2.25, we found that acetoxyated isomers **51** and **52** were formed along with alkene product **50** in addition to the desired cyclopropane.

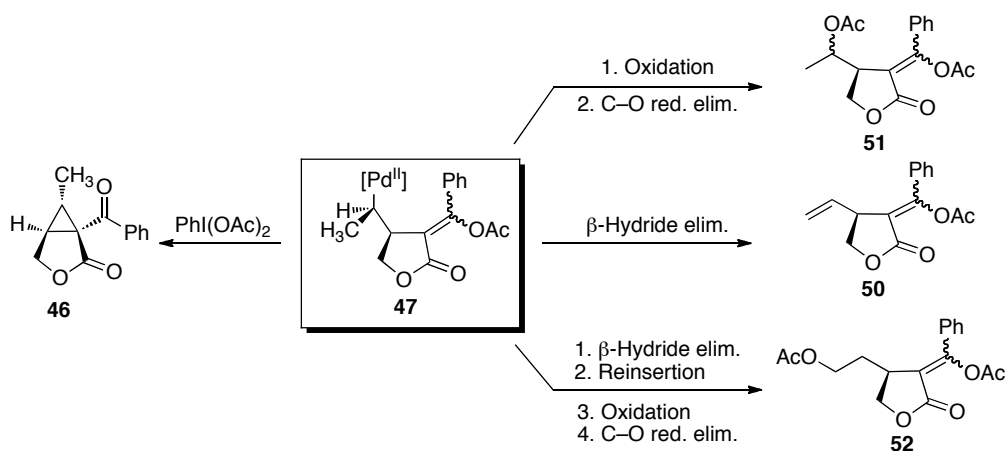
Scheme 2.25 Mixture of Products Formed in Cyclization of Enyne *Z*-**45**



We hypothesized **46** and **50-52** were derived from a common Pd-alkyl intermediate **47** (Scheme 2.26). β -Hydride elimination from this intermediate followed

by alkene dissociation would afford **50**. Oxidation of **47** with $\text{PhI}(\text{OAc})_2$ followed by C–O bond-forming reductive elimination from Pd^{IV} would provide acetoxyated product **51**. Finally, reinsertion of alkene **50** into the Pd–H would afford a linear isomer of **47**, which could then undergo oxidative functionalization with $\text{PhI}(\text{OAc})_2$ to afford **52**. Importantly, C–O bond-forming reductive elimination at unactivated sp^3 carbon centers is well-known at Pd^{IV} , but has not been reported at Pd^{II} .⁴³ As such, the formation of products **51** and **52** provides additional evidence to support a $\text{Pd}^{\text{II/IV}}$ catalytic cycle.

Scheme 2.26 Mechanistic Rationale for Side Product Formation



We noted that acetoxyated side product **51** was formed in >95% diastereoselectivity as determined by ^1H NMR spectroscopy. However, the relative stereochemistry of the two adjacent stereocenters in the molecule could not be determined conclusively using NOE studies or coupling constant analysis. Furthermore, efforts to obtain X-ray quality crystals of **51** were hampered by the fact that this compound is an oil at room temperature. In order to prepare a crystalline product, we replaced the phenyl substituent on the alkyne with a biphenyl group. We anticipated that this modification would alter the physical properties of the product without significantly perturbing the cyclization reaction. The biphenyl-substituted enyne **53** underwent Pd-catalyzed cyclization with $\text{PhI}(\text{OAc})_2$ to afford acetoxyated product **54** as a single detectable diastereomer in 7% isolated yield (Scheme 2.27). X-ray crystallographic analysis of **54** definitively established the stereochemical relationship shown in Figure 2.2.

Scheme 2.27 Pd-Catalyzed Cyclization of Biphenyl-Substituted Enyne

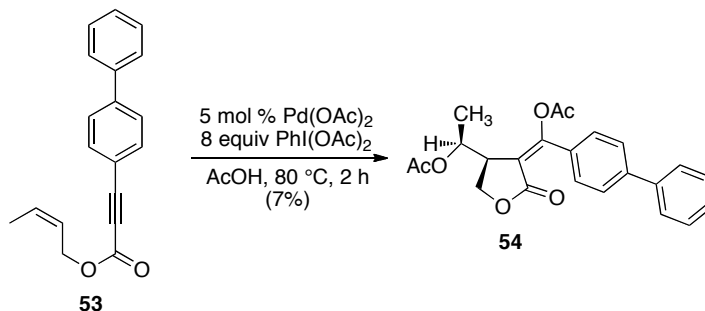
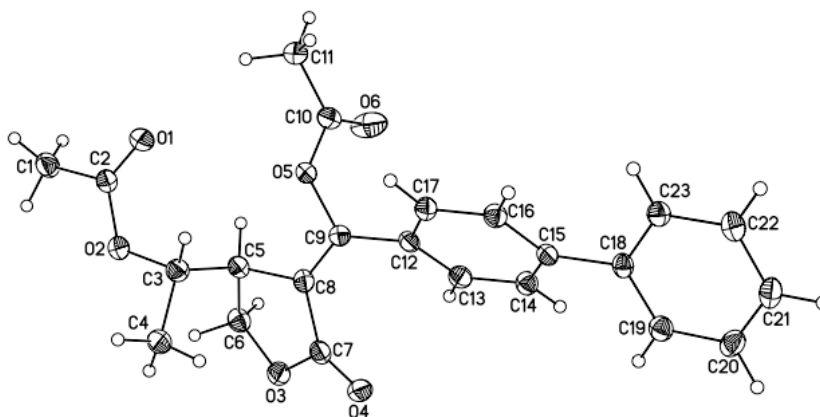
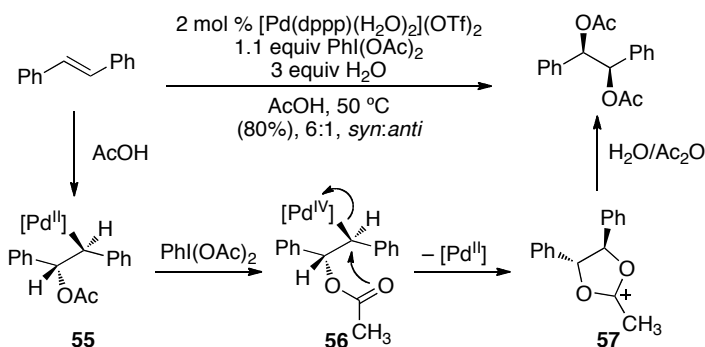


Figure 2.2 X-ray Crystal Structure of Product **54**



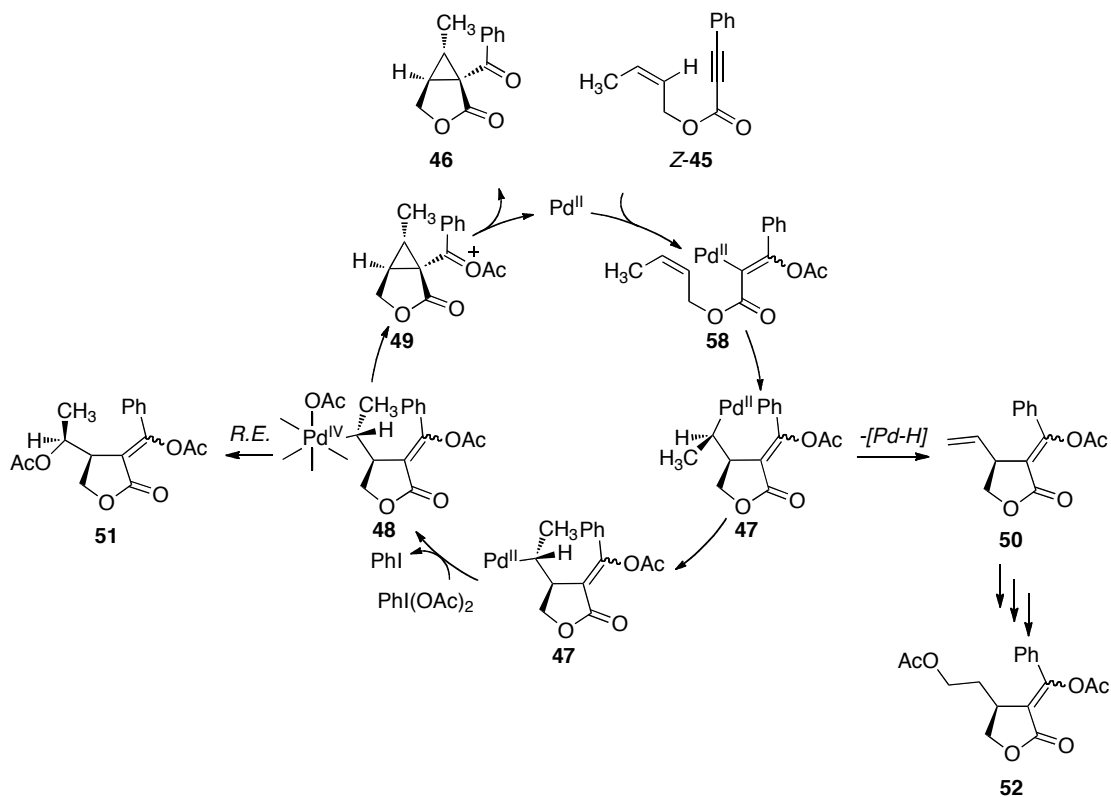
Assuming that the alkene insertion to form the lactone proceeds in a *syn* fashion, **54** is the product of C–OAc bond formation with inversion of configuration at carbon. This result provides strong evidence in support of an S_N2 mechanism for reductive elimination from the Pd^{IV} intermediate in this system. Notably, similar results have been obtained in other C–O bond-forming reactions from Pd^{IV}. The recent diacetoxylation of olefins by Dong and coworkers is one such example (Scheme 2.28).⁴⁴ This reaction proceeds by *trans* acetoxylation of the alkene to give **55**, followed by oxidation with PhI(OAc)₂ to Pd^{IV} intermediate **56**. Finally, intramolecular cyclization forms the acetoxonium intermediate **57** and hydrolysis affords the dihydroxylated product.

Scheme 2.28 Dong's Diacetoxylation Mechanism

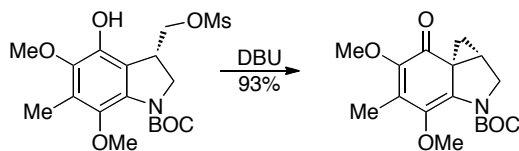


Based on the data described above, a complete catalytic cycle can be proposed for this transformation (Scheme 2.28). The reaction begins with acetoxypalladation of the alkyne followed by intramolecular olefin insertion to afford intermediate **47**. Next, bond rotation followed by oxidation of alkyl palladium complex **47** affords Pd^{IV} intermediate **48**. (The order of these two steps could also be reversed.) Intramolecular nucleophilic attack at C_α by the vinyl acetate then produces organic intermediate **49**. Finally, hydrolysis of highly reactive species X would provide the observed cyclopropane product. Importantly, the high oxidation state of the Pd intermediate renders it an excellent leaving group; as such, this reaction can be considered analogous to intramolecular organic cyclopropane-forming reactions such as that shown in Scheme 2.30.⁴⁰

Scheme 2.29 Proposed Pd^{II/IV} Catalytic Cycle for Cyclopropane Formation With Z-45

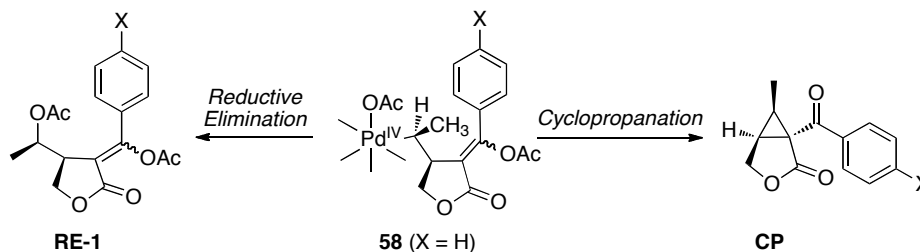


Scheme 2.30 Example of S_N2-Type Organic Cyclopropane-Forming Reaction



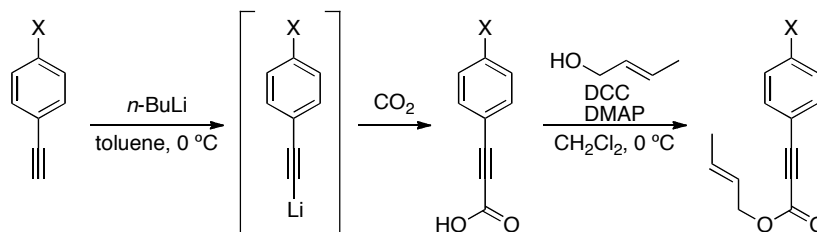
A key intermediate in the proposed reaction mechanism is a Pd^{IV} complex **58**. As discussed above, this complex is believed to undergo two competing reactions: (i) intramolecular nucleophilic attack by the vinyl acetate to afford cyclopropane (**CP**) or (ii) nucleophilic attack by OAc to afford acetoxylated product **RE-1** (Scheme 2.31). As such, we hypothesized that the ratio of cyclopropane to acetate products (18 : 1 in the case of substrate **43**) should be very sensitive to electronic perturbation of one of these two competing reactions. In particular, we reasoned that *p*-substitution on the aromatic group conjugated with the alkyne would significantly influence the electronic nature of the vinyl acetate moiety, and thereby affect the relative rate of cyclopropane formation.

Scheme 2.31 Proposed Competing Pathways



To probe this hypothesis we synthesized a series of electronically different *p*-substituted enynes (Scheme 2.32). These enynes were generally prepared from the substituted arylacetylene. The terminal alkyne was deprotonated with *n*-BuLi and quenched with CO₂ to give the carboxylic acid. Standard DCC coupling with crotyl alcohol then afforded the *E*-enynes in good yield.

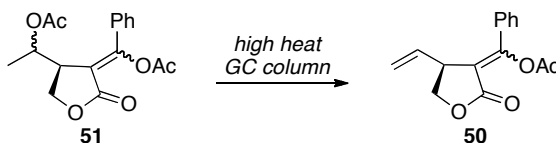
Scheme 2.32 Synthesis of *p*-Substituted Aryl Enynes



These enynes were submitted to our optimized reaction conditions (5 mol % of Pd(OAc)₂ and 8 equiv of PhI(OAc)₂ in AcOH at 80 °C) and assayed by analytical HPLC with yields calibrated against an internal standard. Detection complications prevented us from using more common techniques such as gas chromatography or ¹H NMR spectroscopy. For example, our initial screenings were assayed by gas chromatography against an internal standard. However, after failing to observe the expected **RE-1** product from these reactions, we discovered that the **RE-1** product was undergoing an elimination to the **β-H** product on the GC column (Scheme 2.33). Presumably this was a function of the high temperatures and/or residual metals left on the column itself. Several attempts were made to use ¹H NMR spectroscopy to measure the yields of these products

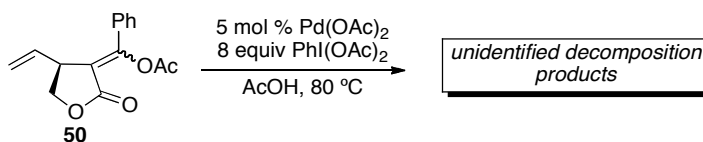
from the crude reaction mixture, but too many proton signals overlapped in a variety of solvents.

Scheme 2.33 GC Promoted Elimination of **RE-1**



However, HPLC analysis allowed us to survey each of the electronically differentiated enynes under our reaction conditions. Interestingly, the reaction time for each substrate varied substantially from 8 h (with X = NO₂) to 10 min (with X = OMe). However, it is important to note that both the cyclopropanes (**CP**) and the acetoxyated products (**RE-1**) were stable under the reaction conditions over the course of 8 h; therefore, all of the reactions were compared at 8 h for consistency. In contrast, significant decomposition of the alkene products (**β-H**) was observed under these conditions (Scheme 2.34). Many small peaks were observed in the GC and HPLC traces of these reactions after 8 h, suggesting the **β-H** decomposes to a mixture of unidentified minor products. We propose this decomposition accounts for the poor mass balance in many of these reactions.

Scheme 2.34 Decomposition of **β-H** Under Standard Reaction Conditions



Gratifyingly, we observed a clear trend in the ratio of **CP/RE-1** (Table 2.6). For example, with the electron deficient *p*-NO₂-substituted derivative, a 5 : 1 ratio of **CP/RE-1** was obtained. In striking contrast, the electron donating *p*-OMe substituent resulted in a >200:1 ratio of these two products. This is consistent with a faster relative rate of cyclopropanation for the more electron rich enynes, as was hypothesized above. Notably, significant quantities of **β-hydride** elimination product **β-H** and the isomeric acetoxyated product **RE-2** were also formed in these reactions, although no clear trends

were observed upon variation of the substituent X. However, this was not unexpected, as both of these products are formed by independent pathways that do not involve competing reactivity of intermediate **58**.

Table 2.6 CP/RE-1 as a Function of Aryl Substituent X

Entry	X	CP	β -H	RE-1	RE-2	Cp/RE-1
1	NO ₂	44%	<< 1%	8%	<< 1%	5 : 1
2	CF ₃	36%	2%	5%	7%	7 : 1
3	H	55%	< 1%	3%	12%	18 : 1
4	Me	56%	2%	1%	5%	56 : 1
5	OMe	66%	2%	<< 1%	<< 1%	>200 : 1

2.4 Conclusion

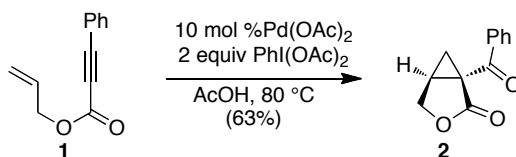
We have demonstrated a new Pd-catalyzed reaction for the stereospecific oxidative cyclization of enynes into bicyclic cyclopropanes. This method allows for the construction of cyclic products from acyclic starting materials with a complementary stereochemical outcome to related Pd^{0/II}, Au^I, and Pt^{II}-catalyzed processes. We have shown that the choice of oxidant is crucial to the construction of these products and that with certain substrates, bidentate ligands improve the cyclization. This reaction is tolerant of a variety of functional groups and proceeds in moderate to good yield with a broad scope of enynes. The observed stereochemistry as well as detailed electronic studies provide strong evidence supporting the formation of a Pd^{IV} intermediate that

undergoes competing C–C bond formation (to generate the cyclopropane product) and C–OAc bond formation (to produce an acetoxyated compound). These studies offer insight into a new mode of reactivity for alkyl–Pd^{IV} species and provide an orthogonal synthetic approach for accessing functionalized bicyclic cyclopropanes.

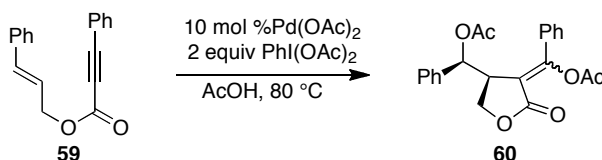
2.5 Subsequent Work

Concurrent with our initial publication, Beller and Tse published a Pd^{II/IV}-catalyzed cyclopropanation of enynes under analogous conditions to our methodology (Scheme 2.35).⁴⁵ Subjection of enyne **1** to 10 mol % of Pd(OAc)₂ and 2 equiv of PhI(OAc)₂ produced the cyclopropane product **2** in 63% yield. Interestingly, under these conditions the enyne **59** produced the acetoxyated isomer **60** as the major product (Scheme 2.36). This product presumably arises from intramolecular *syn* olefin insertion, followed by oxidation to Pd^{IV} and C–OAc bond-forming reductive elimination, similar to **RE-1** discussed above. ¹H NMR coupling constant analysis of this product suggested that reductive elimination proceeded with inversion of stereochemical configuration, consistent with our proposed mechanism above (Scheme 2.29).

Scheme 2.35 Beller and Tse's Pd^{II/IV}-Catalyzed Cyclopropanation



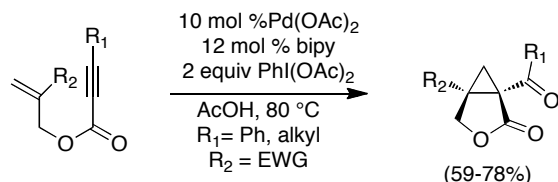
Scheme 2.36 Beller and Tse's S_N2-C-OAc Reductive Elimination Product



Related work by Tong and coworkers has expanded the scope of Pd^{II/IV}-catalyzed cyclopropanation of enynes to Baylis-Hillman type adducts utilizing an electron-withdrawing group on the alkene moiety.⁴⁶ Using similar reaction conditions to our

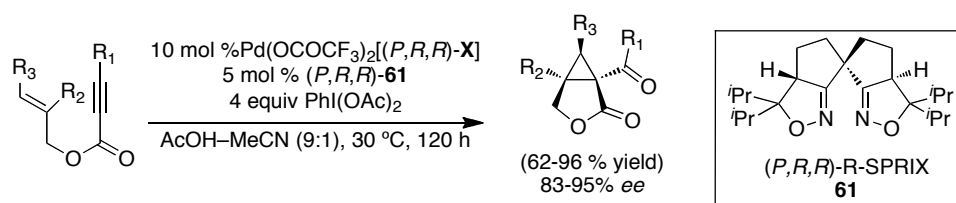
system, a series of 1,1-disubstituted enynes could be cyclized to the desired cyclopropane products in moderate to good yields (Scheme 2.37).

Scheme 2.37 Tong's Pd^{II/IV}-Catalyzed Cyclization of Enynes



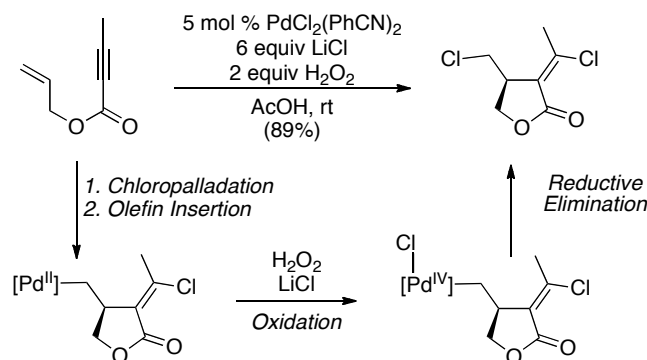
Excitingly, in 2009 Sasai and coworkers were able to demonstrate an enantioselective variant of this Pd^{II/IV}-catalyzed cyclopropanation (Scheme 2.38).⁴⁷ Using a pre-formed Pd-SPRIX complex as the catalyst with additional SPRIX ligand, afforded the cyclopropane in good yield and enantioselectivity. Importantly, this represents the first example of asymmetric catalysis utilizing a Pd^{II/IV} redox couple.

Scheme 2.38 Sasai's Asymmetric Pd^{II/IV}-Catalyzed Cyclopropanation



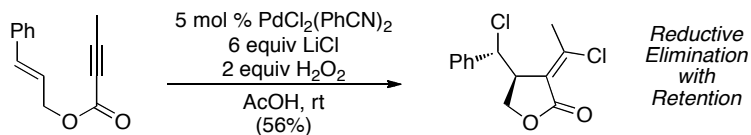
Related work by Lu has shown that the cyclization of enynes with subsequent chlorination can also take place via a Pd^{II/IV} catalytic cycle.⁴⁸ Enynes subjected to 5 mol % of PdCl₂(PhCN)₂, 6 equiv LiCl, and 2 equiv of H₂O₂ underwent cyclization to afford chlorinated products in good yield (Scheme 2.39). This reaction is hypothesized to proceed through chloropalladation of the alkyne, intramolecular alkene insertion, oxidation to Pd^{IV} with H₂O₂, and C-Cl bond-forming reductive elimination to give the chlorinated product.

Scheme 2.39 Lu's Chlorination of Enynes with H₂O₂



Substrates bearing substitution at the terminal position of the alkene moiety led to stereospecific C–Cl bond formation. Surprisingly, the stereochemistry at this position is consistent with C–Cl bond-forming reductive elimination proceeding with retention of configuration (Scheme 2.40). This is in contrast to the above examples of C–OAc bond forming reductive elimination proceeding with inversion, suggesting the mechanism of alkyl–Pd^{IV} reductive elimination may vary significantly as a function of reaction conditions.

Scheme 2.40 Reductive Elimination with Retention of Stereochemistry



2.6 Experimental Procedures

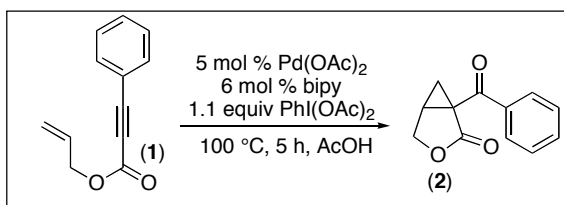
General Procedures: NMR spectra were obtained on a Varian Inova 500 (499.90 MHz for ¹H; 125.70 MHz for ¹³C) or a Varian Inova 400 (399.96 MHz for ¹H; 100.57 MHz for ¹³C; 376.34 MHz for ¹⁹F) spectrometer. ¹H NMR chemical shifts are reported in parts per million (ppm) relative to TMS, with the residual solvent peak used as an internal reference. Multiplicities are reported as follows: singlet (s), doublet (d), doublet of doublets (dd), doublet of doublets of doublets (ddd), doublet of triplets (dt), doublet of quartets (dq), doublet of triplets of doublets, (dtd), triplet (t), triplet of triplets (tt) quartet

(q), quintet (quin), multiplet (m), and broad resonance (br). IR spectra were obtained on a Perkin-Elmer “Spectrum BX” FT-IR spectrometer. Melting points were obtained on a MEL-TEMP 3.0 from Laboratory Devices Inc., USA.

Materials and Methods:

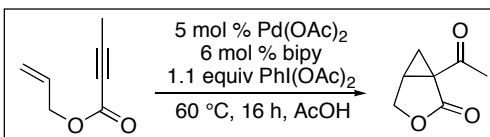
Enyne substrates were prepared according to literature procedures.¹ $\text{PhI}(\text{OAc})_2$ and 2,2'-bipyridine were obtained from Aldrich or Acros and used as received. $\text{Pd}(\text{OAc})_2$ was obtained from Pressure Chemical or Frontier Scientific and used as received. The GC yields reported are corrected GC yields based on calibration curves against an internal standard (biphenyl). Flash chromatography was performed on EM Science silica gel 60 (0.040-0.063 mm particle size, 230-400 mesh) and thin layer chromatography was performed on Merck TLC plates pre-coated with silica gel 60 F254. HPLC separations were performed on a Varian ProStar 210 HPLC using Waters $\mu\text{Porasil}^{\text{®}}$ 10 μm silica (19 x 300 mm) columns. Gas chromatography was performed on a Shimadzu GC-17A equipped with a Restek Rtx $^{\text{®}}$ -5 column (15m, 0.25 mm ID, 0.25 μm df) and an FID detector. GC analysis of all of the products reported herein was carried out using the following method: 100 $^{\circ}\text{C}$ start temperature, ramp 15 $^{\circ}\text{C}/\text{min}$ to 240 $^{\circ}\text{C}$, and hold for 10 min. GCMS analysis was performed on a Shimadzu GCMS QP-5000 equipped with a Restek Rtx $^{\text{®}}$ -5 column (30 m, 0.25 mm ID, 0.25 μm df). Control reactions (in the absence of Pd catalyst) were run for each substrate and showed no reaction.

Experimental Procedures



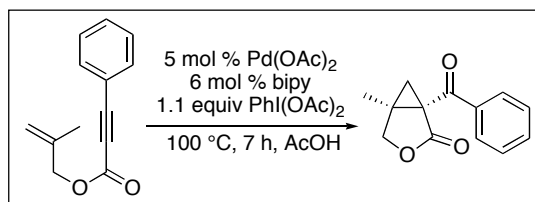
Enyne **1** (0.301 g, 1.6 mmol, 1 equiv), $\text{PhI}(\text{OAc})_2$ (0.571 g, 1.8 mmol, 1.1 equiv), 2,2'-bipyridine (0.016 g, 0.10 mmol, 6 mol %), and $\text{Pd}(\text{OAc})_2$ (0.018 g, 0.082 mmol, 5 mol %) were combined in acetic acid (11.5 mL) in a 20 mL vial. The vial was sealed with a Teflon-lined cap, and the reaction was heated at 100 $^{\circ}\text{C}$ for 5 hours. The reaction

was diluted with water (40 mL) and extracted with ethyl acetate (2 x 50 mL). The combined organic layers were washed with water (3 x 100 mL) and brine (1 x 100 mL) and then dried over anhydrous MgSO₄. The solvent was removed under vacuum, and the resulting oily residue was purified by gradient column chromatography on silica gel (25% ethyl acetate/75% hexanes to 75% ethyl acetate/25% hexanes, R_f = 0.49 in 50% ethyl acetate/50% hexanes). Product **2** was obtained as a pale orange solid (0.259 g, 79% yield). mp = 101.0-103.5 °C. ¹H NMR (500 MHz, CDCl₃): δ 7.89 (dt, 2H, *J* = 8.5, 1.6 Hz), 7.60 (tt, 1H, *J* = 7.2, 1.4 Hz), 7.48 (tt, 2H, *J* = 7.7, 1.5 Hz), 4.58 (dd, 1H, *J* = 9.5, 4.5 Hz), 4.36 (d, 1H, *J* = 10.0 Hz), 2.84 (dtd, 1H, *J* = 8.0, 5.0, 0.7 Hz), 2.13 (dd, 1H, *J* = 8.0, 4.5 Hz), 1.45 (t, 1H, *J* = 5.0 Hz). ¹³C {¹H} NMR (125.7 MHz, CDCl₃): δ 192.0, 172.7, 135.5, 133.7, 129.2, 128.5, 67.9, 35.8, 27.1, 19.2. IR (Thin film): 1771, 1674 cm⁻¹. Anal. Calcd for C₁₂H₁₀O₃: C, 71.28, H, 4.98; found: C, 70.99, H, 4.89.

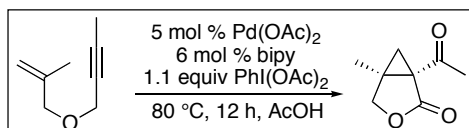


The enyne (0.300 g, 2.4 mmol, 1 equiv), PhI(OAc)₂ (0.857 g, 2.7 mmol, 1.1 equiv), 2,2'-bipyridine (0.023 g, 0.14 mmol, 6 mol %), and Pd(OAc)₂ (0.028 g, 0.12 mmol, 5 mol %) were combined in acetic acid (15 mL) in a 20 mL vial. The vial was sealed with a Teflon-lined cap, and the reaction was heated at 60 °C for 16 hours. The reaction was diluted with water (40 mL) and extracted with ethyl acetate (2 x 50 mL). The combined organic layers were washed with water (3 x 100 mL) and brine (1 x 100 mL) and then dried over anhydrous MgSO₄. The solvent was removed under vacuum, and the resulting oily residue was purified by gradient column chromatography on silica gel (5% ethyl acetate/95% hexanes to 40% ethyl acetate/60% hexanes, R_f = 0.37 in 50% ethyl acetate/50% hexanes). The product was obtained as an orange oil along with a trace amount of an unidentified minor product [0.188 g, 55% isolated yield (99% pure by GC, 76% GC yield)]. ¹H NMR (500 MHz, CDCl₃): δ 4.32 (dd, 1H, *J* = 9.5, 5.0 Hz), 4.18 (d, 1H, *J* = 9.5 Hz), 2.78 (dtd, 1H, *J* = 8.0, 5.0, 0.8 Hz), 2.55 (s, 3H), 2.04 (dd, 1H, *J* = 8.0, 4.2 Hz), 1.40 (dd, 1H, *J* = 5.5, 4.2 Hz). ¹³C {¹H} NMR (125.7 MHz, CDCl₃): δ 200.5,

172.8, 67.2, 36.5, 29.9, 29.3, 24.2. IR (Thin film): 1771, 1698 cm^{-1} . HRMS (EI^+) (m/z): [M^+] calculated for $\text{C}_7\text{H}_8\text{O}_3$: 140.0473; found: 140.0476.

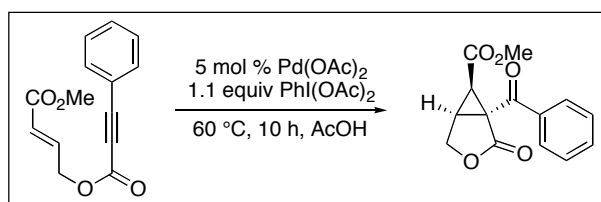


The enyne (0.300 g, 1.5 mmol, 1 equiv), $\text{PhI}(\text{OAc})_2$ (0.533 g, 1.6 mmol, 1.1 equiv), 2,2'-bipyridine (0.014 g, 0.091 mmol, 6 mol %), and $\text{Pd}(\text{OAc})_2$ (0.017 g, 0.075 mmol, 5 mol %) were combined in acetic acid (9.4 mL) in a 20 mL vial. The vial was sealed with a Teflon-lined cap, and the reaction was heated at 100 °C for 7 hours. The reaction was diluted with water (40 mL) and extracted with ethyl acetate (2 x 50 mL). The combined organic layers were washed with water (3 x 100 mL) and brine (1 x 100 mL) and then dried over anhydrous MgSO_4 . The solvent was removed under vacuum, and the resulting oily residue was purified by column chromatography on silica gel ($R_f = 0.22$ in 25% ethyl acetate/75% hexanes). The product was obtained as a cream-colored solid (0.252 g, 77% yield). mp = 108-110 °C. ^1H NMR (500 MHz, CDCl_3): δ 7.72 (d, 2H, $J = 0.7$ Hz), 7.59 (tt, 1H, $J = 7.5, 1.2$ Hz), 7.48 (t, 2H, $J = 7.6$ Hz), 4.43 (d, 1H, $J = 10.0$ Hz), 4.40 (d, 1H, $J = 9.5$ Hz), 2.22 (d, 1H, $J = 5.0$ Hz), 1.44 (d, 1H, $J = 5.0$ Hz), 1.33 (s, 3H). ^{13}C { ^1H } NMR (125.7 MHz, CDCl_3): δ 191.8, 173.9, 136.5, 133.5, 128.7, 128.5, 72.6, 40.2, 37.0, 22.8, 14.3. IR (Thin film): 2969, 1766, 1672 cm^{-1} . Anal. Calcd for $\text{C}_{13}\text{H}_{12}\text{O}_3$: C, 72.21, H, 5.59; found: C, 72.56, H, 5.67.



The enyne (0.114 g, 0.83 mmol, 1 equiv), $\text{PhI}(\text{OAc})_2$ (0.293 g, 0.90 mmol, 1.1 equiv), 2,2'-bipyridine (0.0078 g, 0.050 mmol, 6 mol %), and $\text{Pd}(\text{OAc})_2$ (0.0093 g, 0.041 mmol, 5 mol %) were combined in acetic acid (5.2 mL) in a 20 mL vial. The vial was sealed with a Teflon-lined cap, and the reaction was heated at 80 °C for 12 hours. The

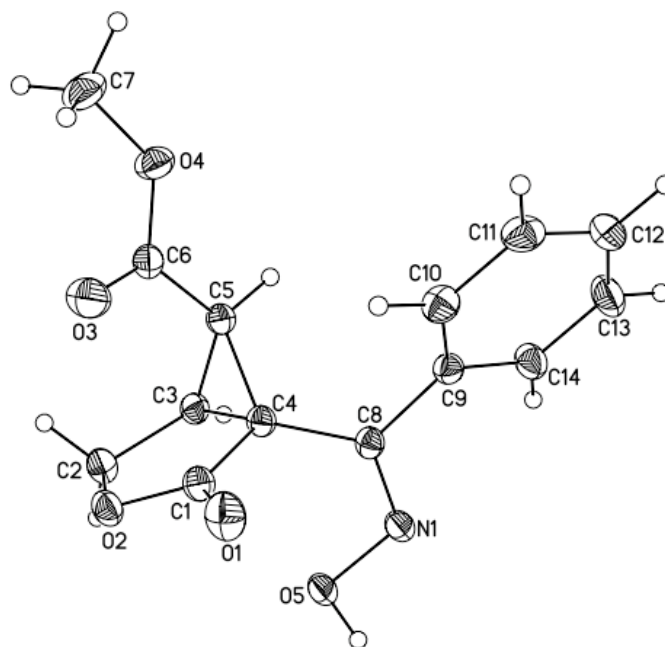
reaction was diluted with water (40 mL) and extracted with ethyl acetate (2 x 50 mL). The combined organic layers were washed with water (3 x 100 mL) and brine (1 x 100 mL) and then dried over anhydrous MgSO_4 . The solvent was removed under vacuum, and the resulting oily residue was purified by column chromatography on silica gel ($R_f = 0.22$ in 25% ethyl acetate/75% hexanes). The product was obtained as a yellow oil (0.0836 g, 66% yield). ^1H NMR (500 MHz, CDCl_3): δ 4.19 (d, 1H, $J = 9.5$ Hz), 4.05 (d, 1H, $J = 9.5$ Hz), 2.43 (s, 3H), 2.04 (d, 1H, $J = 4.0$ Hz), 1.35 (d, 1H, $J = 4.0$ Hz), 1.30 (s, 3H). ^{13}C $\{^1\text{H}\}$ NMR (125.7 MHz, CDCl_3): δ 199.2, 173.8, 72.1, 40.4, 39.2, 30.1, 26.9, 13.1. IR (Thin film): 1770, 1694 cm^{-1} . HRMS (EI^+) (m/z): $[\text{M}^+]$ calculated for $\text{C}_8\text{H}_{10}\text{O}_3$: 154.0630; found: 154.0630.

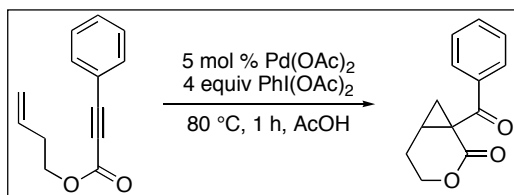


The enyne (42:1 E:Z ratio, 0.301 g, 1.2 mmol, 1 equiv), $\text{PhI}(\text{OAc})_2$ (0.436 g, 1.3 mmol, 1.1 equiv), and $\text{Pd}(\text{OAc})_2$ (0.014 g, 0.061 mmol, 5 mol %) were combined in acetic acid (7.68 mL) in a 20 mL vial. The vial was sealed with a Teflon-lined cap, and the reaction was heated at 60 °C for 10 hours. The reaction was diluted with water (40 mL) and extracted with ethyl acetate (2 x 50 mL). The combined organic layers were washed with water (3 x 100 mL) and brine (1 x 100 mL) and then dried over anhydrous MgSO_4 . The solvent was removed under vacuum, and the resulting oily residue was purified by gradient column chromatography on silica gel (10% ethyl acetate/90% hexanes to 70% ethyl acetate/30% hexanes, $R_f = 0.38$ in 50% ethyl acetate/50% hexanes). The product was obtained as an orange oil (0.253 g, 79% yield, 99% pure by GC). ^1H NMR (400 MHz, CDCl_3): δ 7.91 (d, 2 H, $J = 7.8$ Hz), 7.58 (tt, 1H, $J = 7.4, 1.2$ Hz), 7.46 (t, 2H, $J = 7.6$ Hz), 4.64 (dd, 1H, $J = 10.4, 5.2$ Hz), 4.49 (d, 1H, $J = 10.4$ Hz), 3.77 (s, 3H), 3.12 (ddd, 1H, $J = 8.4, 5.0, 0.8$ Hz), 2.92 (d, 1H, $J = 8.4$ Hz). ^{13}C $\{^1\text{H}\}$ NMR (100.57 MHz, CDCl_3): δ 190.0, 169.6, 166.7, 134.6, 134.0, 129.3, 128.5, 65.1, 52.7, 42.3, 32.1, 30.0. IR (Thin film): 1769, 1738, 1679 cm^{-1} . Anal. Calcd for $\text{C}_{14}\text{H}_{13}\text{NO}_5$ (as the N-

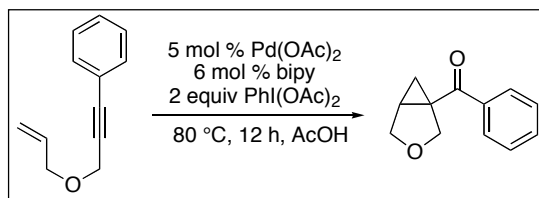
OH oxime): C, 61.09, H, 4.76, N, 5.09; found: C, 61.04, H, 4.89, N, 4.89. The product was converted to an oxime in order to obtain a crystalline material. Needles were grown by the vapor diffusion method (acetone/ hexanes) with the cyclopropyl oxime at 22 °C. The structure is shown below in Figure 1, and it definitively establishes the inversion of stereochemistry in the product. More information about this structure can be found on p. S15.

Figure 2.3 Crystal Structure of Oxime



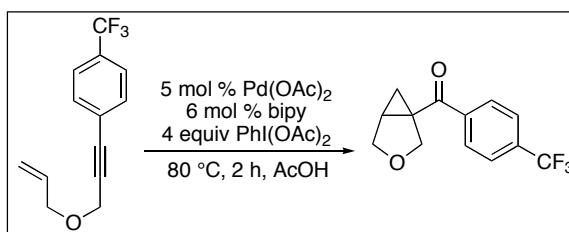


The enyne (0.303 g, 1.5 mmol, 1 equiv), $\text{PhI}(\text{OAc})_2$ (1.928 g, 5.9 mmol, 4 equiv), and $\text{Pd}(\text{OAc})_2$ (0.017 g, 0.75 mmol, 5 mol %) were combined in acetic acid (9.4 mL) in a 20 mL vial. The vial was sealed with a Teflon-lined cap, and the reaction was heated at 80 °C for 1 hour. The reaction was diluted with water (40 mL) and extracted with ethyl acetate (2 x 50 mL). The combined organic layers were washed with water (3 x 100 mL) and brine (1 x 100 mL) and then dried over anhydrous MgSO_4 . The solvent was removed under vacuum, and the resulting oily residue was purified by gradient column chromatography on silica gel (25% ethyl acetate/75% hexanes to 75% ethyl acetate/25% hexanes, $R_f = 0.28$ in 50% ethyl acetate/50% hexanes). The product was obtained as a pale yellow solid (0.182 g, 55% yield). mp = 77.3-80.4 °C. ^1H NMR (500 MHz, CDCl_3): δ 7.83 (dd, 2 H, $J = 8.5, 1.5$ Hz), 7.55 (tt, 1H, $J = 7.5, 1.5$ Hz), 7.45 (tt, 2H, $J = 7.0, 1.5$ Hz), 4.45 (ddt, 1H, $J = 12.0, 6.0, 1.5$ Hz), 4.26 (td, 1H, $J = 12.5, 3.5$ Hz), 2.51 (m, 1H), 2.13 (quin, 1H, $J = 2.0$ Hz), 2.13 (m, 1H), 2.09 (m, 1H), 1.85 (t, 1H, $J = 5.5$ Hz). ^{13}C $\{^1\text{H}\}$ NMR (125.7 MHz, CDCl_3): δ 193.3, 168.8, 135.9, 133.1, 128.6, 128.5, 64.8, 33.7, 23.9, 20.3, 13.3. IR (Thin film): 1722, 1681 cm^{-1} . HRMS (Electrospray) (m/z): $[\text{M}+\text{Na}^+]$ calculated for $\text{NaC}_{13}\text{H}_{12}\text{O}_3$: 239.0684; found: 239.0682.



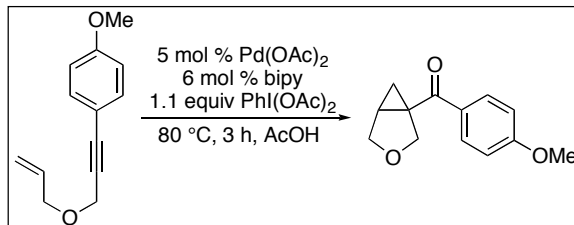
The enyne (0.300 g, 1.7 mmol, 1 equiv), $\text{PhI}(\text{OAc})_2$ (1.13 g, 3.5 mmol, 2 equiv), 2,2'-bipyridine (0.016 g, 0.10 mmol, 6 mol %), and $\text{Pd}(\text{OAc})_2$ (0.019 g, 0.087 mmol, 5 mol %) were combined in acetic acid (7.9 mL) in a 20 mL vial. The vial was sealed with a Teflon-lined cap, and the reaction was heated at 80 °C for 12 hours. The reaction was diluted with water (40 mL) and extracted with ethyl acetate (2 x 50 mL). The combined

organic layers were washed with water (3 x 100 mL) and brine (1 x 100 mL) and then dried over anhydrous MgSO₄. The solvent was removed under vacuum, and the resulting oily residue was purified by gradient column chromatography on silica gel (2% ethyl acetate/98% hexanes to 10% ethyl acetate/90% hexanes, R_f = 0.44 in 25% ethyl acetate/75% hexanes). The product was obtained as a yellow oil (0.158 g, 48% yield). ¹H NMR (500 MHz, CDCl₃): δ 7.70 (d, 2H, *J* = 8.0 Hz), 7.51 (t, 1H, *J* = 7.5 Hz), 7.42 (t, 2H, *J* = 6.7 Hz), 4.19 (dd, 1H, *J* = 8.5, 2.0 Hz), 3.94 (d, 1H, 8.5 Hz), 3.87 (dd, 1H, *J* = 8.5, 2.5 Hz), 3.82 (d, 1H, *J* = 8.5 Hz), 2.38 (m, 1H), 1.53 (dd, 1H, *J* = 4.1, 0.7 Hz), 1.20 (t, 1H, *J* = 4.8 Hz). ¹³C {¹H} NMR (125.7 MHz, CDCl₃): δ 200.4, 138.2, 132.4, 128.5, 127.8, 70.2, 68.7, 38.8, 29.4, 18.9. IR (Thin film): 1665 cm⁻¹. HRMS (EI⁺) (*m/z*): [M⁺] calculated for C₁₂H₁₁O₂: 187.0759; found: 187.0760.

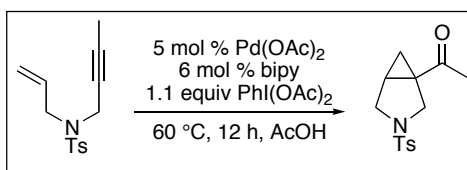


The enyne (0.298 g, 1.2 mmol, 1 equiv), PhI(OAc)₂ (1.598 g, 5.0 mmol, 4 equiv), and Pd(OAc)₂ (0.014 g, 0.063 mmol, 5 mol %) were combined in acetic acid (7.8 mL) in a 20 mL vial. The vial was sealed with a Teflon-lined cap, and the reaction was heated at 80 °C for 2 hours. The reaction was diluted with water (40 mL) and extracted with ethyl acetate (2 x 50 mL). The combined organic layers were washed with water (3 x 100 mL) and brine (1 x 100 mL) and then dried over anhydrous MgSO₄. The solvent was removed under vacuum, and the resulting oily residue was purified by column chromatography on silica gel (R_f = 0.42 in 25% ethyl acetate/75% hexanes). The product was obtained as a pale yellow oil (0.141 g, 44% yield). ¹H NMR (500 MHz, CDCl₃): δ = 7.79 (d, 2H, *J* = 8.0 Hz), 7.72 (d, 2H, *J* = 8.0 Hz), 4.19 (d, 1H, *J* = 9.0 Hz), 3.95 (d, 1H, *J* = 8.5 Hz), 3.91 (d, 1H, *J* = 8.5 Hz), 3.85 (dd, 1H, *J* = 8.5, 3.0 Hz), 2.43 (m, 1H), 1.60 (dd, 1H, *J* = 8.5, 4.2 Hz), 1.29 (t, 1H, *J* = 4.7 Hz). ¹³C {¹H} NMR (125.7 MHz, CDCl₃): δ 199.7, 141.2, 133.7, 128.0, 125.6, 123.5, 69.9, 68.7, 39.0, 30.2, 19.2. ¹⁹F NMR (376.3 MHz, CDCl₃) δ –

63.1. IR (Thin film): 1672 cm^{-1} . HRMS (EI^+) (m/z): $[\text{M}^+]$ calculated for $\text{C}_{13}\text{H}_{10}\text{O}_2$: 255.0633; found: 255.0634.

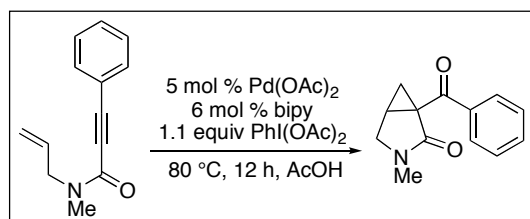


The enyne (0.301 g, 1.5 mmol, 1 equiv), $\text{PhI}(\text{OAc})_2$ (0.526 g, 1.6 mmol, 1.1 equiv), 2,2'-bipyridine (0.014 g, 0.09 mmol, 6 mol %), and $\text{Pd}(\text{OAc})_2$ (0.017 g, 0.075 mmol, 5 mol %) were combined in acetic acid (6.7 mL) in a 20 mL vial. The vial was sealed with a Teflon-lined cap, and the reaction was heated at 80 °C for 3 hours. The reaction was diluted with water (40 mL) and extracted with ethyl acetate (2 x 50 mL). The combined organic layers were washed with water (3 x 100 mL) and brine (1 x 100 mL) and then dried over anhydrous MgSO_4 . The solvent was removed under vacuum, and the resulting oily residue was purified by column chromatography on silica gel ($R_f = 0.31$ in 25% ethyl acetate/75% hexanes). The product was obtained as a yellow oil (0.143 g, 44% yield). ^1H NMR (500 MHz, CDCl_3): δ 7.75 (dt, 2H, $J = 9.0, 1.7$ Hz), 6.91 (dt, 2H, $J = 9.0, 2.0$ Hz), 4.20 (d, 1H, $J = 8.5$ Hz), 3.95 (d, 1H, $J = 8.5$ Hz), 3.87 (d, 1H, $J = 8.5$ Hz), 3.83 (br. s, 4H), 2.35 (m, 1H), 1.45 (dd, 1H, $J = 8.0, 4.0$ Hz), 1.16 (t, 1H, $J = 4.7$ Hz). ^{13}C $\{^1\text{H}\}$ NMR (125.7 MHz, CDCl_3): δ 198.1, 163.1, 130.7, 130.4, 113.7, 70.5, 68.8, 55.4, 38.5, 28.4, 18.5. IR (Thin film): 1661, 1601 cm^{-1} . HRMS (EI^+) (m/z): $[\text{M}^+]$ calculated for $\text{C}_{13}\text{H}_{13}\text{O}_3$: 217.0864; found: 217.0861.



The enyne (0.300 g, 1.1 mmol, 1 equiv), $\text{PhI}(\text{OAc})_2$ (0.408 g, 1.3 mmol, 1.1 equiv), 2,2'-bipyridine (0.011 g, 0.068 mmol, 6 mol %), and $\text{Pd}(\text{OAc})_2$ (0.012 g, 0.055 mmol, 5 mol %) were combined in acetic acid (7.1 mL) in a 20 mL vial. The vial was

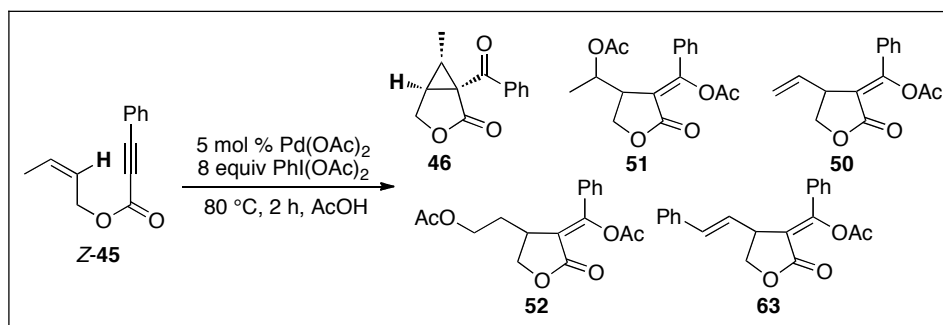
sealed with a Teflon-lined cap, and the reaction was heated at 60 °C for 12 hours. The reaction was diluted with water (40 mL) and extracted with ethyl acetate (2 x 50 mL). The combined organic layers were washed with water (3 x 100 mL) and brine (1 x 100 mL) and then dried over anhydrous MgSO₄. The solvent was removed under vacuum, and the resulting oily residue was purified by column chromatography on silica gel (R_f = 0.40 in 50% ethyl acetate/50% hexanes). The product was obtained as an orange oil (0.226 g, 71% yield). ¹H NMR (500 MHz, CDCl₃): δ 7.67 (d, 2H, J = 8.5 Hz), 7.32 (d, 2H, J = 8.5 Hz), 3.60 (t, 2H, J = 10.0 Hz), 3.37 (d, 1H, J = 9.5 Hz), 3.04 (dd, 1H, 9.5, 3.7 Hz), 2.42 (s, 3H), 2.03 (m, 1H), 1.92 (s, 3H), 1.48 (dd, 1H, J = 8.0, 5.5 Hz) 1.24 (t, 1H, J = 5.2 Hz). ¹³C {¹H} NMR (125.7 MHz, CDCl₃): δ 204.4, 143.8, 132.6, 129.7, 127.6, 49.0, 48.8, 38.8, 27.2, 25.5, 21.5, 17.5. IR (Thin film): 1684, 1346, 1165 cm⁻¹. HRMS (Electrospray) (m/z): [M+Na⁺] calculated for NaC₁₄H₁₇NO₃S: 302.0827; found: 302.0820.



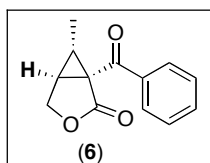
The enyne (0.100 g, 0.54 mmol, 1 equiv), PhI(OAc)₂ (0.191 g, 0.59 mmol, 1.1 equiv), 2,2'-bipyridine (0.0051 g, 0.032 mmol, 6 mol %), and Pd(OAc)₂ (0.0061 g, 0.027 mmol, 5 mol %) were combined in acetic acid (3.4 mL) in a 20 mL vial. The vial was sealed with a Teflon-lined cap, and the reaction was heated at 80 °C for 12 hours. The reaction was diluted with water (40 mL) and extracted with ethyl acetate (2 x 50 mL). The combined organic layers were washed with water (3 x 100 mL) and brine (1 x 100 mL) and then dried over anhydrous MgSO₄. The solvent was removed under vacuum, and the resulting oily residue was purified by column chromatography on silica gel (R_f = 0.19 in 70% ethyl acetate/30% hexanes). The product was obtained as a yellow oil (0.051 g, 44% yield). ¹H NMR (500 MHz, CDCl₃): δ 7.84 (dd, 2H, J = 7, 1.0 Hz), 7.51 (t, 1H, J = 7.5 Hz), 7.41 (t, 2H, J = 7.5 Hz), 3.74 (dd, 1H, J = 10.5, 6.0 Hz), 3.35 (d, 1H, J = 10.5 Hz), 2.80 (s, 3H) 2.38 (dt, 1H, J = 8.0, 2.5 Hz) 1.96 (dd, 1H, J = 8.0, 4.5 Hz), 1.10 (t, 1H,

$J = 4.5\text{Hz}$). ^{13}C $\{^1\text{H}\}$ NMR (125.7 MHz, CDCl_3): δ 194.7, 171.4, 136.5, 133.1, 129.0, 128.3, 49.9, 38.5, 29.7, 22.2, 19.2. IR (Thin Film): 1684, 1598 cm^{-1} . HRMS (EI^+) (m/z): $[\text{M}^+]$ calculated for $\text{C}_{13}\text{H}_{13}\text{NO}_2$: 214.0868; found: 214.0863.

E and *Z* Olefin Studies



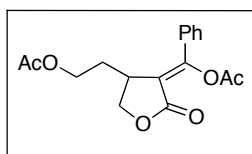
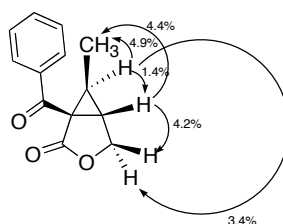
Z-45 (91:9 *Z*:*E* ratio, 0.304 g, 1.5 mmol, 1 equiv), $\text{PhI}(\text{OAc})_2$ (3.865 g, 12 mmol, 8 equiv, dried under vacuum for 24 h), and $\text{Pd}(\text{OAc})_2$ (0.0164 g, 0.073 mmol, 5 mol %) were combined in distilled acetic acid (9.4 mL) in a 20 mL vial. The vial was sealed with a Teflon-lined cap, and the reaction was heated at 80 °C for 2 hours. The reaction was diluted with water (40 mL) and extracted with ethyl acetate (2 x 50 mL). The combined organic layers were washed with water (3 x 100 mL) and brine (1 x 100 mL) and then dried over anhydrous MgSO_4 . The solvent was removed under vacuum, and the resulting oily residue was purified by gradient column chromatography on silica gel (10%/90% to 75% ethyl acetate/25% hexanes) and further purified with HPLC. Products **46** (25% GC yield), **63** (3% GC yield), **52** (19% GC yield), **51** (11% GC yield), **50** (8% GC yield) were isolated from the reaction. [Note: GC yields are calibrated versus an internal standard (biphenyl).]



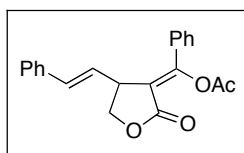
Product **46** was obtained as a white solid in an 13:1 mixture of diastereomers (**6** : **44**) along with a trace amount of an unidentified side product (0.091g, 28% yield, 96%

pure by GC, $R_f = 0.19$ in 25% ethyl acetate/75% hexanes). mp = 109.9-113.0 °C. ^1H NMR (500 MHz, CDCl_3): δ 8.04 (dt, 2 H, $J = 8.0, 1.5$ Hz), 7.62 (tt, 1H, $J = 7.2, 1.4$ Hz), 7.51 (t, 2H, $J = 7.7$ Hz), 4.40 (dd, 1H, $J = 9.0, 5.0$ Hz), 4.29 (d, 1H, $J = 9.5$ Hz), 2.68 (t, 1H, $J = 4.7$ Hz), 1.92 (dq, 1H, $J = 5.9, 5.7$ Hz), 1.10 (d, 3H, $J = 6.0$ Hz). ^{13}C $\{^1\text{H}\}$ NMR (125.7MHz, CDCl_3): δ 191.5, 171.9, 136.0, 133.9, 130.1, 128.4, 67.8, 41.2, 29.1, 28.2, 12.5. IR (Thin film): 1761, 1734 cm^{-1} . HRMS (Electrospray): $[\text{M}+\text{Na}^+]$ calculated for $\text{NaC}_{12}\text{H}_{13}\text{O}_3$: 239.0684, found: 239.0685.

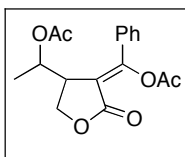
NOE Studies for 46:



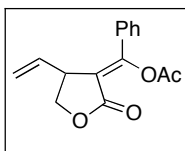
The product was obtained as a pale yellow oil ($R_f = 0.08$ in 30% ethyl acetate/70% hexanes). ^1H NMR (500 MHz, CDCl_3): δ 7.51-7.53 (m, 2H), 7.42-7.44 (multiple peaks, 3H), 4.39 (dd, 1H, $J = 9.0, 7.5$ Hz), 4.14 (dd, 1H, $J = 9.5, 2.5$ Hz), 3.99-4.03 (m, 1H), 3.92-3.96 (m, 1H), 3.59 (m, 1H), 2.30 (s, 3H), 1.93 (s, 3H), 1.78 (m, 2H). ^{13}C $\{^1\text{H}\}$ NMR (125.7 MHz, CDCl_3): δ 170.5, 168.3, 167.8, 153.6, 133.7, 130.5, 128.7, 127.7, 117.6, 69.6, 61.2, 35.5, 32.0, 20.7, 20.6. IR (Thin Film): 1758, 1738, 1669 cm^{-1} . HRMS (Electrospray) calculated for $\text{NaC}_{17}\text{H}_{18}\text{O}_6$ $[\text{M}+\text{Na}^+]$: 341.1001; found: 341.0994.



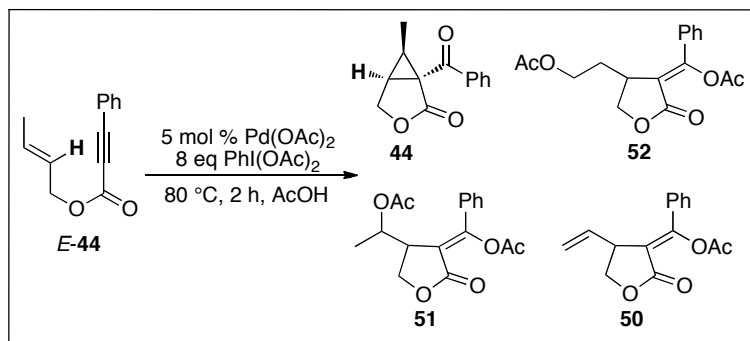
The product was obtained as a pale yellow oil ($R_f = 0.34$ in 30% ethyl acetate/70% hexanes). ^1H NMR (500 MHz, CDCl_3): δ 7.53 (dd, 2H, $J = 9.5, 1.5$, Hz), 7.25-7.44 (multiple peaks, 8H), 6.57 (d, 1H, $J = 19.5$ Hz), 6.16 (dd, 1H, $J = 11, 20$ Hz), 4.53 (m, 1H), 4.06-4.13 (multiple peaks, 2H), 1.96 (s, 3H). ^{13}C $\{^1\text{H}\}$ NMR (125.7 MHz, CDCl_3): δ 168.3, 167.5, 158.5, 136.0, 133.0, 132.2, 130.7, 129.0, 128.8, 128.1, 127.9, 126.4, 126.3, 116.9, 69.3, 43.8, 20.8. IR (Thin Film): 1769, 1733 cm^{-1} . HRMS (Electrospray) calculated for $\text{NaC}_{21}\text{H}_{18}\text{O}_4$ $[\text{M}+\text{Na}^+]$: 357.1103; found: 357.1101.



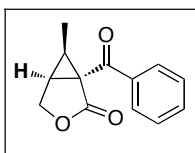
The product was obtained as a yellow oil ($R_f = 0.08$ in 30% ethyl acetate/70% hexanes). ^1H NMR (500 MHz, CDCl_3): δ 7.55 (dd, 2H, $J = 8.0, 1.5$ Hz), 7.38-7.42 (multiple peaks, 3H), 5.26-5.28 (m, 1H), 4.41 (dd, 1H, $J = 12.5, 2.5$ Hz), 4.27 (dd, 1H, $J = 12, 9$ Hz), 3.62-3.65 (m, 1H), 2.29 (s, 3H), 2.05 (s, 3H), 1.24 (d, 3H, $J = 7$ Hz). ^{13}C $\{^1\text{H}\}$ NMR (125.7 MHz CDCl_3): δ 170.3, 168.1, 168.0, 158.3, 131.6, 130.8, 129.0, 128.0, 115.1, 69.5, 65.2, 42.7, 21.2, 20.9, 14.5. IR (Thin Film): 1767, 1739, 1662 cm^{-1} . HRMS (Electrospray) calculated for $\text{NaC}_{17}\text{H}_{18}\text{O}_6$ $[\text{M}+\text{Na}^+]$: 341.1001; found: 341.0998.



The product was isolated as a pale yellow oil ($R_f = 0.29$ in 30% ethyl acetate/70% hexanes). The spectroscopic data for this product was identical to that previously reported in the literature.²



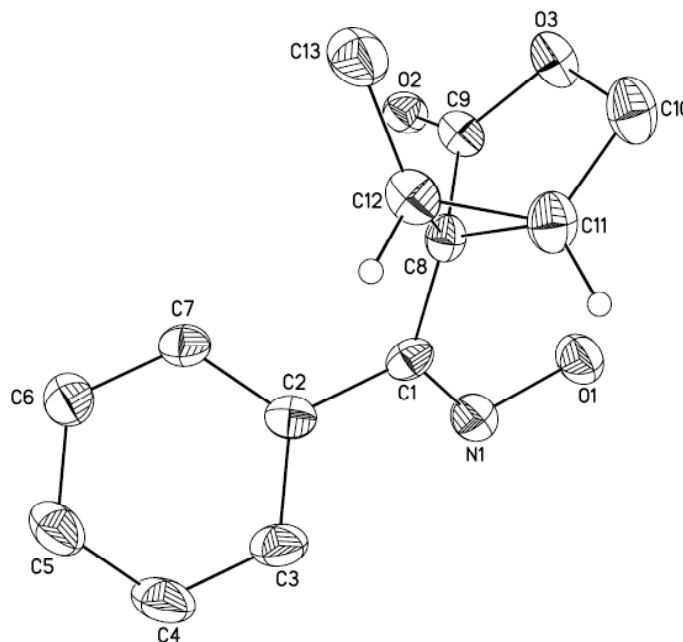
E-43 (86:14 *E:Z* ratio, 0.600 g, 3.9 mmol, 1 equiv), $\text{PhI}(\text{OAc})_2$ (7.727 g, 24.0 mmol, 8 equiv, dried under vacuum for 24 hours), and $\text{Pd}(\text{OAc})_2$ (0.034 g, 0.15 mmol, 5 mol %) were combined in acetic acid (18.7 mL) in a 50 mL pressure flask, and the reaction was heated at 80 °C for 2 hours. The reaction was diluted with water (40 mL) and extracted with ethyl acetate (2 x 50 mL). The combined organic layers were washed with water (3 x 100 mL) and brine (1 x 100 mL) and then dried over anhydrous MgSO_4 . The solvent was removed under vacuum, and the resulting oily residue was purified by gradient column chromatography on silica gel (10% ethyl acetate/90% hexanes to 75% ethyl acetate/25% hexanes). Products **44** (59% GC yield), **52** (8% GC yield), **51** (4% GC yield), and **50** (8% GC yield) were isolated from the reaction. [Note: GC yields are calibrated versus an internal standard (biphenyl).]



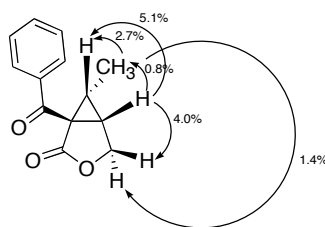
The product was obtained as a white solid as an 11:1 mixture of diastereomers (**44** : **46**) (0.27 g, 42% yield, $R_f = 0.23$ in 25% ethyl acetate/75% hexanes). mp = 107.6-112.1 °C. ^1H NMR (500 MHz, CDCl_3): δ 7.87 (dt, 2H, $J = 7.0, 1.5$ Hz), 7.58 (tt, 1H, $J = 7.5, 1.4$ Hz), 7.47 (t, 2H, $J = 7.7$ Hz), 4.57 (dd, 1H, $J = 10.2, 5.2$ Hz), 4.25 (d, 1H, $J = 10.0$ Hz), 2.89 (ddd, 1H, $J = 8.2, 5.2, 1.0$ Hz), 2.20 (dq, 1H, $J = 7.5, 6.6$ Hz), 1.32 (d, 3H, $J = 6.5$ Hz). ^{13}C $\{^1\text{H}\}$ NMR (126.7 MHz, CDCl_3): $\delta = 192.8, 171.2, 135.7, 133.6, 129.3, 128.5, 64.5, 41.8, 30.9, 25.1, 7.08$. IR (CH_2Cl_2): 1763, 1673 cm^{-1} . HRMS (Electrospray) calculated for $\text{NaC}_{12}\text{H}_{13}\text{O}_3$ [$\text{M}+\text{Na}^+$]: 239.0684, found: 239.0678. The product was converted to an oxime in order to obtain a crystalline material. Needles were grown by

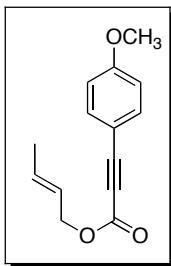
the vapor diffusion method (chlorobenzene/ pentanes) with the cyclopropyl oxime at 22 °C. The structure is shown below in Figure 2.4, and it definitively establishes the inversion of stereochemistry in the product.

Figure 2.4 Crystal Structure of Oxime of 44



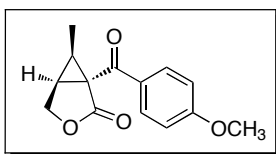
NOE Studies of 44:





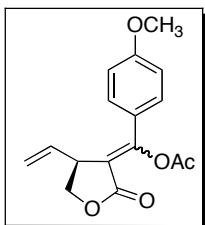
The enyne was obtained as a pale yellow oil ($R_f = 0.39$ in 95% hexanes/5% EtOAc). ^1H NMR (500 MHz, CDCl_3): δ 7.51 (d, $J = 9.0$ Hz, 2H), 6.86 (d, $J = 9.0$ Hz, 2H), 5.85 (dq, $J = 15.0, 6.5$ Hz, 1H), 5.64 (dt, $J = 15.0, 6.5$ Hz, 1H), 4.63 (d, $J = 6.5$ Hz, 2H), 3.81 (s, 3H), 1.73 (d, $J = 2.0$ Hz, 3H). ^{13}C $\{^1\text{H}\}$ NMR (100.6 MHz, CDCl_3): δ 161.4, 154.1, 134.9, 132.6, 124.2, 114.2, 111.3, 87.1, 80.0, 66.5, 55.3, 17.7. HRMS (EI): $[\text{M}]^+$ calcd for $\text{C}_{14}\text{H}_{14}\text{O}_3$: 230.0943. Found: 230.0952. IR (Thin film): 1699 cm^{-1} .

Pd-catalyzed reaction of 48. Substrate **48** (0.300 g, 1.20 mmol, 1 equiv), $\text{PhI}(\text{OAc})_2$ (3.357 g, 10.40 mmol, 8 equiv), and $\text{Pd}(\text{OAc})_2$ (14.6 mg, 5 mol %) were combined in AcOH (8.14 mL) and heated at $80\text{ }^\circ\text{C}$ for 10 min. After the workup described in the standard procedure above, products **48a** and **48b** were isolated from this reaction as described below.

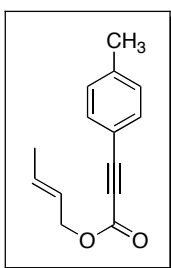


1-(4-methoxybenzoyl)-6-methyl-3-oxabicyclo[3.1.0]hexan-2-one (48a). Product **48a** was purified by gradient column chromatography (gradient = 80% hexanes/20% EtOAc to 50% hexanes/50% EtOAc), and isolated as a pale yellow solid (0.1572 g, 49% yield, mp = $85.0\text{--}87.6\text{ }^\circ\text{C}$, $R_f = 0.17$ in 70% hexanes/30% EtOAc). ^1H NMR (500 MHz, CDCl_3): δ 7.86 (d, $J = 8.5$ Hz, 2H), 6.95 (d, $J = 8.5$ Hz, 2H), 4.54 (dd, $J = 10.0, 5.5$ Hz, 1H), 4.21 (d, $J = 10.0$ Hz, 1H), 3.83 (s, 3H), 2.83 (dd, $J = 8.0, 5.5$ Hz, 1H), 2.09 (dq, $J = 8.0, 6.5$ Hz, 1H), 1.29 (d, $J = 6.5$ Hz, 3H). ^{13}C $\{^1\text{H}\}$ NMR (125.7 MHz, CDCl_3): δ 190.6, 171.4, 163.9, 132.5, 131.8, 113.6, 64.4, 55.4, 41.5, 29.9, 24.6, 7.7. HRMS Electrospray

with Na⁺ added: [M+Na]⁺ calcd for C₁₄H₁₄O₄: 269.0790. Found: 269.0792. IR (Nujol mull): 1756, 1651 cm⁻¹.

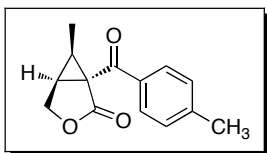


(Z)-(4-methoxyphenyl)(2-oxo-4-vinyldihydrofuran-3(2H)-ylidene)methyl acetate (48b). Product **48b** was purified by gradient column chromatography (gradient = 80% hexanes/20% EtOAc to 50% hexanes/50% EtOAc) and isolated as a yellow oil (34 mg, 9% yield, R_f = 0.23 in 70% hexanes/30% EtOAc). ¹H NMR (500 MHz, CDCl₃): δ 7.50 (d, *J* = 9.0 Hz, 2H), 6.87 (d, *J* = 9.0 Hz, 2H), 5.84 (ddd, *J* = 17.0, 10.0, 9.0 Hz, 1H), 5.21 (dd, *J* = 17.0, 10.0 Hz, 2H), 4.45 (t, *J* = 9.0 Hz, 1H), 4.04 (dd, *J* = 9.0, 5.0 Hz, 1H), 3.89 (td, *J* = 9.0, 5.0 Hz, 1H), 3.82 (s, 3H), 2.12 (s, 3H). ¹³C {¹H} NMR (100.7 MHz, CDCl₃): δ 168.5, 167.4, 161.4, 158.3, 135.7, 130.7, 124.4, 117.1, 115.3, 113.4, 69.2, 55.3, 44.1, 20.8. HRMS Electrospray with Na⁺ added: [M+Na]⁺ calcd for C₁₆H₁₆O₆: 311.0895. Found: 311.0896. IR (Thin film): 1762, 1755 cm⁻¹.

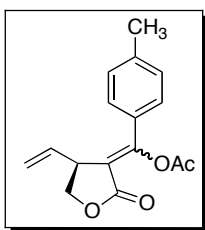


(E)-but-2-enyl 3-*p*-tolylpropiolate. The enyne was obtained as a colorless oil (R_f = 0.36 in 95% hexanes/5% EtOAc). ¹H NMR (500 MHz, CDCl₃) for the *E* isomer: δ 7.46 (d, *J* = 8.5 Hz, 2H), 7.15 (d, *J* = 8.5 Hz, 2H), 5.85 (dq, *J* = 15.0, 7.0 Hz, 1H), 5.64 (tq, *J* = 15.0, 7.0 Hz, 1H), 4.63 (d, *J* = 7.0 Hz, 2H), 2.36 (s, 3H), 1.73 (d, *J* = 7.0 Hz, 3H). ¹³C {¹H} NMR (100.6 MHz, CDCl₃): δ 154.0, 141.2, 132.9, 132.7, 129.3, 124.2, 116.5, 86.8, 80.2, 66.6, 21.7, 17.6. HRMS (EI) [M]⁺ calcd for C₁₄H₁₄O₂: 214.0994. Found: 214.0996. IR (Thin film): 1707 cm⁻¹.

Reaction with enyne (*E*)-but-2-enyl 3-*p*-tolylpropiolate. The substrate (0.700 g, 3.27 mmol, 1 equiv), $\text{PhI}(\text{OAc})_2$ (8.418 g, 26.1 mmol, 8 equiv), and $\text{Pd}(\text{OAc})_2$ (36.6 mg, 5 mol %), were combined in AcOH (20 mL) and heated at 80 °C for 1.5 h. After the workup described in the standard procedure above, products **CP**, **β -H**, **RE-1**, and **RE-2** were isolated from this reaction as described below.

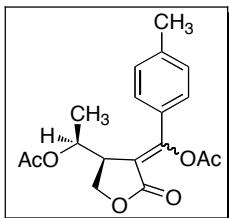


6-methyl-1-(4-methylbenzoyl)-3-oxabicyclo[3.1.0]hexan-2-one. The product was purified by gradient column chromatography (gradient = 80% hexanes/20% EtOAc to 50% hexanes/50% EtOAc) and isolated as a white solid (345 mg, 46 % yield, mp = 112.0–114.0 °C, R_f = 0.26 in 70% hexanes/30% EtOAc). ^1H NMR (500 MHz, CDCl_3): δ 7.81 (d, J = 8.5 Hz, 2H), 7.30 (d, J = 8.5 Hz, 2H), 4.60 (dd, J = 10.0, 5.5 Hz, 1H), 4.27 (d, J = 10.0 Hz, 1H), 2.89 (dd, J = 8.0, 5.5 Hz, 1H), 2.44 (s, 3H), 2.20 (dq, J = 8.0, 6.5 Hz, 1H), 1.34 (d, J = 6.5 Hz, 3H). ^{13}C $\{^1\text{H}\}$ NMR (100.7 MHz, CDCl_3): δ 192.2, 171.3, 144.6, 133.1, 129.5, 129.2, 64.5, 41.8, 30.6, 24.9, 21.8, 7.8. HRMS Electrospray with Na^+ added: $[\text{M}+\text{Na}]^+$ calcd for $\text{C}_{14}\text{H}_{14}\text{O}_3$: 253.0841. Found: 253.0849. IR (Nujol mull): 1760, 1655 cm^{-1} .

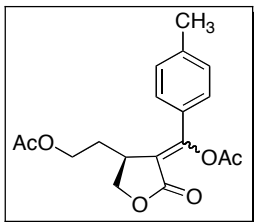


(*Z*)-(2-oxo-4-vinyldihydrofuran-3(2*H*)-ylidene)(*p*-tolyl)methyl acetate. The product was purified by gradient column chromatography (gradient = 80% hexanes/20% EtOAc to 50% hexanes/50% EtOAc) and isolated as a yellow oil (R_f = 0.31 in 70% hexanes/30% EtOAc). Analytically pure material was isolated by further purification by HPLC (85% hexanes/15% EtOAc, 24 mL/min, Waters μ -porasil 19.1 mm). Isolated yield was not

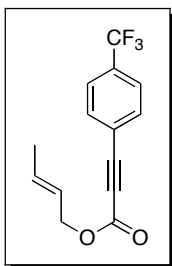
determined due to difficulties in purification, but was found to be 7% by calibrated HPLC after 1.5 hours. Independent experiments show this compound decomposes relative to an internal standard under the optimized reaction conditions. ^1H NMR (400 MHz, CDCl_3): δ 7.46 (d, $J = 8.0$ Hz, 2H), 7.20 (d, $J = 8.0$ Hz, 2H), 5.87 (ddd, $J = 17.2, 10.0, 6.0$ Hz, 1H), 5.25 (dd, $J = 17.2, 10.0$ Hz, 2H), 4.36 (dd, $J = 9.0, 7.2$ Hz, 1H), 4.10 (dd, $J = 9.0, 2.8$ Hz, 1H), 3.93 (m, 1H) 2.38 (s, 3H), 2.34 (s, 3H). ^{13}C $\{^1\text{H}\}$ NMR (100.6 MHz, CDCl_3): δ 168.3, 167.4, 158.5, 141.0, 135.6, 129.3, 128.9, 128.6, 117.2, 116.1, 69.2, 43.9, 21.5, 20.8. HRMS Electrospray with Na^+ added: $[\text{M}+\text{Na}]^+$ calcd for $\text{C}_{16}\text{H}_{16}\text{O}_4$: 295.0946. Found: 295.0942. IR (Thin film): 1765, 1759 cm^{-1} .



(Z)-1-(4-(acetoxymethyl)phenyl)-5-oxotetrahydrofuran-3-yl ethyl acetate. The product was purified by gradient column chromatography (gradient = 80% hexanes/20% EtOAc to 50% hexanes/50% EtOAc) and isolated as a yellow oil ($R_f = 0.20$ in 70% hexanes/30% EtOAc). Analytically pure material was obtained from further purification by HPLC (85% hexanes/15% EtOAc, 24 mL/min, Waters μ -porasil 19.1 mm). The isolated yield was not determined due to loss during purification. However, HPLC analysis of the crude reaction mixture showed that **RE-1** ($\text{X}=\text{CH}_3$) was formed in 2% yield. ^1H NMR (500 MHz, CDCl_3): δ 7.48 (d, $J = 8.0$ Hz, 2H), 7.21 (d, $J = 8.0$ Hz, 2H), 5.29 (m, 1H), 4.42 (d, $J = 10.0$ Hz, 1H), 4.28 (dd, $J = 10.0, 7.5$ Hz, 1H), 3.64 (m, 1H), 2.37 (s, 3H), 2.31 (s, 3H), 2.07 (s, 3H), 1.25 (d, $J = 6.5$ Hz, 3H). ^{13}C $\{^1\text{H}\}$ NMR (100.6 MHz, CDCl_3): δ 168.5, 167.4, 161.4, 158.3, 135.7, 130.7, 124.4, 117.1, 115.3, 113.4, 69.2, 55.3, 53.4, 44.1, 20.8. Note that two peaks in the ^{13}C NMR spectrum coincidentally overlap. HRMS Electrospray with Na^+ added: $[\text{M}+\text{Na}]^+$ calcd for $\text{C}_{18}\text{H}_{20}\text{O}_6$: 355.1158. Found: 355.1160. IR (Thin film): 1760, 1738, 1653 cm^{-1} .



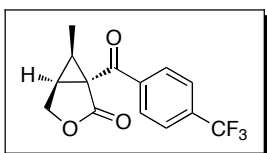
(Z)-2-(4-(acetoxymethyl)methylene)-5-oxotetrahydrofuran-3-yl ethyl acetate. RE-2 (X=CH₃). The product was purified by gradient column chromatography (gradient = 80% hexanes/20% EtOAc to 50% hexanes/50% EtOAc) and isolated as a yellow oil (R_f = 0.16 in 70% hexanes/30% EtOAc). Analytically pure material was obtained from further purification by HPLC (80% hexanes/20% EtOAc, 24 mL/min, Waters μ -porasil 19.1 mm). The isolated yield was not determined due to loss during purification. However, HPLC analysis of the crude reaction mixture showed that **RE-2 (X=CH₃)** was formed in 6% yield. ¹H NMR (500 MHz, CDCl₃): δ 7.43 (d, J = 8.0 Hz, 2H), 7.23 (d, J = 8.0 Hz, 2H), 4.38 (dd, J = 9.0, 7.0 Hz, 1H), 4.14 (dd, J = 9.0, 2.5 Hz, 1H), 4.06-4.01 (m, 1H), 3.96 (dt, J = 11.5, 6.0 Hz, 1H), 3.65-3.61 (m, 1H), 2.38 (s, 3H), 2.30 (s, 3H), 1.95 (s, 3H), 1.83-1.77 (m, 2H). ¹³C {¹H} NMR (100.6 MHz, CDCl₃): δ 170.6, 168.5, 168.1, 154.0, 141.1, 130.9, 129.5, 127.7, 116.8, 69.7, 61.4, 35.7, 32.0, 21.4, 20.8, 20.7. HRMS Electrospray with Na⁺ added: [M+Na]⁺ calcd for C₁₈H₂₀O₆: 355.1158. Found: 355.1160. IR (Thin film): 1749, 1649 cm⁻¹.



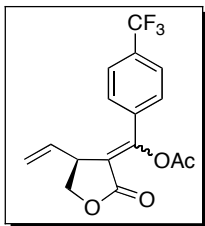
(E)-but-2-enyl 3-(4-(trifluoromethyl)phenyl)propiolate. The enyne was obtained as a clear oil (R_f = 0.32 in 95% hexanes/5% EtOAc). ¹H NMR (500 MHz, CDCl₃): δ 7.70 (d, J = 8.5 Hz, 2H), 7.65 (d, J = 8.5 Hz, 2H), 5.90-5.84 (m, 1H), 5.66-5.59 (m, 1H), 4.66 (d, J = 7.0 Hz, 2H), 1.74 (d, J = 7.0 Hz, 3H). ¹³C {¹H} NMR (100.7 MHz, CDCl₃): δ 153.4, 133.1, 132.2 (q, ² J_{CF} = 33.2 Hz), 131.1, 125.5 (q, ³ J_{CF} = 3.9 Hz), 123.9, 123.5 (q, ¹ J_{CF} =

272.4 Hz), 123.0, 83.9, 82.2, 66.9, 17.8. ^{19}F NMR (376.3 MHz): δ -63.0. HRMS (EI): $[\text{M}]^+$ calcd for $\text{C}_{14}\text{H}_{11}\text{F}_3\text{O}_2$: 268.0711. Found: 268.0709. IR (Thin Film): 1712 cm^{-1} .

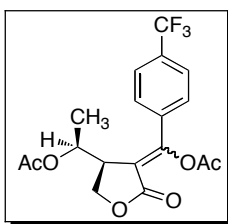
Reaction with enyne (*E*)-but-2-enyl 3-(4-(trifluoromethyl)phenyl)propiolate. The substrate (1.200 g, 3.47 mmol, 1 equiv), $\text{PhI}(\text{OAc})_2$ (11.53 g, 35.8 mmol, 8 equiv), and $\text{Pd}(\text{OAc})_2$ (50.2 mg, 5 mol %) were combined in AcOH (28 mL) and heated at $80\text{ }^\circ\text{C}$ for 6 h. After the workup described in the standard procedure above, products **CP**, **β -H**, **RE-1**, and **RE-2** were isolated from this reaction as described below.



6-methyl-1-(4-(trifluoromethyl)benzoyl)-3-oxabicyclo[3.1.0]hexan-2-one. The product was purified by gradient column chromatography (gradient = 80% hexanes/20% EtOAc to 50% hexanes/50% EtOAc) and isolated as a yellow solid (mp = $78.4\text{--}79.0\text{ }^\circ\text{C}$, $R_f = 0.25$ in 70% hexanes/30% EtOAc). Analytically pure material was obtained from further purification by HPLC (85% hexanes/15% EtOAc, 24 mL/min, Waters μ -porasil 19.1 mm). The isolated yield was not determined due to loss during purification. However, HPLC analysis of the crude reaction mixture showed that **CP** ($X=\text{CF}_3$) was formed in 36% yield. ^1H NMR (400 MHz, CDCl_3): δ 7.96 (d, $J = 8.0$ Hz, 2H), 7.73 (d, $J = 8.0$ Hz, 2H), 4.58 (dd, $J = 10.0, 5.2$ Hz, 1H), 4.27 (dd, $J = 10.0, 1.2$ Hz, 1H), 3.00 (ddd, $J = 8.4, 5.2, 1.2$ Hz, 1H), 2.22 (dq, $J = 8.4, 6.4$ Hz, 1H), 1.36 (d, $J = 6.4$ Hz, 3H). ^{13}C $\{^1\text{H}\}$ NMR (100.6 MHz, CDCl_3): δ 192.5, 170.6, 138.5, 134.8 (q, $^2J_{\text{CF}} = 32$ Hz), 129.7, 125.5 (q, $^3J_{\text{CF}} = 4.0$ Hz), 123.5 (q, $^1J_{\text{CF}} = 271.0$ Hz), 64.4, 42.1, 31.2, 26.7, 7.9. ^{19}F NMR (376.3 MHz): δ -63.3. HRMS Electrospray with Na^+ added: $[\text{M}+\text{Na}]^+$ calcd for $\text{C}_{14}\text{H}_{11}\text{F}_3\text{O}_3$: 307.0558. Found: 307.0547. IR (Nujol mull): $1775, 1680\text{ cm}^{-1}$.

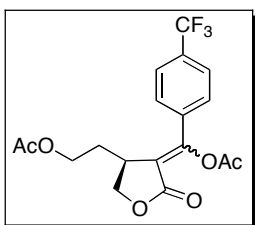


(Z)-2-oxo-4-vinyldihydrofuran-3(2H)-ylidene(4-(trifluoromethyl)phenyl)methyl acetate. The product was purified by gradient column chromatography (gradient = 80% hexanes/20% EtOAc to 50% hexanes/50% EtOAc) and isolated as a yellow oil ($R_f = 0.38$ in 70% hexanes/30% EtOAc). Analytically pure material was obtained from further purification by HPLC (90% hexanes/10% EtOAc, 24 mL/min, Waters μ -porasil 19.1 mm). Isolated yield was not determined due to difficulties in purification, but was found to be 2% by calibrated HPLC after 6 hours. ^1H NMR (400 MHz, CDCl_3): δ 7.63 (s, 4H), 5.83 (ddd, $J = 16.8, 10.0, 8.4$ Hz, 1H), 5.23 (multiple peaks, 2H), 4.47 (t, $J = 8.8$ Hz, 1H), 4.06 (dd, $J = 8.8, 5.2$ Hz, 1H), 3.92 (td, $J = 8.4, 5.2$ Hz, 1H), 2.11 (s, 3H). ^{13}C $\{^1\text{H}\}$ NMR (100.7 MHz, CDCl_3): δ 168.4, 167.5, 152.6, 137.0, 135.4, 132.2 (q, $^2J_{\text{CF}} = 32$ Hz), 128.4, 125.5 (q, $^3J_{\text{CF}} = 3.9$ Hz), 123.6 (q, $^1J_{\text{CF}} = 272.5$ Hz), 118.9, 117.8, 70.2, 43.0, 20.7. HRMS Electrospray with Na^+ added: $[\text{M}+\text{Na}]^+$ calcd for $\text{C}_{16}\text{H}_{13}\text{F}_3\text{O}_4$: 349.0664. Found: 349.0653. IR (Thin film): 1760 cm^{-1} .

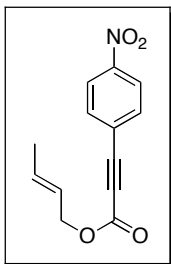


(Z)-1-(4-(acetoxymethyl)-4-(trifluoromethyl)phenyl)methylene-5-oxotetrahydrofuran-3-ylidene ethyl acetate. The product was purified by gradient column chromatography, 80% hexanes/20% EtOAc – 50% hexanes/50% EtOAc, and isolated as a yellow oil ($R_f = 0.18$ in 70% hexanes/30% EtOAc). Analytically pure material was isolated by further purification by HPLC (85% hexanes/15% EtOAc, 24 mL/min, Waters μ -porasil 19.1 mm). The isolated yield was not determined due to loss during purification. However, HPLC analysis of the crude reaction mixture showed that **RE-1** ($X = \text{CF}_3$) was formed in 5% yield. ^1H NMR (400 MHz, CDCl_3): δ 7.67 (multiple peaks, 4H), 5.28 (m, 1H), 4.45

(dd, $J = 9.6, 2.0$ Hz, 1H), 4.31 (dd, $J = 9.6, 7.2$ Hz, 1H), 3.69 (m, 1H), 2.32 (s, 3H), 2.07 (s, 3H), 1.26 (d, $J = 6.4$ Hz, 3H). ^{13}C $\{^1\text{H}\}$ NMR (100.7 MHz, CDCl_3): δ 170.2, 167.9, 167.6, 156.5, 135.1, 132.3 (q, $^2J_{\text{CF}} = 32.6$ Hz), 129.5, 125.0 (q, $^3J_{\text{CF}} = 3.9$ Hz), 123.9 (q, $^1J_{\text{CF}} = 272.1$ Hz), 116.9, 69.3, 65.5, 42.7, 21.1, 20.7, 14.5. ^{19}F NMR (376.3 MHz): δ -63.0. HRMS Electrospray with Na^+ added: $[\text{M}+\text{Na}]^+$ calcd for $\text{C}_{18}\text{H}_{17}\text{F}_3\text{O}_6$: 409.0875. Found: 409.0865. IR (Thin film): 1775, 1757, 1730 cm^{-1} .

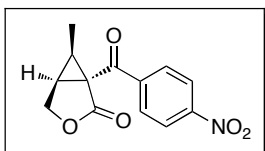


(Z)-2-(4-(acetoxymethylene)-5-oxotetrahydrofuran-3-yl)ethyl acetate. The product was purified by gradient column chromatography (gradient = 80% hexanes/20% EtOAc to 50% hexanes/50% EtOAc) and isolated as a white solid (mp = 141.5-142.4 °C, $R_f = 0.08$ in 70% hexanes/30% EtOAc). Analytically pure material was obtained from further purification by HPLC (85% hexanes/15% EtOAc, 24 mL/min, Waters μ -porasil 19.1 mm). The isolated yield was not determined due to loss during purification. However, HPLC analysis of the crude reaction mixture showed that **RE-2** ($\text{X} = \text{CF}_3$) was formed in 7% yield. ^1H NMR (400 MHz, CDCl_3): δ 7.71 (d, $J = 8.4$ Hz, 2H), 7.66 (d, $J = 8.4$ Hz, 2H), 4.42 (dd, $J = 9.2, 6.8$ Hz, 1H), 4.17 (dd, $J = 9.2, 2.0$ Hz, 1H), 4.05-3.98 (m, 1H), 3.96-3.90 (m, 1H), 3.57-3.51 (m, 1H), 2.32 (s, 3H), 1.92 (s, 3H), 1.81-1.74 (m, 2H). ^{13}C $\{^1\text{H}\}$ NMR (100.7 MHz, CDCl_3): δ 170.8, 167.8, 167.5, 155.3, 135.4, 132.0 (q, $^2J_{\text{CF}} = 32.7$ Hz), 129.4, 124.9 (q, $^1J_{\text{CF}} = 3.8$ Hz), 120.2, 123.5 (q, $^1J_{\text{CF}} = 270.2$ Hz), 69.8, 61.6, 36.6, 32.2, 20.9, 20.8. ^{19}F NMR (376.3 MHz): δ -63.0. HRMS Electrospray with Na^+ added: $[\text{M}+\text{Na}]^+$ calcd for $\text{C}_{18}\text{H}_{17}\text{F}_3\text{O}_6$: 409.0875. Found: 409.0870. IR (Nujol mull): 1763, 1733, 1666 cm^{-1} .



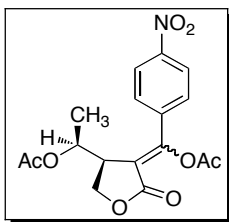
(E)-but-2-enyl 3-(4-nitrophenyl)propiolate. The enyne was obtained as a pale yellow solid (mp = 57.1-58.8 °C, R_f = 0.23 in 95% hexanes/5% EtOAc). ^1H NMR (500 MHz, CDCl_3): δ 8.23 (d, J = 8.5 Hz, 2H), 7.72 (d, J = 8.5 Hz, 2H), 5.91-5.86 (m, 1H), 5.63 (qd, J = 7.0, 1.5 Hz, 1H), 4.67 (d, J = 7.0 Hz, 2H), 1.74, (d, J = 7.0 Hz, 3H). ^{13}C $\{^1\text{H}\}$ NMR (100.7 MHz, CDCl_3): δ 153.1, 133.7, 133.4, 126.3, 123.8, 123.7, 122.9, 84.1, 82.9, 67.1, 17.8. HRMS (EI): $[\text{M}]^+$ calcd for $\text{C}_{13}\text{H}_{11}\text{NO}_4$: 245.0688. Found: 245.0698. IR (Thin film): 1701 cm^{-1} .

Reaction with enyne (E)-but-2-enyl 3-(4-nitrophenyl)propiolate. The substrate (0.452 g, 1.84 mmol, 1 equiv), $\text{PhI}(\text{OAc})_2$ (4.749 g, 14.7 mmol, 8 equiv), and $\text{Pd}(\text{OAc})_2$ (20.7 mg, 5 mol %) were combined in AcOH (11.6 mL) and heated at 80 °C for 8 h. After the workup described in the standard procedure above, products **CP** (X = NO_2) and **RE-1** (X = NO_2) were isolated from this reaction as described below.



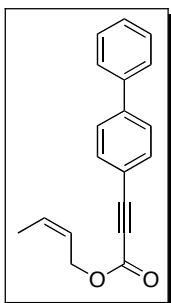
6-methyl-1-(4-nitrobenzoyl)-3-oxabicyclo[3.1.0]hexan-2-one. The product was purified by gradient column chromatography (gradient = 80% hexanes/20% EtOAc to 50% hexanes/50% EtOAc) and isolated as a clear oil (R_f = 0.16 in 70% hexanes/30% EtOAc). Analytically pure material was obtained from further purification by HPLC (85% hexanes/15% EtOAc, 24 mL/min, Waters μ -porasil 19.1 mm). The isolated yield was not determined due to loss during purification. However, HPLC analysis of the crude reaction mixture showed that **CP** (X = NO_2) was formed in 43% yield. ^1H NMR (400 MHz, CDCl_3): δ 8.33 (d, J = 9.0 Hz, 2H), 8.02 (d, J = 9.0 Hz, 2H), 4.59 (dd, J = 10.0, 5.6 Hz,

1H), 4.29 (d, $J = 10.0$ Hz, 1H), 3.07 (ddd, $J = 8.0, 5.2, 1.2$ Hz, 1H), 2.27 (dq, $J = 8.0, 6.0$ Hz, 1H), 1.38 (d, $J = 6.0$ Hz, 3H). ^{13}C $\{^1\text{H}\}$ NMR (100.7 MHz, CDCl_3): δ 192.4, 170.4, 150.3, 140.6, 130.3, 123.6, 64.36, 42.4, 31.6, 27.7, 8.0. HRMS Electrospray with Na^+ added: $[\text{M}+\text{Na}]^+$ calcd for $\text{C}_{13}\text{H}_{11}\text{NO}_5$: 284.0535. Found: 284.0542. IR (Nujol mull): 1766, 1674 cm^{-1} .

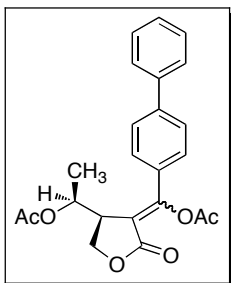


(Z)-1-(4-(acetoxymethylene)-5-oxotetrahydrofuran-3-yl)ethyl acetate.

The product was purified by gradient column chromatography (gradient = 80% hexanes/20% EtOAc to 50% hexanes/50% EtOAc) and isolated as a clear oil ($R_f = 0.11$ in 70% hexanes/30% EtOAc). Analytically pure material was obtained from further purification by HPLC (85% hexanes/15% EtOAc, 24 mL/min, Waters μ -porasil 19.1 mm). The isolated yield was not determined due to loss during purification. However, HPLC analysis of the crude reaction mixture showed that **RE-1** ($\text{X} = \text{NO}_2$) was formed in 8% yield. ^1H NMR (400 MHz, CDCl_3): δ 8.25 (d, $J = 9.2$ Hz, 2H), 7.72 (d, $J = 9.2$ Hz, 2H), 5.27 (dq, $J = 6.8, 4.4$ Hz, 1H), 4.47 (dd, $J = 10.0, 2.0$ Hz, 1H), 4.32 (dd, $J = 10.0, 7.2$ Hz, 1H), 3.72-3.69 (m, 1H), 2.32 (s, 3H), 2.08 (s, 3H), 1.27 (d, $J = 6.8$ Hz, 3H). ^{13}C $\{^1\text{H}\}$ NMR (100.7 MHz, CDCl_3): δ 170.3, 168.0, 167.5, 155.4, 148.7, 137.8, 130.2, 123.2, 118.0, 69.3, 65.7, 42.7, 21.1, 20.7, 14.7. HRMS Electrospray with Na^+ added: $[\text{M}+\text{Na}]^+$ calcd for $\text{C}_{17}\text{H}_{17}\text{NO}_8$: 386.0852. Found: 386.0858. IR (Thin film): 1760, 1738, 1664 cm^{-1} .



(Z)-but-2-enyl 3-(biphenyl-4-yl)propiolate (53). Enyne **53** was obtained as a pale yellow oil ($R_f = 0.11$ in 95% hexanes/5% EtOAc) along with ~10% of an unknown impurity. The impurity was removed by further purification via HPLC (99.5% hexanes/0.5% EtOAc, 60mL/min, Waters μ -porasil 30 mm). ^1H NMR (500 MHz, CDCl_3): δ 7.63 (d, $J = 8.5$ Hz, 2H), 7.58 (multiple peaks, 4H), 7.44 (t, $J = 7.5$ Hz, 2H), 7.24 (t, $J = 7.5$ Hz, 1H), 5.85-5.78 (m, 1H), 5.67-5.61 (m, 1H), 4.82 (d, $J = 7.0$ Hz, 2H), 1.75 (d, $J = 7.5$ Hz, 3H). ^{13}C $\{^1\text{H}\}$ NMR (125.7 MHz, CDCl_3): δ 154.0, 143.3, 139.7, 133.4, 130.7, 128.9, 128.1, 127.1, 127.0, 123.2, 118.2, 86.3, 81.1, 61.4, 13.1. HRMS (EI): $[\text{M}]^+$ calcd for $\text{C}_{19}\text{H}_{16}\text{O}_2$: 276.1150. Found: 276.1157. IR (Thin film): 1707 cm^{-1} .



(Z)-1-(4-(acetoxymethylene)-5-oxotetrahydrofuran-3-yl)ethyl acetate (54). Substrate **53** (0.790 g, 2.86 mmol, 1 equiv), $\text{PhI}(\text{OAc})_2$ (7.362 g, 22.9 mmol, 8 equiv), and $\text{Pd}(\text{OAc})_2$ (32.1 mg, 5 mol %) were dissolved in AcOH (18 mL), and heated at $80\text{ }^\circ\text{C}$ for 2 h. Product **54** was purified by gradient column chromatography (gradient = 80% hexanes/20% EtOAc to 50% hexanes/50% EtOAc) and isolated as a white solid (mp = $150.0\text{-}151.1\text{ }^\circ\text{C}$, $R_f = 0.22$ in 70% hexanes/30% EtOAc). Analytically pure material was obtained from further purification by HPLC (85% hexanes/15% EtOAc, 24 mL/min, Waters μ -porasil 19.1 mm). The isolated yield was not determined due to loss during purification. However, HPLC analysis of the crude reaction mixture showed that **54** was formed in 8% yield. ^1H NMR (500 MHz, CDCl_3): δ 7.67 (d, $J = 8.0$ Hz, 2H), 7.61 (multiple peaks, 4H), 7.45 (t, 7.0 Hz, 2H), 7.37 (t, 7.0 Hz, 1H), 5.31 (m, 1H), 4.45 (dd, $J = 2.0, 9.5$ Hz, 1H), 4.31 (dd, $J = 8.0, 10.0$ Hz, 1H), 3.68 (m, 1H), 2.35 (s, 3H), 2.08 (s, 3H), 1.27 (d, $J = 6.5$ Hz, 3H). ^{13}C $\{^1\text{H}\}$ NMR (100.6 MHz, CDCl_3): δ 170.3, 168.2, 143.7, 140.2, 130.5, 129.5, 128.8, 127.9, 127.2, 126.7, 115.1, 69.6, 65.3, 42.9, 21.2, 20.9,

14.5. Two peaks coincidentally overlap. HRMS (EI): $[M]^+$ calcd for $C_{23}H_{22}O_6$: 394.1416. Found: 394.1417. IR (Nujol mull): 1776, 1758, 1732 cm^{-1} .

2.7 References

1. Zhang, Q. H.; Lu, X. Y. *J. Am. Chem. Soc.* **2000**, *122*, 7604-7605.
2. Trofast, J.; Wickberg, B. *Tetrahedron* **1977**, *33*, 875-879.
3. Koft, E. R.; Smith, A. B. *J. Am. Chem. Soc.* **1982**, *104*, 2659-2661.
4. Brown, R. F. C.; Teo, P. Y. T. *Tetrahedron Lett.* **1984**, *25*, 5585-5588.
5. Ichimura, M.; Ogawa, T.; Katsumata, S.; Takahashi, K.; Takahashi, I.; Nakano, H. *J. Antibiot.* **1991**, *44*, 1045-1053.
6. Boger, D. L.; Garbaccio, R. M.; Jin, Q. *J. Org. Chem.* **1997**, *62*, 8875-8891.
7. Kirkland, T. A.; Colucci, J.; Geraci, L. S.; Marx, M. A.; Schneider, M.; Kaelin, D. E.; Martin, S. F. *J. Am. Chem. Soc.* **2001**, *123*, 12432-12433.
8. Swain, N. A.; Brown, R. C. D.; Bruton, G. *J. Org. Chem.* **2004**, *69*, 122-129.
9. Ok, T.; Jeon, A.; Lee, J.; Lim, J. H.; Hong, C. S.; Lee, H. S. *J. Org. Chem.* **2007**, *72*, 7390-7393.
10. Clive, D. L. J.; Liu, D. Z. *J. Org. Chem.* **2008**, *73*, 3078-3087.
11. Chavan, S. P.; Pasupathy, K.; Shivasankar, K. *Synth. Commun.* **2004**, *34*, 397-404.
12. Doyle, M. P.; Austin, R. E.; Bailey, A. S.; Dwyer, M. P.; Dyatkin, A. B.; Kalinin, A. V.; Kwan, M. M. Y.; Liras, S.; Oalman, C. J.; Pieters, R. J.; Protopopova, M. N.; Raab, C. E.; Roos, G. H. P.; Zhou, Q. L.; Martin, S. F. *J. Am. Chem. Soc.* **1995**, *117*, 5763-5775.
13. Aubert, C.; Buisine, O.; Malacria, M. *Chem. Rev.* **2002**, *102*, 813-834.
14. Mamane, V.; Gress, T.; Krause, H.; Furstner, A. *J. Am. Chem. Soc.* **2004**, *126*, 8654-8655.
15. Harrak, Y.; Blaszykowski, C.; Bernard, M.; Cariou, K.; Mainetti, E.; Mouries, V.; Dhimane, A. L.; Fensterbank, L.; Malacria, M. *J. Am. Chem. Soc.* **2004**, *126*, 8656-8657.
16. Luzung, M. R.; Markham, J. P.; Toste, F. D. *J. Am. Chem. Soc.* **2004**, *126*, 10858-10859.
17. Doyle, M. P.; Pieters, R. J.; Martin, S. F.; Austin, R. E.; Oalman, C. J.; Muller, P. *J. Am. Chem. Soc.* **1991**, *113*, 1423-1424.

18. Doyle, M. P.; Peterson, C. S.; Parker, D. L. *Angew. Chem. Int. Ed.* **1996**, *35*, 1334-1336.
19. Bohmer, J.; Grigg, R.; Marchbank, J. D. *Chem. Commun.* **2002**, 768-769.
20. Meyer, F. E.; Parsons, P. J.; Demeijere, A. J. *J. Org. Chem.* **1991**, *56*, 6487-6488.
21. Owczarczyk, Z.; Lamaty, F.; Vawter, E. J.; Negishi, E. *J. Am. Chem. Soc.* **1992**, *114*, 10091-10092.
22. Grigg, R.; Dorrity, M. J.; Malone, J. F.; Sridharan, V.; Sukirthalingam, S. *Tetrahedron Lett.* **1990**, *31*, 1343-1346.
23. Grigg, R.; Sridharan, V. *Tetrahedron Lett.* **1992**, *33*, 7965-7968.
24. Marco-Martinez, J.; Lopez, V.; Bunel, E.; Simancas, R.; Cardenas, D. J. *J. Am. Chem. Soc.* **2007**, *129*, 1874.
25. Welbes, L. L.; Lyons, T. W.; Cychosz, K. A.; Sanford, M. S. *J. Am. Chem. Soc.* **2007**, *129*, 5836-5837.
26. Lyons, T. W.; Sanford, M. S. *Tetrahedron* **2009**, *65*, 3211-3221.
27. Zhang, Q. H.; Lu, X. Y.; Han, X. L. *J. Org. Chem.* **2001**, *66*, 7676-7684.
28. Zhao, L.; Lu, X.; Xu, W. *J. Org. Chem.* **2005**, *70*, 4059.
29. Heck, R. F. *Org. React.* **1982**, *27*, 345-390.
30. Hartwig, J. F.; Negishi, E.; de Meijere, A., *Handbook of Organopalladium Chemistry for Organic Synthesis*. Wiley-Interscience: New York, NY, 2002.
31. Larhed, M. H., A., In *Handbook of Organopalladium Chemistry for Organic Synthesis*, Negishi, E., Ed. Wiley-Interscience: New York, NY, 2002.
32. Soderberg, B. C., In *Comprehensive Organometallic Chemistry II*, Hegedus, L. S. A., E. W.; Stone, F. G. A., Ed. Pergamon: Oxford, 1995; Vol. 12, pp 259-287.
33. Lu, X. Y.; Zhu, G. X.; Wang, Z. *Synlett* **1998**, 115.
34. Wang, Z.; Zhang, Z.; Lu, X. *Organometallics* **2000**, *19*, 775-780.
35. Zhang, Q. G.; Xu, W.; Lu, X. Y. *J. Org. Chem.* **2005**, *70*, 1505-1507.
36. Muñiz, K.; Hovelmann, C. H.; Streuff, J. *J. Am. Chem. Soc.* **2008**, *130*, 763-773.
37. Liu, G. S.; Stahl, S. S. *J. Am. Chem. Soc.* **2006**, *128*, 7179-7181.

38. Baeckvall, J. E.;Bjoerkman, E. E. *The Journal of Organic Chemistry* **1980**, *45*, 2893-2898.
39. Tichenor, M. S.; Trzupek, J. D.; Kastrinsky, D. B.; Shiga, F.; Hwang, I.;Boger, D. L. *J. Am. Chem. Soc.* **2006**, *128*, 15683-15696.
40. Boger, D. L.;Garbaccio, R. M. *J. Org. Chem.* **1999**, *64*, 8350-8362.
41. Dick, A. R.; Hull, K. L.;Sanford, M. S. *J. Am. Chem. Soc.* **2004**, *126*, 2300-2301.
42. Desai, L. V.; Malik, H. A.;Sanford, M. S. *Org. Lett.* **2006**, *8*, 1141-1144.
43. Dick, A. R.; Kampf, J. W.;Sanford, M. S. *J. Am. Chem. Soc.* **2005**, *127*, 12790-12791.
44. Li, Y.; Song, D.;Dong, V. M. *J. Am. Chem. Soc.* **2008**, *130*, 2962-2964.
45. Tong, X. F.; Beller, M.;Tse, M. K. *J. Am. Chem. Soc.* **2007**, *129*, 4906-4907.
46. Liu, H.; Yu, J.; Wang, L.;Tong, X. *Tetrahedron Lett.* **2008**, *49*, 6924-6928.
47. Tsujihara, T.; Takenaka, K.; Onitsuka, K.; Hatanaka, M.;Sasai, H. *J. Am. Chem. Soc.* **2009**, *131*, 3452-3453.
48. Yin, G.;Liu, G. *Angew. Chem. Int. Ed.* **2008**, *47*, 5442-5445.

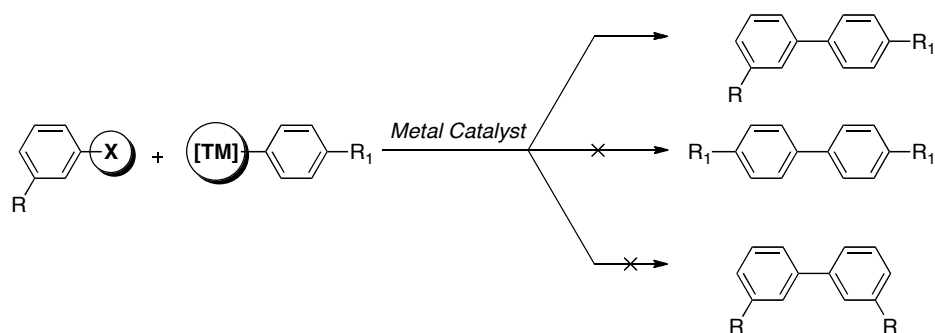
Chapter 3

Controlling Site Selectivity in Palladium-Catalyzed Aryl-Aryl Oxidative Cross-Coupling Reactions

3.1 Background and Significance

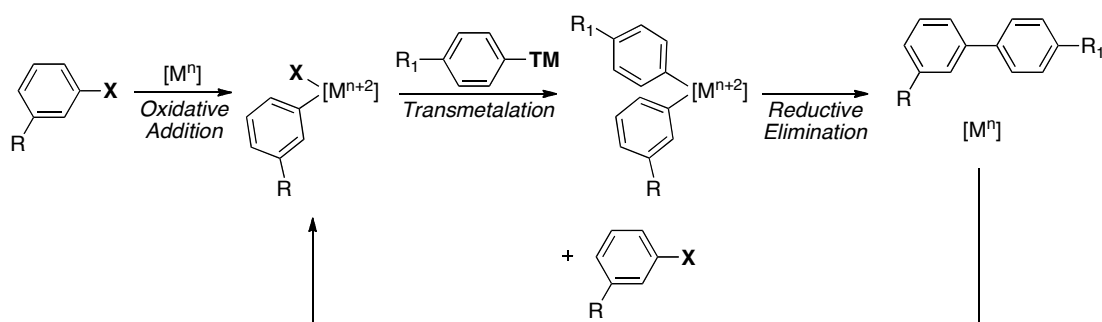
The biaryl linkage is an important structural motif that is prevalent in numerous organic compounds, including natural products,¹⁻³ pharmaceuticals,^{4, 5} agrochemicals,⁶ and conjugated materials⁷. The key aryl-aryl bond forming strategy to construct these moieties has traditionally involved metal-catalyzed cross-coupling using two prefunctionalized arenes.^{8, 9} Typically an aryl-halide is coupled to an aryl group with an appended transmetallating reagent. In this approach, the prefunctionalized aryl-halide and transmetallating reagents control both the selectivity and reactivity of the reaction. The metal catalyst reacts only with the prefunctionalized halide or transmetallating reagent in preference to the relatively unreactive C–H bonds (Scheme 3.1). Additionally, the prefunctionalized coupling partners react with each other in preference to themselves (homocoupling).

Scheme 3.1 Traditional Cross-Coupling



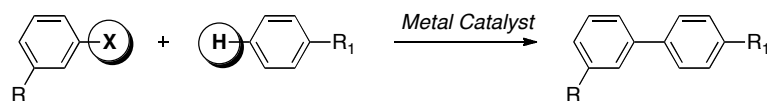
These reactions often proceed by oxidative addition of a low valent metal catalyst $[M^n]$ into the aryl-halide bond, transmetalation with the coupling partner, and reductive elimination to give the biaryl product and regenerate the $[M^n]$ catalyst (Scheme 3.2). Cross-couplings have been carried out with numerous late transition metal catalysts including Pd, Ni, or Cu based catalysts.¹⁰⁻¹⁵ However, the most prevalent and arguably the most versatile catalyst for these reactions, and the focus of our subsequent investigations, has been Pd.

Scheme 3.2 Typical Mechanism for Metal-Catalyzed Cross-Coupling

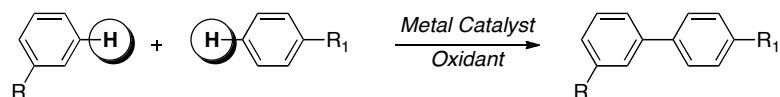


While this cross-coupling strategy continues to be of incredible synthetic importance and utility due to its high catalytic efficiency, it remains fundamentally limited by the necessity for prefunctionalized starting materials. To reduce the need for prefunctionalized materials and increase the atom economy of biaryl synthesis, we and others have pursued two general strategies. The first involves direct arylation, in which one prefunctionalized arene is coupled to an unfunctionalized arene partner (Scheme 3.3).¹⁶⁻²¹ In the context of Pd catalysis this has taken one of two forms; a Pd^{0/II} or a Pd^{II/II+n} reoxidation cycle. The second strategy is known as oxidative coupling, in which two unfunctionalized arenes (aryl-H and aryl'-H) are coupled together, evolving only two equivalents of H⁺ (Scheme 3.4).²²⁻³³

Scheme 3.3 Direct Arylation

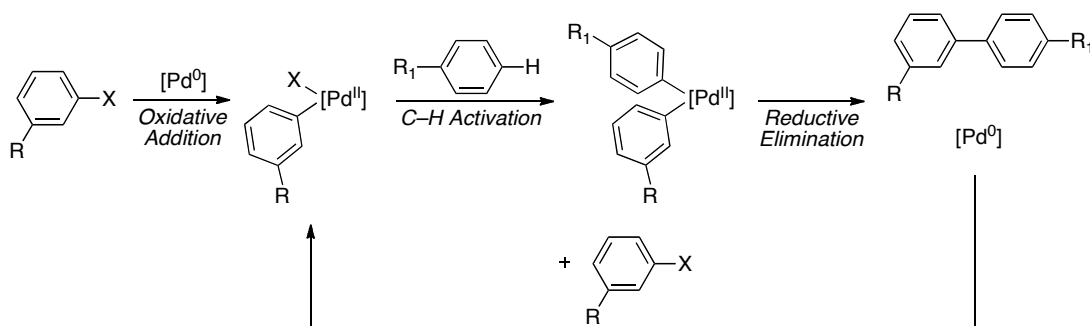


Scheme 3.4 Oxidative Coupling Strategy



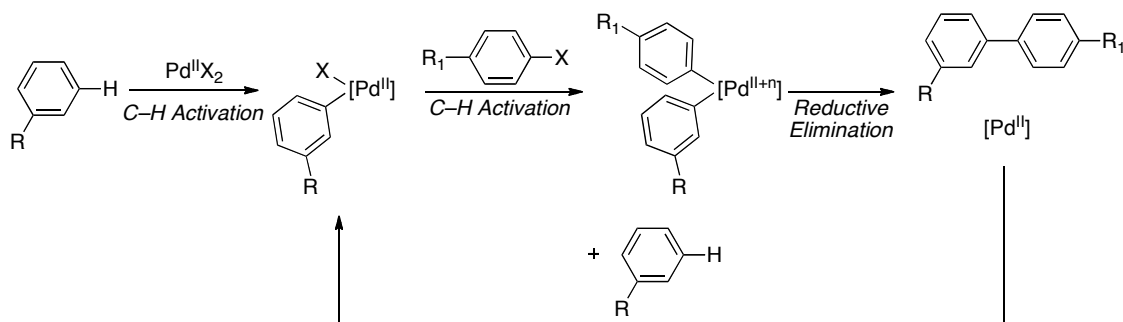
Direct Arylation. One distinct advantage of Pd-catalyzed direct arylation is that prefunctionalization of one coupling partner is no longer required. This eliminates one costly step in biaryl synthesis and reduces the generation of one equivalent of waste, instead producing only one equivalent of H⁺. There are the two common forms of Pd-catalyzed direct arylation involving two different reoxidation cycles. The first typically involves the generation of a Pd^{II}-aryl intermediate from a Pd⁰ catalyst via oxidative addition, then C–H activation of an unfunctionalized arene, and reductive elimination to give the biaryl product (Scheme 3.5).

Scheme 3.5 Mode 1 of Direct Arylation



The second mode of direct arylation generally proceeds by initial C–H activation of an unactivated arene, followed by oxidative functionalization utilizing a prefunctionalized aryl partner (Scheme 3.6). Each mode of direct arylation still has the drawback of generating one equivalent of waste by the use of one prefunctionalized coupling partner.

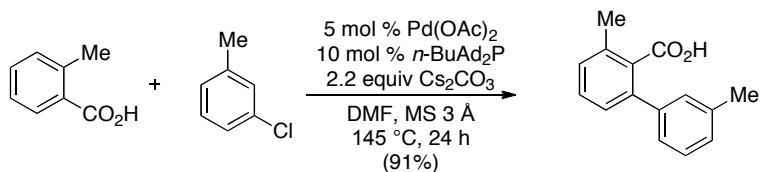
Scheme 3.6 Mode 2 of Direct Arylation



A key challenge for direct arylation methodologies is controlling the site selectivity of the C–H activation step. In order to develop a highly efficient methodology, one C–H bond of the arene must react in preference to all others. This has generally been accomplished in one of three ways; (i) appending a ligand to the substrate, (ii) electronic activation of the substrate, or (iii) steric modification of the substrate.^{18, 21}

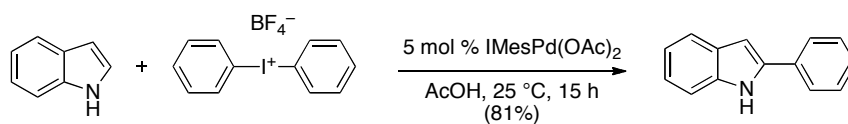
One example of a ligand-directed approach to controlling direct arylation comes from Daugulis and coworkers,³⁴ who were able to show that an appended carboxylic acid could direct activation of the proximal C–H bond (Scheme 3.7). This reaction most likely proceeds through a mechanism similar to that outlined as mode 1 (Scheme 3.5), with oxidative addition into the aryl–Cl bond followed by ligand-directed C–H activation and reductive elimination to give the biaryl product.

Scheme 3.7 Ligand-directed Approach to Direct Arylation (Mode 1)



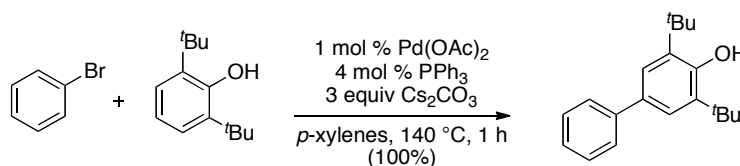
Previous work in our lab has shown that activated arenes such as indoles can be used to control the site selectivity of Pd-catalyzed direct arylation reactions.^{35, 36} These electron rich substrates have been shown to undergo palladation at the more nucleophilic sites of the molecule (C2 and C3). In the presence of a strong diaryliodonium oxidant, the C–H activated indole is oxidized to a high oxidation state Pd-diaryl intermediate and reductive elimination gives the biaryl product (Scheme 3.8).

Scheme 3.8 Activated Arene Approach to Direct Arylation (Mode 2)



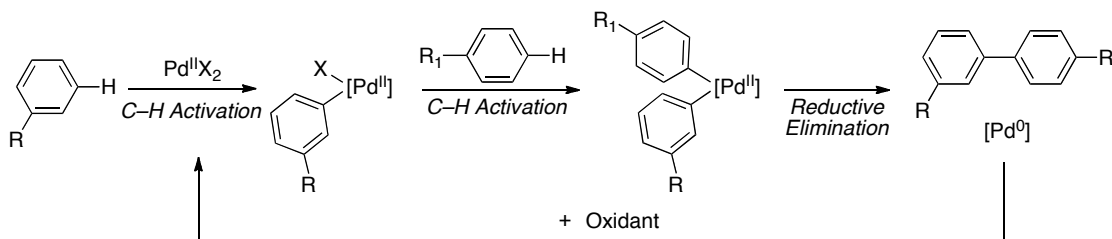
The final approach to controlling site selectivity in Pd-catalyzed direct arylation reactions involves using sterically biased substrates. For example, Miura and coworkers have shown that a sterically encumbered arene like 2,6-di-*tert*-butylphenol will undergo arylation at the most sterically accessible aryl-H bond (Scheme 3.9).³⁷ This reaction also proceeds through mode 1 involving oxidative addition into the aryl-Br bond, C-H activation, and reductive elimination to give the product.

Scheme 3.9 Steric Approach to Direct Arylation (Mode 1)



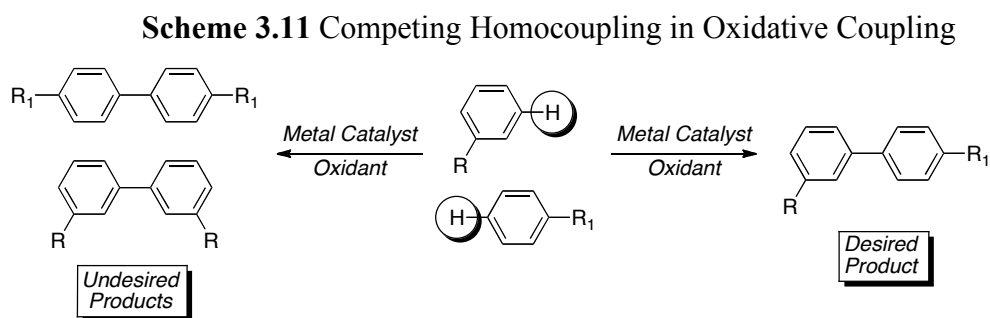
Oxidative Coupling. The second strategy for generating biaryl products uses two unfunctionalized arenes (aryl-H and aryl'-H) in an oxidative coupling to form a C-C bond. This approach is even more atom economical than the direct arylation, as only two equivalents of H^+ are generated from the reaction and there is no need for a prefunctionalization step. Pd-catalyzed oxidative coupling has been developed more recently than the direct arylation strategy and generally proceeds via two sequential C-H activations followed by reductive elimination as seen in Scheme 3.10.

Scheme 3.10 Mechanism of Pd-Catalyzed Oxidative Coupling



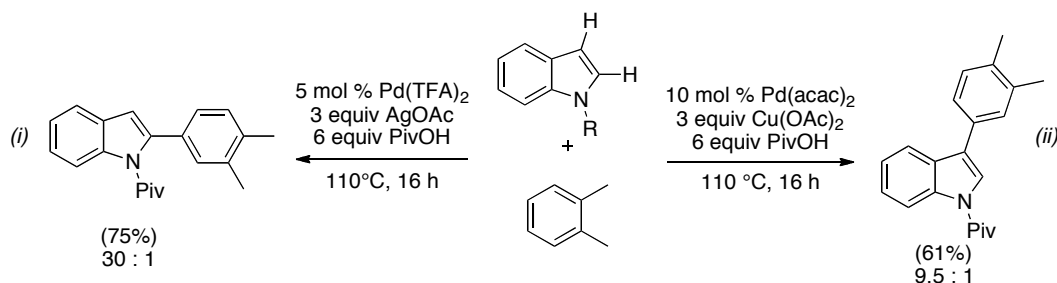
There are three main challenges for Pd-catalyzed C–H oxidative coupling; (i) obtaining site-selectivity for C–H activation, (ii) obtaining chemoselectivity among arene coupling partners, and (iii) choosing an appropriate oxidant to efficiently carry out the transformation. For oxidative coupling to be a practical method a C–H bond on each arene must not only react in preference to others, but that C–H bond must react with the other desired arene in preference to itself. Strategies used to control site-selectivity in this system are analogous to those used in direct arylation and have included appending a ligand to substrates, electronic activation of the substrate, and steric modification of the substrate.

In order to achieve the desired chemoselectivity and prevent homocoupling (Scheme 3.11) a number of strategies have been utilized involving (i) pairing two arenes of different electronics, (ii) pairing one arene with a ligand and one without, and/or (iii) differing the stoichiometry of the two arenes.



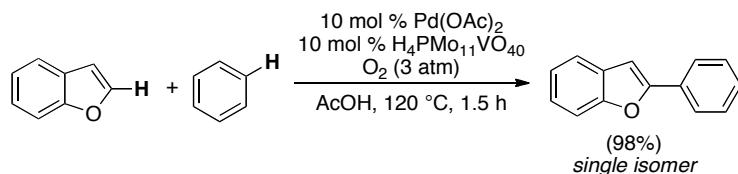
One of the first regioselective examples of Pd-catalyzed oxidative cross-coupling involved the coupling of indoles and benzofurans with arenes developed, concurrently by Fagnou^{25, 26} and DeBoef.²⁷ In Fagnou's premier example, a protected indole was shown to undergo Pd(OAc)₂-catalyzed oxidative coupling with *o*-xylenes. (Scheme 3.12, *i*) Importantly, this initial reaction was highly selective for the C2 position. However, subtle changes to the catalyst and oxidant employed allowed site-selective coupling at the C3 position of the indole (Scheme 3.12, *ii*). A number of other 1,2- and 1,4-disubstituted arenes were used successfully in this methodology giving the least hindered coupling product as the major product.

Scheme 3.12 Fagnou's Oxidative Coupling of *N*-Acetylindole with *o*-xylenes



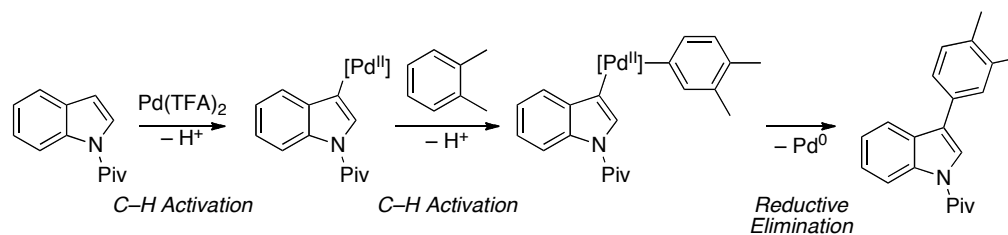
DeBoef was able to show similar reactivity at the C2 position of a benzofuran with benzene using O_2 as the terminal oxidant with $\text{H}_4\text{PMo}_{11}\text{VO}_{40}$ (HMPV) as the co-oxidant (Scheme 3.13). The site selectivity of the simple arene was also controlled by sterics.

Scheme 3.13 DeBoef's Oxidative Coupling of Benzofuran with Benzene



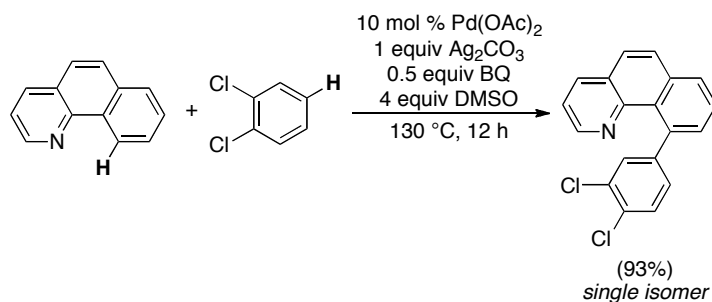
Similar mechanisms have been proposed for each of these transformations. The electron rich heterocycle reacts with the electron poor palladium in an electrophilic palladation step (Scheme 3.14). The palladated intermediate then undergoes C–H activation with the aryl coupling partner at the least hindered aryl–H, and finally reductive elimination gives the biaryl product. Each of these methods utilized the increased reactivity of the oxygen- or nitrogen-containing heterocycles to control the chemoselectivity with simple arenes, and much work has been done to understand the selectivity with these activated heterocycles. In contrast, relatively little work has been done to understand the selectivity of the other coupling partner, the simple arene.

Scheme 3.14 Mechanism of Oxidative Coupling of Indoles



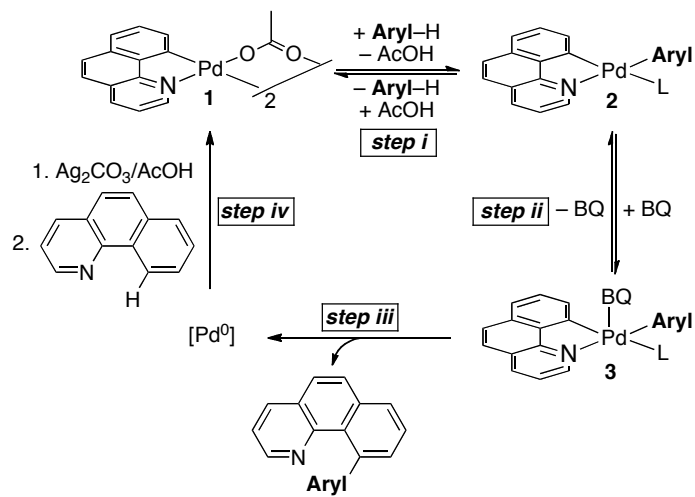
Our group had previously developed a Pd-catalyzed method for the oxidative coupling of benzo[*h*]quinoline (bzq) and arenes using a Ag^I oxidant and benzoquinone (BQ) as a key promoter.³⁸ The strategy implemented to accomplish this oxidative coupling was to use one arene with a tethered ligand in the presence of an excess of another arene coupling partner. This methodology produced the aryl-aryl coupled product in good to excellent yield with generally only one regioisomer (Scheme 3.15).

Scheme 3.15 Previous Pd-Catalyzed Oxidative Coupling



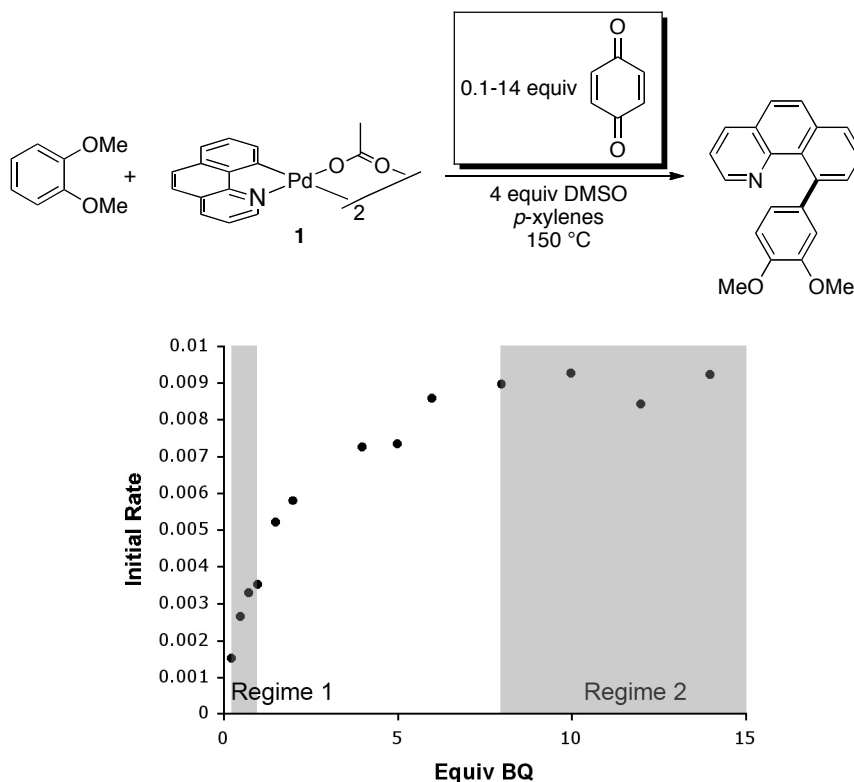
Extensive studies have implicated a mechanism involving: cyclopalladation of bzq to generate [(bzq)Pd(OAc)]₂, reversible activation of aryl-H, BQ binding/BQ-promoted C-C bond-forming reductive elimination, and finally reoxidation of Pd⁰ by Ag^I to regenerate the Pd^{II} catalyst (Scheme 3.16).³⁹ Site selectivity on the bzq was controlled by utilizing the quinoline moiety to direct the Pd to the proximal C-H bond. Chemoselectivity was controlled by taking advantage of the faster relative rate of ligand-directed C-H activation compared to undirected aryl C-H activation. This ensured that the free arene did not undergo homocoupling. The site selectivity of the free arene C-H activation was observed to be controlled by sterics, as the least hindered product predominated.

Scheme 3.16 Mechanism of Pd-Catalyzed Oxidative Coupling



Intriguingly, the rate-determining step of this sequence is dependent on the concentration of the quinone promoter. For example, in the reaction of $[(\text{bzq})\text{Pd}(\text{OAc})_2]$ with 1,2-dimethoxybenzene, a 1st order dependence on $[\text{BQ}]$ was observed at low concentrations of BQ, suggesting that quinone complexation (step *ii*) is rate-determining. In contrast, saturation was observed at high $[\text{BQ}]$, implicating rate-limiting C-H activation (step *i*) under these conditions (Figure 3.1). These two kinetic regimes will be referred to as regime 1 (low $[\text{BQ}]$, 1 equiv) and regime 2 (high $[\text{BQ}]$, 20 equiv) throughout this chapter.

Figure 3.1 Initial Rate vs Equiv of BQ in the Coupling of **1** with 1,2-Dimethoxybenzene



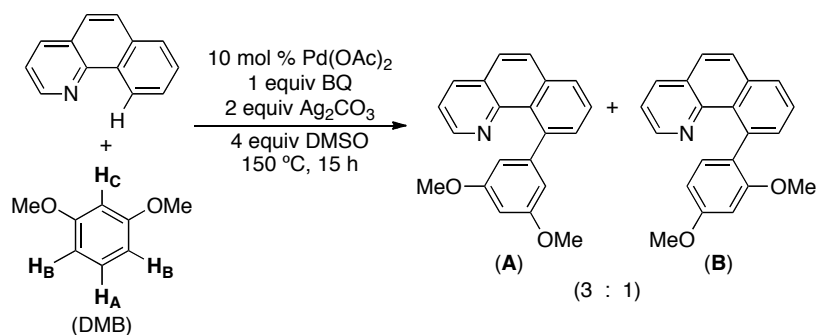
With this mechanistic framework in hand, we turned our attention to understanding and controlling the site selectivity of Aryl-H functionalization of the free arene. We hypothesized that the change in rate-determining step between regimes 1 and 2 might also lead to a change in site selectivity. Furthermore, we reasoned that systematic modification of the ancillary ligands at Pd intermediates **1-3** might enable catalyst control for future methodologies. This chapter describes a detailed investigation of the factors dictating site selectivity in these oxidative coupling reactions. We demonstrate that the X-type ligands have a particularly dramatic influence on selectivity and discuss the origin of these ligand effects in the context of the mechanistic framework in Scheme 3.16.

3.2 Methodology and Stoichiometric Selectivity Studies

We chose 1,3-dimethoxybenzene (DMB) as a test substrate for probing site selectivity. DMB contains three different aromatic hydrogens (H_A , H_B , and H_C) with

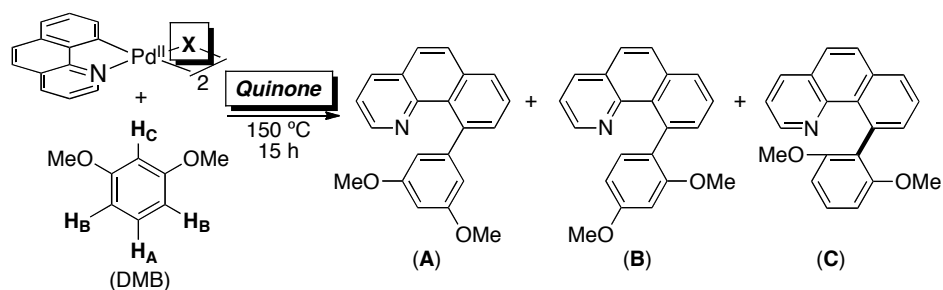
dramatically different steric and electronic properties. H_B and H_C are attached to the most nucleophilic carbons in the molecule, H_A is located at the most sterically accessible position, and H_C is at the most sterically crowded site on the arene. Under the original conditions (10 mol % of $\text{Pd}(\text{OAc})_2$, 1 equiv of BQ, 2 equiv of Ag_2CO_3 , 4 equiv of DMSO), DMB underwent oxidative coupling with benzo[*h*]quinoline to afford a 3 : 1 mixture of isomers **A** : **B** (derived from replacing H_A and H_B , respectively) (Scheme 3.17). This result suggests that there is relatively little inherent selectivity in this system, which renders it an ideal case for studying catalyst control.

Scheme 3.17 Oxidative Coupling of DMB with Benzo[*h*]quinoline



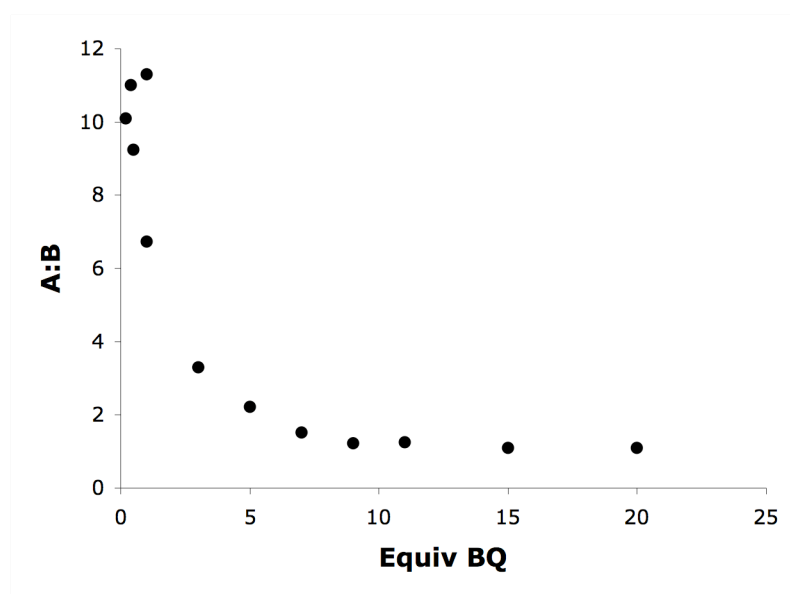
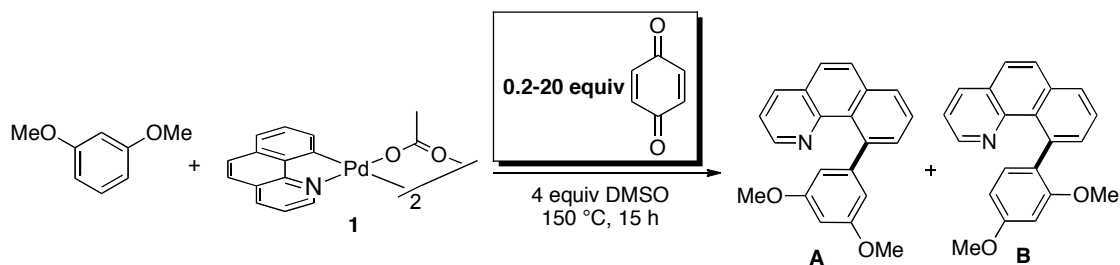
The studies described throughout this chapter involve the reaction of DMB with $[(\text{bzq})\text{PdX}]_2$ to afford mixtures of isomers **A**, **B**, and **C** (Scheme 3.18). This stoichiometric transformation allows us to directly probe DMB functionalization without interference from the cyclometalation or oxidation steps of the catalytic cycle. Most importantly, this approach excludes any influence of oxidant-derived X/L-type ligands on reactivity or selectivity. The results obtained in regime 1 (1 equiv of quinone relative to [Pd]) and regime 2 (20 equiv of quinone relative to [Pd]) are discussed below as a function of three variables: (i) quinone, (ii) carboxylate, and (iii) other X-type ligands.⁴⁰

Scheme 3.18 Model System for Stoichiometric Selectivity Studies



Role of Quinone in Selectivity. The reaction of DMB with [(bzq)Pd(OAc)]₂ was first studied as a function of the concentration of benzoquinone (BQ). The site selectivity showed a clear dependence on [BQ], with the ratio of isomers **A** : **B** ranging from 11 : 1 at 0.005 M (0.2 equiv) to 1.1 : 1 at 0.5 M (20 equiv). (Less than 5% of isomer **C** was observed in any of these reactions.) A plot of **A** : **B** versus equiv of BQ (Figure 3.2)

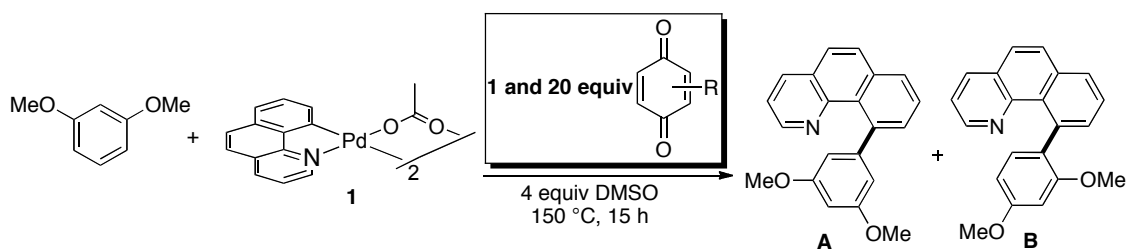
Figure 3.2 **A** : **B** versus Equiv of BQ for the Reaction of **1** with DMB

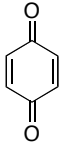
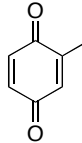
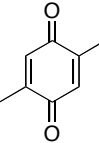
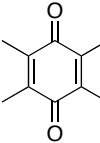
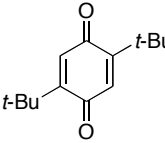


showed that the ratio levels out at approximately 1 : 1 at 0.20 M (8 equiv). This is the same concentration at which saturation is observed in Figure 3.1, consistent with a change in both the rate- and selectivity-determining step between regimes 1 and 2.

This reaction was next studied using a series of commercially available alkyl-substituted quinone promoters. In regime 1 (0.025 M, 1 equiv of quinone), quinone substitution had a dramatic effect on selectivity, with **A** : **B** increasing from 5 : 1 with benzoquinone to 14 : 1 with 2,3,5,6-tetramethylbenzoquinone (Table 3.1). Notably, the improved selectivity was generally accompanied by a decrease in overall yield. In regime 2 (0.5 M, 20 equiv of quinone), the **A** : **B** ratio was significantly lower with all of the quinone derivatives. This ratio dropped even further as [quinone] was increased to 1.0 M (40 equiv).

Table 3.1 Site Selectivity as a Function of Quinone Substitution

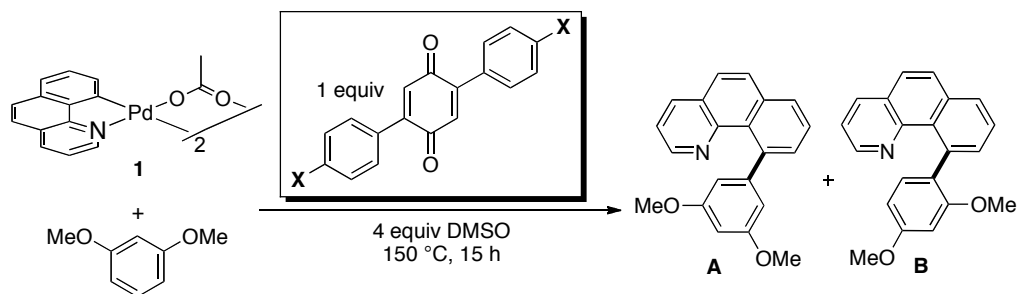


	Equiv of quinone (Regime)					
A : B	1 (Regime 1)	5 : 1	6 : 1	11 : 1	14 : 1	11 : 1
Yield		100%	100%	74%	54%	56%
A : B	20 (Regime 2)	1 : 1	1.5 : 1	4 : 1	8 : 1	5 : 1
Yield		65%	64%	94%	97%	100%
A : B	40 (Regime 2)	1 : 1.7	1 : 1	3 : 1	7 : 1	4 : 1
Yield		61%	59%	82%	66%	99%

Since the electronic and steric nature of the quinone ligand are inextricably linked in the series above, selectivity was also investigated with a series of *para*-substituted 2,5-diarylquinones in order to isolate the electronic influence. These experiments were originally carried out by my colleague Dr. Kami Hull and subsequently repeated and

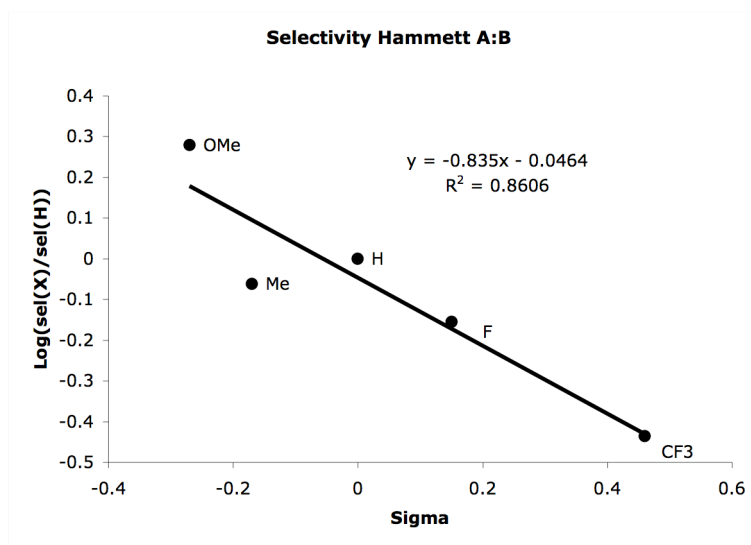
characterized for publication by myself. This study was conducted in regime 1, since this is where the largest effect was expected. In general, the **A** : **B** ratio was higher with more electron donating **X** substituents (Table 3.2). A Hammett plot of $(\log[\mathbf{A}/(\mathbf{A}+\mathbf{B})_{\mathbf{X}}/\mathbf{A}/(\mathbf{A}+\mathbf{B})_{\mathbf{H}}])$ versus σ_{para} (Figure 3.3) showed a reasonable correlation ($R^2 = 0.86$) with a ρ value of -0.8 ± 0.2 .

Table 3.2 Site Selectivity as a Function of Quinone Substitution (Electronic Effects)



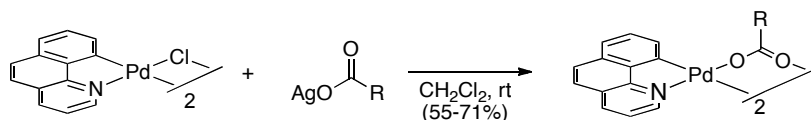
Entry	X	A : B
1	CF ₃	1.1 : 1
2	F	2.1 : 1
3	H	3 : 1
4	Me	2.6 : 1
5	OMe	5.7 : 1

Figure 3.3 Selectivity Hammett Plot



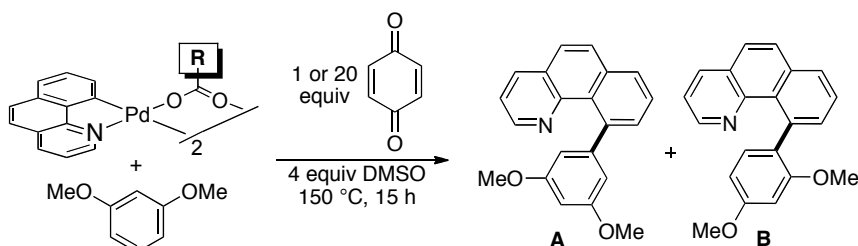
Role of Carboxylate in Selectivity. We next sought to explore the effect of sterics of the carboxylate ligand by reacting a series of [(bzq)Pd(O₂CR)]₂ complexes with DMB. These complexes were synthesized by reacting the appropriate silver carboxylate with [(bzq)PdCl]₂ in CH₂Cl₂ (Scheme 3.19).

Scheme 3.19 Synthesis of [(bzq)Pd(O₂CR)]₂ Complexes



The reaction of DMB with [(bzq)Pd(O₂CR)]₂ was next studied using carboxylate ligands with R = Me, Et, ⁱPr, or ^tBu. These reactions were carried out under our standard conditions with each data point representing the average of two runs. In regime 2, larger R groups provided enhanced preference for isomer **A**; for example, **A** : **B** increased from 1 : 1.5 to 1.8 : 1 upon moving from R = CH₃ to ^tBu (Table 3.3, entries 5-8). Interestingly a similar trend was observed in regime 1, with **A** : **B** changing from 5 : 1 to 9 : 1 for R = CH₃ and ^tBu, respectively (entries 1-4).

Table 3.3 Site Selectivity as a Function of Carboxylate Substitution



Entry	Conditions	R	Yield ^a	A : B
1	1 equiv BQ	Me	76%	5 : 1
2	1 equiv BQ	Et	78%	6 : 1
3	1 equiv BQ	ⁱ Pr	79%	7 : 1
4	1 equiv BQ	^t Bu	84%	9 : 1
5	20 equiv BQ	Me	61%	1 : 1.5
6	20 equiv BQ	Et	62%	1 : 1.2
7	20 equiv BQ	ⁱ Pr	82%	1.5 : 1
8	20 equiv BQ	^t Bu	65%	1.8 : 1

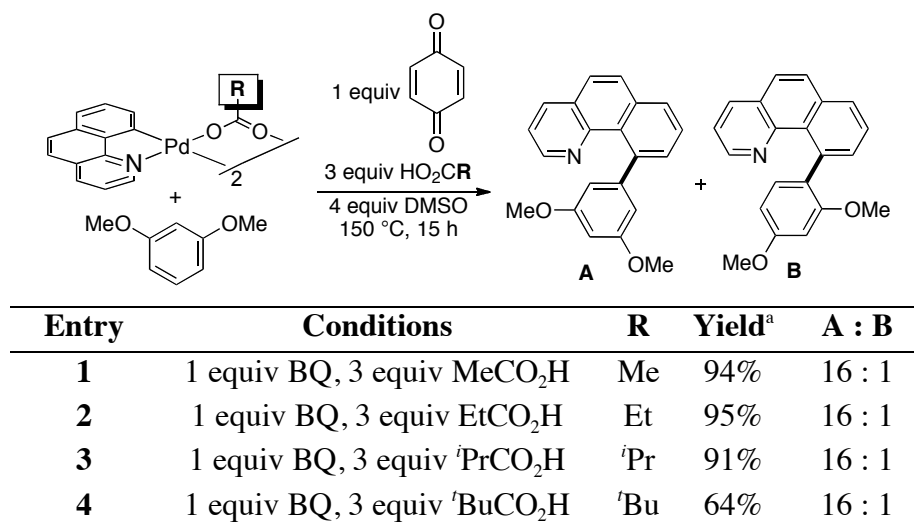
Effect of AcOH on Selectivity in Regime 1. We hypothesized that the observed steric effects in regime 1 might be a consequence of not obtaining rapidly equilibrating C–H activated Pd-aryl intermediates. Thus we examined the effect of added AcOH on the reaction between [(bzq)Pd(OAc)]₂ and DMB. As summarized in Table 3.4, the selectivity for isomer **A** improved as the amount of AcOH was increased up to 3 equiv. Above 3 equiv of AcOH, the selectivity remained approximately constant and the overall yield decreased significantly. This change in selectivity is consistent with the system not reaching equilibrium under our previous reaction conditions.

Table 3.4 Effect of Exogenous AcOH on Selectivity in Regime 1



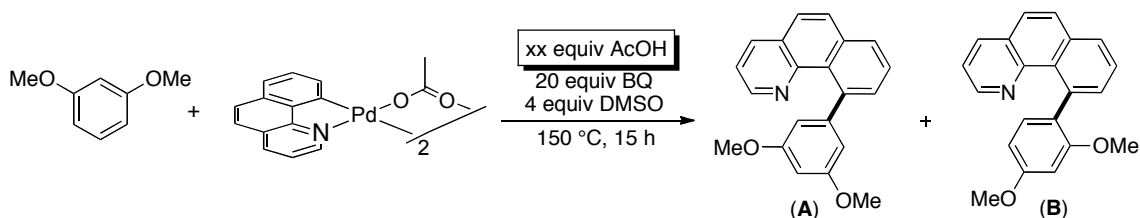
Entry	Equiv AcOH	Ratio A : B	% Yield
1	0.1	8 : 1	87%
2	0.5	12 : 1	100 %
3	1	11 : 1	94 %
4	3	16 : 1	96%
5	5	15 : 1	72 %
6	10	16 : 1	57%

We next added 3 equiv of RCO₂H to the reactions in regime 1 in order to facilitate complete equilibration of the C–H activation step (step *i*, Scheme 1). Under these conditions, **A** : **B** increased from 5 : 1 to 16 : 1. Furthermore, this ratio remained constant over the entire range of carboxylate derivatives (Table 3.5).

Table 3.5 Site Selectivity as a Function of Carboxylate Substitution

^a Yields were determined by GC analysis of the crude reaction mixtures versus an internal standard and represent an average of 2 runs.

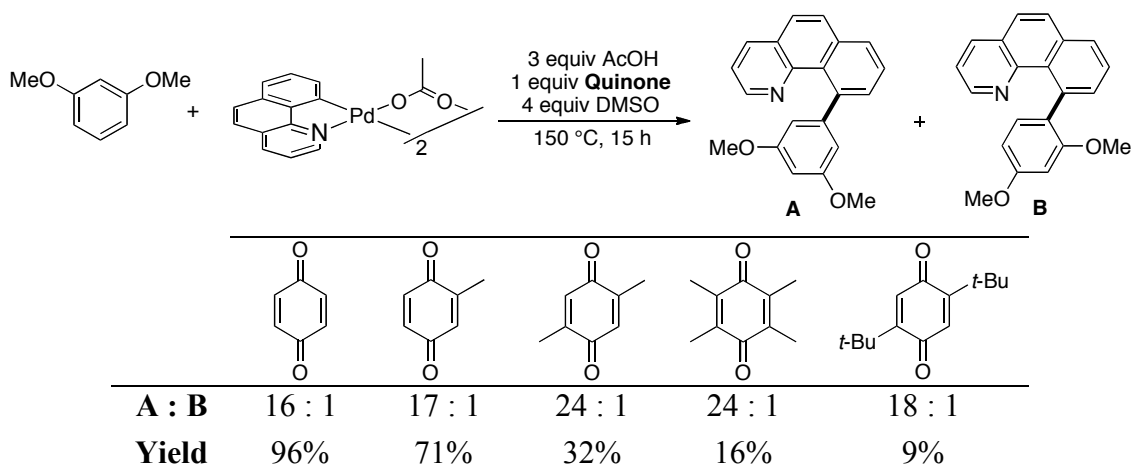
Effect of added AcOH on selectivity in Regime 2. We hypothesized that adding AcOH to the reaction between DMB and [(bzq)Pd(OAc)]₂ under saturation conditions in BQ (regime 2) would perturb the arene C–H activation equilibrium and thereby move the reaction back towards regime 1 (where high selectivity for isomer **A** is observed). As shown in Table 3.6, the expected effect is observed, with the **A** : **B** ratio increasing with increasing [AcOH]. However, the chemical yield drops significantly under these conditions as well.

Table 3.6 Effect of Exogenous AcOH on Selectivity in Regime 2

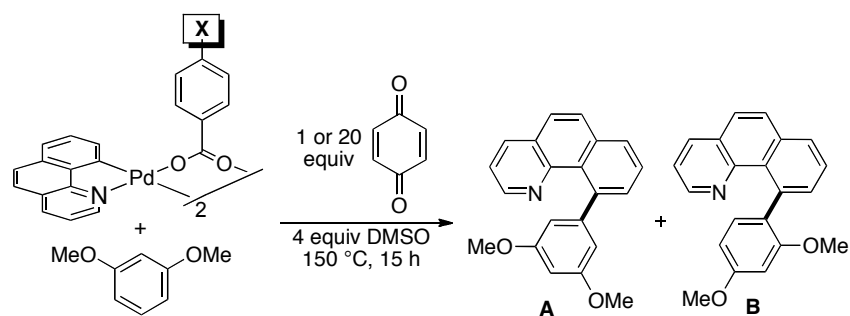
Entry	Equiv AcOH	Ratio A : B	% Yield
1	1	3 : 1	82
2	3	5 : 1	67
3	5	5 : 1	89
4	7	6 : 1	73
5	9	14 : 1	43

Effect of AcOH on Selectivity in Sterically Differentiated Quinones. We repeated the study of substituted quinone derivatives in the presence of 3 equiv of AcOH (conditions that promote more complete equilibration of the C–H activation step). As shown in Table 3.7, the trend in **A** : **B** selectivity under these conditions is very similar to that in Table 3.1; however, there is a marked decrease in chemical yield with the highly substituted quinones.

Table 3.7 Effect of AcOH on Selectivity with Sterically Differentiated Quinones



The electronic influence of the carboxylate ligand was assessed using $[(\text{bzq})\text{Pd}(\text{O}_2\text{C}(p\text{-XC}_6\text{H}_4))]_2$. In regime 1 the *para* substituent X had relatively minimal impact on selectivity (Table 3.8, entries 1-4). The addition of 3 equiv of ArCO_2H slightly enhanced the selectivity for **A** but did not show a correlation with the change in *para* substituent (entries 5-8). In regime 2 small electronic effects were observed, with **A** : **B** ranging from 1 : 1.7 to 1 : 2.9 (entries 9-12). However, there was no clear correlation between **A** : **B** and Hammett σ values in this system.

Table 3.8 Site Selectivity as a Function of Benzoate Substitution (Electronic Effects)

Entry	Conditions	$p\text{-XC}_6\text{H}_4$ (Ar)	Yield	A : B
1	1 equiv BQ	$p\text{-MeOC}_6\text{H}_4$	58%	14 : 1
2	1 equiv BQ	C_6H_5	62%	10 : 1
3	1 equiv BQ	$p\text{-CF}_3\text{C}_6\text{H}_4$	45%	11 : 1
4	1 equiv BQ	$p\text{-NO}_2\text{C}_6\text{H}_4$	39%	11 : 1
5	1 equiv BQ/3 equiv ArCO_2H	$p\text{-MeOC}_6\text{H}_4$	36%	17 : 1
6	1 equiv BQ/3 equiv ArCO_2H	C_6H_5	35%	16 : 1
7	1 equiv BQ/3 equiv ArCO_2H	$p\text{-CF}_3\text{C}_6\text{H}_4$	23%	19 : 1
8	1 equiv BQ/3 equiv ArCO_2H	$p\text{-NO}_2\text{C}_6\text{H}_4$	9%	20 : 1
9	20 (Regime 2)	$p\text{-MeOC}_6\text{H}_4$	36%	1 : 1.7
10	20 (Regime 2)	C_6H_5	40%	1 : 2
11	20 (Regime 2)	$p\text{-CF}_3\text{C}_6\text{H}_4$	38%	1 : 2.9
12	20 (Regime 2)	$p\text{-NO}_2\text{C}_6\text{H}_4$	38%	1 : 2.5

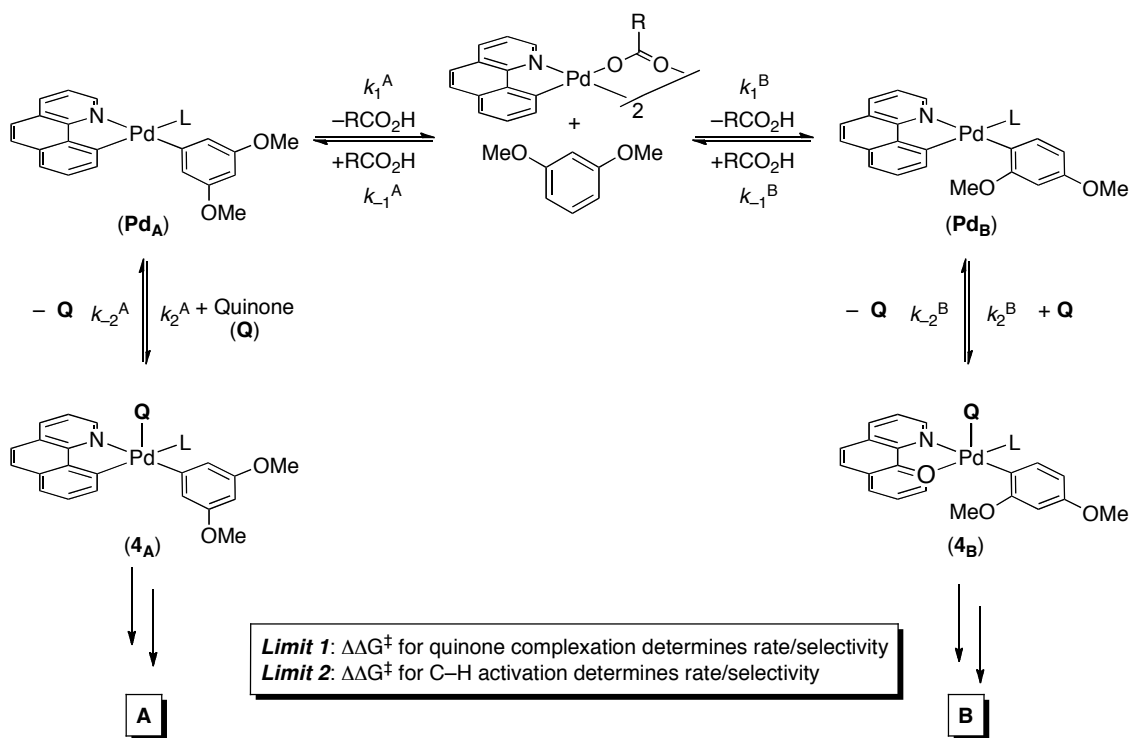
Reaction of [(bzq)Pd(OPiv)]₂ with substituted quinone derivatives. To examine the cumulative effect of sterically large carboxylate substituents and alkyl-substituted quinone derivatives on selectivity, we reacted [(bzq)Pd(OPiv)]₂ with a series of alkyl quinones under the optimized reaction conditions. As summarized in Table 3.9, the overall yields decreased (compared to the analogous reactions of [(bzq)Pd(OAc)]₂), while the A : B selectivity was only modestly increased versus the acetate system.

Table 3.9 [(bzq)Pd(OPiv)]₂ Studies with Substituted Quinones

	R					
A : B	^t Bu	5 : 1	10 : 1	14 : 1	14 : 1	10 : 1
Yield		100%	82%	52%	25%	24%
A : B	Me	5 : 1	6 : 1	11 : 1	14 : 1	11 : 1
Yield		100%	100%	74%	54%	56%

Discussion of Ligand Effects with [(bzq)Pd(O₂CR)]₂. The results described above provide a comprehensive picture of the influence of the quinone promoter and carboxylate ligand on selectivity. A detailed mechanism that is consistent with all of this data is shown in Scheme 3.20, and it implicates two limiting mechanistic scenarios. In the first (*Limit 1*), intermediates **Pd_A** and **Pd_B** are in a fast and reversible equilibrium, where $k_{-1}^{A/B}[\mathbf{Pd}_{A/B}][\text{RCO}_2\text{H}] \gg k_2^{A/B}[\mathbf{Pd}_{A/B}][\text{Quinone}]$. This is a classic Curtin-Hammett situation where the rate and selectivity will be dictated by the relative magnitudes of ΔG^\ddagger for quinone complexation with **Pd_A** versus **Pd_B**, respectively. In the second limiting possibility (*Limit 2*), $k_2^{A/B}[\mathbf{Pd}_{A/B}][\text{Quinone}] \gg k_1[\mathbf{1}][\text{DMB}]$. Under these conditions, the rate and selectivity will be determined by the relative magnitude of ΔG^\ddagger for C–H activation to form **Pd_A** versus **Pd_B**, respectively.

Scheme 3.20 Detailed Mechanism for Coupling between [(bzq)Pd(O₂CR)]₂ and DMB

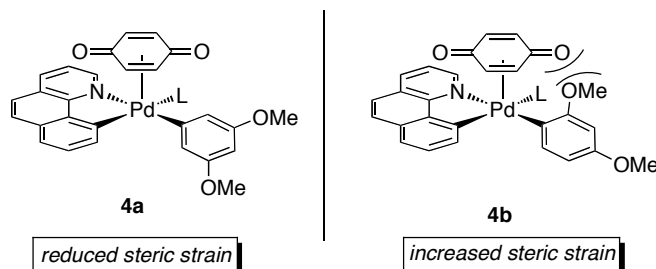


The experiments described above use 1 equiv of quinone (regime 1) and 20 equiv of quinone (regime 2) to approximate these two limiting scenarios. However, changes to the quinone and the carboxylate ligands can clearly influence both the relative and absolute values of the six key rate constants in this system (k_1^A , k_1^B , k_{-1}^A , k_{-1}^B , k_2^A , and k_2^B). As such, the experimental results in regimes 1 and 2 approach, but do not necessarily reach, the limiting scenarios outlined above. In other words, while quinone complexation always dominates the selectivity in regime 1, the C–H activation step can also provide a small contribution under some conditions. Similarly, the C–H activation step always dominates the selectivity in regime 2, but quinone complexation can also have some influence depending on the ligands present and relative rate constants. A detailed discussion of the effects of quinone and carboxylate on regimes 1 and 2 is outlined below.

Discussion of Quinone Promoter. In regime 1, we propose that the rate and selectivity are primarily dictated by quinone complexation through the d_{z^2} orbital of one of two interconverting σ -aryl Pd intermediates (**Pd_A** and **Pd_B**). The d_{z^2} orbital of **Pd_B** is

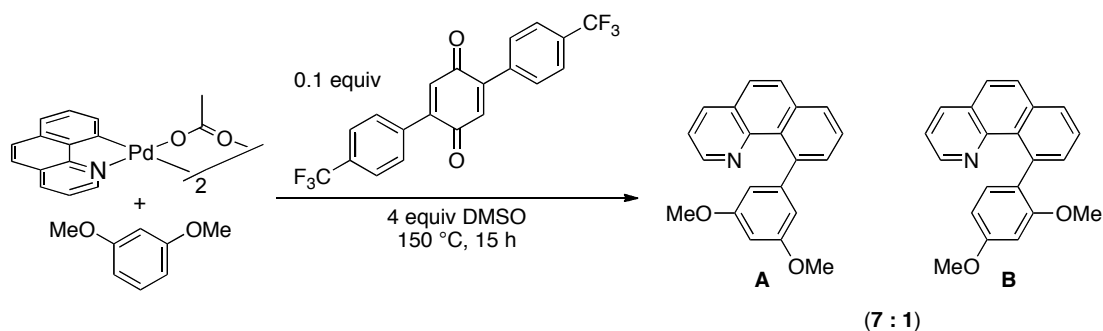
significantly more sterically congested than that of **Pd_A** due to the *ortho*-substituted σ -aryl ligand (Figure 3.4). As a result, we hypothesize that quinone association (and subsequent irreversible bzq–DMB coupling) is slower at **Pd_B** than **Pd_A**, leading to selective formation of isomer **A**.

Figure 3.4 Steric Congestion in BQ Complexation



In regime 1, more electron deficient quinones provided lower **A** : **B** ratios (Table 3.2), and there are likely two factors that contribute to this effect. First, electron deficient BQ derivatives are more reactive π -acids and are thus expected to be less selective in distinguishing between **Pd_A** and **Pd_B**. Second, the higher reactivity of electron deficient quinones should increase k_2^A and k_2^B , leading to a larger contribution of the C–H activation step (which shows less preference for isomer **A**) to selectivity. This hypothesis was confirmed by reacting [bzqPd(OAc)]₂ with DMB in the presence of 10 mol % of the diaryl quinone (X = CF₃) shown below (Scheme 3.21). **A** : **B** selectivity increased from 1.1 : 1, with 1 equiv of diaryl quinone (X = CF₃), to 7 : 1, with 0.1 equiv consistent with the reduced rate of k_2^A and k_2^B .

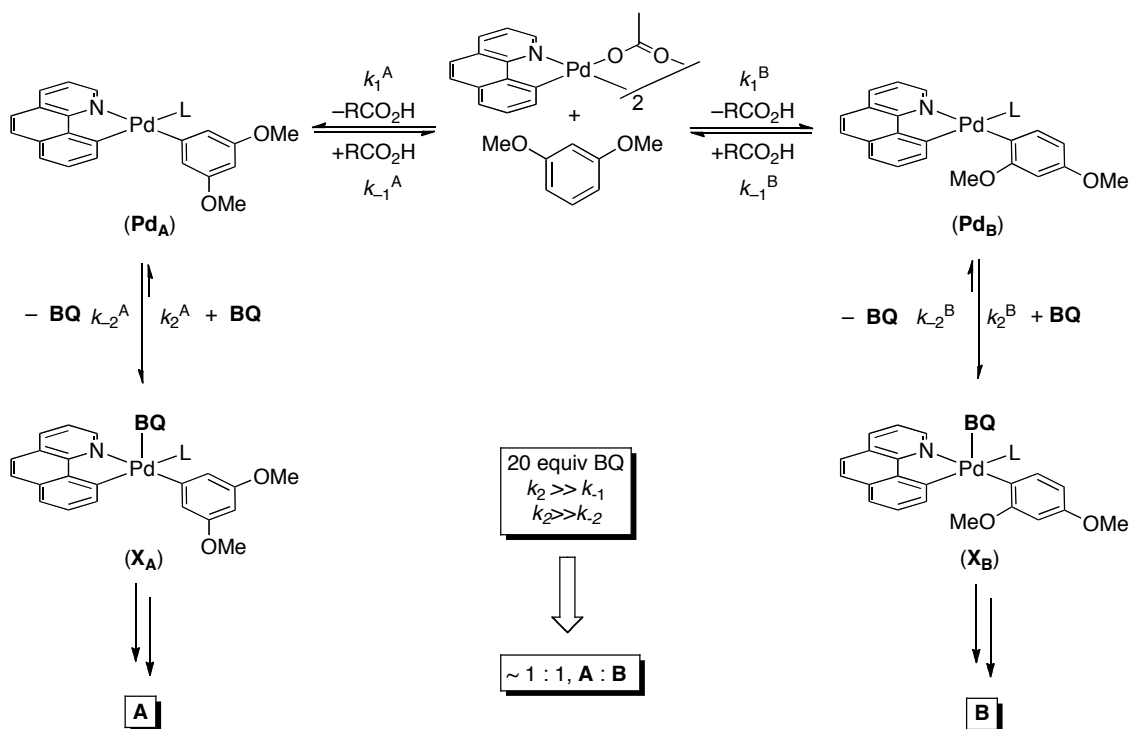
Scheme 3.21 Influence of BQ Stoichiometry on Selectivity



In regime 1, alkyl substituents on the quinone resulted in enhanced selectivity for **A** (Table 3.1). This is likely due to a combination of electronic and steric effects. Alkyl groups are moderately electron donating, which, as discussed above, favors the formation of **A**. Alkyl substitution also increases the size of the quinone, which should exacerbate unfavorable steric interactions in its reaction with **Pd_B**.

In regime 2, the rate and selectivity are dominated by the C–H activation step. Interestingly, under these conditions, this reaction showed almost no selectivity, providing an approximately 1 : 1 ratio of **A** : **B**. This result indicates there is very little kinetic preference for activation of H_A versus H_B at this Pd^{II} center despite the clear steric and electronic differences between these two sites. Notably, most other C–H activation reactions at Pd^{II} are strongly affected by steric/electronic factors; therefore, the low inherent site selectivity of this step is a highly unusual feature of the current transformation.^{21,25,38}

Scheme 3.22 Proposed Mechanism in Regime 2



In regime 2, changes to the quinone structure are expected to have minimal impact on selectivity, since the quinone is not involved in the C–H activation step. As illustrated in Table 3.1, increasing the [quinone] resulted in a decrease of **A** : **B** ratio in all cases. However, even at 1.0 M (40 equiv), the differentially substituted quinones provided somewhat different selectivities. These data suggest that many of these reactions have not completely reached *Limit 2*, and thus the quinone complexation step still provides some contribution to selectivity.

Discussion of Effect of Carboxylate Ligands. In regime 1, sterically larger carboxylates provided enhanced selectivity for **A** (Table 3.3, entries 1-4). We initially considered that the carboxylic acid might serve as the ligand L in \mathbf{Pd}_{AB} (Scheme 3.20). However, this proposal is inconsistent with the inverse 1st order kinetics in AcOH observed during this transformation, which implicate AcOH dissociation prior to the rate-determining step.

Instead we propose that C–H activation is not fully reversible in the presence of 1 equiv of BQ. As a result, a Curtin Hammett situation (involving fast pre-equilibration between \mathbf{Pd}^A and \mathbf{Pd}^B followed by rate- and selectivity-determining BQ complexation) is not fully established. The different relative rates of C–H activation/protonation (k_1^A/k_{-1}^A versus k_1^B/k_{-1}^B) for each carboxylate complex thus contribute to the observed selectivities.

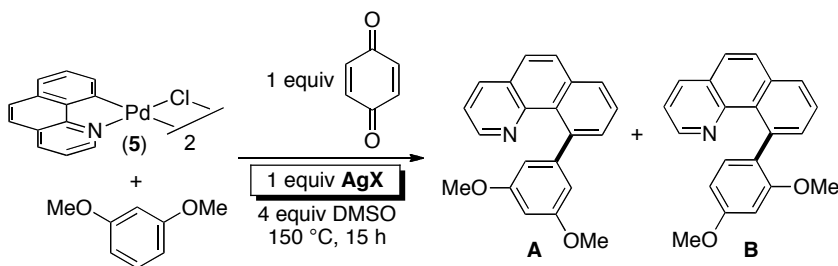
Consistent with this proposal, the **A** : **B** selectivity became independent of R upon the addition of 3 equiv of RCO₂H to these reactions (Table 3.5). The added acid should increase the relative rate of protonation of $\mathbf{Pd}^A/\mathbf{Pd}^B$ ($k_{-1}[\text{RCO}_2\text{H}][\mathbf{Pd}^{AB}]$) compared to that of BQ complexation ($k_2[\text{BQ}][\mathbf{Pd}^{AB}]$). As such, it should promote more complete equilibration of the C–H activation step such that selectivity is dictated solely by $\Delta\Delta G^\ddagger$ for quinone complexation.

In regime 2, the carboxylate ligand is expected to be coordinated to Pd during the rate/selectivity determining C–H activation step. Consistent with this, the **A** : **B** ratio in regime 2 was sensitive to both steric and electronic perturbation of R. Sterically large carboxylate ligands provided enhanced selectivity for functionalization at the least hindered site of DMB (to form **A**), implicating unfavorable steric interactions in the transition state for C–H activation. Small electronic effects were also observed with *p*-substituted benzoate derivatives; however, the modest magnitude and the lack of a clear

trend indicate that electronic perturbations to the complex have minimal effect on site selectivity.

Influence of Varying the X-Type Ligand. On the basis of the studies described above, we reasoned that substituting carboxylates with alternative X-type ligands might further modulate selectivity in these systems. Thus, we examined the reaction of DMB with [(bzq)PdCl]₂ (**5**) in the presence of a variety of AgX salts. Importantly, **5** is unreactive under these conditions on its own (Table 3.10, entry 1), presumably due to its low solubility. Therefore, any observed reactivity indicates at least partial substitution of Cl with X.

Table 3.10 Site Selectivity as a Function of Ag Salt



Entry	AgX	A : B	Yield ^a
1	none	---	nr ^b
2	AgOAc	5 : 1	98%
3	AgOPiv	9 : 1	79%
4	AgO ₂ CCF ₃	1 : 1	13%
5	AgNO ₃	2 : 1	38%
6	Ag ₂ SO ₄	---	nr ^b
7	AgBF ₄	---	nr ^b
8	Ag ₂ CO ₃	1 : 6 ^c	92%

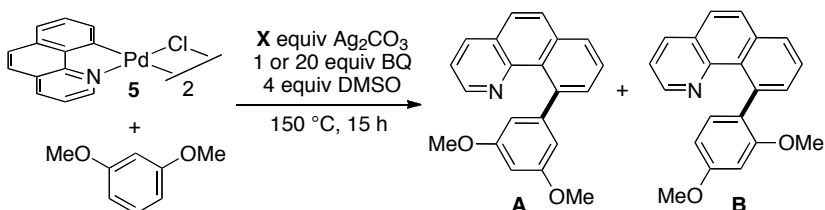
1 mol of Ag was used per mol of Pd (*e.g.*, 1 mol AgOAc per 0.5 mol **5**).^a Yields were determined by GC analysis of the crude reaction mixtures versus an internal standard and represent an average of 2 runs. ^b nr = no reaction observed. ^c Trace amounts (~5%) of C were also observed.

We first examined the reaction of **5** with AgOAc and AgOPiv. The **A** : **B** selectivity in these systems was nearly identical to that obtained using the pre-formed carboxylate bridged dimers (compare Table 3.3, entries 1 and 4, to Table 3.10, entries 2 and 3). This suggests that the reaction between **5** and AgO₂CR generates [(bzq)Pd(O₂CR)] *in situ*.

We next surveyed Ag salts containing weakly coordinating counterions (*e.g.*, CF_3CO_2^- , NO_3^- , BF_4^- , PF_6^-). In all cases, modest to poor yields and low levels of site selectivity were observed (Table 3.10, entries 4-7). In striking contrast, Ag_2CO_3 provided excellent chemical yield (92%) with a complete reversal of selectivity (1 : 6 ratio of **A** : **B**, entry 8). In addition, for the first time, traces (~5%) of isomer **C** (derived from functionalization at the most hindered site on DMB) were observed.

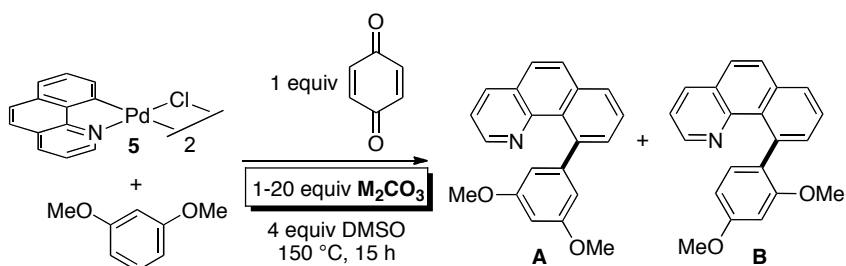
We further explored the influence of this effect by screening both sub- and superstoichiometric amounts of Ag_2CO_3 in both regime 1 and 2. As shown in Table 3.11, the stoichiometry had a dramatic effect on both the selectivity as well as the chemical yield. In regime 1 **A** : **B** selectivity increased from 2 : 1, with 0.25 equiv of Ag_2CO_3 , to 9 : 1, with 2.0 equiv. The same change in Ag_2CO_3 stoichiometry in regime 2 increased the selectivity from 8 : 1, **A** : **B** to 13 : 1.

Table 3.11 Influence of Ag_2CO_3 Stoichiometry on Selectivity



Entry	Equiv Ag_2CO_3	1 Equiv BQ (regime 1)		20 Equiv BQ (regime 2)	
		A : B	Yield	A : B	Yield
1	0.25	2 : 1	25%	8 : 1	16%
2	0.50	3 : 1	53%	9 : 1	38%
3	1.0	6 : 1	92%	10 : 1	56%
4	1.5	8 : 1	96%	11 : 1	92%
5	2.0	9 : 1	100%	13 : 1	92%

Alkali metal carbonate salts provided similar results to Ag_2CO_3 (Table 3.12), and both reactivity and selectivity improved with increasing size of the cation. For example, 1 equiv of Na_2CO_3 afforded 51% yield of product as a 1 : 3 ratio of isomers **A** : **B**, while 1 equiv of Cs_2CO_3 provided quantitative yield of a 1 : 11 mixture of **A** : **B** (entries 1 and 7).

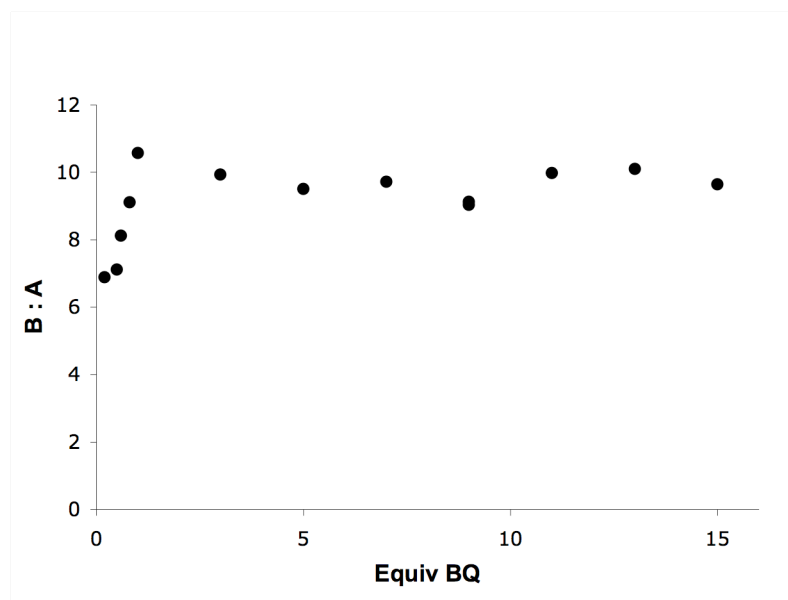
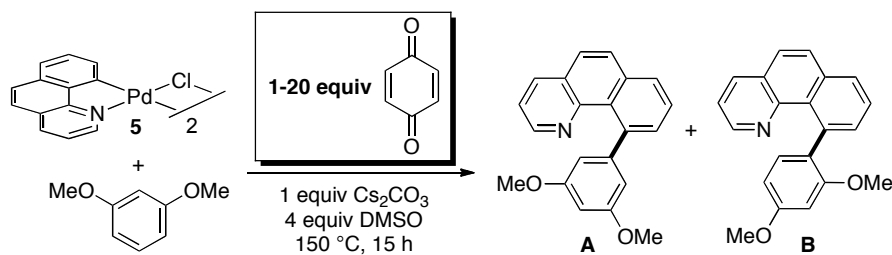
Table 3.12 Selectivity and Yield as a Function of M_2CO_3 

Entry	Equiv M_2CO_3	M_2CO_3	A : B ^a	Yield ^b
1	1	Na_2CO_3	1 : 3	51%
2	20	Na_2CO_3	1 : 3	100%
3	1	K_2CO_3	1 : 2	25%
4	20	K_2CO_3	1 : 10	100%
5	1	Rb_2CO_3	1 : 10	99%
6	20	Rb_2CO_3	1 : 13	71%
7	1	Cs_2CO_3	1 : 11	100%
8	20	Cs_2CO_3	1 : 13	12%

^aLess than 5% of isomer C was observed in these reactions. ^bYields were determined by GC analysis of the crude reaction mixtures versus an internal standard and represent an average of 2 runs.

Finally, we evaluated **A** : **B** selectivity in the carbonate system as a function of quinone concentration (Figure 3.5). Intriguingly, the **A** : **B** ratio changed only a small amount from 0.1 to 20 equiv of BQ (**A** : **B** moved from 1 : 7 to 1 : 11). This is in marked contrast to the much larger effect observed in the acetate system (where **A** : **B** decreased from 11 : 1 to 1.1 : 1 over the same concentration range (Figure 3.2)).

Figure 3.5 Site Selectivity (**B** : **A**) as a Function of Equiv of BQ for the Coupling of **5**/ Cs_2CO_3 with DMB



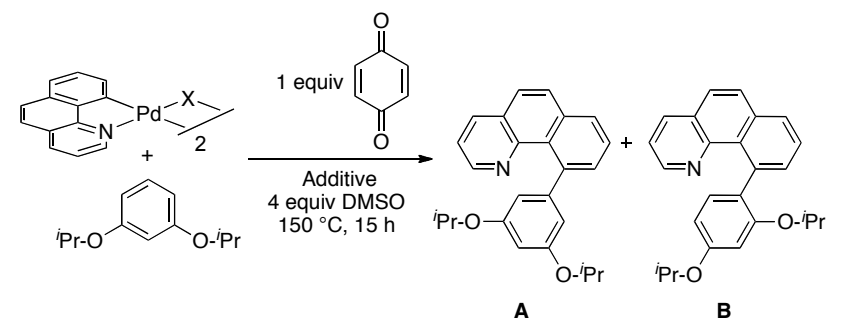
We found that metal carbonate salts are uniquely effective in reversing the selectivity of oxidative coupling between $[(\text{bzq})\text{PdCl}]_2$ and DMB. The generality of this effect with respect to other aromatic substrates and its comparison to the selectivity of the $[(\text{bzq})\text{Pd}(\text{OAc})]_2$ was explored next. Additionally, preliminary investigations into the mechanistic origin of the effect of $[(\text{bzq})\text{PdCl}]_2$ are discussed below.

3.3 Application to Diverse Substrates

The reaction of 1,3-diisopropoxybenzene with $[(\text{bzq})\text{PdX}]_2$ in the presence of 1 equiv of BQ showed nearly identical trends in reactivity and selectivity as with DMB. With $\text{X} = \text{AcO}^-$, **A** : **B** was 6 : 1, and this could be increased to 11 : 1 by using the $\text{X} = \text{OPiv}$ complex. (Table 3.13, entry 1). Similar to DMB, site selectivity could be reversed

through the use of $[(\text{bzq})\text{PdCl}]_2/\text{Cs}_2\text{CO}_3$, which provided the C–C coupled product as a 1 : 6 ratio of **A** : **B** in excellent (85%) yield (Table 3.13, entry 4). Moving from BQ to more electron rich and sterically hindered quinones like 2,3,5,6-tetramethylbenzoquinone also led to significant improvements in selectivity (**A** : **B** increased to 13 : 1); however, this was accompanied by a decrease in chemical yield (49%, Table 3.14).

Table 3.13 Application Oxidative Coupling to 1,3-Diisopropoxybenzene



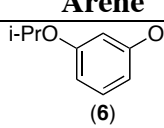
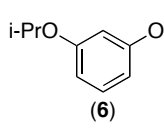
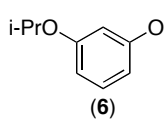
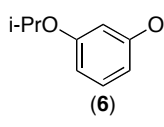
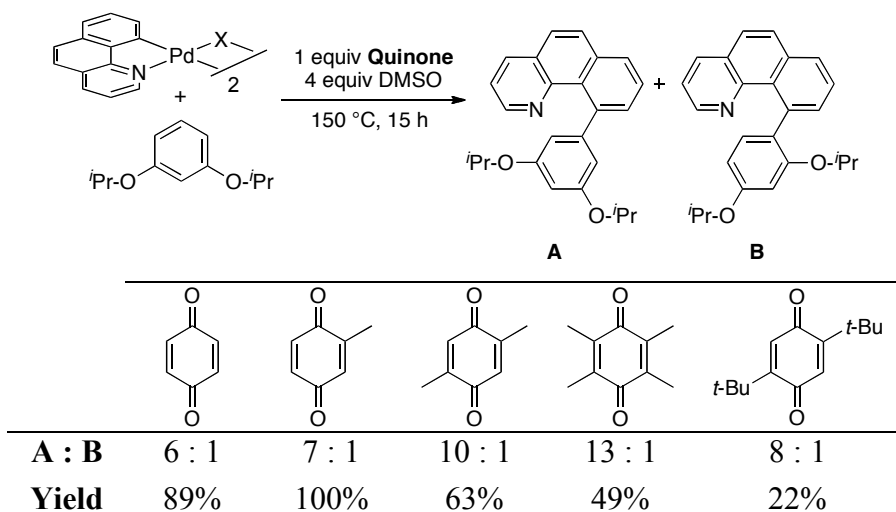
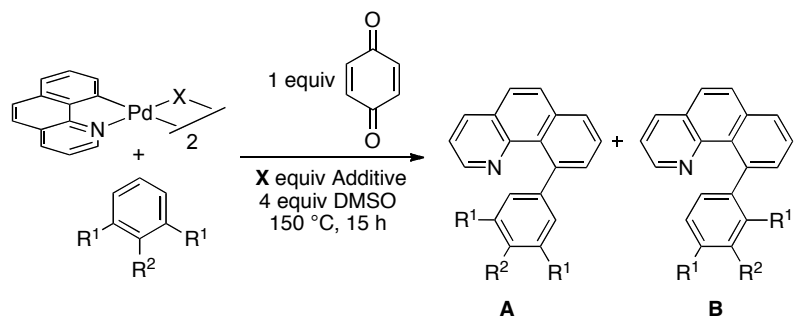
Entry	Arene	X	Additive	A : B	Yield
1		OAc	---	6 : 1	89%
2		OPiv	---	11 : 1	90%
3		OAc	3 equiv AcOH	15 : 1	94 %
4		CO ₃	---	1 : 6	85%

Table 3.14 Substituted Quinones with 1,3-Diisopropoxybenzene

1,2,3-Trisubstituted arenes also reacted with $[(\text{bzq})\text{Pd}(\text{OAc})_2]$ in the presence of 1 equiv of BQ to afford high selectivity for isomer **A** (**A** : **B** was typically $>50 : 1$) (Table 3.15, entries 1, 3, 5, and 7). With $[(\text{bzq})\text{PdCl}]_2/\text{Cs}_2\text{CO}_3$, the site selectivity changed dramatically in all cases; however, the magnitude of this change was subject to the electronic character of the 2-substituent. For example, with a 2-nitro group, **A** : **B** = 1 : 5 (entry 2), while with a methoxy substituent at the 2-position, **A** : **B** = 1 : 1 (entry 6). Additionally, 1,2-dimethoxybenzene (veratrole) also underwent a stark change in **A** : **B** selectivity, giving 56 : 1, with X = OAc, to 1 : 1, with X = CO_3 (entries 9,10).

Table 3.15 Oxidative Coupling Arene Substrate Scope



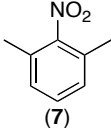
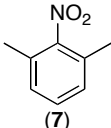
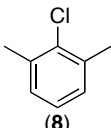
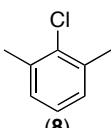
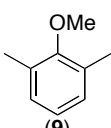
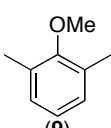
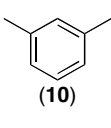
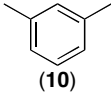
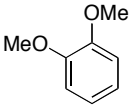
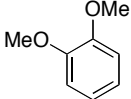
Entry	Arene	X ^a	Additive	A : B	Yield ^a
1	 (7)	OAc	---	64 : 1	100%
2	 (7)	CO ₃	---	1 : 5	69%
3	 (8)	OAc	---	60 : 1	95%
4	 (8)	CO ₃	---	1 : 2	67%
5	 (9)	OAc	---	53 : 1	77%
6	 (9)	CO ₃	---	1 : 1	67%
7	 (10)	OAc	---	55 : 1	84%

Table 3.15 Continued–Oxidative Coupling Arene Substrate Scope

Entry	Arene	X ^a	Additive	A : B	Yield ^a
8	 (10)	CO ₃	---	1 : 1	69%
9		OAc	---	41 : 1	89%
10		CO ₃	---	1 : 1	91%

^a X = CO₃²⁻ generated from [(bzq)PdCl]₂ (0.5 equiv) and Cs₂CO₃ (1 equiv). ^b Yields were determined by GC analysis of the crude reaction mixtures versus an internal standard and represent an average of 2 runs.

Similar trends were observed in complexes with other cyclometallated ligands. For example, [(phpy)PdX]₂ (phpy = 2-phenylpyridine) reacted with DMB to afford an 9 : 1 ratio of **A** : **B** when X = PivO⁻ and a 1 : 6 ratio of **A** : **B** when X = CO₃²⁻ (Table 3.16, entries 4 and 6). This ratio was relatively similar with 3 equiv of AcOH, **A** : **B** = 8 : 1 (entry 5). Similarly, the 8-methylquinoline (mq) complex [(mq)PdX]₂ provided a 4 : 1 ratio of **A** : **B** when X = PivO⁻ and a 1 : 4 ratio of **A** : **B** when X = CO₃²⁻ (entries 7 and 9). The addition of 3 equiv of AcOH with X = AcO⁻ gave only a small increase in selectivity to 5 : 1, **A** : **B** (entry 8). The small differences in selectivity observed by adding AcOH with both [(phpy)PdX]₂ and [(mq)PdX]₂ seem to indicate that the aryl–H equilibrium effects discussed above are sensitive to not only the X ligand, but the cyclometallated ligand as well.

Table 3.16 Scope of Oxidative Coupling Cyclometalating Ligands with DMB

Entry	[Pd]	X ^b	Additive	A : B	Yield ^c
1		OPiv	---	9 : 1	84%
2		OAc	3 equiv AcOH	16 : 1	94%
3		CO ₃	---	1 : 11 ^d	100%
4		OPiv	---	9 : 1	34%
5		OAc	3 equiv AcOH	8 : 1	31%
6		CO ₃	---	1 : 6 ^d	64%
7		OPiv	---	4 : 1	46%
8		OAc	3 equiv AcOH	5 : 1	54%
9		CO ₃	---	1 : 4 ^d	72%

^a Conditions: 1 equiv [Pd], 1 equiv BQ, 4 equiv DMSO, 1 or 0 equiv Cs₂CO₃, 0.8 mL of 1,3-dimethoxybenzene (DMB), 150 °C, 15 h. ^bX = CO₃²⁻ generated from [(bzq)PdCl]₂ (0.5 equiv) and Cs₂CO₃ (1 equiv). ^cYields were determined by GC analysis of the crude reaction mixtures versus an internal standard and represent an average of 2 runs. ^dTraces of isomer C (<5%) were observed in these reactions.

The results in Tables 3.13-3.16 clearly demonstrate that the selectivity trends derived for DMB are applicable across a range of different aromatic substrates and cyclometalating ligands.

3.4 Studies to Understand Selectivity in Carbonate Systems

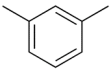
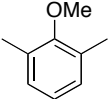
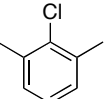
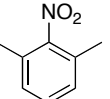
Finally, we sought mechanistic insight into the reversal of site selectivity between the carboxylate and carbonate systems. In the carboxylate system, steric effects appear to dominate selectivity. Particularly in regime 1, the least sterically hindered site (C-H_A) was functionalized with >5 : 1 (and often much higher) selectivity in all substrates examined. The dominance of steric effects is fully consistent with the mechanism outlined in Scheme 3.20.

In marked contrast, the combination of [(bzq)PdCl]₂/Cs₂CO₃ provided modest to high selectivity for functionalization of more sterically hindered C-H_B to afford **B**. Since C-H_B is more nucleophilic than C-H_A (by virtue of being *ortho*- and *para*- to MeO substituents), we first hypothesized that the observed selectivity might arise from an

electrophilic aromatic substitution (S_EAr) type mechanism for C–H cleavage. To test this hypothesis we undertook several computational experiments.

Our first efforts to correlate the S_EAr -type reaction pathway with the observed site-selectivity involved quantifying the electron density in the p-orbitals of a series of 1,2- and 1,2,3-substituted aromatics. The nucleophilicity of a given arene can be predicted by calculating the electron density of the HOMO at a given site.^{41, 42} Using Spartan⁴³ with a semi-empirical AM-1 level of theory the energies of the HOMO and HOMO–1 at C4 and C5 were calculated for each arene along with the appropriate p-orbital coefficient. The sum of the HOMO and HOMO–1 orbital coefficients were used for this calculation due to their comparable energies. As seen in Table 3.17 below, we did not observe a strong correlation between p-orbital coefficients and the observed site selectivity. This evidence suggests against an S_EAr -type reaction pathway.

Table 3.17 Calculated p-orbital Coefficients

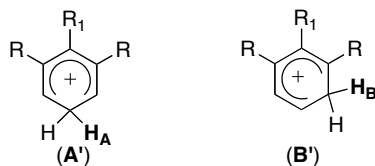
				
p-orbital coefficient C_A	0.5321	0.50249	-0.48392	-0.50299
p-orbital coefficient C_B	0.75049	0.71081	-0.70563	-0.7601
Δ p-orbital coefficient	-0.21839	-0.20832	0.22171	0.25711
Observed Selectivity (B : A)	1 : 1	1 : 1	1.9 : 1	5 : 1

p-orbital coefficients represents the sum of HOMO and HOMO–1 orbitals.

Our next efforts to probe this mechanistic pathway involved conducting AM-1 and DFT calculations to assess the relative energies of S_EAr intermediates **A'** and **B'** (Table 3.18) for a variety of 1,2- and 1,2,3-substituted aromatics. The difference in energy between these intermediates ($E_{A'} - E_{B'}$) represents the energetic preference for S_EAr at C–H_B versus at C–H_A. As shown in Figure 3.6, the calculated $E_{A'} - E_{B'}$ values showed a poor correlation with the experimental **B** : **A** selectivities. We examined **A'** and **B'** rather than the directly analogous palladated intermediates in order to simplify the calculation and reduce computation time. We independently calculated ΔG_{form} for intermediates **A'** and **B'** using both MP-2 and DFT-B3LYP levels of theory.^{44, 45} In order

to correlate these energies with the observed selectivities, the difference in ΔG_{form} for **A'** and **B'** [$\Delta G_{\text{form}}(\mathbf{A}') - \Delta G_{\text{form}}(\mathbf{B}')$] was calculated and plotted against the observed selectivities. Even in 1,3-dimethyl substituted arenes (where the C–H_B bonds are sterically identical), the experimental isomer ratios did not track well with those predicted for S_EAr. The lack of correlation is even more pronounced if transition state theory (TST) is used to estimate the expected isomer distribution. By using the difference in intermediate energies ($E_{\mathbf{A}'} - E_{\mathbf{B}'}$) as an approximation for the relative transition state energies, the expected **B** : **A** selectivities were calculated and listed in Table 3.18. This calculation shows no correlation with the observed selectivities in the series of arenes. As such, we conclude that **B** : **A** selectivity in the [(bzq)PdCl]₂/Cs₂CO₃ system is not due to selectivity-determining electrophilic palladation in an S_EAr pathway.

Table 3.18 Energy Calculations for **A'** and **B'**



$$E_{\mathbf{A}'} - E_{\mathbf{B}'} = \text{energetic preference for } S_E\text{Ar at } C_B\text{-}H_B \text{ versus } C_A\text{-}H_A$$

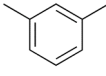
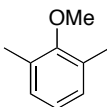
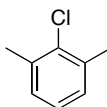
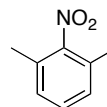
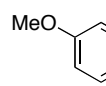
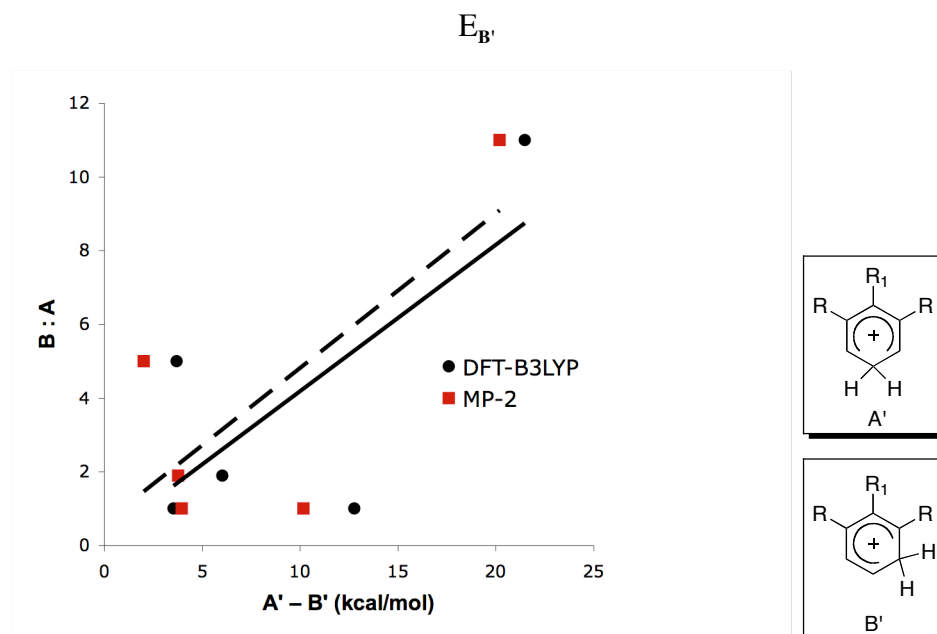
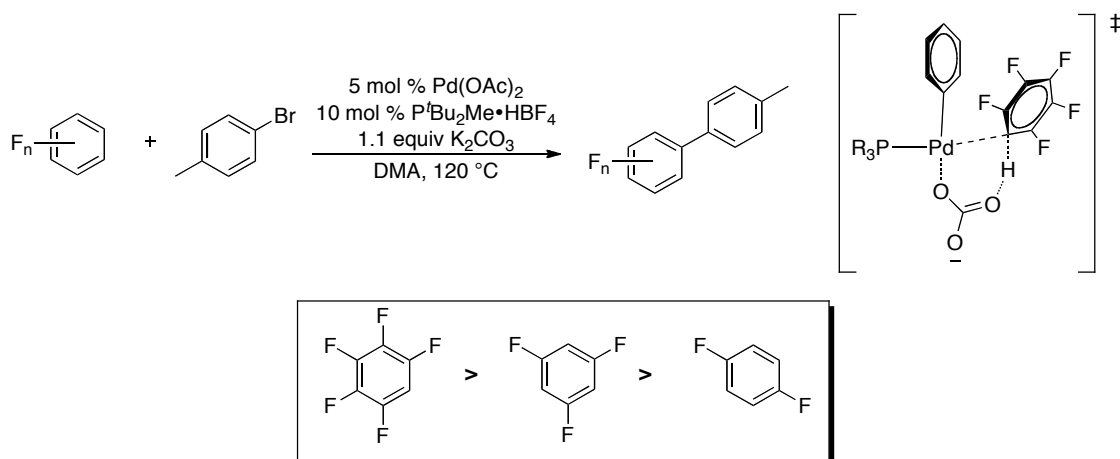
					
Experimental Selectivity (B : A) ^a	1 : 1	1 : 1	1.9 : 1	5 : 1	11 : 1
MP-2 [$\Delta G_{\text{form}}(\mathbf{A}') - \Delta G_{\text{form}}(\mathbf{B}')$] (kcal/mol)	10.18	3.96	3.78	2.01	20.19
DFT [$\Delta G_{\text{form}}(\mathbf{A}') - \Delta G_{\text{form}}(\mathbf{B}')$] (kcal/mol)	12.77	3.54	6.02	3.70	21.49
Selectivity B : A with TST	7.18×10^6 : 1	3 : 1	154 : 1	3580 : 1	2.37×10^{17} : 1

Figure 3.6 Plot of **B** : **A** Ratio (Experimental from Reactions of **5**/ Cs_2CO_3) versus $E_{\text{A}'} - E_{\text{B}'}$



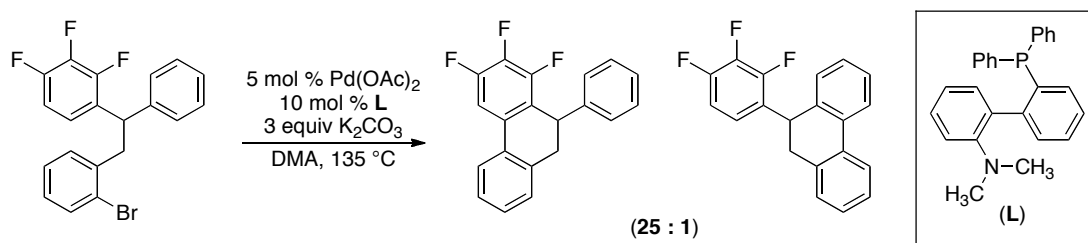
Elegant studies by Fagnou/Gorelsky^{46, 47} and Echavarren⁴⁸ have shown that C–H acidity can play a large role in both reactivity and selectivity in Pd-catalyzed C–H functionalization reactions. Competition experiments between increasingly substituted perfluoroarenes demonstrated a correlation between increased reactivity and the relative acidity of the aryl–H bond. Arenes with more fluorines generally outcompeted their less fluorinated derivatives (Scheme 3.23).

Scheme 3.23 Competition Studies of Perfluoroarenes in Direct Arylation



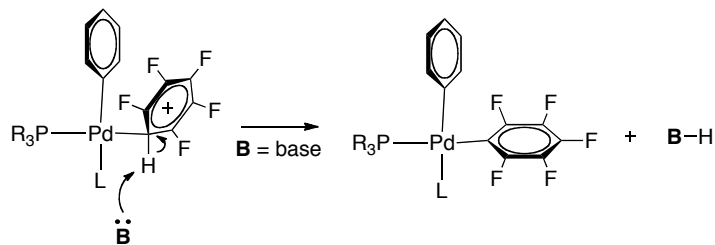
In related work, Echavarren⁴⁸ demonstrated a similar trend in an intramolecular Pd-catalyzed direct arylation. As shown in Scheme 3.24 below, the C–H activation was preferred on the perfluoroarene site over the phenyl ring 25:1. A similar but much more subdued preference was observed when one ring was substituted with electron withdrawing substituents such as 3-Cl- (1.3:1) or 3-CF₃ (1.9:1).

Scheme 3.24 Intramolecular Perfluoroarene Competition in Direct Arylation

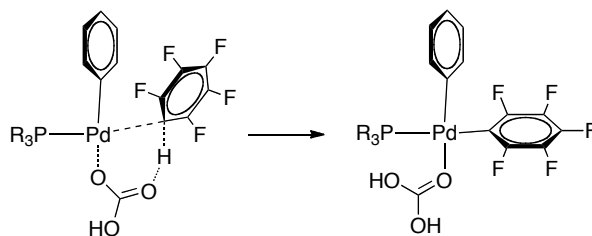


Both this result and the above competition study (Scheme 3.23) are inconsistent with an electrophilic palladation pathway (Scheme 3.26) and instead suggest a concerted metalation-deprotonation (Scheme 3.26) mechanism.

Scheme 3.25 Electrophilic Palladation Mechanism

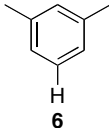
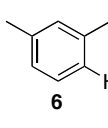
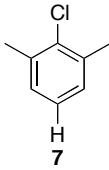
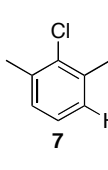
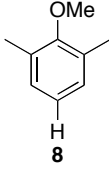
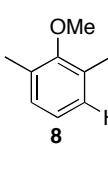
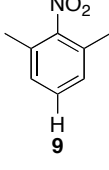
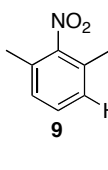
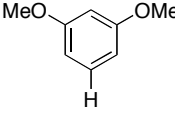
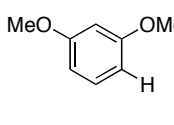


Scheme 3.26 Concerted Metalation-Deprotonation (CMD) Mechanism



With these key studies from the literature in mind we next sought see if there is a correlation between the acidity of aryl-H bonds and the observed site selectivity in our system. To that end we hypothesized that if an analogous effect were responsible for selectivity with [(bzq)PdCl]₂/Cs₂CO₃ then there should be a correlation between ΔpK_a [$pK_a(H_A) - pK_a(H_B)$] and experimental **B** : **A** ratios. DFT calculations were performed using a B3LYP method to determine the pK_a of H_A and H_B in a series of 1,3- and 1,2,3-substituted aromatics shown below in Table 3.19. The details of these calculations are reported in the experimental section.

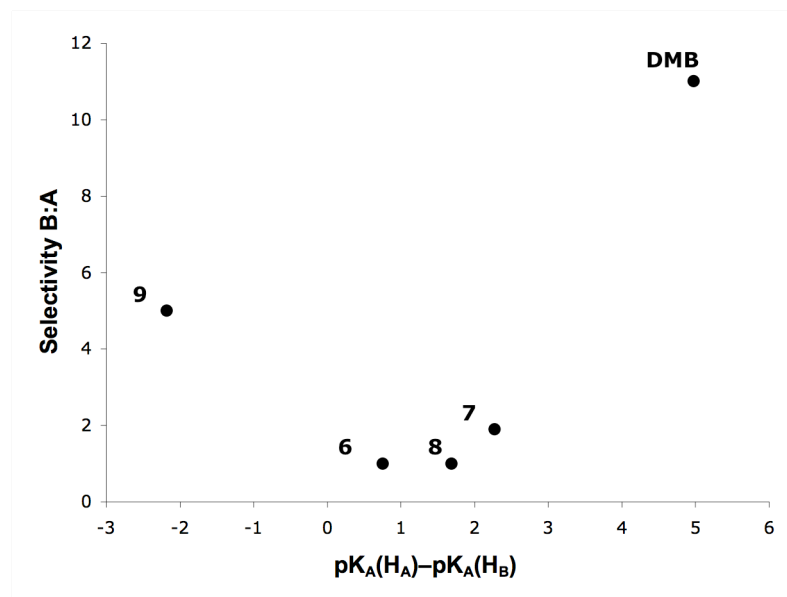
Table 3.19 Calculated pK_a values

Arene	pK_a	Arene	pK_a
	44.42		43.67
	39.43		37.16
	43.96		42.27
	29.99		32.17
	42.51		37.54

The data shown above were used to calculate [$pK_a(H_A) - pK_a(H_B)$] and were then plotted against experimental **B** : **A** ratios. As shown in Figure 3.7, there was no clear

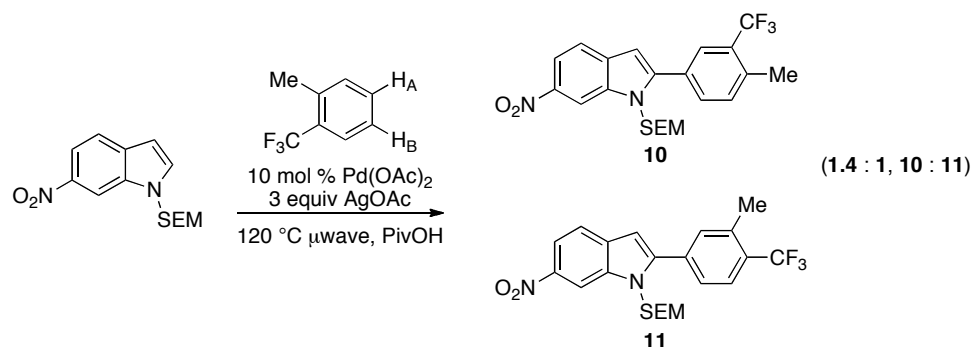
relationship between the observed **B** : **A** ratios and the calculated $[pK_a(H_A) - pK_a(H_B)]$ values. Even in the sterically similar arenes **6-9**, **B** : **A** ratios were poorly correlated with $pK_a(H_A) - pK_a(H_B)$. These data indicate that a thermodynamically-controlled deprotonation is not the selectivity-determining step of this transformation.

Figure 3.7 Plot of Selectivity (**B** : **A**, experimental) versus ΔpK_a



C–H Bond Length Studies. A recent report by DeBoef has proposed that a given C–H bond's ability to participate in a concerted metallation-deprotonation (CMD) mechanism can be predicted by its bond length.²⁹ In the example below H_A is the most acidic, while H_B is predicted to be the most nucleophilic, however the lack of selectivity observed in the oxidative coupling experiment suggests that neither of these factors has a significant influence over the selectivity (Scheme 3.27). The aryl C–H bonds are identical in length (1.075 Å) and the authors suggest that this is responsible for the lack of site selectivity.

Scheme 3.27 Unselective Oxidative Coupling with C–H Bonds of Equivalent Lengths



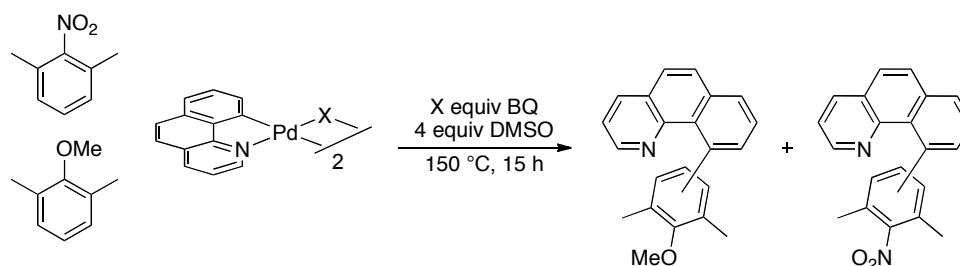
To test this hypothesis on our system, we examined the bond lengths of C–H_A and C–H_B in DMB and other 1,2- and 1,2,3 trisubstituted arenes. As seen in Table 3.20, there is not a clear correlation between aryl–H bond length and selectivity in the carbonate system. This is particularly evident in DMB where C–H_B (Table 3.20, entry 5) is the preferred site of functionalization with the carbonate system, but is shorter in length than C–H_A.

Table 3.20 Calculated C–H Bond Lengths and Selectivities

Entry	Arene	C–H _A Bond Length (Å)	C–H _B Bond Length (Å)	B : A (carbonate system)
1		1.087	1.085	1 : 1
2		1.100	1.100	1 : 1
3		1.100	1.100	1.9 : 1
4		1.088	1.090	5 : 1
5		1.087	1.085	11 : 1

These calculations suggest [(bzq)Pd(OAc)]₂ and [(bzq)PdCl]₂/Cs₂CO₃ could be proceeding through different mechanisms for determining selectivity. We next aimed to pursue experiments to directly compare the mechanism of these two systems.

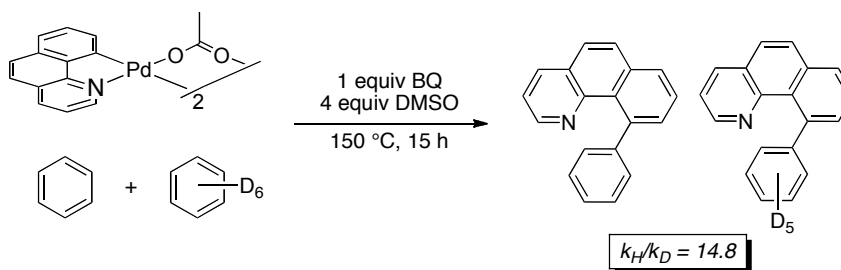
Electronic Competition Studies. We hypothesized that if the reaction of [(bzq)Pd(OAc)]₂ and [(bzq)PdCl]₂/Cs₂CO₃ were operating under fundamentally different mechanisms, the preference for each complex would be different in a mixture of an electron rich and electron poor arenes. To test this notion, each complex was reacted with an equimolar amount of 2-methoxy-1,3-dimethylbenzene and 1,3-dimethyl-2-nitrobenzene. As seen in Table 3.21, the electronic preference for the two Pd complexes is rather small. The [(bzq)Pd(OAc)]₂ system gives a small preference for electron poor arenes at 1 equiv of BQ (1 : 1.1, OMe : NO₂, entry 1), while [(bzq)PdCl]₂ has a moderate preference for electron rich arenes at 1 equiv of BQ (1.26 : 1, OMe : NO₂, entry 2). The preference shifts rather dramatically with [(bzq)Pd(OAc)]₂ under saturation conditions (20 equiv BQ; 2.1 : 1, OMe : NO₂, entry 3), consistent with a change in rate/selectivity determining step. In contrast, very little change in arene selectivity was observed with [(bzq)PdCl]₂ upon increasing the equiv of BQ (1.1 : 1, OMe : NO₂, entry 4). The selectivity difference observed between the [(bzq)Pd(OAc)]₂ and [(bzq)PdCl]₂/Cs₂CO₃ systems is consistent with these two systems operating under different mechanisms. Additionally, the selectivity dependence on [BQ] with [(bzq)Pd(OAc)]₂ observed in this experiment is either not occurring, or not occurring to nearly the same magnitude with [(bzq)PdCl]₂/Cs₂CO₃, indicating another difference in reactivity.

Table 3.21 Arene Electronics Competition Study

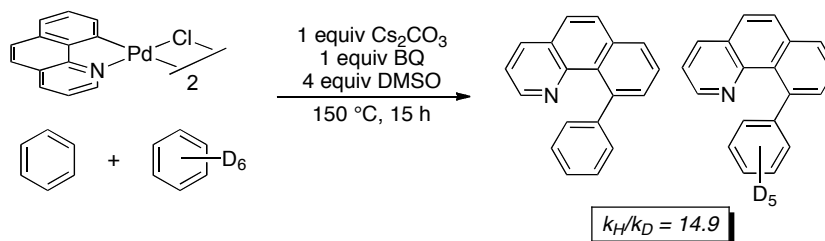
Entry	X	Equiv BQ	% Yield OMe	% Yield NO ₂	Ratio OMe:NO ₂
1	OAc	1	41.5%	45.8%	1 : 1.1
2 ^a	Cl/CO ₃	1	22.2%	17.6%	1.26 : 1
3	OAc	20	49%	23.5%	2.1 : 1
4 ^a	Cl/CO ₃	20	11.5%	10.5%	1.1 : 1

^a Experiments were performed with 1 equiv of Cs₂CO₃

KIE Studies. In an effort to understand the mechanism of C–H activation with [(bzq)PdCl]₂/Cs₂CO₃ and distinguish it from [(bzq)Pd(OAc)]₂ we undertook a series of kinetic isotope effect (KIE) studies. We first examined the competition KIE between H₆-benzene and D₆-benzene with both [(bzq)Pd(Cl)]₂/Cs₂CO₃ and [(bzq)Pd(OAc)]₂. Surprisingly, both reactions gave an unusually high KIE of 14.8 and 14.9 (Schemes 3.28 and 3.29). This indicates a large preference for aryl–H bonds over the aryl–D in both reactions.

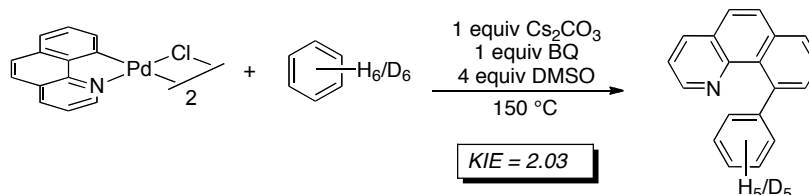
Scheme 3.28 Competition KIE with [(bzq)Pd(OAc)]₂

Scheme 3.29 Competition KIE with [bzqPdCl]₂/Cs₂CO₃ with H₆- and D₆-benzene



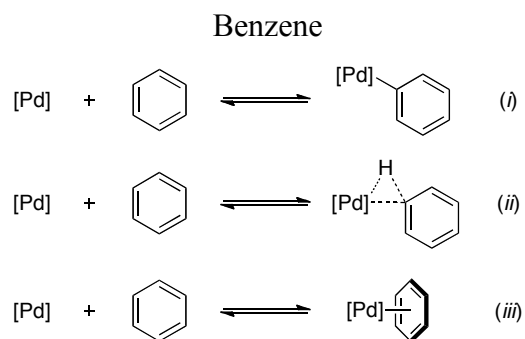
We next looked at the intermolecular isotope effects of [bzqPdCl]₂/Cs₂CO₃ by examining the initial rates of reaction with H₆-benzene and D₆-benzene. As shown in Scheme 3.30 we observed a KIE = 2.03 ± 0.15, consistent with Aryl–H bond breaking in the transition state. This KIE was slightly smaller than that observed with [bzqPd(OAc)₂] and significantly smaller than the competition KIE observed above ($k_H/k_D = 14.9$).

Scheme 3.30 Initial Rates KIE of Oxidative Coupling of [bzqPdCl]₂/Cs₂CO₃ and Benzene



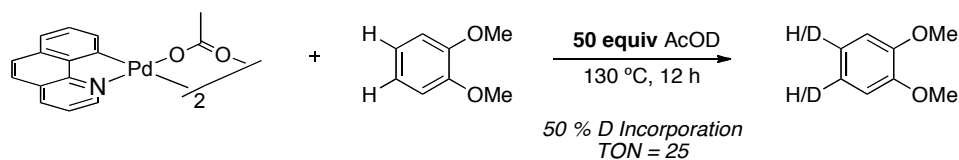
One mechanistic possibility that the KIE data above suggests is a pre-equilibrium event prior to the rate-limiting step. A system in which the selectivity of the products was determined solely by the relative rate of H₆-benzene vs D₆-benzene would be expected to have a 2:1 ratio of H₅/D₅ bzq-benzene coupled products in an intramolecular competition reaction. However, as shown in Scheme 3.29, a $k_H/k_D = 14.9$ is observed suggesting other steps in the reaction are impacting selectivity. One possible explanation is a reversible step prior to C–H bond cleavage. This could include one or more of the following three possible reversible steps (i) reversible aryl–H activation similar to that seen with the [bzqPd(OAc)₂] (Scheme 3.32, i), (ii) a reversible agostic complex interaction (Scheme 3.32, ii), or finally, (iii) there could be reversible π -bond binding to the aryl ring (Scheme 3.32, iii).

Scheme 3.32 Possible Reversible Steps in Oxidative Coupling of $[(\text{bzq})\text{PdCl}]_2/\text{Cs}_2\text{CO}_3$ and

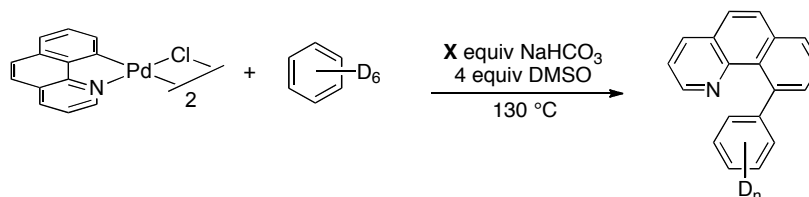


Previous work with $[(\text{bzq})\text{Pd}(\text{OAc})]_2$ had shown that aryl-H activation was reversible. The key experiment used to determine this was an H/D exchange reaction with 1,2-dimethoxybenzene and $[(\text{bzq})\text{Pd}(\text{OAc})]_2$ in the presence of excess $\text{AcOD-}d_4$. As shown in Scheme 3.33, the reaction proceeded with 50 equiv of $\text{AcOD-}d_4$ to give 50% deuterium incorporation by ^2D NMR. This experiment strongly supported a mechanism involving reversible aryl-H activation. We next aimed to explore if aryl-H activation was reversible with $[(\text{bzq})\text{PdCl}]_2/\text{Cs}_2\text{CO}_3$.

Scheme 3.33 H/D Exchange Studies with $[(\text{bzq})\text{Pd}(\text{OAc})]_2$



Several attempts were made to quantify the reversibility of C-H activation in the $[(\text{bzq})\text{PdCl}]_2/\text{Cs}_2\text{CO}_3$ system however, finding suitable conditions proved to be quite challenging. Our efforts to mimic this experiment with $[(\text{bzq})\text{PdCl}]_2$ involved using NaHCO_3 with D_6 -benzene and monitoring for proton incorporation by GCMS. The GCMS chromatogram was then analyzed according to the method of Hickman et. al. to determine the amount of benzene isomers formed.⁴⁹ As shown in Scheme 3.22 below there was not a significant amount of proton incorporation observed in the product relative to the control reaction.

Table 3.22 H/D Exchange Experiments

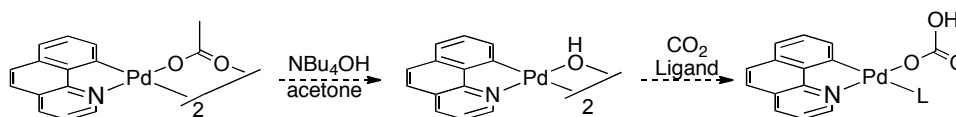
Entry	Equiv NaHCO ₃	C ₆ H ₆	C ₆ H ₅ D	C ₆ H ₄ D ₂	C ₆ H ₃ D ₃	C ₆ H ₂ D ₄	C ₆ HD ₅	C ₆ D ₆
1	1	--	--	3.3	--	--	--	96.7
2	10	--	--	3.3	--	--	--	96.7
3	20	--	--	3.3	--	--	--	96.7
4	--	--	--	3.5	--	--	--	96.5

These data suggest either C–H activation is irreversible under these reaction conditions or that the method of proton incorporation was insufficient. One challenge to this approach was detecting the small amount of H_n-benzene relative to the large amount of the D₆-benzene. In order to address this issue a series of experiments were performed with varying amounts of mesitylene as a cosolvent, however these experiments showed insignificant amounts of proton incorporation as well. Additionally, efforts to synthesize NaDCO₃ from NaHCO₃ for experiments with H₆-benzene produced only small amounts of deuterium incorporation in a mixture that was difficult to characterize. Thus we can conclude there is most likely a reversible step in this reaction prior to the aryl–H bond breaking event, but the nature of that event is unclear at this time.

The studies above rule out two limiting possibilities for selectivity in the [(bzq)PdCl]₂/Cs₂CO₃ reactions: (i) selectivity-determining palladation via an S_EAr pathway and (ii) selectivity-determining thermodynamically controlled deprotonation. The origin of selectivity in this system will remain the subject of ongoing investigations. We are currently considering at least two alternative possibilities: (i) the selectivity-determining step changes as a function of the arene substrate (for example, involving C–H cleavage via electrophilic palladation with certain arenes and concerted metallation-deprotonation with others), and/or (ii) this transformation involves a mechanistically unique selectivity-determining step that remains to be elucidated.

Future work in this area will need to focus on isolable Pd complexes with the CO_3^{2-} moiety. While the desired complex has not been reported in the literature, similar aryl-Pd complexes have been isolated with CO_3^{2-} ligands by CO_2 insertion into the hydroxo-bridged dimers. One potential synthetic approach to these desired compounds involves the synthesis of the hydroxo dimer from $[(\text{bzq})\text{Pd}(\text{OAc})_2]_2$, which can then undergo CO_2 insertion in the presence of a ligand to give the $[(\text{bzq})\text{Pd}(\text{HCO}_3)\text{L}]$ monomer.^{50, 51} Stoichiometric selectivity and rate studies with this complex would be invaluable in determining the mechanism of $[(\text{bzq})\text{PdCl}]_2/\text{CO}_3$ aryl-H activation.

Scheme 3.34 Potential Synthetic Route



3.5 Conclusion

By examining the factors controlling site selectivity under the two regimes outlined above, we have gained insights into the mechanism of Pd catalyzed aryl-aryl oxidative cross coupling. We have shown that the steric and electronic environment at [Pd] can be tuned to control the site selectivity of arene C-H functionalization. In the process we have also discovered new ways of altering the preferred regioisomer formed in these transformations. In general, the less sterically hindered isomer **A** is with carboxylate X-type ligands in the presence of ≤ 1 equiv quinone, with added RCO_2H , and with alkyl-substituted quinones. Switching to carbonate as the X-type ligand at [Pd] reverses the selectivity to favor isomer **B**. The ability to achieve this type of catalyst-based control over site selectivity is a significant advance, and the observed effects may be more broadly applicable to other C-H arylation reactions.

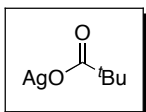
3.6 Experimental Procedures

General Procedures: NMR spectra were obtained on a Varian Inova 500 (499.90 MHz for ^1H ; 125.70 MHz for ^{13}C), a Varian Inova 400 (399.96 MHz for ^1H ; 100.57 MHz for

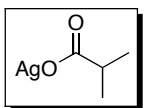
^{13}C ; 376.34 MHz for ^{19}F), or a Varian Mercury 300 (300.07 MHz for ^1H ; 75.45 MHz for ^{13}C NMR; 282.35 MHz for ^{19}F) spectrometer. ^1H and ^{13}C NMR chemical shifts are reported in parts per million (ppm) relative to TMS, with the residual solvent peak used as an internal reference. ^{19}F NMR spectra are referenced based on the unified scale, where the frequency of the residual solvent peak in the ^1H NMR spectrum acts as the single primary reference. ^{19}F NMR spectra are proton coupled. Multiplicities are reported as follows: singlet (s), doublet (d), doublet of doublets (dd), doublet of doublet of doublets (ddd), doublet of triplets (dt), doublet of quartets (dq), triplet (t), triplet of doublets (td), quartet (q), quartet of doublets (qd), and multiplet (m). Unless otherwise indicated, the ^1H and ^{13}C NMR spectra were recorded at room temperature.

Materials and Methods: Chemicals that were purchased from commercial sources and used as received are indicated in the experimental section below. Benzoquinone was obtained from Acros and was purified by vacuum sublimation. 2-Methyl-, 2,5-dimethyl-, 2,3,5,6-tetramethyl-, and 2,5-di-*tert*-butylbenzoquinone were obtained from Aldrich and used as received. The 2,5-diarylquinones were synthesized according to a literature procedure.⁵² Cs_2CO_3 (99.9%) was obtained from Aldrich and used as received. Gas chromatography was carried out using a Shimadzu 17A using a Restek Rtx®-5 (Crossbond 5% diphenyl – 95% dimethyl polysiloxane; 15 m, 0.25 mm ID, 0.25 mm ID, 0.25 μm df) column. All GC and isolated yields are the average of two reactions.

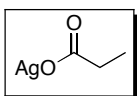
A. Synthesis of Ag Carboxylates



AgOPiv was synthesized from pivalic acid (Sigma) and AgNO_3 (Sargent-Welch) according to a published procedure.⁵³

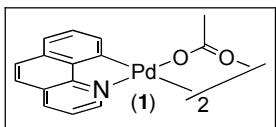


Silver isobutyrate was synthesized from isobutyric acid (Sigma) and AgNO_3 (Sargent-Welch) according to a published procedure.⁵³

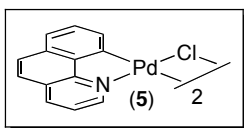


Silver propionate was synthesized from propionic acid (Sigma) and AgNO₃ (Sargent-Welch) according to a published procedure.⁵³

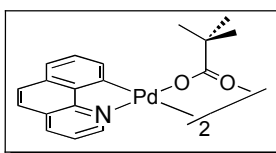
B. Synthesis of Pd Complexes



[(bzq)Pd(OAc)₂] (**1**) was synthesized via the reaction of Pd(OAc)₂ (Pressure Chemical) with benzo[*h*]quinoline (Pfaltz and Bauer) using a published procedure.³⁹ The spectroscopic data matched that reported in the literature.

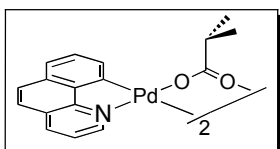


[(bzq)PdCl₂] was synthesized by the reaction [(bzq)PdOAc]₂ with LiCl (Mallinckrodt AR) according to a published procedure.³⁹ The spectroscopic data matched that reported in the literature.

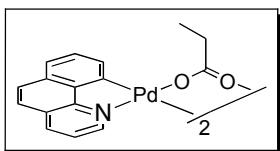


[(bzq)PdCl₂] (500 mg, 0.78 mmol, 0.5 equiv) and AgOPiv (326.5 mg, 1.56 mmol, 1 equiv) were weighed into a round bottom flask and then dissolved in CH₂Cl₂ (173 mL). The resulting solution was stirred at rt for 15 h, during which time it changed color from pale yellow to orange. The reaction mixture was filtered through a plug of Celite, and the solvent was removed *in vacuo*. The resulting orange solid was recrystallized from CH₂Cl₂/hexanes to provide [(bzq)Pd(OPiv)₂] as an orange solid (330.6 mg, 55% yield). ¹H NMR (500 MHz, 95% CDCl₃ : 5% pyridine-*d*₅): δ 8.74 (dd, *J* = 5.0, 1.5 Hz, 1H), 8.27 (dd, *J* = 8.0, 1.5 Hz, 1H), 7.72 (d, *J* = 8.0 Hz, 1H), 7.58 (d, *J* = 8.0 Hz, 1H), 7.54 (d, *J* =

8.0 Hz, 1H), 7.47 (dd, $J = 8.0, 5.0$ Hz, 1H), 7.23 (m, 1H), 6.48 (d, $J = 7.0$ Hz, 1H), 1.15 (s, 9H). ^{13}C { ^1H } NMR (125 MHz, 95% CDCl_3 : 5% pyridine- d_5): δ 185.1, 155.0, 151.2, 148.3, 141.7, 136.9, 133.0, 130.3, 128.8, 128.2, 126.4, 123.1, 122.4, 121.1, 39.6, 28.4. IR (KBr): 1558 cm^{-1} . Analysis calculated for $\text{C}_{36}\text{H}_{34}\text{N}_2\text{O}_4\text{Pd}_2$: C: 56.04, H: 4.44, N: 3.63, found: C: 55.94, H: 4.27, N: 3.70

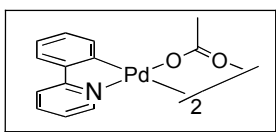


$[(\text{bzbq})\text{PdCl}]_2$ (500 mg, 0.78 mmol, 0.5 equiv) and silver *iso*-butyrate (AgOi-Pr) (304.2 mg, 1.56 mmol, 1 equiv) were weighed into a round bottom flask and then dissolved in CH_2Cl_2 (173 mL). The resulting solution was stirred at rt for 15 h, during which time it changed color from pale yellow to dark yellow. The reaction mixture was filtered through a plug of Celite, and the solvent was removed *in vacuo*. The resulting orange solid was recrystallized from CH_2Cl_2 /hexanes to provide $[(\text{bzbq})\text{Pd}(\text{Oi-Bu})]_2$ as a yellow solid (411.7 mg, 71% yield). ^1H NMR (400 MHz, 95% CDCl_3 : 5% pyridine- d_5): δ 8.68 (dd, $J = 5.0, 1.0$ Hz, 1H), 8.21 (dd, $J = 8.0, 1.0$ Hz, 1H), 7.66 (d, $J = 8.0$ Hz, 1H), 7.51 (t, $J = 8.0$ Hz, 2H), 7.41 (dd, $J = 8.0, 5.0$ Hz, 1H), 7.22 (t, $J = 8.0$ Hz, 1H), 6.44 (d, $J = 8.0$ Hz, 1H), 2.48 (sept, $J = 7.0$ Hz, 1H), 1.10 (d, $J = 7.0$ Hz, 6H). { ^1H } NMR (100 MHz, 95% CDCl_3 : 5% pyridine- d_5): δ 184.1, 155.1, 150.9, 148.4, 141.7, 137.1, 133.2, 130.4, 128.8, 128.3, 126.5, 123.3, 122.6, 121.1, 37.0, 20.5. IR (KBr): 1593 cm^{-1} . Analysis calculated for $\text{C}_{34}\text{H}_{30}\text{N}_2\text{O}_4\text{Pd}_2$: C: 54.93, H: 4.07, N: 3.77, found: C: 54.15, H: 4.06, N: 3.53.

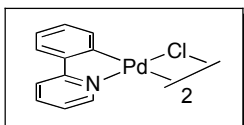


$[(\text{bzbq})\text{PdCl}]_2$ (500 mg, 0.78 mmol, 0.5 equiv) and silver propionate (AgOProp) (282.3 mg, 1.56 mmol, 1 equiv) were weighed into a round bottom flask and then dissolved in CH_2Cl_2 (173 mL). The resulting solution was stirred at rt for 15 h, during which time it changed color from pale yellow to dark yellow. The reaction mixture was filtered through a plug of Celite, and the solvent was removed *in vacuo*. The resulting orange solid was

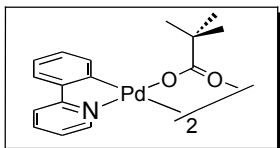
recrystallized from CH₂Cl₂/hexanes to provide [(bzq)Pd(OProp)]₂ as a yellow solid (362.7 mg, 65% yield). ¹H NMR (400 MHz, 95% CDCl₃ : 5% pyridine-*d*₅): δ 8.68 (dd, *J* = 5.0, 1.0 Hz, 1H), 8.19 (dd, *J* = 8.0, 1.0 Hz, 1H), 7.65 (d, *J* = 8.0 Hz, 1H), 7.49 (t, *J* = 8.0 Hz, 2H), 7.41 (dd, *J* = 8.0, 5.0 Hz, 1H), 7.21 (t, *J* = 8.0 Hz, 1H), 6.40 (d, *J* = 8.0 Hz, 1H), 2.28 (q, *J* = 8.0 Hz, 2H), 1.10 (t, *J* = 8.0 Hz, 3H). ¹³C {¹H} NMR (100 MHz, 95% CDCl₃ : 5% pyridine-*d*₅): δ 181.2, 155.0, 150.8, 148.4, 141.7, 137.1, 133.1, 130.4, 128.8, 128.3, 126.5, 123.2, 122.6, 121.1, 31.4, 11.1. IR (KBr): 1588 cm⁻¹. Analysis calculated for C₃₂H₂₆N₂O₄Pd₂: C: 53.72, H: 3.66, N: 3.92, found: C: 53.03, H: 3.58, N: 3.82.



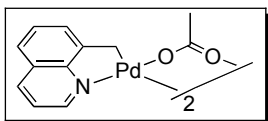
2-Phenylpyridine (1.56 g, 0.011 mol, 1 equiv, Matrix Scientific) was added to a solution of Pd(OAc)₂ (2.50 g, 0.011 mol, 1 equiv) in MeOH (180 mL) and stirred at rt for 6 h, during which time a yellow solid precipitated from solution. The precipitate was collected at the top of a plug of Celite, and the solids were washed with hexanes (3 x 30 mL). The yellow residue at the top of the Celite plug was then washed through with CH₂Cl₂ (2 x 300 mL). The solvent was removed *in vacuo*, and the resulting solid was recrystallized from CH₂Cl₂/hexanes to afford the product as a yellow solid (3.02 g, 86% yield). The spectroscopic data matched that reported in the literature.⁵⁴



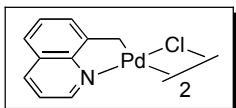
LiCl (2.65 g, 0.0625 mol, 20 equiv, Mallinckrodt AR) was added to a solution of [(phpy)Pd(OAc)]₂ (1.0 g, 0.0031 mol, 0.5 equiv dimer) in EtOH (25 mL) at 0 °C. The resulting solution was warmed to rt and then stirred for 15 h, during which time a gray solid precipitated from solution. The precipitate was collected on a fritted filter, washed with water (3 x 20 mL), MeOH (3 x 20 mL), and diethyl ether (3 x 20 mL), and then dried under vacuum. The product was obtained as a gray solid (0.555 g, 60% yield). The spectroscopic data matched that reported in the literature.⁵⁵



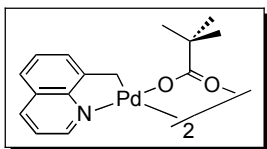
[(phpy)PdCl]₂ (444.1 mg, 0.75 mmol, 0.5 equiv) and AgOPiv (313.0 mg, 1.5 mmol, 1 equiv) were weighed into a round bottom flask and then dissolved in CH₂Cl₂ (167 mL). The resulting solution was stirred at rt for 15 h, during which time it changed color from pale yellow to orange. The reaction mixture was filtered through a plug of Celite, and the solvent was removed *in vacuo*. The resulting orange solid was recrystallized from CH₂Cl₂/hexanes to provide [(phpy)Pd(OPiv)]₂ as an orange solid (385.2 mg, 71% yield). ¹H NMR (500 MHz, 95% CDCl₃ : 5% pyridine-*d*₅): δ 8.52 (dd, *J* = 6.0, 1.0 Hz, 1H), 7.79 (td, *J* = 8.0, 2.0 Hz, 1H), 7.64 (d, *J* = 8.0 Hz, 1H), 7.43 (dd, *J* = 8.0, 1.0 Hz, 1H), 7.13 (ddd, *J* = 7.0, 6.0, 1.0 Hz, 1H), 7.06 (td, *J* = 7.0, 1.0 Hz, 1H), 6.90 (td, *J* = 8.0, 1.0 Hz, 1H), 6.23 (dd, *J* = 8.0, 1.0 Hz, 1H), 1.15 (s, 9H). ¹³C {¹H} NMR (100 MHz, 95% CDCl₃ : 5% pyridine-*d*₅): δ 184.6, 165.4, 153.6, 149.5, 145.8, 138.6, 133.3, 129.1, 124.2, 123.1, 121.9, 118.1, 39.5, 28.4. IR (KBr): 1559 cm⁻¹. Analysis calculated for C₃₂H₃₄N₂O₄Pd₂: C: 53.13, H: 4.74, N: 3.87, found C: 53.43, H: 4.74, N: 3.99.



8-Methylquinoline (0.7159 g, 5.0 mmol, 1 equiv) was added to a solution of Pd(OAc)₂ (1.122 g, 5.0 mmol, 1 equiv) in AcOH, and the resulting mixture was stirred at 100 °C for 2 h, during which time a yellow-orange solid precipitated from solution. The precipitate was collected at the top of a plug of Celite, and the solids were washed with hexanes (3 x 50 mL). The yellow-orange residue at the top of the Celite plug was then washed through with CH₂Cl₂ (2 x 200 mL). The solvent was removed *in vacuo*, and the resulting solid was recrystallized from EtOAc/hexanes to afford the product as a yellow-orange solid (1.398 g, 91% yield). The spectroscopic data matched that reported in the literature.⁵⁶



LiCl (8.47 g, 0.200 mol, 20 equiv) was added to a solution of [(mq)Pd(OAc)]₂ (3.076 g, 1 equiv, 0.0100 mol) in EtOH (80 mL). The resulting solution was stirred for 15 h at 0 °C, during which time a gray solid precipitated from solution. The precipitate was collected on a fritted filter, washed with water (3 x 20 mL), MeOH (3 x 20 mL), and diethyl ether (3 x 20 mL), and then dried under vacuum. The product was obtained as a gray solid (1.850 g, 65% yield). The spectroscopic data matched that reported in the literature.⁵⁷

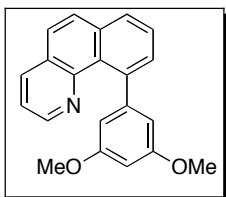


[(mq)PdCl]₂ (424.4 mg, 0.75 mmol, 0.5 equiv) and AgOPiv (313.0 mg, 1.5 mmol, 1 equiv) were weighed into a round bottom flask and then dissolved in CH₂Cl₂ (167 mL). The resulting solution was stirred at rt for 15 h, during which time it changed color from pale yellow to orange. The reaction mixture was filtered through a plug of Celite, and the solvent was removed *in vacuo*. The resulting solid was recrystallized from CH₂Cl₂/hexanes to provide [(mq)Pd(OPiv)]₂ as an orange solid (236.1 mg, 45% yield). ¹H NMR (500 MHz, 95% CDCl₃ : 5% pyridine-*d*₅): δ 8.71 (dd, *J* = 5.0, 1.0 Hz, 1H), 8.18 (dd, *J* = 8.0, 1.0 Hz, 1H), 7.51 (d, *J* = 8.0 Hz, 1H), 7.47 (dd, *J* = 8.0, 1.0 Hz, 1H), 7.40 (t, *J* = 8.0 Hz, 1H), 7.33 (dd, *J* = 8.0, 5.0 Hz, 1H), 3.33 (s, 2H), 1.14 (s, 9H). ¹³C {¹H} NMR (100 MHz, 95% CDCl₃ : 5% pyridine-*d*₅): δ 184.6, 153.2, 149.4, 148.5, 137.1, 128.7, 128.2, 127.7, 123.2, 121.2, 39.6, 28.5, 24.3. IR (KBr): 1564 cm⁻¹. Analysis calculated for C₃₁H₃₈N₂O₄Pd₂: C: 52.52 H: 4.90, N: 4.01, found: C: 52.61, H: 4.97, N: 3.93

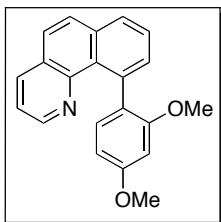
C. Oxidative Coupling Reactions

General Procedure A (Isolation of C–C Coupled Products). The appropriate palladium dimer (0.15 mmol dimer, 0.5 equiv), BQ (0.3 mmol, 1 equiv), Cs₂CO₃ (0.3 mmol, 1 equiv, Aldrich), and DMSO (1.2 mmol, 4 equiv) were combined in a 20 mL scintillation vial. The resulting mixture was diluted with arene (12 mL). The vial was sealed with a Teflon-lined cap, and the reaction mixture was stirred vigorously at 150° C for 15 h.

Upon completion, the reaction was transferred to a round bottom flask, and the solvent was removed via distillation under reduced pressure. The product was then purified by chromatography on silica gel.

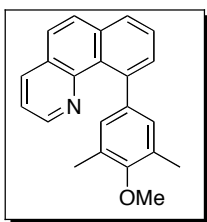


The product 10-(3,5-dimethoxyphenyl)benzo[*h*]quinoline was synthesized according to general procedure A, using [(bzq)Pd(OAc)]₂ (103.1 mg, 0.15 mmol, 0.5 equiv) and 1,3-dimethoxybenzene (12 mL, TCI) without added Cs₂CO₃. The crude product contained a 5 : 1 mixture of isomers **A** and **B**. Pure samples of **A** were obtained via flash chromatography on silica gel (*R*_f (isomer **A**) = 0.30 in 90% hexanes/10% ethyl acetate). This product was isolated as a white solid (67 mg, 71% yield, mp = 131.0-132.3 °C). ¹H NMR (CDCl₃): δ 8.52 (d, *J* = 4.0 Hz, 1H), 8.08 (d, *J* = 8.0 Hz, 1H), 7.92 (d, *J* = 8.0 Hz, 1H) 7.85 (d, *J* = 8.0 Hz, 1H), 7.78 (d, *J* = 8.0 Hz, 1H), 7.67 (d, *J* = 8.0 Hz, 1H), 7.58 (d, *J* = 8.0 Hz, 1H), 7.34 (dd, *J* = 8.0, 4.0 Hz, 1H), 6.55 (s, 2H), 6.51 (s, 1H), 3.78 (s, 6H). ¹³C {¹H} NMR (CDCl₃): δ 160.0, 148.4, 147.0, 146.6, 141.4, 135.1, 134.9, 131.1, 128.9, 128.2, 127.2, 126.9, 125.0, 121.1, 107.1, 98.2, 55.3. HRMS ESI with Formic Acid (*m/z*): [M+H]⁺ calcd for C₂₁H₁₇NO₂, 316.1338; found, 316.1336.

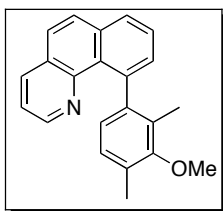


The product 10-(2,4-dimethoxyphenyl)benzo[*h*]quinoline was synthesized according to general procedure A, using [(bzq)PdCl]₂ (96 mg, 0.15 mmol, 0.5 equiv) and 1,3-dimethoxybenzene (12 mL, TCI) in the presence of Cs₂CO₃. The crude product contained a 1 : 11 mixture of isomer **A** : **B**. This mixture was purified via flash chromatography on silica gel to afford a yellow solid containing a > 20 : 1 ratio of **B** : **A** (56.8 mg, 61% yield, *R*_f (isomer **B**) = 0.27 in 90% hexanes/10% ethyl acetate, mp = 122.0-123.5 °C). Samples

of isomer **B** for NMR analysis were further purified by HPLC. ^1H NMR (CDCl_3): δ 8.49 (dd, $J = 4.0, 2.0$ Hz, 1H), 8.07 (dd, $J = 8.0, 2.0$ Hz, 1H), 7.90 (d, $J = 8.0$ Hz, 1H), 7.86 (d, $J = 8.0$ Hz, 1H), 7.68 (dd $J = 15.0, 8.0$ Hz, 2H), 7.53 (d, $J = 8.0$ Hz, 1H), 7.31 (dd, $J = 8.0, 4.0$ Hz, 1H), 7.19 (d, $J = 8.0$ Hz, 1H), 6.61 (dd, $J = 8.0, 2.0$ Hz, 1H), 6.51 (d, $J = 2.0$ Hz, 1H), 3.92 (s, 3H), 3.80 (s, 3H). ^{13}C $\{^1\text{H}\}$ NMR (CDCl_3): δ 159.7, 158.5, 147.4, 146.9, 137.6, 134.9, 134.5, 131.5, 129.9, 129.1, 128.4, 128.0, 127.2, 126.7, 125.7, 120.8, 103.1, 98.1, 55.4, 55.2 (two ^{13}C NMR resonances coincidentally overlap). HRMS ESI with Formic Acid (m/z): $[\text{M}+\text{H}]^+$ calcd for $\text{C}_{21}\text{H}_{17}\text{NO}_2$, 316.1338; found, 316.1335.

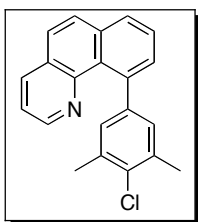


Authentic samples of 10-(4-methoxy-3,5-dimethylphenyl)benzo[*h*]quinoline were obtained using a previously reported procedure,³² and the characterization data matched that reported in the literature.³² A GC calibration curve was made using nonadecane as an internal standard.

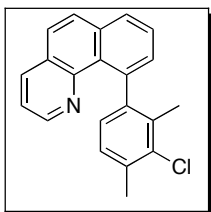


The product 10-(3-methoxy-2,4-dimethylphenyl)benzo[*h*]quinoline was synthesized according to general procedure A, using $[(\text{bzq})\text{PdCl}]_2$ (96 mg, 0.15 mmol, 0.5 equiv) and 2-methoxy-1,3-dimethylbenzene (12 mL, Aldrich) in the presence of Cs_2CO_3 . The crude product contained a 1 : 1 mixture of isomer **A** : **B**. This mixture was purified via flash chromatography on silica gel to afford a clear oil containing a 5 : 1 ratio of **B** : **A** (29 mg, 31% yield, R_f (isomer **B**) = 0.20 in 95% hexanes/5% ethyl acetate). Samples of isomer **B** for NMR analysis were further purified by HPLC. ^1H NMR (CDCl_3): δ 8.45 (dd, $J = 4.0, 2.0$ Hz, 1H), 8.08 (dd, $J = 8.0, 2.0$ Hz, 1H), 7.94 (dd, 8.0, 1.0 Hz, 1H), 7.87 (d, $J = 9.0$

Hz, 1H), 7.72-7.68 (multiple peaks, 2H), 7.49 (dd, $J = 7.0, 1.0$ Hz, 1H), 7.31 (dd, $J = 8.0, 4.0$ Hz, 1H), 7.10 (d, $J = 8.0$ Hz, 1H), 6.89 (d, $J = 8.0$ Hz, 1H), 3.78, (s, 3H), 2.44 (s, 3H), 1.77, (s, 3H). ^{13}C $\{^1\text{H}\}$ NMR (CDCl_3): δ 156.4, 147.3, 147.0, 145.9, 140.8, 135.1, 134.6, 130.8, 129.5, 129.2, 128.5, 128.0, 127.9, 127.5, 127.2, 127.0, 125.8, 123.5, 120.9, 59.7, 16.2, 13.3. HRMS ESI with Formic Acid (m/z): $[\text{M}+\text{H}]^+$ calcd for $\text{C}_{22}\text{H}_{19}\text{NO}$, 314.1545; found, 314.1542.

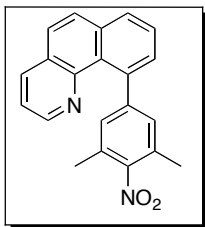


Authentic samples of 10-(4-chloro-3,5-dimethylphenyl)benzo[*h*]quinoline were obtained using a previously reported procedure, and the characterization data matched that reported in the literature.³² A GC calibration curve was made using nonadecane as an internal standard.

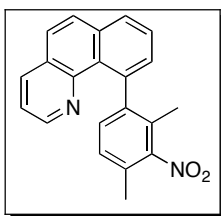


The product 10-(3-chloro-2,4-dimethylphenyl)benzo[*h*]quinoline was synthesized according to general procedure A, using $[(\text{bzq})\text{PdCl}]_2$ (96 mg, 0.15 mmol, 0.5 equiv) and 2-chloro-1,3-dimethylbenzene (12 mL, Aldrich) in the presence of Cs_2CO_3 . The crude product contained a 1 : 2 mixture of isomer **A** : **B**. This mixture was purified via flash chromatography on silica gel to afford a clear oil containing a 7 : 1 ratio of **B** : **A** (20 mg, 21% yield, R_f (isomer **B**) = 0.26 in 95% hexanes/5% ethyl acetate, mp = 122.0-123.5 °C). Samples of isomer **B** for NMR analysis were further purified by HPLC. ^1H NMR (CDCl_3): δ 8.46 (dd, $J = 4.5, 2.0$ Hz, 1H), 8.08 (dd, $J = 8.0, 2.0$ Hz, 1H), 7.95 (d, $J = 8.0$ Hz, 1H), 7.87 (d, $J = 8.0$ Hz, 1H), 7.70 (dd, $J = 8.0, 4.5$ Hz, 2H), 7.43 (d, $J = 8.0$ Hz, 1H), 7.32 (dd, 8.0, 4.5 Hz, 1H), 7.15 (d, $J = 8.0$ Hz, 1H), 6.99 (d, $J = 8.0$ Hz, 1H), 2.52 (s, 3H),

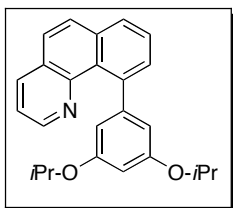
1.92 (s, 3H). ^{13}C $\{^1\text{H}\}$ NMR (CDCl_3): δ 147.5, 146.8, 145.6, 140.5, 135.1, 134.6, 134.3, 134.1, 133.5, 130.8, 129.4, 128.3, 128.1, 127.2, 127.1, 127.0, 125.9, 125.8, 121.0, 21.0, 18.1. HRMS ESI with Formic Acid (m/z): $[\text{M}+\text{H}]^+$ calcd for $\text{C}_{21}\text{H}_{16}\text{ClN}$, 318.1050; found, 318.1045.



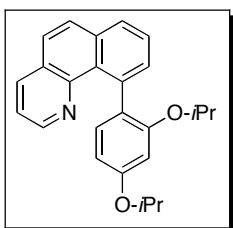
Authentic samples of 10-(3,5-dimethyl-4-nitrophenyl)benzo[*h*]quinoline were obtained using a previously reported procedure, and the characterization data matched that reported in the literature.³² A GC calibration curve was made using nonadecane as an internal standard.



The product 10-(2,4-dimethyl-3-nitrophenyl)benzo[*h*]quinoline was synthesized according to general procedure A, using $[(\text{bzq})\text{PdCl}]_2$ (96 mg, 0.15 mmol, 0.5 equiv) and 1,3-dimethyl-2-nitrobenzene (12 mL, TCI) in the presence of Cs_2CO_3 . The crude product contained a 1 : 5 mixture of isomer **A** : **B**. This mixture was purified via flash chromatography on silica gel to afford a yellow oil containing a 11 : 1 ratio of **B** : **A** (28 mg, 30% yield, R_f (isomer **B**) = 0.11 in 98% hexanes/2% ethyl acetate). Samples of isomer **B** for NMR analysis were further purified by HPLC. ^1H NMR (acetone- d_6): δ 8.44 (dd, $J = 4.0, 2.0$ Hz, 1H), 8.31 (dd, $J = 8.0, 2.0$ Hz, 1H), 8.12 (d, $J = 8.0$ Hz, 1H), 8.02 (d, $J = 9.0$ Hz, 1H), 7.88 (d, $J = 9.0$ Hz, 1H), 7.80 (7, $J = 8.0$ Hz, 1H), 7.49-7.45 (multiple peaks, 2H), 7.26 (d, 8.0 Hz, 1H), 7.15 (d, 8.0 Hz, 1H), 2.38 (s, 3H), 1.76 (s, 3H). ^{13}C $\{^1\text{H}\}$ NMR (acetone- d_6): δ 153.3, 148.2, 147.0, 146.8, 139.3, 136.3, 135.6, 131.3, 130.1, 129.8, 129.6, 129.1, 128.5, 128.3, 128.0, 127.7, 127.0, 126.6, 122.3, 17.0, 15.1. HRMS ESI with Formic Acid (m/z): $[\text{M}+\text{H}]^+$ calcd for $\text{C}_{21}\text{H}_{16}\text{N}_2\text{O}_2$, 329.1290; found, 329.1281.

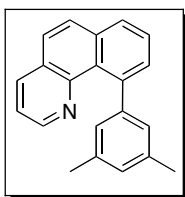


The product 10-(3,5-diisopropoxyphenyl)benzo[*h*]quinoline was synthesized according to general procedure A, [(bzq)Pd(OAc)₂] (103.1 mg, 0.15 mmol dimer, 1 equiv) and 1,3-di-*i*-propoxybenzene (12 mL, Aldrich) without added Cs₂CO₃. The crude product contained a 9 : 1 mixture of isomer **A** : **B**. This mixture was purified via flash chromatography on silica gel to afford a clear oil containing a 10 : 1 ratio of **A** : **B** (73.1 mg, 66% yield, R_f (isomer **A**) = 0.25 in 95% hexanes/5% ethyl acetate). Samples of isomer **A** for NMR analysis were further purified by HPLC. ¹H NMR (CDCl₃): δ 8.52 (dd, *J* = 4.5, 2.0 Hz, 1H), 8.08 (dd, *J* = 8.0, 2.0 Hz, 1H), 7.91 (dd, *J* = 8.0, 1.0 Hz, 1H), 7.84 (d, *J* = 8.0 Hz, 1H), 7.68 (d, *J* = 9.0 Hz, 1H), 7.65 (d, *J* = 9.0 Hz, 1H), 7.57 (dd, *J* = 7.0, 1.0 Hz, 1H), 7.32 (dd, *J* = 8.0, 4.0 Hz, 1H), 6.49 (d, *J* = 2.0 Hz, 2H), 6.47 (t, *J* = 2.0 Hz, 1H), 4.85 (septet, *J* = 6.0 Hz, 2H), 1.26 (d, *J* = 6.0 Hz, 12H). ¹³C {¹H} NMR (CDCl₃): δ 158.3, 148.3, 147.1, 146.8, 141.7, 135.0, 134.9, 131.0, 129.0, 128.2, 127.9, 127.2, 126.9, 125.9, 121.0, 109.1, 102.4, 69.8, 22.1. HRMS ESI with Formic Acid (*m/z*): [M+H]⁺ calcd for C₂₅H₂₅NO₂, 372.1964; found, 372.1969.

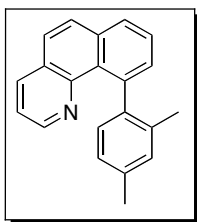


The product 10-(2,4-diisopropoxyphenyl)benzo[*h*]quinoline was synthesized according to general procedure A, using [(bzq)PdCl]₂ (96 mg, 0.15 mmol, 0.5 equiv) and 1,3-di-*i*-propoxybenzene (12 mL, Aldrich) in the presence of Cs₂CO₃. The crude product contained a 1 : 9 mixture of isomer **A** : **B**. This mixture was purified via flash chromatography on silica gel to afford a clear oil containing a >20 : 1 ratio of **B** : **A** (73 mg, 66% yield, R_f (isomer **B**) = 0.24 in 95% hexanes/5% ethyl acetate). Samples of

isomer **B** for NMR analysis were further purified by HPLC. ^1H NMR (CDCl_3): δ 8.49 (dd, $J = 4.0, 2.0$ Hz, 1H), 8.06 (dd, $J = 7.5, 2.0$ Hz, 1H), 7.88 (dd, $J = 7.5, 1.0$ Hz, 1H), 7.82 (d, $J = 9.0$ Hz, 1H), 7.68-7.64 (multiple peaks, 2H), 7.54 (dd, $J = 7.5, 2.0$ Hz, 1H), 7.31 (q, $J = 4.0$ Hz, 1H), 7.23 (d, $J = 7.5$ Hz, 1H), 6.60 (dd, $J = 7.5, 2.0$ Hz, 1H), 6.44 (d, $J = 2.0$ Hz, 1H), 4.64 (sep, $J = 6.0$ Hz, 1H), 4.06 (sep, $J = 6.0$ Hz, 1H), 1.43 (d, $J = 6.0$ Hz, 3H), 1.41 (d, $J = 6.0$ Hz, 3H), 0.85 (d, $J = 6.0$ Hz, 3H), 0.39 (d, $J = 6.0$ Hz, 3H). (*Restricted rotation around the aryl-aryl bond*) ^{13}C $\{^1\text{H}\}$ NMR (acetone- d_6): δ 158.5, 157.3, 148.2, 147.5, 139.3, 135.8, 135.3, 132.2, 130.9, 130.3, 130.2, 129.0, 128.3, 127.8, 127.7, 127.5, 126.3, 121.8, 70.2, 70.0, 22.4, 22.3, 22.2, 21.5. (*Two aromatic signals coincidentally overlap*) HRMS ESI with Formic Acid (m/z): $[\text{M}+\text{H}]^+$ calcd for $\text{C}_{25}\text{H}_{25}\text{NO}_2$, 372.1964; found, 372.1971.

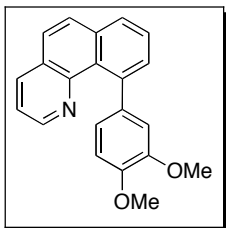


Authentic samples of 10-(3,5-dimethylphenyl)benzo[*h*]quinoline were obtained using a previously reported procedure, and the characterization data matched that reported in the literature.³² A GC calibration curve was made using nonadecane as an internal standard.

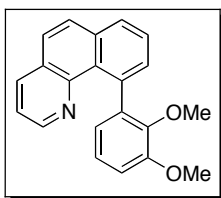


The product 10-(2,4-dimethylphenyl)benzo[*h*]quinoline was synthesized according to general procedure A, using $[(\text{bzq})\text{PdCl}]_2$ and *m*-xylene (12 mL, Aldrich) in the presence of Cs_2CO_3 . The crude product contained a 1 : 1 mixture of isomer **A** : **B**. This mixture was purified via flash chromatography on silica gel to afford a clear oil containing a 1 : 1 ratio of **B** : **A** (56 mg, 66% yield, R_f (isomer **B**) = 0.39 in 95% hexanes/5% ethyl acetate). Samples of isomer **B** for NMR analysis were further purified by HPLC. ^1H NMR (500 MHz, CDCl_3): δ 8.46 (dd, $J = 4.0, 2.0$ Hz, 1H), 8.08 (dd, $J = 8.0, 2.0$ Hz, 1H), 7.94 (dd, J

= 8.0, 1.0 Hz, 1H), 7.87 (d, $J = 9.0$ Hz, 1H), 7.70 (multiple peaks, 2H), 7.47 (dd, $J = 8.0$, 2.0 Hz, 1H), 7.31 (dd, $J = 8.0$, 4.0 Hz, 1H), 7.09 (overlapping peaks, 2H), 7.08 (s, 1H), 2.46 (s, 3H), 1.82 (s, 3H). ^{13}C $\{^1\text{H}\}$ NMR (100 MHz, d_6 -acetone): δ 148.1, 147.7, 144.4, 141.9, 136.2, 135.9, 135.7, 135.5, 131.7, 130.2, 129.2, 128.8, 128.6, 128.1, 127.9, 126.8, 126.4, 122.1, 21.2, 20.3 (two ^{13}C NMR resonances coincidentally overlap). HRMS ESI with Formic Acid (m/z): $[\text{M}+\text{H}]^+$ calcd for $\text{C}_{21}\text{H}_{17}\text{N}$, 284.1439; found, 284.1428.

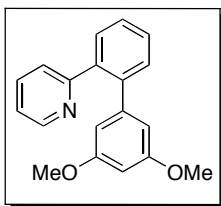


Authentic samples of 10-(3,4-dimethoxyphenyl)benzo[*h*]quinoline were obtained using a previously reported procedure, and the characterization data matched that reported in the literature.³² A GC calibration curve was made using nonadecane as an internal standard.

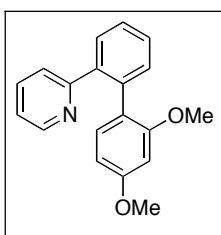


The product 10-(2,3-dimethoxyphenyl)benzo[*h*]quinoline was synthesized according to general procedure A, using [(bzq)PdCl]₂ (96 mg, 0.15 mmol, 0.5 equiv) and 1,2-dimethoxybenzene (12 mL, Aldrich) in the presence of Cs₂CO₃. The crude product contained a 1 : 1 mixture of isomer **B** : **A**. This mixture was purified via flash chromatography on silica gel to afford a clear oil in 95% purity. (76.1 mg, 80% yield, R_f (isomer **B**) = 0.07 in 90% hexanes/10% ethyl acetate). Samples of isomer **B** for NMR analysis were further purified by HPLC. ^1H NMR (400 MHz, d_6 -acetone): δ 8.42 (dd, $J = 4.4$, 2.0 Hz, 1H), 8.24 (dd, $J = 8.0$, 2.0 Hz, 1H), 8.03 (dd, $J = 8.0$, 1.0 Hz, 1H), 7.95 (d, $J = 8.8$ Hz, 1H), 7.81 (d, $J = 8.8$ Hz, 1H), 7.72 (t, $J = 7.2$ Hz, 1H), 7.47 (dd, $J = 7.2$, 1.0 Hz, 1H), 7.40 (dd, $J = 8.4$, 4.4 Hz, 1 H), 7.06-7.00 (overlapping peaks, 2H), 6.73 (dd, $J = 6.8$, 2.8 Hz, 1H), 3.88 (s, 3H), 3.26 (s, 3H). ^{13}C $\{^1\text{H}\}$ NMR (100 MHz, d_6 -acetone): δ 153.3, 147.9, 147.8, 147.1, 141.8, 138.8, 136.1, 135.6, 131.8, 130.4, 129.1, 128.8, 127.9, 127.7,

126.7, 123.7, 122.7, 122.1, 111.9, 59.5, 56.2. HRMS ESI with Formic Acid (m/z): $[M+H]^+$ calcd for $C_{21}H_{17}NO_2$, 316.1332; found, 316.1331.

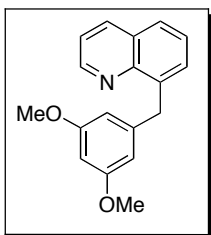


The product 2-(3',5'-dimethoxy-[1,1'-biphenyl]-2-yl)pyridine was synthesized according to general procedure A, using $[(\text{phpy})\text{Pd}(\text{OAc})_2]$ (95.9 mg, 0.15 mmol, 0.5 equiv) and 1,3-dimethoxybenzene (12 mL, TCI) without added Cs_2CO_3 . The crude product contained a 4 : 1 mixture of isomer **A** : **B**. This mixture was purified via flash chromatography on silica gel to afford a clear oil containing a 11 : 1 ratio of **A** : **B** (28.4 mg, 33% yield, R_f (isomer **A**) = 0.09 in 80% hexanes/20% ethyl acetate). Samples of isomer **A** for NMR analysis were further purified by HPLC. ^1H NMR (500 MHz, CDCl_3): δ 8.65 (d, $J = 5.0$ Hz, 1H), 7.69 (dd, $J = 7.5, 1.0$ Hz, 1H), 7.48-7.41 (multiple peaks, 4H), 7.12 (dd, $J = 5.0, 1.0$ Hz, 1H), 6.96 (d, $J = 8.0$ Hz, 1H), 6.33 (t, $J = 2.0$ Hz, 1H), 6.31 (d, $J = 2.0$ Hz, 2H), 3.62 (s, 6H). ^{13}C $\{^1\text{H}\}$ NMR (CDCl_3): δ 160.3, 159.3, 149.3, 143.3, 140.5, 139.5, 135.3, 130.3, 130.1, 128.5, 127.8, 125.3, 121.3, 107.8, 99.4, 55.2. HRMS ESI with Formic Acid (m/z): $[M+H]^+$ calcd for $C_{19}H_{17}NO_2$, 292.1338; found, 292.1335.

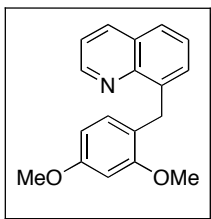


The product 2-(2',4'-dimethoxy-[1,1'-biphenyl]-2-yl)pyridine was synthesized according to general procedure A, using $[(\text{phpy})\text{PdCl}_2]$ (88.8 mg, 0.15 mmol, 0.5 equiv) and 1,3-dimethoxybenzene (12 mL, TCI) in the presence of Cs_2CO_3 . The crude product contained a 1 : 6 mixture of isomer **A** : **B**. This mixture was purified via flash chromatography on silica gel to afford a yellow oil containing a >20 : 1 ratio of **B** : **A** (24.4 mg, 56% yield, R_f (isomer **B**) = 0.11 in 80% hexanes/20% ethyl acetate). Samples of isomer **B** for NMR

analysis were further purified by HPLC. ^1H NMR (500 MHz, CDCl_3): δ 8.61 (d, $J = 5.0$ Hz, 1H), 7.71 (m, 1H), 7.45-7.42 (multiple peaks, 2H), 7.40-7.35 (multiple peaks, 2H), 7.12 (d, $J = 8.0$ Hz, 1H), 7.07 (ddd, $J = 8.0, 5.0, 1.0$ Hz, 1H), 6.93 (d, $J = 8.0$ Hz, 1H), 6.48 (dd, $J = 8.0, 2.5$ Hz, 1H), 6.29 (d, $J = 2.5$ Hz, 1H), 3.29 (s, 3H), 2.93 (s, 3H). ^{13}C $\{^1\text{H}\}$ NMR (125 MHz, CDCl_3): δ 160.4, 159.8, 157.0, 149.0, 140.2, 136.8, 135.1, 131.8, 131.2, 129.6, 128.3, 127.4, 123.6, 121.0, 116.1, 104.4, 98.5, 55.3, 54.9. HRMS ESI with Formic Acid (m/z): $[\text{M}+\text{H}]^+$ calcd for $\text{C}_{19}\text{H}_{17}\text{NO}_2$, 292.1338; found, 292.1343.



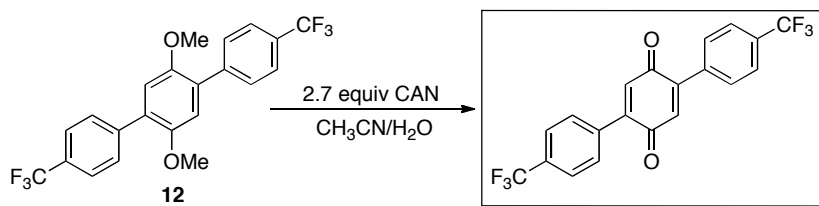
The product 8-(3,5-dimethoxybenzyl)quinoline was synthesized according to general procedure A, using $[(\text{mq})\text{PdOAc}]_2$ (92.3 mg, 0.15 mmol, 0.5 equiv) and 1,3-dimethoxybenzene (12 mL, TCI) without added Cs_2CO_3 . The crude product contained a 1.5 : 1 mixture of isomer **A** : **B**. This mixture was purified via flash chromatography on silica gel to afford a yellow oil containing a 10 : 1 ratio of **A** : **B** (20.9 mg, 25% yield, R_f (isomer **A**) = 0.33 in 85% hexanes/15% ethyl acetate). Samples of isomer **A** for NMR analysis were further purified by HPLC. ^1H NMR (500 MHz, CDCl_3): δ 8.97 (dd, $J = 7.5, 1.5$ Hz, 1H), 8.15 (dd, $J = 7.5, 1.5$ Hz, 1H), 7.69 (dd, $J = 7.5, 1.5$ Hz, 1H), 7.46 (m, 2H), 7.41 (q, $J = 4.0$ Hz, 1H), 6.49 (d, $J = 2.0$ Hz, 2H), 6.31 (t, $J = 2.0$ Hz, 1H), 4.63 (s, 2H), 3.74 (s, 6H). ^{13}C $\{^1\text{H}\}$ NMR (125 MHz, CDCl_3): δ 160.7, 149.5, 146.7, 143.7, 139.7, 136.3, 129.5, 128.4, 126.4, 126.3, 121.0, 107.5, 97.9, 55.2, 37.0. HRMS ESI with Formic Acid (m/z): $[\text{M}+\text{H}]^+$ calcd for $\text{C}_{18}\text{H}_{17}\text{NO}_2$, 280.1338; found, 280.1340.



The product 8-(2,4-dimethoxybenzyl)quinoline was synthesized according to general procedure A, using [(mq)PdCl]₂ (85.2 mg, 0.15 mmol, 0.5 equiv) and 1,3-dimethoxybenzene (12 mL, TCI) in the presence of Cs₂CO₃. The crude product contained a 1 : 4 mixture of isomer **A** : **B**. This mixture was purified via flash chromatography on silica gel to afford a clear oil containing a >20 : 1 ratio of **B** : **A** (29.7 mg, 35% yield, R_f (isomer **B**) = 0.35 in 85% hexanes/15% ethyl acetate). Samples of isomer **B** for NMR analysis were further purified by HPLC. ¹H NMR (500 MHz, CDCl₃): δ 8.98 (dd, *J* = 4.0, 1.5 Hz, 1H), 8.15 (dd, *J* = 8.0, 1.5 Hz, 1H), 7.66 (d, *J* = 8.0 Hz, 1H), 7.41 (multiple peaks, 2H), 7.34 (d, *J* = 7.0 Hz, 1H), 7.05 (d, *J* = 8.0 Hz, 1H), 6.52 (d, *J* = 2.0 Hz, 1H), 6.41 (dd, *J* = 8.0, 2.0 Hz, 1H), 4.62 (s, 2H), 3.79 (overlapping s, 6H). ¹³C{¹H} NMR (100 MHz, CDCl₃): δ 159.3, 158.6, 149.3, 146.9, 140.1, 136.3, 131.2, 128.9, 128.3, 126.4, 125.8, 121.8, 120.8, 104.0, 98.6, 55.4, 55.3, 30.3. HRMS ESI with Formic Acid (*m/z*): [M+H]⁺ calcd for C₁₈H₁₇NO₂, 280.1338; found, 280.1338. C₁₈H₁₇NO₂, 280.1338; found, 280.1338.

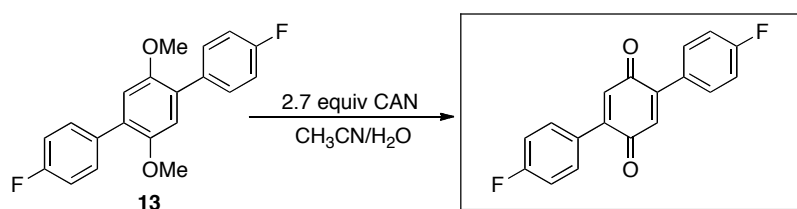
D. Synthesis of 2,5-Diarylquinone Derivatives

The 2,5-diarylquinone derivatives used in this article were synthesized according to a literature procedure, and their spectroscopic data matched that previously reported.⁵² Details of the synthesis and characterization of derivatives that have not been reported previously are described below.



General Procedure for the Synthesis of Diarylquinones. A hot solution of **12**⁵² (653.3 mg, 1.53 mmol, 1.0 equiv) dissolved in a minimal amount of CH₃CN was added dropwise to a stirring room temperature solution of CAN (2.26 g, 4.13 mmol, 2.7 equiv) in H₂O (3.82 mL). The resulting brown solution was stirred for 45 min at rt, and it gradually changed color to yellow as a pale yellow precipitate formed. H₂O (10.4 mL)

was added, and yellow precipitate was collected on a fritted filter and dried under vacuum. The quinone was recrystallized from hot CH₂Cl₂/EtOH to afford a pale yellow solid (392.3 mg, 65% yield, mp = 220.8–221.5 °C). ¹H NMR (400 MHz, CDCl₃): δ 7.74 (d, *J* = 8.0 Hz, 4H), 7.66 (d, *J* = 8.0 Hz, 4H), 7.03 (s, 2H). ¹⁹F NMR (376 MHz, CDCl₃): δ –62.8. ¹³C{¹H} NMR (100 MHz, CDCl₃): δ 185.9, 144.6, 135.6, 133.9, 132.1 (q, *J*_{C-F} = 32.5 Hz), 129.7, 125.5 (q, *J*_{C-F} = 3.8 Hz), 123.8 (q, *J*_{C-F} = 270.1 Hz). IR (KBr): 1646 cm⁻¹. HRMS ESI with Formic Acid (m/z): [M+H]⁺ calcd for C₂₀H₁₀F₆O₂, 396.0585; found, 396.0591.



A hot solution of **13**⁵² (1.152 g, 3.53 mmol, 1.0 equiv) dissolved in a minimal amount of CH₃CN was added dropwise to a stirring room temperature solution of CAN (5.22 g, 9.53 mmol, 2.7 equiv) in H₂O (8.8 mL). The resulting brown solution was stirred for 45 min at rt, during which time an orange precipitate formed. The precipitate was collected via vacuum filtration, washed with H₂O (30 mL) and hexanes (30 mL), and dried under vacuum to afford the quinone product as an orange solid (575.2 mg, 55% yield, mp = 282.3–283.4 °C). ¹H NMR (400 MHz, CD₃CN at 70 °C): δ 7.62 (m, 4H), 7.23 (m, 4H), 6.96 (s, 2H). ¹⁹F NMR (376 MHz, CD₃CN at 70 °C): δ –112.9. The quinone was not sufficiently soluble to obtain a ¹³C NMR spectrum. IR (KBr): 1651 cm⁻¹. HRMS ESI with Formic Acid (m/z): [M+H]⁺ calcd for C₁₈H₁₀F₂O₂, 296.0649; found, 296.0645. Analysis calculated for C₁₈H₁₀F₂O₂: C: 72.97, H: 3.40, F: 12.83, found C: 72.98, H: 3.31, F: 12.58.

Selectivity Studies

General Procedure B (Selectivity Studies in Tables 3.1, 3.2, 3.7, 3.9-3.11, 3.13-3.16, Figure 3.2 and 3.5). The palladium dimer (0.01 mmol) was weighed into a 2 mL scintillation vial, and the appropriate combination of reagents (benzoquinone, M₂CO₃, DMSO, etc) was added. The resulting mixture was diluted with the arene substrate (0.8

mL). The vial was then sealed with a Teflon-lined cap, and the reaction mixture was stirred vigorously at 150 °C for 15 h.⁵⁸ The reactions were allowed to cool to room temperature, nonadecane (0.01 mmol of a stock solution in EtOAc) was added as an internal standard to the crude reaction mixture, and the reactions were analyzed by gas chromatography. The yields of **A** and **B** were determined based on a calibration curve.

Selectivity Dependence on Carboxylate and Benzoate Derivatives. (Tables 3.3-3.6 and 3.8). A slight variation of general procedure B was used for these reactions as follows. [(bzq)Pd(O₂CR)]₂ (0.01 mmol, 0.5 equiv) was weighed into a 2 dram vial. To this solid was added 0.8 mL of a stock solution containing (per aliquot): benzoquinone (1 or 20 equiv), DMSO (4 equiv, 5.7 μL), and 1,3-dimethoxybenzene (0.8 mL). The vial was then sealed with a Teflon-lined cap, and the reaction mixture was stirred vigorously at 150 °C for 15 h. The reactions were allowed to cool to room temperature, nonadecane (0.01 mmol of a stock solution in EtOAc) was added as an internal standard to the crude reaction mixture, and the reactions were analyzed by gas chromatography. The yields of **A** and **B** were determined based on a calibration curve.

Selectivity Hammett plot for [(bzq)Pd(OAc)]₂ (Table 3.2 and Figure 3.3). A Hammett plot was constructed for the reaction of [(bzq)Pd(OAc)]₂ with various 2,5-diarylquinone derivatives based on the data presented in Table 2. The reagents for these experiments were as follows: [(bzq)Pd(OAc)]₂ (6.9 mg, 0.01 mmol, 0.5 equiv), quinone (0.02 mmol, 1 equiv), DMSO (5.7 μL, 0.08 mmol, 4 equiv), and 1,3-dimethoxybenzene (0.8 mL). The reactions were stirred at 150 °C for 15 h, nonadecane was added as an internal standard, and the yield and **A** : **B** ratio was determined by GC. The yields of these reactions ranged from 56-72%. The Hammett plot was obtained by plotting $\log\left[\frac{A/(A+B)_X}{A/(A+B)_H}\right]$ versus σ . Each point represents the average of three runs.

General Procedure for Rate Studies. The palladium dimer (0.01 mmol) was weighed into a 2 mL custom-made Schlenk tube, and the appropriate combination of reagents (benzoquinone, M₂CO₃, DMSO, etc) was added. The resulting mixture was diluted with the arene (benzene or *d*₆-benzene) substrate (0.8 mL) and sealed with a Teflon screw-on

stopper. Data points were collected every 10 minutes for the first 30% of conversion with each Schlenk tube representing one time point. Additionally, each time point was run in duplicate and calibrated against an internal standard (nonadecane).

Figure 3.8 H₆-benzene Reaction Kinetics with [(bzq)PdCl]₂/CO₃

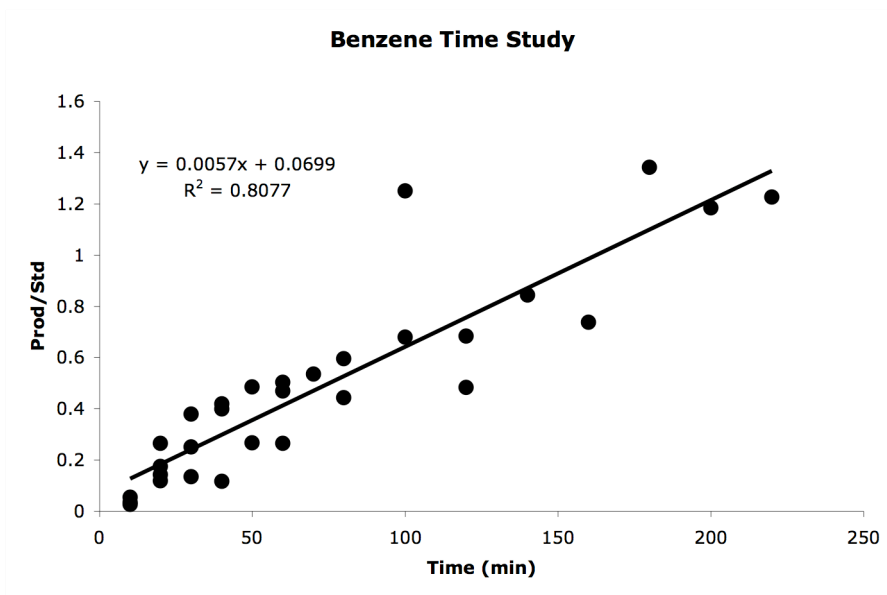
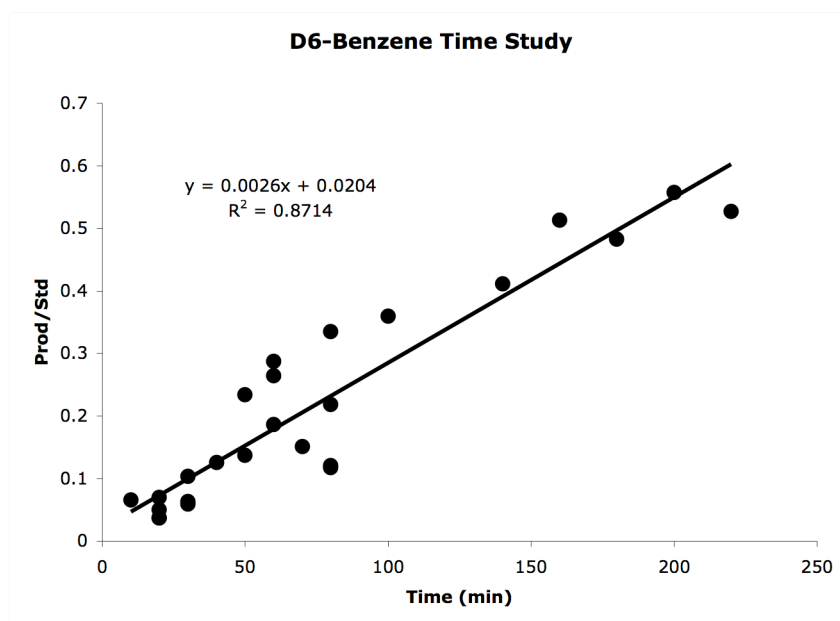


Figure 3.9 D₆-benzene Reaction Kinetics with [(bzq)PdCl]₂/CO₃



V. Computational Experiments

All density functional theory (DFT) calculations were carried out using the Spartan '08⁴³ suite of programs. The B3LYP (Becke's three-parameter hybrid functional⁵⁹ using the LYP correlation functional containing both local and nonlocal terms of Lee, Yang, and Parr)⁶⁰ functional and 6-31+G* or 6-31G** (for anion and cation, respectively) basis set was used for all calculations. Calculations were optimized with constrained symmetry and with IR and thermodynamic corrections using default settings in Spartan. All energies are reported in kcal/mol. Analogous MP-2 calculations were performed in Spartan 08 using identical basis sets and thermodynamic corrections.

Wheland intermediate energies and selectivity. We used DFT to calculate the energies of Wheland intermediates **A'** and **B'** for a series of different 1,3- and 1,2,3-substituted aromatic substrates. We examined **A'** and **B'** rather than the directly analogous palladated intermediates in order to simplify the calculation and reduce computation time. We independently calculated ΔG_{form} for intermediates **A'** and **B'** using both MP-2 and DFT-B3LYP levels of theory. In order to correlate these energies with the observed selectivities, the difference in ΔG_{form} for **A'** and **B'** [$\Delta G_{\text{form}}(\mathbf{A}') - \Delta G_{\text{form}}(\mathbf{B}')$]

was calculated and plotted against the observed selectivities. As seen in Table 3.18 and Figure 3.6 we did not observe a strong correlation with either MP-2 or DFT calculations.

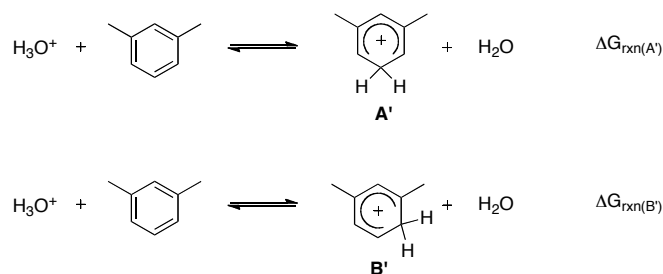
Transition State Theory Approximations. Using the Transition State Theory equation (Figure S3) the rate constant k , was calculated for H_A and H_B of each arene at 298.15K using the ΔG_{rxn} for formation of **A'** or **B'** as an approximation for the ΔG^\ddagger . k_B , h , κ , R , T represent the Boltzmann constant, Planck's constant, the transmission coefficient, gas constant, and temperature (Kelvin) respectively. The predicted product ratio reflects the ratio of rates (k) for **A'** vs **B'**. Hydronium (H_3O^+) and water (H_2O) were used as the acid and conjugate base for these equations respectively. Gas phase DFT calculations were performed with B3LYP/6-31G** using Spartan.

Figure 3.10. Transition State Theory Equation

$$k = \kappa \left(\frac{k_B T}{h} \right) e^{(-\Delta G^\ddagger / RT)}$$

$$k = 2.083 \times 10^{10} T e^{(-\Delta G^\ddagger / RT)}$$

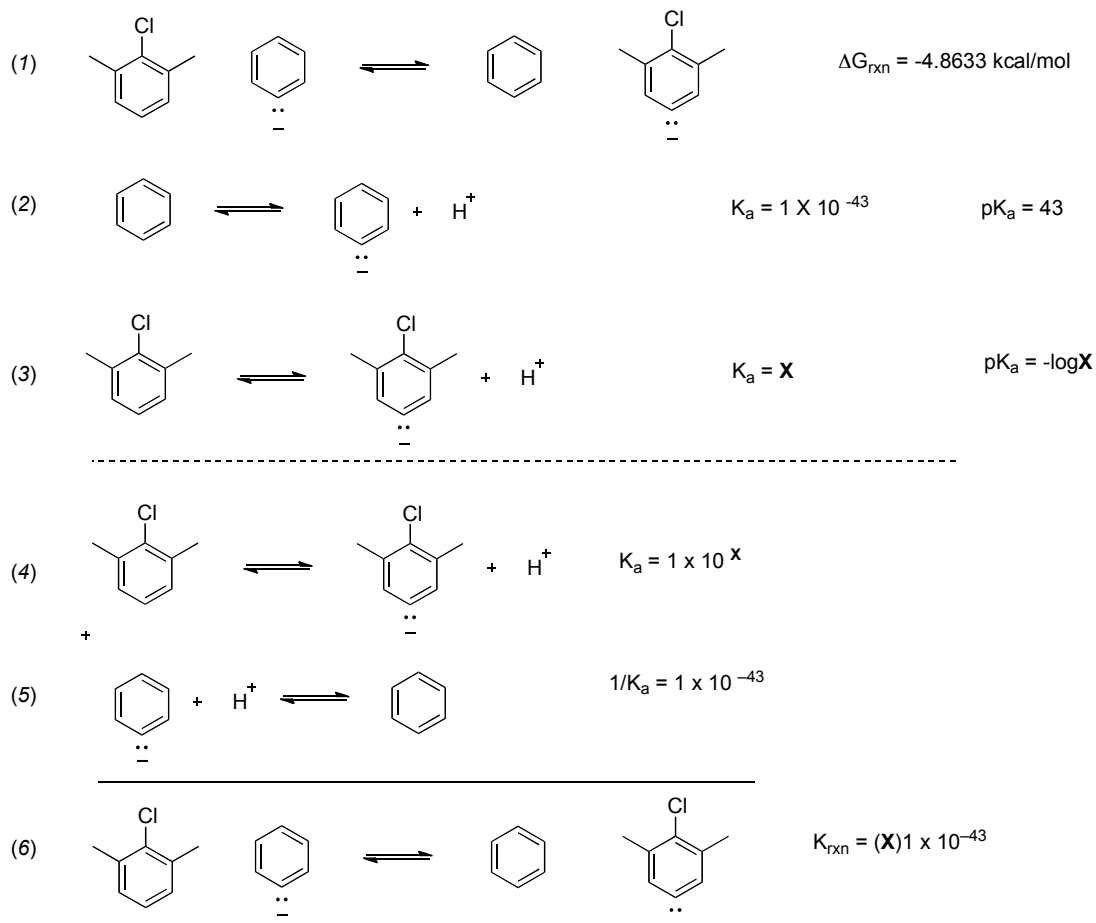
Scheme 3.35. Arene Protonation Reactions



Acidity Calculation. In order to calculate the pK_a of the Aryl- H_A and Aryl- H_B bonds, ΔG_{rxn} for each arene reacting with a benzene anion was calculated. The individual ΔG_{form} energies for each molecule were calculated separately, and the ΔG_{rxn} was established using the equation: $\Delta G_{\text{rxn}} = \Delta G_{\text{products}} - \Delta G_{\text{reactants}}$. This calculation is demonstrated for H_A of 1-chloro-2,6-dimethylbenzene below (Figure 3.10). The equilibrium for H_A is shown in eq. 1. Using Hess' Law this reaction can be broken down into two components (eq. 2 and 3). Eq. 2 represents the pK_a calculation for benzene, which is known⁶¹ and eq. 3 represents the pK_a calculation for the unknown C-H bond.

These two equations can be summed together (eq. 4 + eq. 5) to give the final expression (eq. 6), with the equilibrium constant expressed in terms of the unknown variable. The equilibrium constant can also be expressed in terms of ΔG_{rxn} and thus X can be determined using simple algebra. This value can then be used in eq. 3 to give the desired pK_a .

Figure 3.11 Example Calculation of pK_a from Computational ΔG_{rxn} Calculations



$$\Delta G = -RT \ln(K_{\text{rxn}})$$

$$-4863.3 \text{ cal/mol} = -(1.987 \text{ cal/mol}\cdot\text{K})(298.15 \text{ K}) \ln(K_{\text{rxn}})$$

$$K_{\text{rxn}} = 3674.4$$

$$K_{\text{rxn}} = (X) 1 \times 10^{-43}$$

$$X = 3674.4 \times 10^{-40}$$

$$pK_a = -\log(3.6744 \times 10^{-40})$$

$$pK_a = 39.43$$

3.7 References

1. Thomas, R. H., *The Chemistry of Natural Products*. Blackie and Son: Glasgow, 1985.
2. Baudoin, O. G., F., In *Studies in Natural Product Chemistry*, 2003; Vol. 29, pp 335-417.
3. Kozlowski, M. C.; Morgan, B. J.;Linton, E. C. *Chem. Soc. Rev.* **2009**, *38*, 3193-3207.
4. Rao, A. V. R.; Gurjar, M. K.; Reddy, K. L.;Rao, A. S. *Chem. Rev.* **1995**, *95*, 2135-2167.
5. Nicolaou, K. C.; Boddy, C. N. C.; Bräse, S.;Winssinger, N. *Angew. Chem. Int. Ed.* **1999**, *38*, 2096-2152.
6. Cepanec, I., *Synthesis of Biaryls*. Elsevier Inc.: San Diego, CA, 2004.
7. Roncali, J. *Chem. Rev.* **1992**, *92*, 711-738.
8. Jiang, L.; Buchwald, S. L.; Diederich, F.;Stang, P. J., *Metal-Catalyzed Cross-Coupling Reactions*. 2004; p 699.
9. Hassan, J.; Sevignon, M.; Gozzi, C.; Schulz, E.;Lemaire, M. *Chem. Rev.* **2002**, *102*, 1359-1470.
10. Stille, J. K. *Angew. Chem. Int. Ed.* **1986**, *25*, 508-524.
11. Farina, V. K., V.; Scott, W.J. *Org. React.* **1997**, *40*.
12. Miyaura, N.;Suzuki, A. *Chem. Rev.* **1995**, *95*, 2457-2483.
13. Suzuki, A. *J. Organomet. Chem.* **1999**, *576*, 147-168.
14. Beletskaya, I. P.;Cheprakov, A. V. *Chem. Rev.* **2000**, *100*, 3009-3066.
15. Denmark, S. E.;Sweis, R. F. *Acc. Chem. Res.* **2002**, *35*, 835-846.
16. Campeau, L. C.;Fagnou, K. *Chem. Commun.* **2006**, 1253-1264.
17. Godula, K.;Sames, D. *Science* **2006**, *312*, 67-72.
18. Alberico, D.; Scott, M. E.;Lautens, M. *Chem. Rev.* **2007**, *107*, 174-238.
19. Beccalli, E. M.; Broggini, G.; Martinelli, M.;Sottocornola, S. *Chem. Rev.* **2007**, *107*, 5318-5365.

20. McGlacken, G. P.;Bateman, L. M. *Chem. Soc. Rev.* **2009**, *38*, 2447-2447.
21. Lyons, T. W.;Sanford, M. S. *Chem. Rev.* **2010**, *110*, 1147-1169.
22. Ashenhurst, J. A. *Chem. Soc. Rev.* **2010**, *39*, 540-548.
23. Li, R.; Jiang, L.;Lu, W. *Organometallics* **2006**, *25*, 5973-5975.
24. Rong, Y.; Li, R.;Lu, W. *Organometallics* **2007**, *26*, 4376-4378.
25. Stuart, D. R.;Fagnou, K. *Science* **2007**, *316*, 1172-1175.
26. Stuart, D. R.; Villemure, E.;Fagnou, K. *J. Am. Chem. Soc.* **2007**, *129*, 12072-12073.
27. Dwight, T. A.; Rue, N. R.; Charyk, D.; Josselyn, R.;DeBoef, B. *Org. Lett.* **2007**, *9*, 3137-3139.
28. Xi, P.; Yang, F.; Qin, S.; Zhao, D.; Lan, J.; Gao, G.; Hu, C.;You, J. *J. Am. Chem. Soc.* **2010**, *132*, 1822-1824.
29. Potavathri, S.; Pereira, K. C.; Gorelsky, S. I.; Pike, A.; LeBris, A. P.;DeBoef, B. *J. Am. Chem. Soc.* **2010**, *132*, 14676-14681.
30. Hull, K. L.; Lanni, E. L.;Sanford, M. S. *J. Am. Chem. Soc.* **2006**, *128*, 14047-14049.
31. Xia, J.-B.;You, S.-L. *Organometallics* **2007**, *26*, 4869-4871.
32. Hull, K. L.;Sanford, M. S. *J. Am. Chem. Soc.* **2007**, *129*, 11904-11905.
33. Li, B.-J.; Tian, S.-L.; Fang, Z.;Shi, Z.-J. *Angew. Chem. Int. Ed.* **2008**, *47*, 1115-1118.
34. Chiong, H. A.; Pham, Q.-N.;Daugulis, O. *J. Am. Chem. Soc.* **2007**, *129*, 9879-9884.
35. Deprez, N. R.; Kalyani, D.; Krause, A.;Sanford, M. S. *J. Am. Chem. Soc.* **2006**, *128*, 4972-4973.
36. Deprez, N. R.;Sanford, M. S. *J. Am. Chem. Soc.* **2009**, *131*, 11234-11241.
37. Kawamura, Y. S., T.; Miura, M.; Nomura, M. *Chemical Letters* **1998**, *27*, 931-932.
38. Hull, K. L.;Sanford, M. S. *J. Am. Chem. Soc.* **2007**, *129*, 11904-11905.
39. Hull, K. L.;Sanford, M. S. *J. Am. Chem. Soc.* **2009**, *131*, 9651-9653.

40. Lyons, T. W.; Hull, K. L.; Sanford, M. S. *J. Am. Chem. Soc.* **2010**, *In Press*.
41. Galabov, B.; Ilieva, S.; Schaefer, H. F. *J. Org. Chem.* **2006**, *71*, 6382-6387.
42. Galabov, B.; Nikolova, V.; Wilke, J. J.; Schaefer, H. F.; Allen, W. D. *J. Am. Chem. Soc.* **2008**, *130*, 9887-9896.
43. Shao, Y. M., L. F.; Jung, Y.; Kussmann, J.; Ochsenfeld, C.; Brown, S. T.; Gilbert, A. T. B.; Slipchenko, L.V.; Levchenko, S. V.; O'Neill, D. P.; DiStasio Jr, R. A.; Lochan, R. C.; Wang, T.; Beran, G. J. O.; Besley, N. A.; Herbert, J. M.; Lin, C. Y.; Van Voorhis, T.; Chien, S. H.; Sodt, A.; Steele, R. P.; Rassolov, V. A.; Maslen, P. E.; Korambath, P. P.; Adamson, R. D.; Austin, B.; Baker, J.; Byrd, E. F. C.; Dachsel, H.; Doerksen, R. J.; Dreuw, A.; Dunietz, B. D.; Dutoi, A. D.; Furlani, T.; Gwaltney, S. R.; Heyden, A.; Hirata, S.; Hsu, C.-P.; Kedziora, G.; Khalliulin, R. Z.; Klunzinger, P.; Lee, A. M.; Lee, M. S.; Liang, W. Z.; Lotan, I.; Nair, N.; Peters, B.; Proynov, E. I.; Pieniazek, P. A.; Rhee, Y. M.; Ritchie, J.; Rosta, E.; Sherrill, C. D.; Simmonett, A. C.; Subotnik, J. E.; Woodcock III, H. L.; Zhang, W.; Bell, A. T.; Chakraborty, A. K.; Chipman, D. M.; Keil, F. J.; Warshel, A.; Hehre, W. J.; Schaefer, H. F.; Kong, J.; Krylov, A. I.; Gill, P. M. W.; Head-Gordon, M. *Phys. Chem. Chem. Phys.* **2006**, *8*, 3172-3191.
44. Hehre, W. J. R., L.; Schleyer, P.R.; Pople, J.A., *Ab Initio Molecular Orbital Theory*. John Wiley & Sons: New York, 1986.
45. Maksic, Z. B.; Kovacek, D.; Eckert-Maksic, M.; Zrinski, I. *The Journal of Organic Chemistry* **1996**, *61*, 6717-6719.
46. Lafrance, M.; Fagnou, K. *J. Am. Chem. Soc.* **2006**, *128*, 16496-16497.
47. Gorelsky, S. I.; Lapointe, D.; Fagnou, K. *J. Am. Chem. Soc.* **2008**, *130*, 10848-10849.
48. Garia-Cuadrado, D.; Braga, A. A. C.; Maseras, F.; Echavarren, A. M. *J. Am. Chem. Soc.* **2006**, *128*, 1066-1067.
49. Hickman, A. J.; Villalobos, J. M.; Sanford, M. S. *Organometallics* **2009**, *28*, 5316-5322.
50. Serrano, J. L.; García, L.; Pérez, J.; Pérez, E.; García, J.; Sánchez, G.; López, G.; Liu, M. *Eur. J. Inorg. Chem.* **2008**, *2008*, 4797-4806.
51. Ruiz, J.; Martinez, M. T.; Florenciano, F.; Rodriguez, V.; Lopez, G.; Pérez, J.; Chaloner, P. A.; Hitchcock, P. B. *Inorg. Chem.* **2003**, *42*, 3650-3661.
52. Palmgren, A.; Thorarensen, A.; Backvall, J.-E. *J. Org. Chem.* **1998**, *63*, 3764-3768.

53. Edwards, D. A. H., R. M.; Mahon, M. F.; Molloy, K. C. *Inorg. Chim. Acta* **2002**, 328, 134.
54. Constable, E. C. C. T., A. M. W.; Leese, T. A.; Reese, D. G. F. *Inorg. Chim. Acta* **1991**, 182, 93.
55. Pugliese, T. G., N.; Aiello, I.; Ghedini, M.; La Deda, M. *Inorg. Chem. Commun.* **2006**, 9, 93-95.
56. Zhang, J. K., E.; Anderson, N. P.; Zavalij, P. Y.; Vedernikov, A. N. *Chem. Commun.* **2008**, 3625-3626.
57. Pfeffer, M. *Inorg. Synth.* **1989**, 26, 211-212.
58. Heating/stirring were conducted on an aluminum reaction block with stirring set at the highest rpm (IKA stirplate setting of 11).
59. Becke, A. D. *J. Chem. Phys.* **1993**, 98, 5648-5653.
60. Lee, C. Y., W.; Parr, R. G. *Phys. Rev.* **1998**, B37, 785.
61. Streitwieser, A.; Scannon, P. J.; Niemeyer, H. M. *J. Am. Chem. Soc.* **1972**, 94, 7936-7937.

Chapter 4

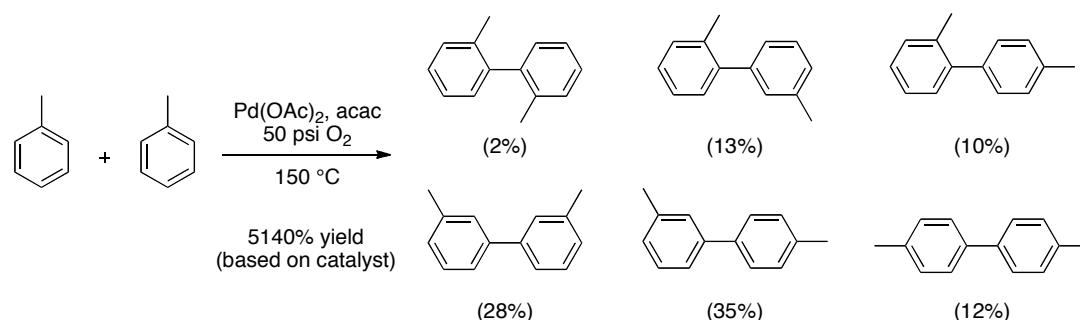
Progress Toward Catalytic Regioselective Oxidative Cross-Coupling Reactions and Application to Direct Arylation

4.1 Background and Significance

One of the key challenges for Pd-catalyzed oxidative coupling is achieving catalytic turnover with a stoichiometric oxidant. Traditional cross coupling relies on the facile oxidative addition of a Pd⁰ catalyst into an aryl halide bond. Thus, the aryl halide serves as not only the arene coupling partner, but the oxidant as well. Similar effects are at work in direct arylation, in which the oxidant is either an aryl halide or an aryl-containing oxidant such as a diaryliodonium salt. In both traditional cross coupling and direct arylation, the oxidant contains the aryl coupling partner. In sharp contrast, oxidative coupling requires an exogenous stoichiometric oxidant. This reagent must successfully reoxidize the metal to the necessary oxidation state without inhibiting the catalyst from undergoing other steps in the catalytic cycle (e.g., C–H activation, reductive elimination), or oxidizing the starting materials or products. There are several key examples in the literature that have demonstrated the feasibility of a variety of oxidants for Pd-catalyzed oxidative coupling.

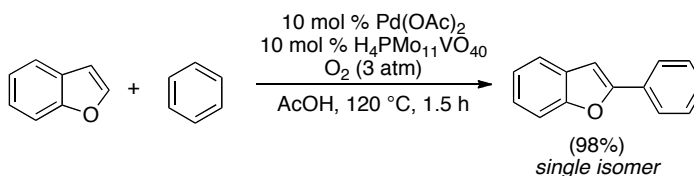
A particularly desirable oxidant for these transformations would be O₂ because it is cheap and readily available. One of the first examples of using O₂ in a Pd-catalyzed oxidative coupling reaction comes from Itatani in the dimerization of toluene.¹ Using a Pd(OAc)₂ catalyst, with an acetylacetonate (acac) ligand in the presence of 50 psi of O₂, the dimerization of toluene was accomplished in good yield (Scheme 4.1). Though the selectivity of the reaction was quite low, producing a mixture of all the available isomers, it did demonstrate the viability of O₂ as an efficient oxidant for oxidative coupling.

Scheme 4.1 Seminal Example of O₂ as Terminal Oxidant in Pd-Catalyzed Oxidative Coupling



A separate example highlighting the use of O₂ as an oxidant is DeBoef's Pd-catalyzed coupling of benzofurans with simple arenes (Scheme 4.2).² Here, a Pd(OAc)₂ catalyst is used in the presence of O₂ as the terminal oxidant with a heteropolyacid (HPA) co-oxidant to provide the aryl–aryl coupled product in good yield. Importantly, HPA salts have proven to be effective reagents for the reoxidation of Pd catalysts with O₂, by facilitating electron transfer between the Pd⁰ catalyst and stoichiometric oxidant O₂.

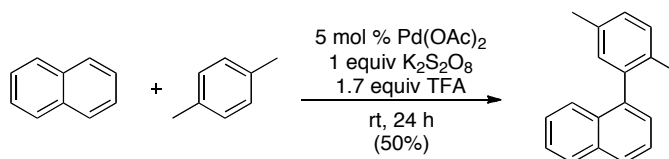
Scheme 4.2 DeBoef's Arylation of Benzofurans



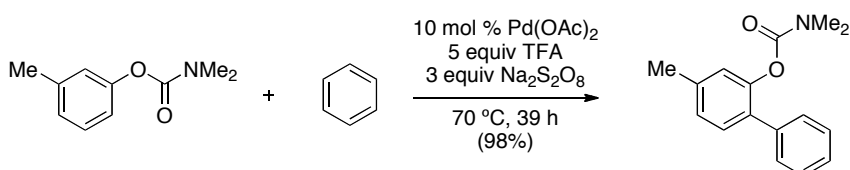
Peroxydisulfate salts represent another stoichiometric oxidant capable of providing catalyst turnover in Pd-catalyzed oxidative coupling reactions. Lu and coworkers have used K₂S₂O₈ in the coupling of naphthalene with a variety of simple arenes (Scheme 4.3).³ In the presence of super-stoichiometric TFA, naphthalene was coupled with *p*-xylenes in 50% yield at room temperature with 77% selectivity for the desired cross coupling products over competing homo-coupling pathways. More recently, the related Na₂S₂O₈ oxidant has been used for the oxidative cross-coupling between *o*-phenylcarbamates and simple arenes with high yield and selectivity (Scheme 4.4).⁴ Using a ligand directed approach analogous to ours, Dong and coworkers showed that 10 mol %

of Pd(OAc)₂, 3 equiv Na₂S₂O₈ as the oxidant, and 5 equiv TFA can provide excellent yields of the biaryl products at mild temperatures.

Scheme 4.3 Pd-Catalyzed Oxidative Coupling of Naphthalene with Simple Arenes

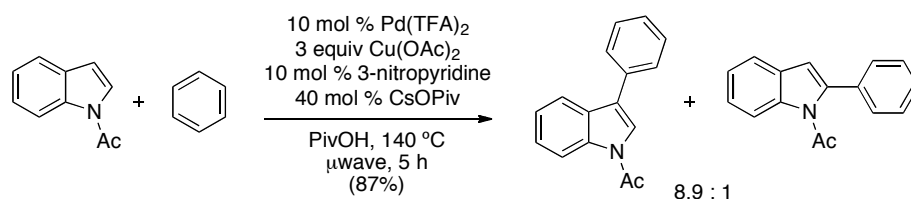


Scheme 4.4 Pd-Catalyzed Oxidative Coupling of Naphthalene with Simple Arenes

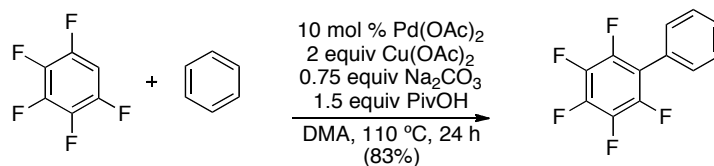


Cu^{II} salts have also proven effective for regenerating Pd^{II} catalysts for oxidative cross coupling. Cu(OAc)₂ was used by Fagnou and coworkers for the regioselective oxidative coupling of indoles and simple arenes (Scheme 4.5).^{5, 6} Interestingly, this oxidant was also crucial to obtaining C3 selectivity. Switching to AgOAc as the oxidant resulted in the C2 arylated isomer predominating. More recently, Cu(OAc)₂ was used for the oxidative cross-coupling of polyfluoroarenes with simple arenes (Scheme 4.6).⁷ Su has demonstrated that Cu(OAc)₂ can be an efficient oxidant for Pd-catalyzed cross coupling in the presence of pivalic acid (PivOH) and a Na₂CO₃ base, giving the biaryl cross-coupled products in good yields.

Scheme 4.5 Fagnou's Oxidative Cross-Coupling of Indoles and Simple Arenes

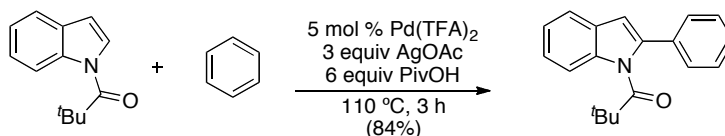


Scheme 4.6 Su's Oxidative Cross-Coupling of Polyfluoroarenes and Simple Arenes

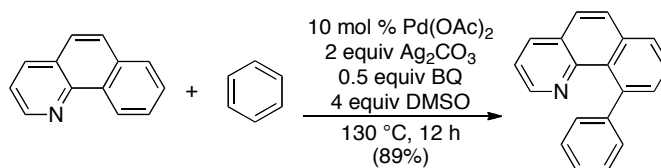


A final class of terminal oxidant shown to be effective in Pd-catalyzed oxidative cross coupling is Ag^I salts. AgOAc was shown by Fagnou and coworkers to be an effective reagent for the coupling of indoles with simple arenes in the presence of 5 mol % of Pd(TFA)₂ and 6 equiv of PivOH (Scheme 4.7).⁶ In related work, our group has shown that Ag₂CO₃ is uniquely effective in promoting catalyst turnover in the cross coupling of benzoquinoline and simple arenes (Scheme 4.8).⁸ In both of these transformations, at least 2 equiv of Ag^I are required to oxidize the Pd⁰ product after reductive elimination back to the Pd^{II} oxidation state required for C–H activation (Scheme 4.9).⁹

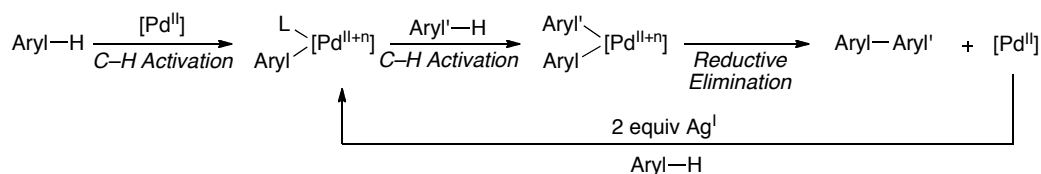
Scheme 4.7 Fagnou's Oxidative Cross Coupling of Indoles and Simple Arenes



Scheme 4.8 Sanford's Oxidative Cross Coupling of Benzoquinoline with Simple Arenes

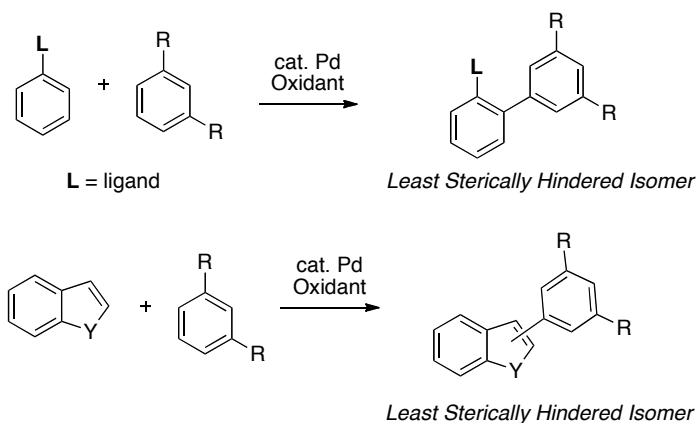


Scheme 4.9 Mechanism of Pd-Catalyzed Oxidative Cross Coupling with Ag^I Oxidants



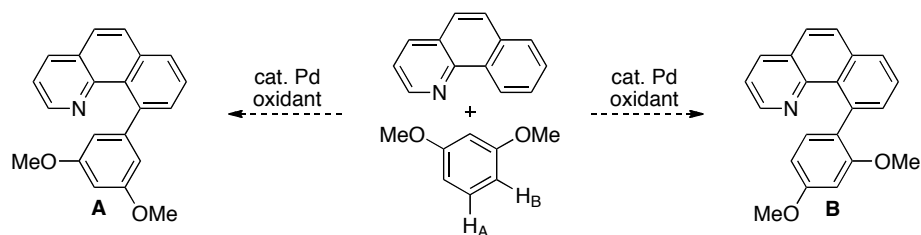
Each of these methodologies has undoubtedly advanced the field of oxidative coupling, providing numerous ways to enhance catalytic turnover and expand substrate scope. Each of the previously reported methodologies proceeds to give the least sterically hindered regioisomer as the major product (Scheme 4.10). As such, the site selectivity of Pd-catalyzed aryl–aryl oxidative coupling remains a key challenge in this field.

Scheme 4.10 Site Selectivity of Previous Oxidative Coupling Methods



With an assortment of established protocols for achieving catalyst turnover in Pd-catalyzed oxidative cross coupling, we aimed to afford an analogous catalytic system with complementary site selectivity using the findings from Chapter 3. Several strategies were shown to improve selectivity in the oxidative coupling of benzoquinoline with DMB to give isomer **A** as the preferred product. These included sterically bulky quinones, carboxylates, or small amounts of AcOH. Additionally, carbonate salts were uniquely effective in reversing the site selectivity to give isomer **B** as the major product. Thus, we sought to develop a modifiable catalyst system for the coupling of benzoquinoline with simple arenes by implementing the findings from Chapter 3 (Scheme 4.11).

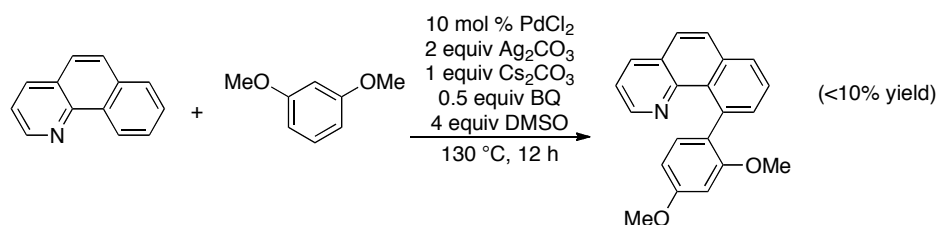
Scheme 4.11 Potential Modifiable Catalytic System



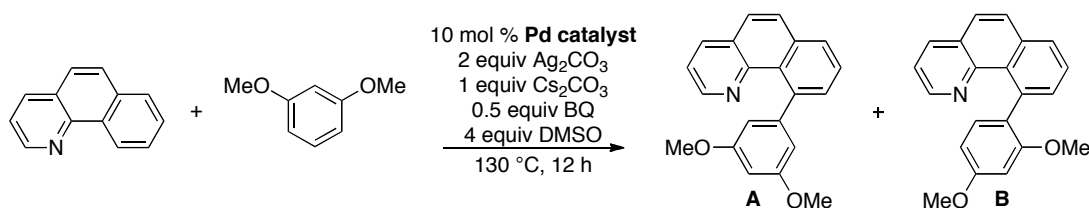
4.2 Methodology Development and Oxidant Screening

Our first efforts at developing this system were focused on finding suitable conditions for the carbonate system to undergo catalysis. We hypothesized that similar conditions to our original report⁸ could be used to effect the desired transformation using PdCl₂ in place of Pd(OAc)₂ with Ag₂CO₃ as the stoichiometric oxidant. Unfortunately, our initial screening of this reaction yielded less than 10% yield of the desired product (Scheme 4.12). The starting materials, benzoquinoline and DMB made up the vast majority of the material remaining after the reaction.

Scheme 4.12 Initial Efforts at PdCl₂/CO₃-Catalyzed Oxidative Cross Coupling



While PdCl₂ failed to produce catalytic turnover under our initial conditions, numerous other Pd salts could be screened. Importantly, PdCl₂ is quite insoluble in many organic solvents, and we hypothesized that a more soluble Pd salt would be more effective in this transformation. To that end we screened a number of Pd-Cl derivatives with the previously reported oxidative coupling protocol. However, as shown in Table 4.1, none of these Pd catalysts provided any improvement over PdCl₂. Even 10 mol % of [(bzq)PdCl]₂, failed to product catalytic turnover.

Table 4.1 Catalyst Screening for Pd/CO₃-Catalyzed Oxidative Coupling

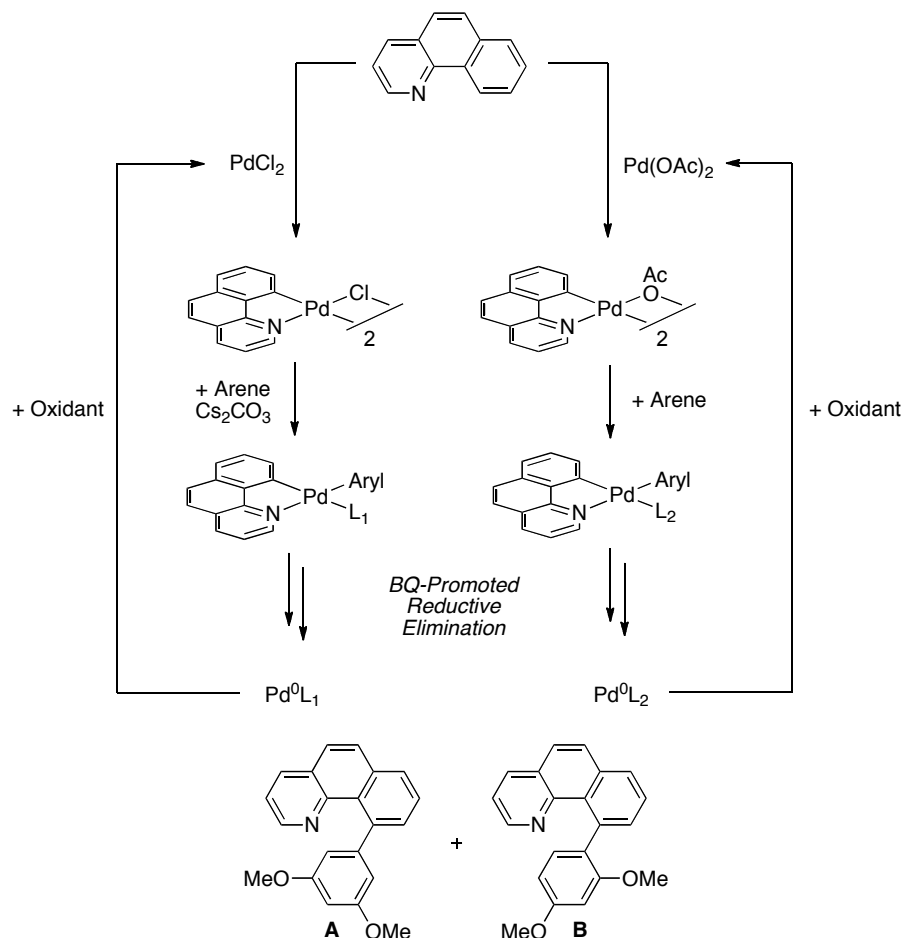
Entry	Catalyst	B : A	Yield
1	PdCl ₂	4 : 1	10%
2	PdCl ₂ (dppf)	---	n.r.
3	PdCl ₂ (PPh ₃) ₂	3 : 1	<5%
4	PdCl ₂ (PhCN) ₂	4 : 1	10 %
5	Li ₂ PdCl ₄	---	n.r.
6	PdCl ₂ (BrCH ₂ CN) ₂	---	n.r.
7	Pd(bipy)Cl ₂	2 : 1	<5%
8	Na ₂ PdCl ₄	---	n.r.
9	[(bzq)PdCl] ₂	5 : 1	10%

n.r. indicates no reaction

The lack of turnover with [(bzq)PdCl]₂ (Table 4.1, entry 9) is particularly surprising because the Pd⁰ product formed should be quite similar to the one produced using Pd(OAc)₂ reported previously (Scheme 4.13).⁸ We envisioned a mechanism for PdCl₂/Cs₂CO₃ analogous to the one proposed for Pd(OAc)₂ (Scheme 4.13). This would involve cyclometallation of bzq, followed by ligand exchange of Cl for CO₃ in the presence of Cs₂CO₃. Then aryl-H activation and BQ promoted reductive elimination would give mixtures of isomers **A** and **B** as well as the Pd⁰ product. Thus, we anticipated similar oxidants (Ag₂CO₃) could be effective in carrying out the transformation with PdCl₂/Cs₂CO₃. The lack of catalyst turnover in these experiments suggests several possibilities: (i) the Pd⁰ product formed from PdCl₂/Cs₂CO₃ is not analogous to the Pd⁰ formed with the Pd(OAc)₂ system, (ii) reoxidation is occurring but the newly formed Pd^{II} cannot undergo cyclometallation, or (iii) an alternative catalyst decomposition pathway is

occurring. We next chose to investigate the cyclometallation step with a variety of Pd catalysts.

Scheme 4.13 Comparable Mechanisms for PdCl₂- and Pd(OAc)₂-Catalyzed Oxidative Coupling



One key step that is present in the catalytic reaction that is absent in the stoichiometric reaction is benzoquinoline cyclopalladation (Scheme 4.14). While we anticipated this step would be facile, a series of Pd salts were screened in a stoichiometric reaction, absent oxidant. As shown in Table 4.2 below several Pd salts were able to mediate the desired stoichiometric oxidative coupling between benzoquinoline and DMB. PdCl₂, Li₂PdCl₄, Na₂PdCl₄, PdCl₂(PhCN)₂, and PdCl₂(BrCH₂CN)₂ (entries 1-5) all provided the oxidative coupling products in good yield and high selectivity for isomer **B**, ranging from **B** : **A** = 9 : 1 to **B** : **A** = 5 : 1. These experiments suggest against

cyclometallation being the problematic step in catalysis and instead point to oxidation as the critical step needing improvement. These experiments also provided a unique opportunity to observe the effects of other ligands on this transformation. Electron rich phosphine ligands like PPh₃ and 1,1'-bis(diphenylphosphino)ferrocene (dppf) slowed or completely inhibited reactivity (Table 4.2, entries 6, 8). Other ligands such as bipy and acac (entries 7, 9) had similar deleterious effects, suggesting that choice of ligand in these experiments is crucial to affording the desired reactivity.

Scheme 4.14 Benzoquinoline Cyclometallation

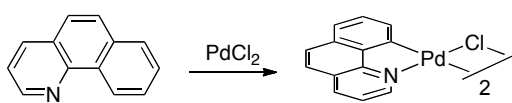
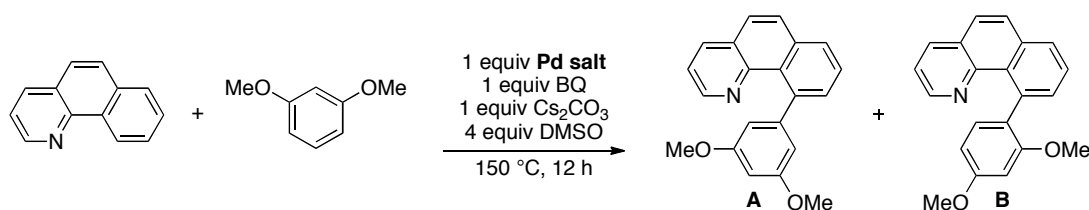


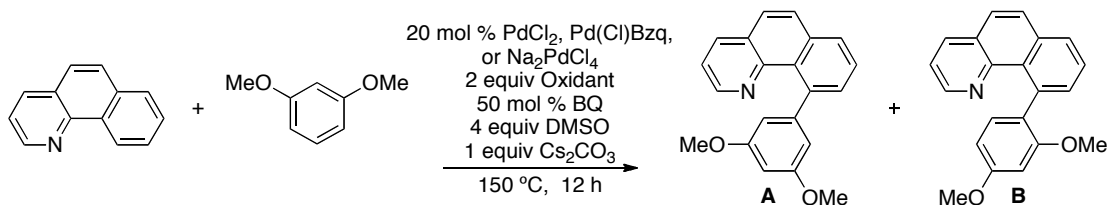
Table 4.2 Stoichiometric Studies with Pd Salts



Entry	Pd Salt	B : A	Yield
1	PdCl ₂	9 : 1	100%
2	Li ₂ PdCl ₄	6 : 1	90 %
3	Na ₂ PdCl ₄	6 : 1	100%
4	PdCl ₂ (PhCN) ₂	5 : 1	85%
5	PdCl ₂ (BrCH ₂ CN) ₂	6 : 1	100%
6	PdCl ₂ (PPh ₃) ₂	4 : 1	40 %
7	Pd(bipy)Cl ₂	4 : 1	13%
8	PdCl ₂ (dppf)	---	n.r.
9	Pd(acac) ₂	10 : 1	6%
10	PdI ₂	2 : 1	24 %
11	Pd(OTf) ₂	4.5 : 1	47%

Following these studies, we next turned our attention to finding a new oxidant for this transformation. Screening three different Pd complexes with a wide array of known stoichiometric oxidants produced the results shown in Table 4.3 below. Most of these oxidants appeared to be ineffective at providing catalyst turnover in the desired transformation. Strong two electron oxidants like $\text{PhI}(\text{OAc})_2$ or $\text{K}_2\text{S}_2\text{O}_8$ did not provide any catalytic turnover (entries 1,2 and 3–5). Additionally, Cu^{II} salts were largely ineffective; $\text{Cu}(\text{OAc})_2$ was an exception and produced an **B** : **A** ratio of 1 : 1.4 in 67% yield. The selectivity for isomer **A** in this reaction is more similar to that observed with $\text{Pd}(\text{OAc})_2$, suggesting that $\text{Pd}(\text{OAc})_2$ was the active catalyst under these conditions. Finally, a number of other oxidants (including iron- and cerium salts) also inhibited the reaction (entries 3, 10–17), implying that these oxidants promote unproductive pathways.

Table 4.3 Oxidant Screening with Bzq and DMB



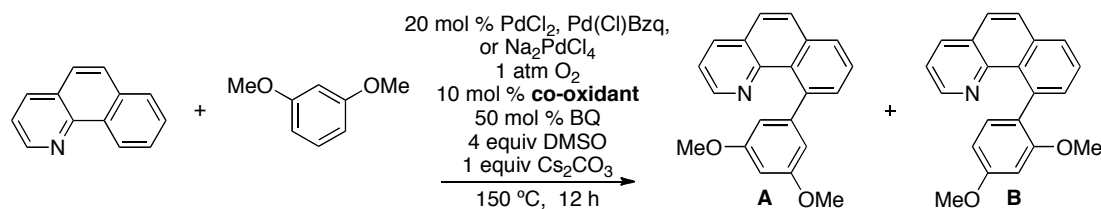
Entry	Oxidant	B : A	Yield
1	$\text{PhI}(\text{OAc})_2$	5 : 1	19%
2	$\text{K}_2\text{S}_2\text{O}_8$	5 : 1	18%
3	Oxone	---	n.r.
3	IOAc^{a}	5 : 1	19%
4	NCS	4 : 1	15%
5	NIS	5 : 1	16%
6	CuO	6 : 1	20%
7	CuCl_2	5 : 1	18%
8	CuF_2	4.5 : 1	20%
9	$\text{Cu}(\text{OAc})_2$	1 : 1.4	67%
10	$\text{Cu}(\text{acac})_2$	---	n.r.
11	$\text{Cu}(\text{OTf})_2$	---	n.r.

Table 4.3 Continued Oxidant Screening with Bzq and DMB

Entry	Oxidant	B : A	Yield
12	FeCl ₃	---	n.r.
14	FeCp ₂ BF ₄	---	n.r.
15	CAN	---	n.r.
16	CAS	---	n.r.
17	N-F-pyr	---	n.r.

^a Formed *in situ* from I₂/PhI(OAc)₂. CAS = ceric(IV) ammonium sulfate. CAN = ceric(IV) ammonium nitrate. N-F-pyr = *N*-fluoropyridinium triflate.

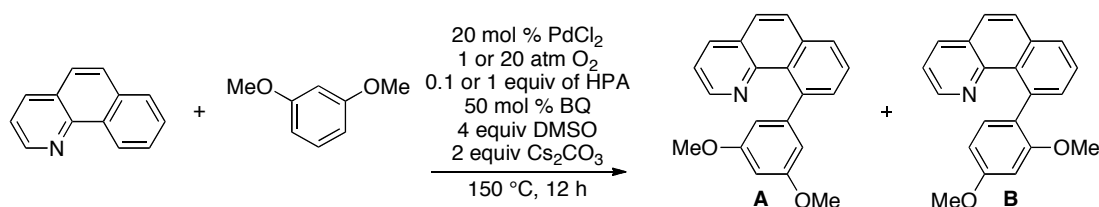
We next chose to look at O₂ as the stoichiometric oxidant along with a number of other co-oxidants. A series of Cu^{II} salts were screened as co-oxidants with 1 atm O₂, 50 mol % BQ, 1 equiv Cs₂CO₃, and 4 equiv DMSO (Table 4.4). These conditions failed to produce catalytic turnover with substoichiometric amounts of [(bzq)PdCl]₂ or with other Pd salts previously shown to work under stoichiometric conditions.

Table 4.4 Oxidant Screenings with O₂ and Cu^{II} Co-oxidants

Entry	Co-Oxidant	B : A	Yield
1	CuCl ₂	5 : 1	19%
2	CuO	6 : 1	20%
3	CuF ₂	4.5 : 1	20 %
4	Cu(OAc) ₂	1 : 1	18%
5	Cu(OTf) ₂	---	n.r.
6	Cu(acac) ₂	---	n.r.
7	None	4 : 1	18%

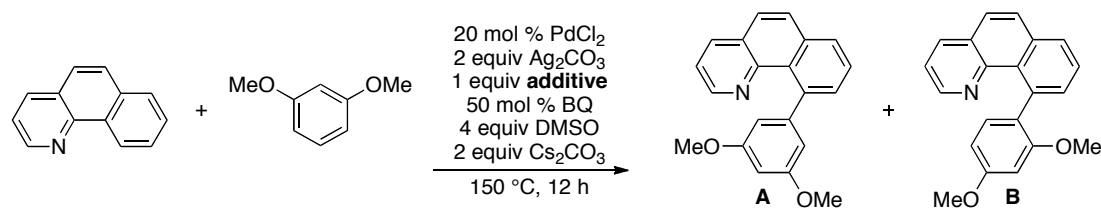
We next examined the use of O₂ as a terminal oxidant with a series of HPA salts as co-oxidants analogous to a previous report by DeBoef (Scheme 4.5).² We screened these reactions at atmospheric pressure of O₂ using a balloon (1 atm) as well as at pressures as high as 20 atm with the use of a Parr reactor. These experiments also failed to effect catalyst turnover in our system. Instead these conditions appeared to inhibit the reaction giving no observable product.

Table 4.5 O₂ as the Terminal Oxidant with HPA Co-oxidants



Entry	HPA	B : A	Yield
1	H ₄ PMo ₁₁ VO ₄₀ (1 or 0.1 equiv)	---	n.r.
2	H ₅ PMo ₁₀ V ₂ O ₄₀ (1 or 0.1 equiv)	---	n.r.
3	H ₆ PMo ₉ V ₃ O ₄₀ (1 or 0.1 equiv)	---	n.r.

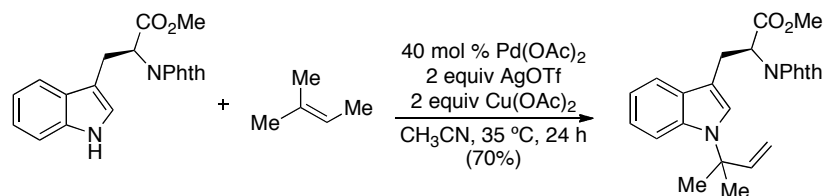
Various additives were also used to try to effect the desired transformation (Table 4.6). Each of these additives has been shown in C–H activation/functionalization reactions to improve reactivity. Chloride salts have been shown to improve ligand coordination as well as have a productive influence in PdCl₂ catalyzed reactions, presumably by aiding in generating the active PdCl₂ catalyst.¹⁰ Separately, Mn salts have also proven to be effective additives in C–H activation reactions by improving catalyst turnover (Table 4.6, entries 4-6).¹¹ A variety of other phosphorous and nitrogen ligands were also added to these reactions in an effort to stabilize the Pd⁰ product and limit deposition of Pd⁰ black (entries 7–13). Unfortunately, none of these additives resulted in catalyst turnover.

Table 4.6 Additive Screening

Entry	Additive	B : A	Yield
1	LiCl	---	n.r.
2	NaCl	---	n.r.
3	HMPA	---	n.r.
4	Mn(OAc) ₂	---	n.r.
5	MnCO ₃	---	n.r.
6	MnO	5 : 1	18%
7	PPh ₃	5 : 1	19%
8	P(<i>o</i> -tolyl) ₃	4.5 : 1	18%
9	3-NO ₂ -pyridine	---	n.r.
10	Dbp	---	n.r.
11	pyridine	---	n.r.
12	DMSO	5 : 1	20%
13	DMF	---	n.r.

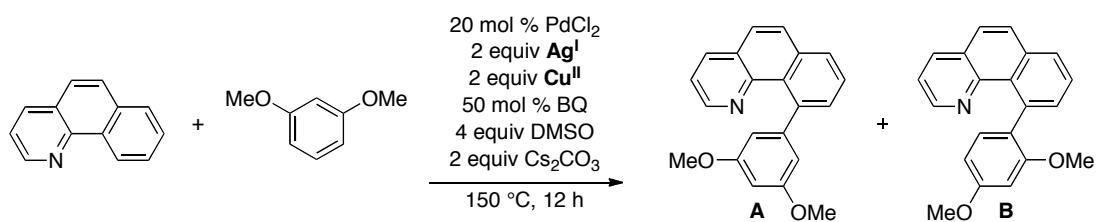
Recent work by Baran and coworkers has shown that combinations of Ag^I and Cu^{II} salts can provide catalytic turnover, even when each oxidant separately does not.¹² The chemoselective *N-tert*-prenylation of indoles was accomplished with 40 mol % of Pd(OAc)₂ as the catalyst and two equivalents of both AgOTf and Cu(OAc)₂ as the stoichiometric oxidants (Scheme 4.15). Interestingly, neither AgOTf nor Cu(OAc)₂ was able to afford the *N-tert*-prenylated product in yields greater than the catalyst loading (22% and 31% respectively).

Scheme 4.15 Baran's *N*-*tert*-prenylation of Indoles



Using this interesting result as inspiration, we next sought to screen combinations of Ag^I and Cu^{II} salts in an effort to obtain catalytic turnover in our oxidative coupling system. As seen in Table 4.7, all these combinations failed to produce catalytic turnover in our system.

Table 4.7 Oxidant Screening with Ag^I and Cu^{II} Salts



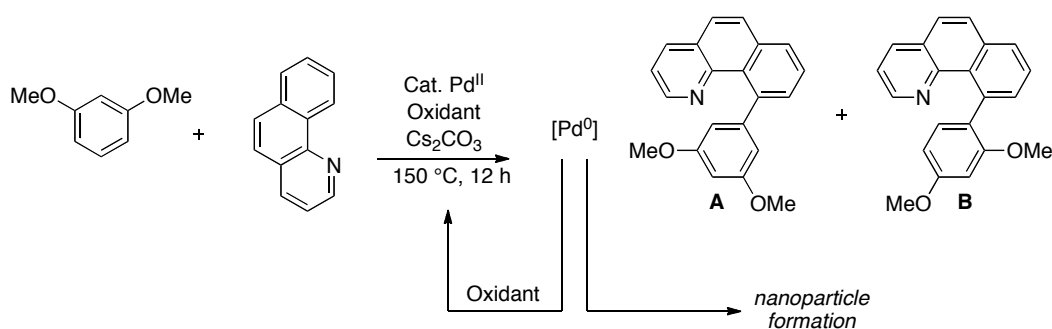
Entry	Oxidant	B : A	Yield
1	AgOTf/Cu(OAc) ₂	---	n.r.
2	AgOTf/CuCl ₂	---	5%
3	AgOTf/Cu(OTf) ₂	---	5%
4	AgOTf/CuF ₂	---	5%
5	Ag ₂ CO ₃ /Cu(OAc) ₂	---	5%
6	Ag ₂ CO ₃ /CuCl ₂	4.5 : 1	16%
7	Ag ₂ CO ₃ /Cu(OTf) ₂	---	5%
8	Ag ₂ CO ₃ /CuF ₂	5 : 1	18%

All of these studies illustrate the great challenge of finding a suitable oxidant for Pd-catalyzed oxidative coupling. We pursued numerous strategies in order to facilitate catalytic turnover in our desired system; however, we have thusfar been unable to identify suitable conditions. From these observations we can conclude that changing the

ligand environment of the Pd-catalyst from OAc^- to CO_3^{2-} not only affects the site selectivity of aryl C–H activation, but also influences the regeneration of the Pd^{II} catalyst.

One possible explanation for this lack of catalytic turnover is that the Pd^0 byproduct formed upon reductive elimination forms Pd–nanoparticles in preference to reoxidation (Scheme 4.16). Several papers suggest that the conditions needed in this system to reverse regioselectivity are the same used to synthesize Pd–nanoparticles.¹³⁻¹⁵ For example Adak and coworkers have shown that Pd–nanoparticles are readily formed in solution using a PdCl_2 starting material in the presence of a carbonate base, strikingly similar to conditions required for our oxidative coupling transformation.¹⁴ A competitive aggregation to Pd–nanoparticles would prevent re-oxidation to the desired PdCl_2 catalyst, rendering catalysis impossible under these conditions.

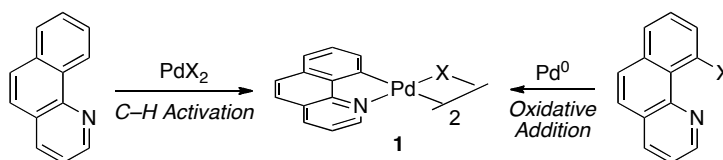
Scheme 4.16 Potential Nanoparticle Formation



4.3 Applications to Direct Arylation

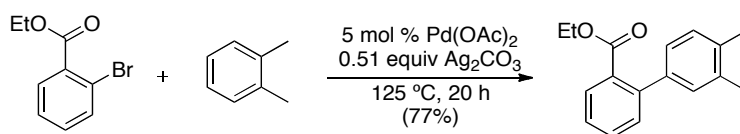
While we have thusfar been unable to find suitable conditions for a Pd/CO_3^- -catalyzed oxidative coupling protocol, we hypothesized that the factors controlling site selectivity in Chapter 3 might also be applied to direct arylation reactions. We noted that cyclopalladated starting material **1** could be accessed either by C–H activation or by oxidative addition (Scheme 4.17). Thus, we next sought to use halogenated benzoquinoline as the oxidant in this system, applying the methods found in Chapter 3 (CO_3^{2-} , and OAc^- ligands) to control site selectivity with free arenes.

Scheme 4.17 C–H Activation and Oxidative Addition Routes to **1**

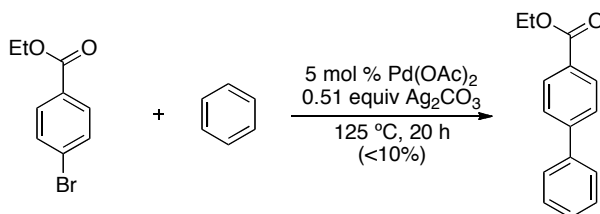


Importantly, the use of aryl–X bonds with adjacent directing groups has been demonstrated recently for direct arylation reactions and proven essential for obtaining reactivity. Charette and coworkers have shown that weakly coordinating ligands such as ethyl esters promote the direct arylation of simple arenes under relatively mild conditions.¹⁶ For example, the arylation of ethyl-2-bromobenzoate with *o*-xylenes proceeded cleanly with a Pd(OAc)₂ catalyst in the presence of 0.51 equiv of Ag₂CO₃ (Scheme 4.18). Interestingly, when ethyl-4-bromobenzoate was used with benzene, the reaction was far less efficient, giving less than 10% yield (Scheme 4.19). This precedent demonstrates the importance of an adjacent directing group on the aryl halide in accelerating direct arylation. However, it is important to note that this reaction proceeds with similar site selectivity as other literature protocols – generally giving the least sterically hindered isomer as the major product (Scheme 4.18).

Scheme 4.18 Charette's Direct Arylation of Ethyl-2-bromobenzoate



Scheme 4.19 Charette's Direct Arylation of Ethyl-4-bromobenzoate



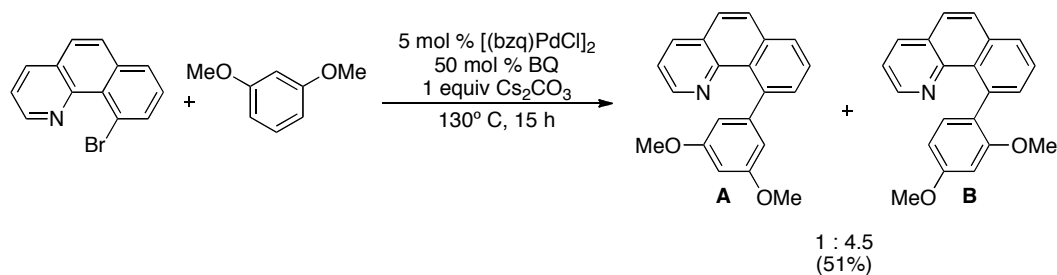
We aimed to develop two protocols for direct arylation to achieve complementary site selectivity. In the first, we anticipated that regenerating a Pd–OAc intermediate

through the use of AgOAc would favor the formation of isomer **A**. In the second, we hypothesized that the addition of a carbonate salt would favor the formation of isomer **B**. To test this hypothesis, we submitted substoichiometric amounts of [(bzq)Pd(OAc)]₂ (Scheme 4.20) and [(bzq)PdCl]₂ (Scheme 4.21) to reaction conditions with DMB and 10-bromobenzo[*h*]quinoline (Br-bzq) as the coupling partners. Gratifyingly, in our initial attempts with 10 mol % of [(bzq)Pd(OAc)]₂, 50 mol % of BQ, and 1 equiv of AgOAc, we observed 59% yield of the desired products with an **A** : **B** ratio of 7 : 1 (Scheme 4.20). Changing these conditions to 10 mol % of [(bzq)PdCl]₂ with 50 mol % of BQ, and 1 equiv Cs₂CO₃, reversed the site selectivity giving **A** : **B** = 1 : 4.5 in 51% yield (Scheme 4.21).

Scheme 4.20 Direct Arylation of Br-bzq and DMB with [(bzq)Pd(OAc)]₂



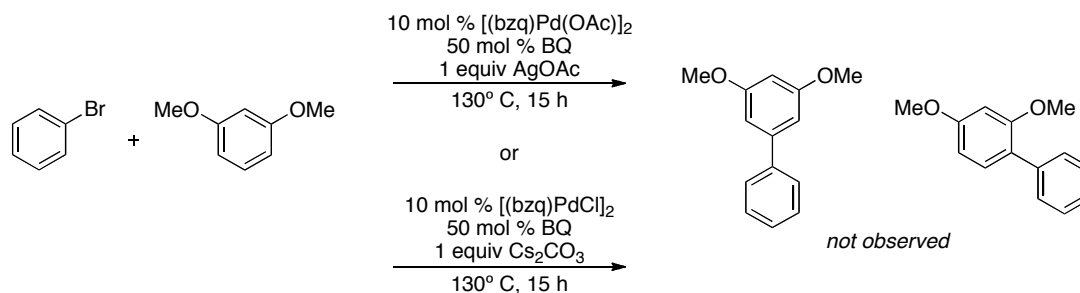
Scheme 4.21 Direct Arylation of Br-bzq and DMB with [(bzq)PdCl]₂



Interestingly, applying the same conditions to coupling an aryl halide without an appended directing group resulted in none of the cross-coupled product (Scheme 4.22). This observation is consistent with that of Charette, who reported significantly reduced yields for aryl halides without *ortho* directing groups. These results suggest that an adjacent ligand such as quinoline in bzq is crucial for obtaining the desired reactivity.

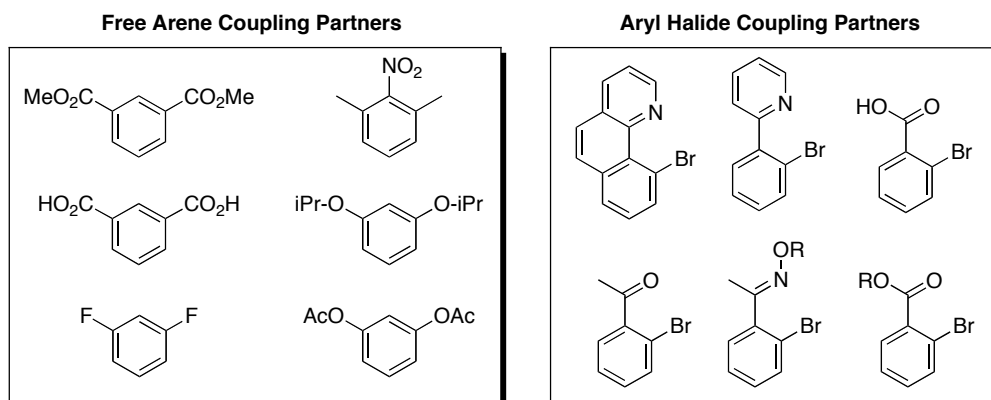
Furthermore, reoxidation with an aryl halide such as Br-bzq seems to be faster than the other pathways to Pd–nanoparticles.

Scheme 4.22 Direct Arylation Attempts with Bromobenzene and DMB



These initial findings are incredibly exciting, and we anticipate pursuing a number of different arenes as well as halogenated starting materials in the future. One can envision using many of the same arenes utilized in Chapter 3 as well as other 1,3-disubstituted benzene derivatives shown below in Figure 1. Additionally, a number of aryl halides could be used for this chemistry with both strongly coordinating directing groups such as pyridines or weakly coordinating directing groups, such as ketones and esters.

Figure 4.1 Potential Arene and Aryl Halide Coupling Partners



4.4 Conclusion

In summary, we have been unable to find suitable conditions for to achieve the catalytic oxidative coupling of benzo[*h*]quinoline with DMB to afford isomer **B** as the major product. Our efforts involved screening numerous oxidation protocols including O₂ and other stoichiometric oxidants in conjunction with a variety of additives and ligands to facilitate oxidation. However, we were able to provide preliminary evidence that the methods of controlling site selectivity developed in Chapter 3 can be applied to a new direct arylation protocol using Br-bzq as the coupling partner/oxidant.

4.5 Experimental Procedures

General Procedures: NMR spectra were obtained on a Varian Inova 500 (499.90 MHz for ¹H; 125.70 MHz for ¹³C), a Varian Inova 400 (399.96 MHz for ¹H; 100.57 MHz for ¹³C; 376.34 MHz for ¹⁹F), or a Varian Mercury 300 (300.07 MHz for ¹H; 75.45 MHz for ¹³C NMR; 282.35 MHz for ¹⁹F) spectrometer. ¹H and ¹³C NMR chemical shifts are reported in parts per million (ppm) relative to TMS, with the residual solvent peak used as an internal reference. ¹⁹F NMR spectra are referenced based on the unified scale, where the frequency of the residual solvent peak in the ¹H NMR spectrum acts as the single primary reference. ¹⁹F NMR spectra are proton coupled. Multiplicities are reported as follows: singlet (s), doublet (d), doublet of doublets (dd), doublet of doublet of doublets (ddd), doublet of triplets (dt), doublet of quartets (dq), triplet (t), triplet of doublets (td), quartet (q), quartet of doublets (qd), and multiplet (m). Unless otherwise indicated, the ¹H and ¹³C NMR spectra were recorded at room temperature.

Materials and Methods: Chemicals that were purchased from commercial sources and used as received are indicated in the experimental section below. Benzoquinone was obtained from Acros and was purified by vacuum sublimation. 10-bromo-benzo[*h*]quinoline was synthesized according to literature methods.¹⁷ Cs₂CO₃ (99.9%) was obtained from Aldrich and used as received. Gas chromatography was carried out using a Shimadzu 17A using a Restek Rtx®-5 (Crossbond 5% diphenyl – 95% dimethyl

polysiloxane; 15 m, 0.25 mm ID, 0.25 mm ID, 0.25 μ m df) column. All GC and isolated yields are the average of two reactions.

General Procedure for Pd-Catalyzed Oxidative Coupling. Benzo[*h*]quinoline was weighed (0.04 mmol) into a 2 mL scintillation vial and the appropriate combination of reagents (Pd catalyst, benzoquinone, M_2CO_3 , DMSO, oxidant etc) was added. The resulting mixture was diluted with the arene substrate (0.8 mL). The vial was then sealed with a Teflon-lined cap, and the reaction mixture was stirred vigorously at 150 °C for 15 h.¹⁸ The reactions were allowed to cool to room temperature, nonadecane (0.02 mmol of a stock solution in EtOAc) was added as an internal standard to the crude reaction mixture, and the reactions were analyzed by gas chromatography. The yields of **A** and **B** were determined based on a calibration curve.

General Procedure for Pd-Catalyzed Direct Arylation. 10-bromo-benzo[*h*]quinoline was weighed (0.02 mmol) into a 2 mL scintillation vial and the appropriate combination of reagents (Pd catalyst, benzoquinone, M_2CO_3 etc) was added. The resulting mixture was diluted with DMB (1.6 mL). The vial was then sealed with a Teflon-lined cap, and the reaction mixture was stirred vigorously at 130 °C for 15 h.¹⁸ The reactions were allowed to cool to room temperature, nonadecane (0.01 mmol of a stock solution in EtOAc) was added as an internal standard to the crude reaction mixture, and the reactions were analyzed by gas chromatography. The yields of **A** and **B** were determined based on a calibration curve.

4.6 References

1. Yashimoto, H.;Itatani, H. *Bull. Chem. Soc. Jpn.* **1973**, *46*, 2490-2492.
2. Dwight, T. A.; Rue, N. R.; Charyk, D.; Josselyn, R.;DeBoef, B. *Org. Lett.* **2007**, *9*, 3137-3139.
3. Li, R.; Jiang, L.;Lu, W. *Organometallics* **2006**, *25*, 5973-5975.
4. Zhao, X.; Yeung, C. S.;Dong, V. M. *J. Am. Chem. Soc.* **2010**, *132*, 5837-5844.
5. Stuart, D. R.;Fagnou, K. *Science* **2007**, *316*, 1172-1175.
6. Stuart, D. R.; Villemure, E.;Fagnou, K. *J. Am. Chem. Soc.* **2007**, *129*, 12072-12073.
7. Wei, Y.;Su, W. *J. Am. Chem. Soc.* **2010**, *132*, 16377-16379.
8. Hull, K. L.;Sanford, M. S. *J. Am. Chem. Soc.* **2007**, *129*, 11904-11905.
9. He, C.-Y.; Fan, S.;Zhang, X. *J. Am. Chem. Soc.* **2010**, *132*, 12850-12852.
10. Goosen, L. J. P., *J. Angew. Chem., Int. Ed.* **2002**, *41*, 1237-1241.
11. Reddy, B. V. S.; Reddy, L. R.;Corey, E. J. *Org. Lett.* **2006**, *8*, 3391-3394.
12. Luzung, M. R.; Lewis, C. A.;Baran, P. S. *Angew. Chem. Int. Ed.* **2009**, *48*, 7025-7029.
13. Horinouchi, S.; Yamanoi, Y.; Yonezawa, T.; Mouri, T.;Nishihara, H. *Langmuir* **2006**, *22*, 1880-1884.
14. Ranu, B. C.; Chattopadhyay, K.;Adak, L. *Org. Lett.* **2007**, *9*, 4595-4598.
15. Bianchini, C.;Shen, P. K. *Chem. Rev.* **2009**, *109*, 4183-4206.
16. Mousseau, J. J.; Vallée, F.; Lorion, M. M.;Charette, A. B. *J. Am. Chem. Soc.* **2010**, *132*, 14412-14414.
17. Dick, A. R.; Hull, K. L.;Sanford, M. S. *J. Am. Chem. Soc.* **2004**, *126*, 2300-2301.
18. Heating/stirring were conducted on an aluminum reaction block with stirring set at the highest rpm (IKA stirplate setting of 11).